IMPACT DAMAGE IN CARBON FIBRE COMPOSITES

by

W. J. CANTWELL

Thesis submitted for the degree of

Doctor of Philosophy

in the faculty of Engineering

University of London

1986.

Department of Aeronautics,
Imperial College,
London SW7 2BY.

BIBL
LONDON
UNIV.

ACKNOWLEDGEMENTS

I would like to acknowledge the Ministry of Defence (Procurement Executive) who provided the financial funding for this research contract.

I would also like to take this oppurtunity to thank Ray Wilkins and the other technicians of the Aeronautics workshop for helping with the various technical problems encountered during the project.

I wish to extend my extreme gratitude to my supervisor, Dr. John Morton, who has been a source of great help and inspiration throughout this research programme.

Finally, I wish to thank my dear wife Linda for her love and understanding throughout the last three years.

There are different kinds of service to God,

but it is the same Lord we are serving.

1 Corinthians 12:5

ABSTRACT

The impact response of a multi-angle fibrous composite has been assessed by conducting low and high velocity impact tests on a standard carbon fibre reinforced plastic.

Initially, the initiation and propagation of impact damage in a series of composite beams is monitored using a variety of destructive and non-destructive test techniques.

By accounting for the dissipation of energy during the impact process, a number of simple models are developed to predict the impact response of a laminated composite. The accuracy and suitability of these models is then assessed by comparing their predictions with the relevant experimental data.

The effect of impact damage on residual strength is then assessed by conducting monotonic tension tests on a range of damaged composites. By modelling the region of impact fracture as a simple notch and using a fracture model the residual tensile strength of the impact damaged composites is predicted.

Finally, the influence of target geometry on impact response is considered by conducting tests on a variety of composite structures. Further, the capabilities of the impact models are extended to predict the impact response of a more typical structure; the ensuing predictons are again compared with corresponding experimental data.

MAIN INDEX

		Page
Chapter 1.	Introduction.	1
Chapter 2.	Experimental procedure.	26
Chapter 3.	The low velocity impact response of CFRP.	40
Chapter 4.	Residual strength assessment of low velocity impact damaged CFRP.	87
Chapter 5.	The high velocity impact response of CFRP.	107
Chapter 6.	Residual strength assessment of high velocity impact damaged CFRP.	136
Conclusions		147
Appendices		295

NOTATION

A	Membrane tension coefficient fo a circular plate
[A]	Extensional stiffness matrix
a	Radius of area of contact
a	Plate radius
a	Semi-crack length
a_o	Characteristic damage size
b_i	Notch length in i th coupon
b_o	Size of the damage zone
[B]	Coupling stiffness matrix
d_o	Characteristic damage size
[D]	Bending stiffness matrix
Dx	Bending stiffness in x direction
E	Young's modulus
K	Flexural stiffness of target
Kt+Kp	Parameter describing elastic properties of impactor and target
Kic	Fracture toughness
L	Beam length
m	Projectile mass
M	Beam mass
Mx,My	Bending moments in x and y directions respectively
[M]	Moment resultant
[N]	Force resultant
P	Total plate or beam load
Pcr	Critical load
Pp	Plate flexural load
Pm	Plate membrane load

$\bar{Q}ij$	Transformed stiffness term
q	Surface Pressure
q_0	Maximum surface pressure
qx,y	Surface pressure at x, y
Rp	Projectile radius
r	Radius of applied load
t	Target thickness
V_f	Volume fraction of fibres
w	Specimen Width
Y	Width correction factor
α	Length of intense energy region
α	Contact deformation
γ	Overall fracture energy of composite
γ_m	Fracture energy of matrix
γ_f	Fracture energy of fibres
γ_d	Fracture energy of delamination
γ_t	Transverse fracture energy
δ	Target deflection
σ_0	Unnotched tensile strength
σ_c	Unnotched compressive strength
σ_r	Residual tensile strength
σ_i	Notched strength of i'th coupon
ν	Poisson's ratio
ϵ	Laminate membrane strains
κ	Laminate Curvatures

1. INTRODUCTION

		page
1.1	Background	2
1.2	Impact of Composite Materials	7
1.3	Review of the literature	7
1.3.1	Impact fracture mechanisms	8
1.3.2	The influence of fibre properties on impact response	13
1.3.3	The effect of fibre surface treatment on impact response	15
1.3.4	The influence of resin properties on impact response	15
1.3.5	The influence of laminate stacking sequence on impact response	17
1.3.6	Residual strength of impact damaged composites	20
1.3.7	The influence of target geometry on impact response	21
1.4	Aims of the research programme	23

INTRODUCTION

1.1 Background

With the rapid increase in fuel costs during the early 1970's fuel efficiency became a major consideration in aircraft design. During the same period, aerospace engineers were beginning to examine the feasability of employing the high strength, high stiffness properties of composite materials in the construction of many aircraft secondary structures. The potential of composite materials had long been known. The ancient Egyptians realized that laminated wood structures displayed strengths far superior to those of similar plain wood structures and that straw prevented cracking of mud bricks when drying.

In general, modern day composites comprise of strong, stiff fibres embedded in a polymeric matrix. Most composites are manufactured by laying sheets of unidirectional resin-impregnated fibres in a specific sequence, the exact order being determined by the anticipated operational conditions. The resulting panel is positioned in an autoclave and subjected to a complex curing procedure involving the application of high temperatures and pressures. The resulting component is both strong and light, offering superior properties in the principal fibre directions. With the recent improvement in processing techniques, composites are now being manufactured with specific strengths (defined as the strength per unit volume)

up to seven times greater than those of conventional aeronautical materials. Figure 1 presents a comparison between one such composite, carbon fibre reinforced plastic (CFRP) and three conventional aeronautical metals (1). The superiority of this high performance composite is clearly evident.

However, it is not just in static conditions that composites excel. For example, their fatigue behaviour is far superior to that of standard metals. The fatigue limit of notched CFRP is typically sixty five per cent of the ultimate strength, this compares with a value of thirty per cent for most notched metals (1). Another potential advantage of the use of composites is that, despite the high cost of the raw materials, structures may be manufactured at lower cost than many of their metallic counterparts. Here, the good formability characteristics of composite materials permits the fabrication of complex geometries and removes the need for the complex bonding and jointing procedures.

It is becoming clear that the potential for employing composite materials in the constuction of aeronautical components is enormous. In the past, however, aerospace companies have been hesitant, even reluctant, to contemplate replacing conventional metallic structures with these new high performance plastics. More recently, the successful trial deployment of composites in the secondary structures of the General Dynamics F-111 (boron-epoxy) and the Boeing 737 (carbon-epoxy) has served to allay many of these initial

fears. Following this, NASA in collaboration with McDonald-Douglas conducted a rigorous test programme to examine the feasability of manufacturing a large tail-fin structure with carbon fibre reinforced plastic (2). Several composite DC-10 fins were manufactured and tested. The first of these failed prematurely during testing. Following minor modifications a subsequent fin was designed and tested. This section fin failed at 167 per cent of its ultimate design load, representing a load-carrying margin of 17 per cent over the safety factor design limit. Furthermore, this was achieved with a weight saving of over twenty three per cent! Many of the current generation of civil aircraft now employ laminated composites in their secondary structures. One example of this is the Boeing 767, see figure 2. Here the control surfaces in the wing and tail are manufactured from carbon fibre and Kevlar-carbon fibre epoxy composites bonded to a light honeycomb core. Such utilisation of these high performance materials in sandwich configurations yielded a structural weight saving of over 500 kilograms, this corresponding to a fuel saving of 1.5 million litres a year (3).

It is perhaps in the military sector where the impact of composite technology will be greatest. Modern day fighters must be light, fast but yet highly manoeuverable under the rigours of combat conditions. Current aircraft, such as the

F-14, F-15, YF-16 and the AV-8B, all employ composites in their wing and tail structures. Perhaps the most innovative programme being undertaken at present is that by Grummans in the design of the X-29A forward swept wing aircraft (4). Forward-sweep technology is not new, it has long been known that forward swept wings yield improved lift, better low speed handling and reduced drag at subsonic speeds. To date, however, due to material limitations, it has been impossible to design aircraft wings with sufficient sweep angles to fully benefit from these advantages. However, with the advent of this new generation of high performance materials this problem has now been overcome. A carbon fibre forward-swept wing structure with its fibres orientated at 0°,+/-45° and 90° has been designed and fully tested. Early indications are very favourable. The composite wing section has been subjected to and survived loads considerably in excess of those likely to be encountered in operational conditions.

Early fears suggested that composites may have inadequate resistance to transverse impact loading. These fears were compounded when a major aerospace company used carbon fibre /epoxy turbine blades in one of its production engines. During a flight test through a severe thunderstorm, the turbine blades were severly damaged and, although the plane landed safely, the near disaster raised serious concerns regarding the suitability of composite materials for future aircraft design.

Most laminated composites are manufactured by stacking layers of unidirectional fibres in a predetermined sequence. As a result, layers of resin enrichment exist between the plies in the final cured composite which, when subjected to large direct or interlaminar stresses, fracture resulting in the formation of planes of delamination.

However, composites are by no means inferior to metals in their ability to absorb incident impact energies. Most metals deform when strains exceed about 0.1 % so that the elastic energy absorbed per unit volume is approximately 35 KJ/M^2 (taking E as 70 GPa). Subsequent plastic deformation allows strains of more than 10 % suggesting that the plastic energy absorption may be as high as 50 MJ/M^2. In composites failure strains are of the order of one to two per cent so that the maximum elastic energy absorbed may be of the order 3.5-14 MJ/M^2 . Also the development of new systems promise even higher values. However, transverse impact on composites also leads to energy dissipating mechanisms which affect the structural integrity. Indeed, strength reductions of up to fifty per cent have been recorded in composites displaying little or no visible damage (5).

Concerned by these limitations, this research programme was inaugurated to examine the response of a standard carbon fibre composite when subjected to localised transverse impact loading.

The programme concentrates on examining the overall response of a standard carbon fibre composite to both low and high velocity impact loading. Much attention is given to examining the processes by which impact damage propagates in these materials. Further, by considering the impact process in more detail, attempts are made to develop simple models suitable for predicting the response of laminated composites when subjected to localised impact loading

1.2 Impact of Composite Materials

Before undertaking this programme of research a comprehensive review of the literature was conducted in order to fully appreciate the current 'state of the art' and to highlight those areas requiring further examination. The important findings of this literature survey will be discussed in the following section.

1.3 Review of the Literature

Despite early worries, it is becoming clear that composites are by no means inferior to metals in their ability to absorb energy in both elastic and fracture mechanisms, indeed in some cases they may be superior(6).

When subjected to localised impact loading, composite

structures respond in bending, allowing energy to be accommodated in elastic deformations. At sufficiently large impact energies a stress system may be generated which exceeds the local strength of the material and failure ensues. The following section details the various damage mechanisms common to composites.

1.3.1 Impact Fracture Mechanisms

On a macroscopic scale, impact on composite materials generates a complex damage zone consisting of regions of delamination, matrix cracking and transverse fibre fracture (7,8). The first of these, delamination, propagates mainly in the resin rich regions at the ply interfaces, occurring as a result of locally large interlaminar and direct stresses (9). In general, since delamination does not involve the destruction of fibres it displays a fracture energy comparable to that of the pure matrix system. Typical fracture energies for epoxy resins range between $700J/M^2$ and $3800\ J/M^2$ (10,11). Although these figures are relatively low, the area of delamination may be considerable indicating that this form of interlaminar fracture is a major energy absorbing mechanism in impacted laminated composites. Indeed, it has been suggested that laminates which encourage the growth of delamination offer superior resistances to localised impact loading (12-16).

Delamination is also instrumental in determining the post-impact performance of a damaged composite (17,18). In tension, the presence of delamination around a notch or defect frequently reduces the stress concentrating effect of the damage leading to a considerably improved tensile capability (17). In compression, however, the problem is more serious. Here, delamination precipitates a reduction in support around load-bearing fibres which ultimately leads to a premature buckling failure (18). Figure 3 shows the variation in post-impact compression strength with impact energy for a sixteen ply (0,+/-45) laminate. Reductions in compression strength were recorded here in coupons displaying little or no sign of visible damage. Attempts to inhibit the growth of delamination have been made by stitching laminates with Kevlar thread or by using some form of 3-D reinforcement (19). However, both techniques are costly and are therefore impractical from a manufacturing point of view.

The second damage mechanism, matrix cracking, propagates in the regions of resin between individual fibres. During initial crack propagation, matrix cracking exhibits a fracture energy similar in magnitude to that of the neat matrix material. However, as the matrix cracks continue to grow they are bridged by local fibres. Now, more energy is required in order to propagate the crack resulting in a

substantial increase in fracture energy (20).

Wilkins (21), in considering the effect of matrix damage on residual properties, suggested that matrix cracking does not influence significantly the residual strength of a composite structure. These conclusions are questionable however. Under certain tensile loading conditions where the crack does not extend to delamination matrix cracking can impose large stress concentrations on the load-bearing fibres and, in certain circumstances, lead to premature failure.

Transverse fibre fracture exhibits the greatest fracture energy of the damage modes considered here. Typical values for transverse fracture energy in C.F.R.P. range between 30 KJ/M^2 (22) and 60 KJ/M^2 (20). Although transverse fibre fracture is generally limited to regions local to the point of impact it can be a source of considerable energy absorption.

Because fibre fracture frequently involves the destruction of the load-bearing constituents of the composite structure it can precipitate significant reductions in load carrying capability, particularly in tension (23). Figure 4 shows the effect of low velocity impact loading on the residual tensile strength of a typical sixteen ply (0,+/-45) composite. Significant reductions in tensile strength were first recorded at the onset of fibre damage, above this threshold the strength declines rapidly.

One other, although less reported, fracture mechanism common

to fibrous composites is fibre spallation. When a fast moving missile strikes a composite target a system of compression stress waves are generated around the point of impact (24,25). These waves then propagate through the thickness of the composite structure with velocities up to 2500 m/s (26). Upon encountering a free surface, usually the rear surface of the target, the compression waves are reflected to form tensile waves which, upon reaching a ply interface, generate large through thickness stresses resulting in the removal of the lower surface fibres.

Attempts to limit damage due to stress wave propagation have centred on using woven fabrics as surface protection or employing through thickness reinforcing fibres similar to those discussed earlier (26).

On a microscopic level fracture mechanisms such as fibre-matrix debonding and fibre pull-out are frequently observed in impact damaged fibrous composites (27,28). Debonding occurs extensively in those composites with low levels of fibre surface treatment. Debonding results when the stress field near the crack tip exceeds the local strength of the local fibre-matrix interface. With continuing crack propagation the fracture surfaces seperate causing many fibres to pull out of their surrounding matrix. During this pulling out process energy is expended in overcoming local frictional forces.

Based on the evidence of scanning electron microscope studies, a number of simple models have been developed to predict energy dissipation in these micromechanical processes (29). It has been shown that the fracture energy for debonding can be written as

$$E_d = \frac{V_f \sigma_f^2 y}{4E_f}$$

and the fracture energy for fibre pull-out as

$$E_{po} = \frac{V_f \sigma_f l_c^2}{12.1}$$

where

l_c = critical transfer length = $\frac{\sigma_f r}{\tau}$

V_f = the volume fraction of fibres

σ_f = the tensile strength of the fibres

E_f = the Young's modulus of the fibres

y = the debonded length

τ = the fibre-matrix interfacial shear strength

r = the radius of fibre

l = length of fibre

It is now generally accepted that both fracture mechanisms contribute significantly to the overall impact toughness of a fibrous composite (30-33). Phillips and Tetelman (34) found that fibre pull-out was the dominant fracture mechanism in C.F.R.P. containing type 1 fibres, quoting fracture energies for debonding and pull-out of

$1.5KJ/M^2$ and $26KJ/M^2$ respectively.

From the preceeding paragraphs it is becoming clear that energy absorption in impacted composite materials occurs through a variety of vastly differing fracture mechanisms. As a result, engineers possess the capability to design composite structures to absorb incident impact energies in large areas of matrix damage or more localised regions of fibre fracture. The ultimate choice of failure mode will depend upon, amongst other things, the environmental conditions encountered during operational service and upon the in-service loading spectrum.

1.3.2 The Influence of Fibre Properties.

The mechanical properties of the fibres are known to influence directly the impact resistance and subsequent load-carrying capacity of a fibrous composite (35-40).

It is known that the impact resistance of a multi-layered composite is determined by its ability to absorb energy in elastic deformations. For a fibrous material the stored strain energy is known to be proportional to the term σ_f^2 / E_f where ' σ_f ' and ' E_f ' are the tensile strength and Young's modulus of the fibres respectively. This suggests therefore, that a composite manufactured from high strength, low stiffness fibres will offer an improved resistance to impact loading. Indeed, Chamis et al (33)

having examined the Charpy impact energies of a wide range of fibrous composites have identified a strong correlation between this strain energy term and impact resistance. This suggests, therefore, that the strain energy model, although simple, is adequate for ranking the impact response of materials of this nature.

The development of a new generation of high strain to failure carbon fibres has precipitated marked improvements in post-impact residual properties. This is most apparent under in-plane tensile loading where improvements in static strength of up to forty per cent have been recorded, see figure 5a (39). In compression however, improvements in residual strength are not as great, figure 5b. It is now generally accepted that the compression strength of a fibrous composite is not influenced greatly by changes in fibre properties but instead is sensitive to variations in matrix and interface properties.

Rich and Bunsell (41) examined the influence of fibre diameter on impact response in a boron-aluminium composite system. They found that slight improvements in impact resistance could be achieved by increasing the diameter of the in-situ fibres. However, from these results it is not clear if all, or even part, of this improvement was achieved by varying the fibre diameter or whether these trends were just a consequence of inadvertantly varying the fibre volume

fraction of the composite.

1.3.3 The Effect of Fibre Surface Treatment on Impact Response

Fibre surface treatment is a process employed for increasing the adhesion between the in-situ fibre and the surrounding matrix. The effect of such treatment on the impact resistance and subsequent mechanical properties of a composite is complex and therefore beyond the scope of this survey. Briefly, however, fibre surface treatment is known to increase the transvers tensile strength of the composite resulting in higher energy thresholds for first damage (42).

At large incident energies the low transverse fracture energy of surface treated composites means that extensive fibre fracture is frequently incurre resulting in poor post-impact tensile properties.

1.3.4 The Influence of Resin Properties on Impact Response

Although many workers have attempted to assess the role of matrix properties in determining impact response their conclusions appear to differ (36,42). Rogers et al (42) conducted high velocity impact tests on a limited number of

carbon fibre-epoxy systems. They suggested that the mechanical properties of the resin affect the impact resistance only marginally. This is somewhat surprising, however, since delamination, which is primarily a resin controlled mode of failure, is known to be a major energy absorbing mechanism under impact conditions and should be influenced by changes in matrix properties.

A more comprehensive test programme has been undertaken by Williams, Rhodes and Starnes (44). They considered a range of over twenty different resin systems from low strain to failure epoxy resins to elastomeric resins with strains to failure as high as twenty four per cent. Here, it was observed that matrix properties are indeed significant in determining the level of damage incurred in a laminated composite. Figure 7 shows the outlines of a series of C-scans taken from two entirely different resin systems. System 1 is a conventional brittle matrix composite and system 2 a high strain to failure matrix composite. The evidence clearly shows that the high strain matrix incurs considerably less damage. The authors suggest that for improved impact resistance the resin must be present in sufficient amounts to permit the formation of a plastic zone between the fibres and therefore blunting of the propogating crack system.

Attempts to further enhance the impact resistance of these

composites by the use of plasticizers did not, however, yield conclusive results (44).

At present, much interest is being focussed on examining the potential for using high performance thermoplastics in aeronautical applications(45). Carbon fibre/PEEK systems have already displayed considerable toughness under drop-weight impact loading. Ultrasonic C-scans and optical micrographs of carbon fibre/PEEK laminates have indicated that impact damage is generally more localised to the point of impact than in conventional carbon fibre systems suggesting that more energy is being dissipated in contact deformations, fibre fracture or both. Carbon fibre/PEEK composites, although exhibiting slightly greater notch sensitivity than most composites, offer excellent post-impact characteristics with residual strengths up to twenty five per cent greater than those of conventional carbon fibre systems.

1.3.5 The Influence of Laminate Stacking Sequence on Impact Response

The effect on impact resistance of varying the fibre lay-up is not fully understood. Under low velocity impact the flexural stiffness of the target, a function of the composites lay-up, will determine its ability to absorb energy elastically. Assuming a maximum strain failure criterion, stiffer targets, with the greater ability to accommodate elastic energy, will display superior impact resistances. Indeed, testing has shown

this to be the case (46). However, the situation is not as simple as this since the maximum elastic energy absorbed is limited by some failure criteria which depend upon lay-up in a complex manner.

Under high velocity impact conditions, the strain energy contribution is likely to be small since light, fast moving projectiles generate only a local mode of target response. However, the fibre stacking configuration may still be important since this will determine the extent and location of the resulting impact fracture. This view is supported by Ross and Sierakowski(47) who found that composites possessing many interfaces displayed considerably improved resistance to high velocity perforation.

Figure 7 suggests a lay-up effect in post-impact residual strength. Here, the variation of residual tensile strength with impact energy for a pair of two millimetre thick carbon fibre composites is shown. The composite with its zero degree fibres outermost displays a superior residual strength capability. Bishop (48) found that the specific positioning of the +/-45° plies in a (0,+/-45) composite can be crucial. Placing a +45° layer and -45° layer either side of a zero degree layer precipiates the growth of planes of delamination under tensile loading leading to a reduction in stress concentrations on the load bearing zero degree fibres.

Significant improvements in impact resistance have been achieved with hybrid composites (50-53). Here, structures can be designed to combine the high impact capability of say glass or Kevlar with the high strength and stiffness properties of carbon fibres.

Two types of hybridised composite exist, namely intraply and interply. The former involves combining fibres with different properties in the same layer of material. This can,however, present problems in the manufacturing process and frequently results in laminates displaying extensive regions of resin enrichment. As a result, intraply composites are not widely favoured and have found little use. Interply hybrids are manufactured by mixing discrete plies of two or more materials within the same laminate. As a result, improvements in impact resistance well above those predicted by a simple rule of mixtures approach have been realised (50). It is now generally accepted that the improved impact resistance of these hybrid composites is in part due to the increased number of energy absorbing fracture mechanisms incurred. Extensive testing has shown that the most promising hybrid in terms of impact toughness is one containing an inner core of carbon fibes covered by an outer layer of either glass or Kevlar fibres (53,54). The outer layers absorb much of the incident energy of the impactor while the inner carbon layers, being relatively undamaged, provide the necessary

residual stiffness and strength properties for subsequent operation.

However, with the development of high strain to failure carbon fibres it may be that the subsequent advantages of hybridising these fibres with Kevlar or glass fibres will be small.

1.3.6 Residual Strength of Impact Damaged Composites

In operational service, aeronautical structures are continually subjected to a complex spectrum of static and dynamic loads. In an attempt to simulate these conditions, several workers have subjected pre-loaded composite structures to localised impact loading (55-58). Butcher (56) found that the combined impact and tensile loading on a composite target is more severe than similar impact on corresponding unloaded structure. He suggested that these differences are not a result of any significant dynamic effect but more likely a consequence of a combination of the impact and in-plane stress fields.

The effects of compression pre-loading are more serious however (57). When a projectile strikes a target, out of plane displacements will be generated which result in a reduction in target stability. At large incident energies the structure will become unstable probably failing in an overall buckling mode at relatively low pre-loads.

The post impact fatigue properties of damaged carbon fibre composites have received much attention (18,23). Interestingly, 0-Tension (R=-1) and 0-compression (R=100) fatigue cycling does not appear to degrade residual properties of a previously damaged composite (18,59). Indeed, extensive testing has shown that 0-tension cycling generates delamination local to the zone of damage leading to reductions in stress concentrations and therefore improved tensile strength (18).

The combined effects of tension-compression fatigue (R=-1) on an impact damaged composite have been considered by Stellbrink and Aoki (54). They found that fully reversed cycling was particularly detrimental to the integrity of a damaged composite. Similar tests on centre-notched carbon fibre composites have shown that areas delamination generated in the tensile component on the fatigue cycle precipiated failure in buckling in the compression half of the cycle (49)

1.3.7 The Influence of Target Geometry on Impact Response.

One of the most important factors in determining impact response is likely to be the geometry of the target structure. However, to date, little work has been undertaken to fully assess the dominance of this parameter.

Due to convenience and economic limitations screening is

frequently conducted on small coupons supported in an idealized manner. However, it may be that basing component design on the knowledge yielded by these tests is unwise because such coupons will under-estimate the impact resistance (due to their low volume) and not necessarily anticipate the correct mode of failure.

Several workers have attempted to apply simple beam theory to predict the influence of target geometry on the impact response of small composite coupons (60,61). Bradshaw et al (24) have shown that the location and nature of first damage in small coupons depends on two parameters, the span to depth ratio of the target and the longitudinal strength to shear strength ratio of the target material. They found that short, thick beams failed in an interlaminar mode, whereas long, thin beams failed in overall a flexural mode.

The effect of structural geometry on high velocity impact response has recieved little attention. Husman and Whitney (36) found that the geometrical size of the target was important under high velocity impact conditions. However, since all of their work was conducted on small, narrow coupons where damage propagated to the specimen edges it appears that these tests are unrepresentative.

Few workers have examined the impact response of a larger, more realistic composite structure. Demuts et al (62) conducted ballistic impact tests on a series of multi-spar

and multi-rib wing designs. Their findings suggested that the location of the impact strike is critical. Contrary to expectation, they found that impact at the mid-bay areas was more detrimental than that at the spar or rib attachments.

1.4 Aims of the Research Programme

From these results it is clear that the fracture process in laminated fibrous composites is complex with energy being accommodated in a variety of widely differing micro and macro-scopic damage mechanisms. The available experimental evidence suggests that the matrix or, more likely, the fibre-matrix interface is the Achilles heel of these materials when subjected to impact loading.

Subsequent strength testing has shown that such damage, although frequently innocuous, precipitates significant reductions in residual strength (particularly in compression).

Clearly, in designing composite structures for impact resistance and damage tolerance it is necessary to highlight and understand those mechanisms responsible for damage initiation and propagation. To date,however, little work has been done in this area. One of the goals of this research project was, therefore, to understand and, if possible, predict the development of impact damage in a standard carbon fibre epoxy laminate when subjected to low and high

velocity loading.

Some disagreement exists regarding the effect of the various damage mechanisms on the subsequent load-carrying ability of these laminated structures.

In an attempt to cast light on this area, many of the impact damaged composites will be tested for their residual strength. In this project attention is limited to considering only the residual strength in tension since, although not necessarily the most severe loading condition, such tests were simple and removed the need for complex or ineffective loading jigs.

Finally, this research programme examines the geometrical factor in impact testing. As stated previously, for reasons of both simplicity and economy much of the work to date has been conducted on unrepresentative small coupons. In this programme it is intended to examine the reliability of such tests by comparing the response of these 'idealistic' coupons with those of larger, more realistic structures. The experimental details and resulting findings of this research programme are presented in the following chapters. Chapter 2 details the experimental procedure for achieving a broad range of impact velocities encompassing low velocity (drop-weight) impact tests undertaken to simulate the 'dropped tool' impact problem and the high velocity impact situation characteristic of runway debris damage. Following

this, the report is divided into two parts, chapters 3 and 4 will examine the low velocity impact problem and chapters 5 and 6 will consider the high velocity impact response of CFRP. Both sections commence by examining the development of impact damage using a variety of destructive and non-destructive test techniques. Then, by considering the mechanisms of energy dissipation during the impact process a number of simple models are developed to predict the low and high velocity impact response of this carbon fibre-epoxy system. Both sections then continue by examining the influence of target geometry on impact resistance. Here, the impact responses of a number of simple geometries are compared with that of a larger circular plate.

Finally, the effect of impact damage on residual strength is assessed by conducting monotonic tension tests on both the drop-weight and ballistically impacted laminates.

2. EXPERIMENTAL PROCEDURE

		page
2.1	Programme overview	27
2.2	Laminate production	28
2.3	Specimen preparation	29
2.4	Impact testing	29
2.4.1	The drop-weight impact test rig	30
2.4.2	The gas gun	31
2.5	Residual strength assessment of damaged composites	33
2.6	Damage detection and assessment	33
2.6.1	Ultrasonic C-scanning	33
2.6.2	The X-ray technique	35
2.6.3	The Deply technique	36
2.6.4	Optical microscopy	37
2.6.5	Scanning electron microscopy	38
2.7	Summary	39

CHAPTER 2.

EXPERIMENTAL PROCEDURE

2.1 Programme Overview

In the last chapter it was noted that composite materials are at present being utilized in the manufacture of many secondary structures for civil and military aircraft. In operational service these components may encounter a wide range of impact threats ranging from a simple dropped tool travelling at a few metres per second to runway debris travelling at velocities of up to 600 m/s. In order to simulate these threats a drop-weight test rig (capable of achieving impact velocities of up to 7 metres per second) and a nitrogen powered gas gun (for ballistic velocities) were employed.

The following chapter details the experimental procedure employed in this programme for examining the impact response of a standard carbon fibre-epoxy composite. In order to fully understand this complex process it is necessary to monitor the development of the resulting impact damage. In this programme a variety of destructive and non-destructive damage detection techniques will be employed, details of the procedures followed will also be discussed in this chapter.

Since a damaged component will be subjected to a variety of loading conditions in its subsequent operational service it is necessary to understand the full consequence of impact damage on residual strength. Here, this is assessed by determining the residual tensile strength of the damaged composites.

2.2 Laminate Production

The laminates examined in this study were manufactured from 0.125mm thick sheets of unidirectional Grafil XAS high strength surface treated carbon fibres in Ciba-Geigy BSL914C epoxy resin. This material system was favoured since it was thought typical of many of those finding employment in the construction of present day aeronautical components.

Carbon fibre panels with dimensions 300mm x 300mm x thickness were prepared by laying sheets of unidirectional warp sheet according to the laminate stacking configurations given in table 1. A range of seven different laminates were examined in this research programme. The (+/-45) composites were selected since it is believed that these laminates might be used in the construction of future aircraft wing skins (63). The 8 and 16 ply (0, +/-45) lay-ups, although generally notch sensitive, were favoured since they are characteristic of laminates currently being employed in the construction of many aircraft secondary structures (3,4).

After laying up, the panels were cured in an autoclave according to the manufacturers specifications. The cure cycle for all but the thickest panel is shown in figure 8. The sixty-four ply laminate, due to its increased thickness, was cured according to the modified cure cycle shown in figure 9.

After manufacture, all panels were post-cured in an air circulating oven for four hours at a temperature of 190°C. The post-curing process improves the high temperature performance of the composites and also enhances their machinability.

2.3 Specimen Preparation.

After manufacture, the panels were scanned using an ultrasonic scanning machine. The resulting C-scans gave an indication of the overall quality of the panel and were useful for determining the location of small voids and defects which were then avoided in subsequent testing.

Individual test specimens were cut from the manufactured panels using a high speed diamond tipped slitting wheel. Initial testing was conducted on beam coupons with dimensions 25mm x 50mm. These small coupons were chosen for economy and to allow comparisons with the published work of Dorey (53,64). During the course of this study it became necessary to vary the dimensions of the target, in these cases the full details of the geometrical configuration are given at the appropriate location in the text.

2.4 Impact Testing.

In order to simulate the radically differing impact threats encountered in operational service a simple drop-weight impact rig and a high velocity gas gun were employed. The following

sections details the construction and operation of these test rigs.

2.4.1 The Drop-Weight Test Rig.

The drop-weight rig shown in figure 10 comprises of a falling carriage, two parallel guide rails, an opto-electric trigger and a target support strurcture. The impacting head, a six millimetre diameter steel hemisphere, was fixed to the lower side of the drop-weight carriage resulting in an overall carriage mass of 0.7 Kg. In order to examine the impact process in more detail, a load cell was attached to the impact carriage immediately above the impactor head. Before undertaking any impact testing it was necessary to calibrate the load cell, details of this procedure are given in appendix 1.

Impact energies up to twelve Joules were achieved by raising the carriage to a predetermined height and releasing it. The falling carriage was guided by two parallel, well lubricated rails ensuring a normal impact on the test structure. Just prior to impact, a non-reflective flag attached to the falling carriage intercepted a pair of opto-electric switches positioned 40mm apart enabling the incident energy of the impactor to be determined accurately. Where necessary, the rebounding carriage was caught in order to avoid further impacts.

Several support structures were used during the course of testing. Initially, composite beams were supported on two 12.7mm diameter simple supports positioned at distance between 50mm and 200mm apart. In order to simulate the impact response of a larger, more realistic composite structure tests were conducted on a series of flat panels clamped between two 130mm internal diameter ring supports.

2.4.2 The Gas Gun

In order to achieve impact velocities up to and above Mach one the gas gun shown in detail in figures 11 and 12 was designed and constructed. The gun comprises of a nitrogen gas reservoir, a driver chamber, a long uniform barrel, a tapered tube and a specimen support structure.

Bottled nitrogen gas was fed via a normally closed solenoid valve to the driver chamber located at the end of the gun barrel. Here the gas was restrained by a plastic diaphragm clamped between the faces of the driver chamber and the barrel mounting block. The projectile, usually a six millimetre diameter, one gram steel ball, was placed in a holder, usually termed a "sabot", and positioned approximately twenty millimetres in front of the diaphragm as shown in figure 13(a). A typical sabot geometry is shown in figure 13(b). The sabots were made from wood, nylon or steel the choice depending on the incident velocity required. The heavier

masses were used for low velocity firings when excessively low gas pressures have been required.

Rupture of the plastic diaphragm was achieved by passing an electric current through a length of resistance wire located at its centre. The resulting rapid expansion of gas accelerated the sabot/projectile combination along the two metre long barrel. At the end of the barrel the sabot intercepted two infra-red light beams triggering an electronic counter enabling the incident velocity of the projectile to be determined. Upon leaving the barrel the sabot was decelerated in the tapered steel tube leaving the projectile to continue in free flight and strike the neighbouring target structure.

The incident velocity of the projectile was varied in three ways, by changing the diaphragm thickness, by altering the sabot mass and by varying the chamber pressure at diaphragm burst.

The composite targets were supported in supports similar to those employed in the drop-weight test programme. For purposes of safety, the target and its supporting structure were housed in a large steel box.

Where necessary, the post-perforation velocity of the projectile was obtained by measuring the time taken for it to break two fine wire meshes located immediately behind the target.

2.5 Residual Strength Assessment of Damaged Composites.

Before testing for residual tensile strength, aluminium end-plates were bonded to the specimen ends in order to protect them from the powerful gripping action of the testing machine jaws. A strong bond between specimen and end-plate was achieved by first abrading the specimen ends with wire wool and then cleaning them with trichloroethane solution.

Residual testing was conducted on an Instron Universal testing machine. This machine has a capacity of ten tonnes and can accommodate specimen geometries up to 50mm wide. All residual testing was conducted in a displacement mode of control with a crosshead speed of two millimetres per minute.

2.6 Damage Detection and Assessment

Fracture in the impacted specimens was assessed using a variety of destructive and non-destructive damage detection techniques. Ultrasonic C-scanning, X-radiography, thermal deplying, optical and scanning electron microscopy were all used extensively during the course of the research programme. A brief summary of these procedures and their relative merits will now be given.

2.6.1 Ultrasonic C-scanning.

Ultrasonic detection methods are widely used in the aerospace industry due to their simplicity and overall versatility. The

ultrasonic technique involves passing high frequency sound waves through a test specimen and monitoring the resulting attenuation in signal strength. Signal attenuation usually results from three sources, namely, viscoelastic effects in the resin, the heterogeneity of the composite and internal damage such as delamination and matrix cracking. By selecting the appropriate sound wave frequency the attenuation due to internal damage mechanisms can be maximised allowing an overall assessment of internal damage to be made.

In this programme, a Meccasonics pulse-echo ultrasonic scanner was used. To provide a uniform coupling medium for wave transmission, the test specimens were immersed in water. Sound waves with a frequency of 10MHz were emitted from a spherically focussed transducer located 50mm above the surface of the specimen. By reflecting the sound waves off a flat glass surface located directly beneath the specimen the sound waves were made to pass through the composite twice before returning to the ultrasonic transducer. The resulting attenuation of the signal was monitored by comparing its amplitude with that of the emitted signal, the level of attenuation being indicative of the quality of the composite. A series of discriminator circuits were calibrated to generate an electric current inversely proportional to the level of signal attenuation. These electric signals were then passed to an electric pen enabling all the information to be recorded on

current sensitive drawing paper.

The resulting C-scans yielded only a planar view of the composite and the region of damage. As a consequence, C-scans are incapable of distinguishing between the various prevailing damage mechanisms, nor do they give information on the through-thickness location of the damage. In this programme the C-scan technique was useful for detecting regions of localised impact damage which may then be examined in greater detail using X-radiography.

2.6.2 The X-ray Technique

X-radiography involves passing X-rays through a potentially damaged component and recording the resulting information on photographic film. To obtain a good level of contrast in the photographic recordings it is customary to apply an X-ray opaque fluid to the region of damage. A number of enhancing fluids are commercially available, these include tetrabromoethane, diodobutane, diodomethane and zinc iodide. The first three are extremely toxic and are not generally favoured, consequently zinc iodide, a safe, non-toxic chemical, was used in this research programme. The zinc iodide solution was made by mixing 60g of zinc iodide, 10ml of absolute alcohol, 10ml of water and a few drops of commercially available wetting agent.

The damaged composites were soaked in the zinc iodide solution

for approximately ten minutes, washed and then dried. The specimens were then laid on Polaroid Type 52 film, placed in a Faxitron 43504 X-ray cabinet and X-rayed. In all cases the accelerating voltage of the X-ray tube was set to a value of 15KV. The period of exposure varied with specimen thickness, typically, for a two millimetre thick CFRP composite this was five minutes.

X-radiography is a useful technique for observing matrix cracking and delamination. Standard X-radiographs give a two dimensional representation of the damage zone. A three dimensional effect can be achieved by making two exposures, one at $+15^{\circ}$ and the other at -15° to the X-ray beam and by viewing the pair through a stereoscope.

The success of the X-ray technique depends on the ability of the enhancing fluid to diffuse into the fracture zone. This can be improved by applying the enhancing fluid under vacuum conditions or introducing the penetrant to a specimen which is under load.

In this programme thermal deplying has proved to be a valuable damage detection technique since it yielded a three dimensional representation of the damage zone giving a clear insight into the impact process in these materials.

2.6.3 The Deply Technique

Although a destructive damage detection technique, thermal

deplying is very useful for examining fibre fracture and delamination in damaged composites.

Damaged coupons were supported on a wire mesh and placed in a furnace maintained at a temperature of 420°C for approximately one hour. After pyrolizing, the specimens were removed from the furnace and allowed to cool to room temperature. The specimens were then seperated into individual plies using transparent tape and a sharp blade. These deplied layers were subsequently mounted on cardboard for further observation.

2.6.4 Optical Microscopy

Optical microscopy has been used by metallurgists for many years. It is now becoming a popular technique for examining the fracture surfaces in composite materials. Optical micrographs, although yielding only a two dimensional view of the damage zone, are particularly useful since they are capable of distinguishing between the many forms of damage incurred by filamentary composites.

Small sections were cut form the damaged composites using a diamond wheel and mounted in Metaserv Type FT resin and left to harden. The resulting moulded specimens were then ground on a rotary grinder until all excess resin was removed and a flat surface remained. The mounted composites were polished for approximately one hour on a rotating nylon cloth using Brasso metal polish.

The fracture surfaces within the composite were subsequently examined and photographed using a high power Olympus photomicroscope.

This destructive damage detection technique was greatly favoured here since it was capable of detecting very low levels of impact damage and highlighting the mechanisms of first failure in this fibrous composite.

2.6.5 Scanning Electron Microscopy

The scanning electron microscope is a particularly useful tool for obtaining a clear three-dimensional view of a fracture surface.

In this study, a Jeol Technics JSM T200 scanning electron microscope was used. Before examination, the specimens were coated with a thin film of gold in order to prevent excessive heating by the electron beam. The specimens were then mounted on a solid base, earthed and placed on the operating stage of the photomicroscope. For optimum resolution and an adequate depth of field, the electron tube within the microscope was maintained at a voltage of 25KV. All relevant information was recorded on photographic film using the appropriate camera attachment.

Although not used extensively in this programme, the SEM is particularly useful for observing fibre pull-out and fibre-matrix debonding, damage mechanisms not readily detected

by the other tecniques.

2.7 Summary

In this chapter the fabrication technique, testing procedure and damage detection methods have been reviewed. It has been stated that thermal deplying and optical microscopy although necessarily destructive techniques are ideally suited for assessing the initiation and growth of damage in impacted composites.

The following chapters examine the effect of impact loading on the response of a carbon fibre composite. Since the low and high velocity impact response of this material is likely to differ considerably it has been elected to consider these problems separately. Therefore, the following chapters, chapters 3 and 4 will be concerned with analysing the low velocity impact response and post-impact capability of this material system. Chapters 5 and 6 will examine the response of CFRP when subjected to high velocity impact loading.

The next chapter, chapter 3, commences by examining the processes of damage development in a series of beam coupons. Supported by this knowledge, a number of simple models are developed to predict the low velocity impact response of a composite structure. Finally, the influence of target geometry on impact response is considered by conducting impact tests on a series of larger geometries.

3. THE LOW VELOCITY IMPACT RESPONSE OF CFRP

		page
3.1	Background	42
3.2	Low velocity impact damage studies	43
3.2.1	Damage development in CFRP	43
3.2.1.1	Eight ply (+/-45) composite	44
3.2.1.2	Eight ply (0,+/-45) composite	46
3.2.1.3	Sixteen ply (0,+/-45) composite	47
3.2.1.4	Thirty-two ply (+/-45) composite	49
3.2.2	Summary of damage studies	50
3.3	Analysis of the low velocity impact response of a composite beam	53
3.3.1	Background	53
3.3.2	Energy dissipation during low velocity impact loading	56
3.3.3	Assessment of the flexural stiffness of a composite beam	57
3.3.4	Energy balance for predicting first damage	59
3.3.5	Determination of the flexural stress field	62
3.3.6	Determination of the contact stress field	64
3.3.7	Comparison of predicted damage thresholds with experimental data	67
3.3.8	Prediction of fibre fracture threshold	68
3.3.9	Prediction of perforation threshold	69

		Page
3.3.9.1	Estimation of energy for shear out	70
3.3.9.2	Estimation of energy dissipated in delamination	71
3.3.10	Comparison of predicted perforation thresholds with Experimental data	72
3.4	The effect of target geometry on low velocity impact response	73
3.4.1	Background	74
3.4.2	The size effect in composite beams	75
3.4.2.1	The variation of the damage threshold energy with beam length	75
3.4.2.2	The variation of fibre fracture threshold with beam length	77
3.4.2.3	The variation of perforation energy with beam length	77
3.4.3	The low velocity impact response of a circular composite plate	78
3.4.3.1	Analysis	78
3.4.3.2	Prediction of first damage in circular composite plates	81
3.4.3.3	Prediction of perforation in circular composite plates	82
3.5	Summary of low velocity impact studies	83

CHAPTER 3.

LOW VELOCITY IMPACT STUDIES

3.1 Background

This chapter examines the response of a series of carbon fibre composite structures when subjected to localised low velocity impact loading by a large mass. Under low velocity impact conditions the contact time between the impactor and target is long and the target deforms in a primary mode of response adopting an overall 'quasi-static' flexural mode. This behaviour allows part, or sometimes all, of the incident energy of the projectile to be accommodated elastically.

The low velocity impact response of fibrous composites has been considered by many workers (8,12,14,52). In-depth experimental and analytical studies have shown that parameters such as target geometry (45), laminate properties (39), fibre stacking sequence (18), impactor geometry (12) and target support conditions (9) all influence the low velocity impact response of a composite structure.

Initially, by employing a variety of destructive and non-destructive damage detection techniques, this chapter examines the processes by which impact damage develops in a carbon fibre structure. Then, by accounting for the dissipation of energy during the impact process, a number of simple models are developed to predict the impact capability

of a composite beam.

Finally, the influence of target geometry on low velocity impact response is assessed by conducting drop-weight impact tests on a variety of larger structures.

3.2 Low Velocity Impact Damage Studies

The process of fracture in composite materials has been discussed in chapter 1. It is clear that composites possess the ability to absorb incident impact energies through a variety of widely differing fracture processes. On a macroscopic scale, fracture mechanisms such as matrix cracking, delamination and fibre fracture are frequently observed in impacted composites (8). On a microscopic level, fibre-matrix debonding and fibre pull-out are common to fibrous composites (27). In this section the development of impact damage in the Ciba Geigy XAS-914C system is examined using a number of destructive and non-destructive damage detection techniques, these include penetrant enhanced X-radiography, ultrasonic C-scanning, optical microscopy and thermal deplying.

3.2.1 Damage Development in CFRP

The following section concentrates on the development of impact damage in the four carbon fibre XAS-914C composites

detailed below, (full details of the stacking sequences are given in table 1).

8 ply	(+/-45)
8 ply	(0,+/-45,0)
16 ply	(0 ,+/-45)
32 ply	(+/-45)

These lay-ups were selected since they represented a broad cross-section of the laminates tested here and permitted a comparison to be made between the (+/-45) and (0,+/-45) composites. Also, the processes of damage development in them were believed typical of those incurred in most laminated composites.

Since the mechanisms of failure varied with fibre stacking configuration, the development of damage in each laminate will now be discussed seperately.

The processes of damage development is assessed through a series of photographs, micrographs, C-scans and radiographs.

3.2.1.1 Eight ply (+/-45) Composite.

The development of impact damage in this one millimetre thick laminate is shown in the micrographs, figure 14, and the photographs, figure 15.

Damage initiated in the matrix between the lower surface fibres after an impact energy of 0.63 Joules, figure 14a. This damage appears to be a result of the flexural response of the beam, the lower surface flexural stresses exceeding the local strength of the composite. The resulting C-scan and X-radiograph failed to highlight this localised damage. After 0.81 Joules this lower surface matrix crack had extended up through the lowest lamina to form a plane of delamination at the lowest ply interface. Now, damage was clearly visible to the naked eye and also apparent in the corresponding C-scan and X-radiograph, figure 16a.

After 1.2 Joules damage was extensive. Here, a complex array of translaminar matrix cracks and delaminations extending well away from the point of impact, were recorded. This evidence suggested that two independent fracture mechanisms prevailed, the first due to the flexural action of the beam and the second due to the complex contact stress field. Damage resulting from the contact stress field involved a system of delaminations and matrix cracks. Here, the matrix cracks propagate away from the top surface point of contact as shown schematically in figure 17a. The lower surface flexure mechanism also comprises of a system of delaminations linked by an array of matrix cracks. However, these matrix cracks appear to extend upwards, away from the

point of initial failure as depicted in figure 17b

After an incident energy of 1.33 Joules, the deplied sections highlighted a region of fibre fracture in the lowest but one ply. As before, it seems that such damage resulted from the large tensile stresses generated by the flexural action of the beam.

Intuition suggests that such fibre fracture should initiate in the lower surface fibres, that is, those fibres furthest from the neutral axis of the composite. However, the low level of constraint on the lower surface fibres allows them to peel off during the impact process leaving the neighbouring fibres exposed and heavily stressed.

At larger incident energies fibre fracture and delamination were extensive in most plies, this is clearly seen in the deplied layers shown in figure 18. After 3.3 Joules the hemispherical nose of the impact carriage completely perforated the composite target removing much of the material from around the region of contact, figure 14d. Examination of the damage zone indicates that the perforation process has resulted in the removal of a frustrum shaped shear plug.

3.2.1.2 Eight ply (0,+/-45) Composite

Although this composite was similar in thickness to the eight ply +/-45 laminate the process of damage initiation

and propagation was quite different. Damage, in the form of lower surface fibre cracking was first detected after an incident energy of 1.0 Joules, figure 19a. Visual examination of the coupon indicated that this damage was just detectable, figure 20a. This damage appears to be a result of the excessive flexural stress field generated by the beam response. By 1.2 Joules this region of localised fibre fracture initiated a plane of delamination between the lower surface plies, figure 19b, this damage was detected in the C-scan and X-radiograph, figure 21a. At larger incident energies damage was extensive through the thickness of the target and was clearly visible on both the upper and lower surfaces of the target, figure 20b.

The micrograph taken after 2.75 Joules clearly shows the formative stages of the shear plug, figure 19d, which is completely ejected by 2.9 Joules again resulting in a characteristic conical shear zone.

3.2.1.3 Sixteen ply (0,+/-45) Composite

The fibre stacking configuration of this (0,+/-45) laminate yielded a laminate that was approximately twenty times stiffer than that of the eight ply (+/-45) target.

The initiation and development of low velocity impact damage in this composite is depicted in figures 22 to 24.

The optical micrographs indicated that damage in the form of

a matrix crack initiated between the top surface fibres after an incident energy of 1.6 Joules, figure 23a. This change in the location of first failure appears to be a consequence of the increased flexural stiffness of the target. Due to this increased stiffness a large impact force (energy) is required to initiate a lower surface flexural failure. Instead, top surface failure occurs at loads below this value as a result of the large contact stress field generated around the impactor. Closer examination of this initial failure revealed that the matrix crack had developed at or near the edge of the area of contact. In considering the contact problem between a flat plate and a sphere Greszczuk (66) showed that the the tensile stress system reaches its maximum at the top surface of the target local to the perimeter of the contact zone, that is, the region where damage was first detected in this two millimetre thick target. It appears therefore that this localised damage results from a tensile failure either in the matrix, or more likely, the fibre-matrix interface.

After 1.9 Joules two small fibre cracks were noted either side of the impact location, these are just visible in the photograph, figure 22a. These small cracks are perhaps a result of a combined compression-buckling failure precipitated by a destabilizing plane of delamination near the top surface of the composite.

The micrograph taken after 2.4 Joules shows the existence of a complex array of matrix cracks spreading away from the area of contact. However, these cracks do not appear to converge towards one particular point as noted previously, instead they are focussed towards a number of different locations near the point of initial contact. This phenomenon was explained by considering the contact process in more detail. When the projectile impinges upon the target a series of matrix cracks focussed towards the point of impact are generated. As the projectile continues to impinge upon the target the area of contact changes and a new system of cracks are generated. This whole process is shown in schematic form in figure 25.

Target perforation occurred after an energy of 6.6 Joules. The resulting micrograph, figure 23c, indicates that the shear zone is again frustrum-like in configuration.

3.2.1.4 Thirty-two ply (+/-45) composite

This four millimetre thick composite represents the thickest and stiffest laminate considered in this discussion.

Damage was first detected after an incident energy of 0.4 Joules, a matrix crack extending from the edge of the area of contact is clearly visible in the micrograph shown in figure 26a. As before, it appears that this localised damage was a result of the tensile component of the contact

stress field exceeding the local strength of the composite. With increasing incident energy, the characteristic pattern of delaminations and matrix cracks developed in the uppermost plies, figure 26b.

Target perforation occurred after an incident energy of 24 Joules. Here, damage was extensive spreading to regions near the structure supports. Interestingly, examination of the perforated region again revealed the presence of the characteristic conical fracture zone similar to that observed in the previous laminates.

3.2.2 Summary of Damage Studies.

From the preceeding observations it is becoming clear that the impact resistance of a laminated composite is determined by its fibre stacking sequence. The orientation of the fibres governs the flexural stiffness of the composite structure and therefore its ability to accommodate energy elastically. Using Engineer's theory of bending it can be shown that the strain energy capacity of an isotropic beam increases linearly with its flexural stiffness, doubling the flexural stiffness doubles the strain energy capability. Although the behaviour of these composite materials is more complex, it is likely that similar laws will govern their ability to absorb energy elastically.

The relative orientation of the plies in a laminated

composite will also govern the mode of failure. Fracture in the eight ply (+/-45) composite initiated at the fibre matrix interface between the lower surface fibres as a result of the large flexural strains. This suggests that the threshold energy for first damage could be enhanced by the surface treatment of the fibres. Indeed, limited experimental evidence supports this view (24). However, surface treating the fibres lowers the transverse fracture energy of the composite. This therefore promotes extensive fibre fracture at large energies and results in poor post-impact tensile properties.

Damage in the eight ply (0,+/-45) initiated in the lower surface fibres, again as a result of the flexural response of the target. When tested for its subsequent tensile strength, it was noted that this localised damage had precipitated a fifteen per cent loss in strength. This was considered alarming since no damage was visible at the top surface and it proved very difficult to detect using the non-destructive test methods.

Fracture in the stiffer sixteen and thirty-two ply composites initiated at the top surface of the target local to the point of impact. It was sugested that this damage has resulted from the contact generated tensile stress system. If this is so, it is likely that the impact resistance of a composite structure can be enhanced by covering it with a

ply of heavily surface treated fibres, thus giving the top surface of the target high strength in the transverse direction.

Initial fibre fracture in the stiff targets appears to have resulted from a top surface buckling instability. This damage appears to be a result of a contactor-induced plane of delamination forming between the uppermost plies during the early stages of the impact process. Such delamination would reduce the support on the top surface fibres thereby encouraging premature failure in a combined compression-buckling mode. Since this damage is easily detectable it does not present the problems posed by the corresponding eight ply composite.

At energies above the damage threshold the incident energy of the projectile is dissipated in forming areas of matrix and fibre fracture. Although the fracture energy for delamination is considerably below that of fibre fracture (700 J/M^2 compared to 37.5 KJ/M^2) its considerable extent highlighted it as being a major energy absorbing mechanism under impact conditions. The fracture energy for delamination is controlled by many parameters, including matrix properties and the level of fibre surface treatment. However, much more work needs to be done in order to fully appreciate the consequences of varying these properties on impact response.

Target perforation resulted in the generation of extensive damage spreading well away from the point of impact. Examination of the resulting fracture surfaces highlighted a characteristic frustrum-shaped fracture surface. Since this shear-out process involved considerable damage to the fibres it is likely that much of the incident energy of the projectile has been dissipated in this mechanism.

From these tests it appears that three damage thresholds might be of particular interest to the designer, namely, the threshold for first damage (where reductions in compressive strength will occur), fibre fracture where significant reductions in tensile strength will be incurred and target perforation (where the residual strength is least).

The following chapter details an approach which attempts to predict the incident energies for these three thresholds. The suitability and accuracy of these models is then assessed by comparing their predictions with the relavant experimental data.

3.3 Analysis of the Low Velocity Impact Response of a Composite beam

3.3.1 Background

The low velocity impact response of a homogeneous isotropic structure has in the past received considerable attention. Theoretical models of the impact problem have been numerous ranging from rigorous analytical approaches to strictly

empirical techniques. However, attempts to extend this knowledge to study the dynamic response of composite materials have been few. McQuillen et al (67) modelled the low velocity impact response of a graphite-epoxy beam using a Bernoulli-Euler beam analysis. The solutions of this analysis were expanded in the eigenfunctions of the free vibration problem using Galerkin's method. For impact velocities up to six metres per second the analytical model displayed good correlation with the experimental results. However, the analysis was simplified by considering only the flexure-induced stress field, top surface contact stresses were assumed small in comparison. Consequently, this technique is only suited for analysing the impact response of flexible targets impacted by large radius projectiles where, as assumed, the contact stresses are small.

Oplinger and Slepetz (38) considered the drop-weight impact response of a series of graphite-honeycomb sandwich panels. They approached the problem by modelling the distribution of the impact load and target displacement by a pair of double Fourier series expansions. It was found that agreement between the theoretical and experimental data was good only for target displacements less than half a millimetre. At larger displacements crushing of the honeycomb core encouraged debonding of the graphite face sheets resulting in a significant reduction in target flexural stiffness.

Caprino et al (68) modelled the impact problem by considering the response of a massless spring subjected to a time varying input force. Although simple, this technique was successful in predicting the impact force required to precipitate target flexural failure. However, their assumptions regarding an effectively massless target renders this solution suitable only for analysing the response of small coupons where this holds.

The approaches detailed above have, in the main, concentrated on the beam impact problem. Most have sought to neglect the top surface contact problem by assuming the impact problem to be that of a large radius sphere striking a relatively thin, flexible target. In practice, however, the impact situation is rarely as simple. For example, the thickness of the composite skins in the Harrier GR5 range between two and fifteen millimetres. Further, the offending impactor is not necessarily a large radius solid but more likely to be small in radius or even sharp. Under such impact conditions flexural failure is unlikely, instead, failure may occur local to the point of impact as a result of the top surface contact stress field.

The following sections consider the impact response of a number of carbon fibre structures when subjected to loading by a small radius steel projectile. By accounting for the dissipation of energy during the impact process, a number of

simple models are developed to predict the incident impact energies to precipitate first damage, fibre fracture and target perforation. The accuracy and suitability of these models is then assessed by comparing their predictions with the relevant experimental data.

3.3.2 Energy Dissipation During Low Velocity Impact Loading

Under localised impact conditions the incident energy of the projectile will be dissipated in a variety of mechanisms, principal amongst these being

1) elastic flexure
2) contact deformations
3) fracture mechanisms
4) stress wave propagation
5) vibrational effects
6) inertial effects

In the case of low velocity impact loading, energy is dissipated mainly in the first three mechanisms, the relative distribution depending upon paramters such as impactor geometry (12), target properties (39), target support conditions (9) and the impact velocity (9). In developing this analysis it is therefore assumed that the energy losses in stress wave propagation, vibrational and

inertial effects are sufficiently small to warrant neglection.

Previous tests on CFRP when tested in modes which are fibre dominated have shown that this material is relatively rate insensitive over many decades of strain rate loading (69). This suggests therefore, that elastic response of the impacted target can be modelled using simple quasi-static theory. This procedure was adopted here to predict the impact capability of a number of composite geometries. The following section considers the low velocity impact response of a simply suported composite beam. Initially, the flexural properties of the target beam are assessed experimentally and theoretically. Then, by accounting for the dissipation of energy in the impact process the incident energies for initial damage, fibre fracture and perforation are estimated.

3.3.3 Assessment of the Flexural Stiffness of a Composite Beam

Here, classical laminate theory (CLT) was used to model the flexural stiffness of the laminated composite beams. The principles behind CLT will be discussed in greater detail in section 3.3.5. However, it can be shown that the longitudinal flexural stiffness per unit length can be

written as

$$D_{11} = EI/\text{Unit length} \qquad (1)$$

where $$D_{11} = \frac{1}{3}\sum_{1}^{n}\left[z_k^3 - z_{k-1}^3\right]\bar{Q}_{ij} \qquad (2)$$

where $\bar{Q}ij$ is the transformed stiffness.

The term D_{11} , and therefore EI, can easily be determined knowing the elastic properties and stacking configuration of the target.

Now, for a simply supported beam subjected to central loading the beam deflection is related to the applied load by the relationship

$$P = \frac{48EI\delta}{L^3} \qquad (3)$$

By substituting the value for EI in equation 3 it should therefore be possible to predict the variation of target displacement with applied load. This was undertaken for a simply supported sixteen ply (0,+/-45) beam and the resulting curve is shown in figure 27. Included in this figure is the corresponding experimental curve determined by applying a line load to the composite beam and measuring the resulting variation of target displacement with applied

load. In these tests the impact load was applied through a six millimetre diameter hemisphere, therefore such a quasi-static bend test was also undertaken, the resulting curve also being shown in the figure. It is clear that CLT predicts the flexural stiffness of the target with some success (the level of accuracy only being as good as the input data). Therefore, this approach was to predict the flexural stiffness of all the laminates considered here.

3.3.4 Energy Balance for Predicting First Damage

Now, consider the response of a simply supported beam when subjected to central impact loading. Up to the point of initial fracture, the incident energy of the projectile is accommodated mainly in flexural and contact deformations. By equating the incident energy of the projectile to the energy absorbed in these elastic flexure and contact deformations it is possible to write an energy balance for the impact process. This is,

$$\frac{mv^2}{2} = \int_0^{\delta_1} P d\delta + \int_0^{\alpha_1} P d\alpha \qquad (4)$$

The first integral in the above equation accounts for energy dissipation in elastic flexure and the second integral for energy dissipation in top surface contact deformations.

The Hertzian contact analysis states that the

force-deformation relationship for contact between a sphere and an isotropic target is given as

$$P = n\alpha^{3/2} \tag{5}$$

where P is the applied load, α the contact deformation and

$$n = \left[\frac{4}{3\pi\left[K_t + K_p\right]}\right]\sqrt{R_p} \tag{6}$$

By combining equations 4, 5 and 6 and evaluating the integrals, the energy balance can be rewritten as

$$\frac{mv^2}{2} = P^2\left[\frac{L^3}{96EI}\right] + P^{5/3}\left[\frac{2}{5n^{2/3}}\right] \tag{7}$$

The term $(K_t + K_p)$ in equation 6 characterizes the elastic properties of the impactor and target. In this programme this term was determined experimentally by conducting a series quasi-static indentation tests. Details of the indentation rig are shown in figure 28. Here, a composite coupon was placed on a flat steel block and loaded normally by a six millimetre diameter hemispherical head. During the test, the variation of contact deformation with applied load was recorded and plotted. A typical curve for the two millimetre, sixteen ply (0,+/-45) composite is shown in figure 29. The value of the material constant $(K_t + K_p)$ was

then determined by plotting the applied load, P, against the deformation parameter, $\alpha^{3/2}$, and equating the resulting gradient of the curve to the right hand side of equation 5 . This approach yielded a value for the term $(K_t + K_p)$ of 1.1E-10 M^2/N .The dependence of this parameter on fibre stacking sequence was found to be small and therefore this value was used in all subsequent impact analyses.

Now, by using the energy balance outlined in equation 7, it is possible to estimate the variation of impact force with projectile incident energy. This approach was applied to predict the impact force variation in the (+/-45) composites. The results of this analysis are shown in figure 30. It is clear that the impact load for a given impact velocity is strongly dependent on the flexibilty of the target, the dynamic force decreasing with increasing target flexibility. The accuracy of this approach was assessed by comparing its predictions with data yielded from a series of impact tests on sixteen ply (0,+/-45) composite beams with dimensions 50mm x 25mm. In each case, the maximum impact force was determined from the readings yielded by the instrumented load cell. The results of these tests are shown in figure 31. Although the impact model over-estimates the experimental data agreement is satisfactory.

By determining the stress field generated by these impact loads it should be possible to predict failure in a

composite beam. In this analysis account is made for the flexural stress field and also for the contact stress field.

3.3.5 Determination of the Flexural Stress Field

In this study the flexural stress field was assessed using classical laminate theory. This states that the moment resultants [N] and [M] acting on a composite are related to the middle surface strains and curvatures ε and κ as follows

$$\begin{aligned} [N] &= [A][\varepsilon] + [B][\kappa] \\ [M] &= [B][\varepsilon] + [D][\kappa] \end{aligned} \qquad (8)$$

where

$$A_{ij} = \sum_{1}^{n}\left[Z_k - Z_{k-1}\right]\overline{Q}_{ij}$$

$$B_{ij} = \frac{1}{2}\sum_{1}^{N}\left[Z_k^2 - Z_{k-1}^2\right]\overline{Q}_{ij}$$

$$Dij = \frac{1}{3}\sum_{1}^{N}\left[Z_k^3 - Z_{k-1}^3\right]\overline{Q}_{ij}$$

The 'A_{ij}' terms in equation 8 are extensional stiffnesses, the 'B_{ij}' terms coupling stiffnesses and the 'D_{ij}' terms bending stiffnesses. The presence of non-zero 'B_{ij}' terms in equation 8 terms implies coupling between laminate bending

and mid-plane extension. Under such circumstances an applied extensional load results in not only extensional deformations but also twisting curvatures. Conversely, an applied bending moment induces both twisting and extensional deformations. In this study, all laminates were balanced and symmetric in nature. Consequently, the 'B_{ij}' terms in equation 8 are all zero and no extension-twisting coupling will result. By an involved process of matrix inversion, equation 8 can be solved to yield the membrane strains and laminate curvatures in terms of the applied loads.

For speed and accuracy, a computer programme was written to determine the 'A', 'B' and 'D' matrices for any arbitrary laminate given the basic material properties E11, E22, V12 and G12. The listing of this computer programme is given in appendix 3. Material properties for the XAS-914C system considered here were taken from references 70 and 71 and are given in table 2.

For the particular case of impact on a composite beam, it was assumed that all the load and moment resultants were zero except Mx.

Using simple beam theory it can be shown that the bendir moment at the centre of the beam is

$$M = \frac{P\,L}{4} \qquad (9)$$

The bending moment per unit length was then determined b dividing this value by the target width.

In this analysis flexural failure was assumed when the lowe surface strains attained the relevant failure strain of th material.

3.3.6 Determination of the Contact Stress FIeld

The contact stress field was analysed by combining a Hertzia contact analysis with a procedure developed by Love (72) fo predicting the sub-surface stress field in a semi-infinit isotropic target subjected to a varying surface pressure.

The distribution of the surface pressure over the area o contact could be written in the form (66)

$$q_{x,y} = q_o \left[1 - \frac{x^2}{a^2} - \frac{y^2}{a^2} \right] \qquad (10)$$

By summing the surface pressures and equating them to the applied load the maximum surface pressure can be written as

$$q_o = \frac{3P}{2\pi a^2} \qquad (11)$$

Given a varying surface pressure of the type detailed in equation 11, Love (72) developed an analysis for predicting the resulting sub-surface stress system in a semi-infinite isotropic target. Here, it was shown that the stress

distribution takes the form

$$\sigma_r = \frac{3P}{2\pi a^2}\left[\frac{1-2\sigma}{3}\frac{a^2}{\rho^2}\left\{1-\left(\frac{z}{\sqrt{\lambda_1}}\right)^3\right\}+(1+\sigma)\frac{z}{a}\tan^{-1}\frac{a}{\sqrt{\lambda_1}}\right.$$
$$\left.+(1-\sigma)\frac{z\sqrt{\lambda_1}}{a^2+\lambda_1}-2\frac{z}{\sqrt{\lambda_1}}+\frac{a^2z^3}{(\lambda_1^2+a^2z^2)\sqrt{\lambda_1}}\right],$$

$$\sigma_\theta = \frac{3P}{2\pi a^2}\left[-\frac{1-2\sigma}{3}\frac{a^2}{\rho^2}\left\{1-\left(\frac{z}{\sqrt{\lambda_1}}\right)^3\right\}+(1+\sigma)\frac{z}{a}\tan^{-1}\frac{a}{\sqrt{\lambda_1}}\right. \qquad (12)$$
$$\left.-(1-\sigma)\frac{z\sqrt{\lambda_1}}{a^2+\lambda_1}-2\sigma\frac{z}{\sqrt{\lambda_1}}\right],$$

$$\sigma_z = -\frac{3P}{2\pi}\frac{z^3}{(\lambda_1^2+a^2z^2)\sqrt{\lambda_1}}, \quad \tau_{rz} = -\frac{3P}{2\pi}\frac{\rho z^2\sqrt{\lambda_1}}{(\lambda_1^2+a^2z^2)(a^2+\lambda_1)}.$$

where λ_1 is the positive root of the equation

$$\frac{\rho^2}{a^2+\lambda}+\frac{z^2}{\lambda}=1. \qquad (13)$$

Since the solution procedure for the above equations is lon and tedious a computer programme was written to save time an reduce the likelihood of errors. Typical stress contours fo an impact velocity of 6 m/s are shown in figures 32 and 33 For clarity, the stress contours in these figures have bee normalised with respect to the maximum surface pressure q_0. I is evident that the maximum compressive stresses occur, a expected, directly under the point of impact. However, a small distances away from the impact location thes compressive stresses decay rapidly and, although not marked

they become tensile in regions near the edge of the area c contact.

From these equations it is possible to determine the magnitud and location of the maximum tensile and compressive stresse developed in the target. These are

$$\sigma_t = \left[\frac{1 - 2\nu}{3}\right] q_o \qquad (14)$$

$$\sigma_c = q_o$$

where $$q_o = \frac{3P}{2\pi a^2}$$

The locations of these maximum stresses are shown i figure 34. Interestingly, the maximum tensile stress occurs a the perimeter of the region of contact, that is, the regio where damage was first detected in the stiffer sixteen pl (0,+/-45) and the thirty-two ply (+/-45) laminates. Thi suggests therefore, that top surface damage of the typ observed here is a consequence of the tensile contact stresse exceeding the transverse tensile strength of the material.

By determining the minimum impact force to precipitate eithe a top surface or a flexural failure and substituting thi value in the energy balance, equation 7, it is possible t estimate the incident impact energy to cause target failure.

3.3.7 Comparison of Predicted Damage Thresholds with Experimental Data

The accuracy of the impact model was examined by comparing its predictions with corresponding experimental data. Table 3 presents a comparison between the predicted and experimental damage thresholds for a number of composite beams. Also, for clarity, much of this information is presented in graphical form in figures 35 and 36. Included in the table are the experimentally determined energies for first damage and the corresponding location. First, consider the (+/-45) composites shown in figure 35. For target thicknesses up to and including two millimetres, the incident energy for first damage increases in an approximate linear fashion with increasing target thickness. In this region failure initiated in the matrix between the lower surface fibres as a result of the flexural response of the beam. Here, agreement between the theoretical and experimental values is very good. At larger thicknesses failure initiates between the top surface fibres as a result of the local contact stress field. In this region, the critical incident energy for initial damage first decreases rapidly and then asymptotes towards the value for a semi-infinite target. Although the experimental points in this range confirm this trend, there appears to quite a sizeable discrepancy between experiment and prediction. This departure may in part be due to the neglect of transverse shear effects in the impact model.

The corresponding damage thresholds for the (0,+/-45) composites, figure 36, display similar trends in the first damage threshold with target thickness. The impact model suggests that first damage in the eight ply target will be a top surface compressive failure of the fibres. Experimentally it was found that fibre fracture first initiated in the lowest ply. It seems likely that this lower surface failure was induced by the combination of membrane stretching around the projectile and the flexural response of the beam.

3.3.8 Prediction of Fibre Fracture Threshold

The incident impact energy to initiate fibre fracture was estimated using the approach outlined above for predicting first damage. Here, fibre failure was assumed when the strain field exceeded the fibre failure strain. The predictions yielded by this approach are given in table 4. It is immediately clear that agreement is very poor with the impact model tending to over-estimate the experimental data. These discrepancies are probably a result of the loss in target flexural stiffness during the impact process. During impact, it is likely that matrix cracking and delamination preceed any form of fibre damage. If this is so, the flexural stiffness of the target may be reduced substantially precipitating fibre failure at a lower impact

load (energy) than anticipated. To illustrate this point, quasi-static flexure tests were conducted on a number of damaged composites. Figures 37 and 38 show the resulting variation of flexural stiffness with incident energy. Examination of the figures highlights two trends. Firstly, no reduction in flexural stiffness occurs when matrix damage is localised to the rear surface of the target, that is, in the region where the flexural stresses are tensile. First reductions in flexural strength coincide with the onset of top surface damage, here the flexural stresses are compressive. These figures suggest that the flexural stiffness of the target at the onset of fibre fracture may be considerably below its undamaged value. For example, consider the sixteen ply (0,+/-45) composite. Figure 38 suggests that the loss in flexural stiffness at the onset of fibre fracture is approximately fifteen per cent. If this value is used in the impact model a prediction for first damage of 1.8 Joules is yielded, this compares more favourably with the experimental value of 1.7 Joules.

3.3.9 Prediction of Perforation Threshold

This section details a procedure for estimating the drop-weight perforation energy of a composite beam. Here, account is made for energy dissipation in target flexure, contact deformations, delamination and shear-out. The procedures for estimating energy dissipation in contact and flexural deformations are outlined in section 3.3.4. The

following sections assess the dissipation of impact energy in shear-out and delamination.

3.3.9.1 Estimation of Energy Dissipated in Shear-Out

The micrographic studies discussed earlier in this chapter indicated that perforation resulted in the formation of a frustrum-shaped shear zone. The energy required to create a shear zone of this geometry was estimated by determining the product of the area of fracture and the transverse fracture energy of the composite. The first of these, the area of fracture, was determined using geometrical principles. It can be shown that the surface area of fracture for this fracture zone is

$$A_s = \sqrt{2}\pi t\left[t + 2r\right]$$

where 'r' is the radius of the projectile and 't' the laminate thickness.

The transverse fracture energy of a composite can be determined in a variety of ways. A popular technique is the notched beam test shown in figure 39a (34). Here a 'V'-notched beam is subjected to a central transverse load as shown. During loading, the variation of beam displacement with applied load is recorded. By integrating the area under the resulting load-displacement curve the energy expended during crack propagation can be determined. Although useful for determining the fracture energy of most metals, this

technique is not ideally suited to analysing composites since the propagating crack path is frequently deflected precipitating undesirable modes of fracture. In this work, the transverse fracture energy of the composite was determined using the test rig shown in figure 39b. Here a thin test coupon was clamped between two rectangular supports and positioned in a Tensometer testing machine. Transverse failure at the clamped end was ensured by advancing a square crosshead along the face of the supports as shown. During the test, the variation of crosshead displacement with applied load was recorded and plotted. Typical load-displacement curves for the four ply (0°) and four ply ($+/-45^{\circ}$) composites are shown in figure 40. From these curves fracture energies of 38.9 and 38.0 KJ/M^2 were determined for the unidirectional and (+/-45) composites respectively. The fact that these two fracture energies are similar in magnitude is not surprising since the surface area of fibres fractured is effectively the same in both cases. In subsequent analyses an averaged value of 38.45 KJ/M^2 was used to represent the transverse fracture energy of the composites.

3.3.9.2 Estimation of Energy Dissipated in Delamination

The energy expended in generating delamination was estimated by determining the product of the area of interlaminar fracture as observed in the deplies and the fracture energy for delamination. The latter has been determined for the

XAS-914C system by Austin and Walters (10). Here dynamic burst tests on a series of circular plates yielded a fracture energy of delamination of approximately 700 J/M^2.

3.3.10 Comparison of Predicted Perforation Thresholds with Experimental Data

By summing the above predictions with those for elastic flexure and contact effects it is possible to estimate the energy required to perforate a composite beam. This was undertaken for the laminates considered in this programme and the results of this analysis are given in table 5 and in figure 41.

It appears that the simple model predicts perforation with some success. The graphical presentation clearly shows the non-linear trend of perforation energy with target thickness.

In order to gain an understanding of how energy is dissipated during the impact process an energy map was developed and is shown in figure 42. The map indicates that shear-out is a dominant energy absorbing mechanism for all thicknesses. It is interesting to note that the flexural response is less important in the thicker composites, here energy dissipation in delamination becomes dominant.

The variation of delaminated area with target thickness is shown by the points in figure 43. The model as it stands is

incapable of predicting this variation of delaminated area with impact energy, instead this information is obtained from a series of experimental tests. Developing an analysis to predict the extent of delamination at the perforation threshold would be enormously difficult probably impossible. However, examination of the micrographs indicated that, at perforation, damage was more extensive towards the rear surface of the target. If the region of delamination is assumed to resemble that shown schematically in figure 44 it should be possible to estimate the trend in delaminated area with target thickness. This was undertaken for the (+/-45) composites and the resulting curve is included in figure 43. Here, the value of the length 'L' in figure 44 was determined by curve fitting the model to the point corresponding to the thirty-two ply composite. Although this is simply a curve fitting procedure the simple model does anticipate the trends in experimental data with reasonable success.

The applicability of the impact model was further examined by manufacturing and testing an eight millimetre thick, sixty-four ply (+/-45) composite. The result of this test along with data for the other (+/-45) composites are shown in figure 45. At first glance agreement appears good. However, when the laminate was sectioned and examined it was observed that the shear zone did not conform to that assumed

in the impact model. Instead of being frustrum-shaped, the shear zone was more cylindrical in configuration, see figure 46. This suggests therefore, that the level of agreement apparent in figure 45 is purely fortuitous.

3.4 The Effect of Target Geometry on Low Velocity Impact Response

3.4.1 Background

From the preceeding observations it is becoming clear that the low velocity impact response of a composite target is strongly dependent upon its ability to absorb energy elastically. This ability to accommodate energy elastically is dependent upon many parameters, prominent amongst these being the target geometry. To date, little work has been undertaken to examine in depth the influence of target geometry on impact response. It is unclear if small scale laboratory tests provide a valuable insight into the impact behaviour of larger structures or whether they yield just a grossly pessimistic overview of the problem.

The following chapter sets out to examine the influence of target geometry on impact response. Initially, to gain an understanding of the problem, attention is given to examining the size effect in simple composite beams. Supported by this evidence, the the impact response of a large circular plate is examined, this being considered more representative of bays or panels of a large structure and

still maintaining geometrical simplicity for analytical treatment.

3.4.2 The Size Effect in Composite Beams

The effect of varying beam geometry on impact response is clearly demonstrated in the C-scans shown in figure 47. Here, the C-scans of a series of sixteen ply (0,+/-45) composites are shown after incident energies of 4.2 and 6.0 Joules. It is evident that the level of impact damage decreases with increasing beam length. Consider the 50mm and 150mm beams. In the former, damage is extensive, at this energy the impactor almost perforated the target. In the longer 150mm beam however, damage is barely discernable indicating that this represents the damage threshold energy. Clearly, the longer beam was able to accommodate almost all of the incident energy of the impactor in elastic deformations, whereas the shorter beam, with a lower strain energy capability, absorbed much of the incident energy in extensive matrix and fibre fracture.

Having observed such a variation in impact resistance with target geometry, the impact models developed earlier were implemented in order to determine if these geometrical effects could be predicted.

3.4.2.1 The Variation of the Damage Threshold Energy with Beam Length

Consider first the flexural response of an isotropic beam.

Using Engineer's Theory of Bending it can be shown that the energy absorbing capability of an isotropic beam increases linearly with increasing beam length, therefore, doubling the length of the beam doubles the elastic energy which may be accommodated. Although the response of composite materials is not so simple, similar trends will almost certainly apply.

It has already been stated that energy dissipation in composites when subjected to low velocity impact loading can occur through a variety of elastic and fracture processes. By accounting for this energy expenditure as outlined in section 3.3.4 the variation of the incident energy for first damage with beam length was estimated. The resulting predictions are compared with the experimental evidence in figure 48. At first, it appears that the impact model predicts the experimental trends with some success. However, this is misleading. The impact model anticipates a change in failure mode from top surface contact fracture in the short beams to lower surface fibre flexural failure in the longer beams. However, examination of the micrographs indicated that the longer beams did not fail in the predicted fashion. Instead, fracture initiated between the fibres at the lower surfaces of the beams, probably as a result of the transverse curvatures generated around the impactor. Again such agreement is purely fortuitous.

3.4.2.2 The Variation of the fibre fracture Threshold with Beam Length.

The variation of fibre fracture threshold with beam geometry for the sixteen ply (0,+/-45) laminate is shown in figure 49. Here, as before, the length of the beam is significant in determining the incident energy for this form of fracture. It is clear that the fibre fracture threshold increases with beam length.

3.4.2.3 The Variation of Perforation Energy with Beam Length

Examination of the C-scans at perforation indicated that the planar area of damage at perforation varied little with beam geometry suggesting that the energy expended in generating delamination was invariant of beam length. Also, the size and geometry of the resulting shear zone did not appear to vary significantly in the beams again indicating that the energy expended in shear-out was not a function of beam length.

The variation of the perforation energy with beam length was estimated using the procedure outlined in section 3.3.9. Here, as before, energy dissipation in contact deformations, beam flexure, delamination and shear-out is considered. The ensuing predictions for perforation in the sixteen ply

(0,+/-45) laminate are shown in figure 50.

It appears that the perforation model predicts perforation with some success, agreement being good for all beam lengths.

These tests clearly demonstrate the influence of target geometry in determining impact response. The longer beams, that is, those with a greater ability to accommodate energy elastically, incur less damage and will therefore possess superior post-impact residual properties. However, such geometries are not typical of those encountered in operational service and do not necessarily characterize the impact response of their larger counterparts. In an attempt to close this gap, the following section examines the low velocity impact response of 'more realistic' circular composite.

3.4.3 The Low Velocity Impact Response of a Circular Composite Plate.

3.4.3.1 Analysis

Consider the response of a large circular plate subjected to a transverse central load. For small deflections, the plate will respond in a flexural mode with the applied load being resisted by the flexural stress field. When the deflection of the plate greatly exceeds its thickness, a membrane

action is induced which results in mid-plane stretching of the plate. Elber (73) states that for a given plate deflection the total plate load can be expressed in terms of the flexural reaction P_p and membrane reaction P_m as

$$P = P_m + P_p \qquad (15)$$

For an isotropic plate, radius 'a' the flexural load is given as

$$P_p = \frac{4\pi E t^3 \delta}{3a^2(1-\nu^2)} \qquad (16)$$

and the membrane plate load as

$$P_m = \frac{AEt\delta^3}{a^2} \qquad (17)$$

The term 'A' in equation 17 is the membrane tension coefficient, included to describe the plate loading conditions. For a point load, 'A' approaches zero whereas for a fully distributed load 'A' approaches 2. The complete variation of A with r/a (r = radius of applied load and a = radius of plate) is given in figure 51.

At present, no analysis exists for determining the flexural stiffness of an anisotropic laminate, therefore this term was determined experimentally. Here, the composite plate was clamped between two 65mm internal radius rings and loaded transversely at its centre by a three millimetre radius

hemispherical head. During the test, the variation of plate displacement with applied load was determined and plotted. Using a curve fitting procedure, equations 15 and 16 was fitted to the experimental data thereby yielding a value for the effective plate modulus, E.

The energy expended in deforming the plate is given as

$$En = \int P d\delta \qquad (18)$$

In order to determine the energy stored in the plate at failure it is necessary to determine the critical load. Here, as before, the contact stress field was modelled using the Love analysis outlined in section 3.3.6. The flexural stress field was analysed using anisotropic plate theory. For a circular anisotropic plate subjected to loading at its centre the bending moments per unit length are

$$M_x = \frac{P}{4\pi D'}\left[D_x + D_1\right]\left[Ln(a/r) + \frac{r^2}{4a^2}\right] \qquad (19)$$

$$M_y = \frac{P}{4\pi D'}\left[D_y + D_1\right]\left[Ln(a/r) + \frac{r^2}{4a^2}\right]$$

where 'a' is the radius of the applied load, taken as the radius of area of contact here

and $$D' = \frac{1}{3}\left[3D_x + 3D_y + 4D_{xy} + D_1\right] \qquad (20)$$

$$D_1 = \frac{\nu_{21}E_{11}t^3}{12(1-\nu_{12}\nu_{21})}$$

The terms Dx, Dy and Dxy are the bending stiffness terms and were determined using the laminate analysis programme shown in appendix 3.

The resulting stress and strain field was examined using classical laminate theory. Here, reiterating equation 8, the force and moment resultants are related to the laminate strains and curvatures by the expressions

$$\begin{bmatrix} N \end{bmatrix} = \begin{bmatrix} A \end{bmatrix}\begin{bmatrix} \varepsilon \end{bmatrix} + \begin{bmatrix} B \end{bmatrix}\begin{bmatrix} \kappa \end{bmatrix} \qquad (21)$$

$$\begin{bmatrix} M \end{bmatrix} = \begin{bmatrix} B \end{bmatrix}\begin{bmatrix} \varepsilon \end{bmatrix} + \begin{bmatrix} D \end{bmatrix}\begin{bmatrix} \kappa \end{bmatrix}$$

Therefore, knowing the applied load, P, it is possible to determine the distribution of strains throughout the laminated plate. Conversely, by a reversed process, using the composite failure strains it is possible to calculate the critical load to initiate fracture.

3.4.3.2 Prediction of First Damage in Circular Composite Plates

This procedure was undertaken to predict the critical loads, and therefore the critical energies, to precipitate failure

under impact conditions. The results of this analysis are presented in table 6 and figure 52. Included in this table are the experimentally determined damage thresholds. Here, tests were conducted on a number of composite plates clamped between two 65mm internal diameter rings. For continuity, the impact head was a three millimetre radius hemisphere.
Examination of the data suggests that the analysis predicts the energies for first damage with some success. The model does not, however, predict with any accuracy failure in the sixteen ply (0,+/-45) composite. The reasons for this are not clear, the model did however predict the correct mode of failure, a lower surface interfacial fracture.

3.4.3.3 Prediction of Perforation in Circular Composite Plates

Perforation of these circular plates was predicted using the procedure outlined in section 3.3.9. In this instance, the energy absorbed by the target in elastic flexure was estimated using the procedure presented above.
Table 7 and figure 53 present the findings of this analysis and compare its predictions with the relevant experimental data. Once again agreement is acceptable. Interestingly, the model tends to over-estimate the perforation threshold in the thin, flexible targets whereas it over-estimates perforation in the thicker laminates

3.5 Summary of Low Velocity Impact Studies

From these experimental and theoretical studies it is becoming clear that the low velocity impact behaviour of fibrous composites is inherently complex. However, by considering the process of energy absorption in these materials it has been possible to predict the impact capability of a laminated composite with some success.

In this programme the impact threat was simplified as being a small radius hemisphere. Under these impact conditions it was found that the impact resistance of a composite target was strongly dependent upon its flexural stiffness. In thin, flexible targets damage initiated at the lower surface of the target (usually at the fibre-matrix interface) as a result of the flexural response of the beam. At larger impact loads this lower surface fracture precipitated the growth of further damage within the composite. Since such damage is frequently difficult to detect and may in some cases lead to premature failure it is desirable to inhibit its initiation. This may be possible by covering the lower surface of the target with a layer of heavily surface treated fibres, that is, a ply with a high transverse tensile strength.

Fracture in the stiffer targets developed between the fibres in the uppermost ply. It was found that this damage developed at the edge of the area of contact and was probably a result of the tensile component of the contact stress field exceeding the local fibre-matrix strength.

Again, at larger incident energies this initial fracture precipitated further damage. It may be possible to improve the impact resistance of such stiff targets in several ways. Firstly, since this damage appears to initiate at the fibre-matrix interface it may be advantageous to apply a top surface covering of more heavily surface treated fibres. Secondly, the contact analysis discussed in section 3.3.6 indicated that the top surface stress field is dependent upon the material parameter ($K_t + K_p$). It can be shown that by increasing the value of this term, that is, reducing the transverse stiffness of the composite, the magnitude of the top surface tensile stress field for a given applied load (energy) is diminished.

At energies above the damage threshold energy is expended chiefly in forming planes of fracture. On a macroscopic scale several fracture mechanisms are incurred most prominant being delamination and fibre fracture. The former, delamination, although possessing a fracture energy considerably below that of fibre fracture (700 J/M^2 compared to 37.5KJ/M^2) accounts for considerable energy dissipation, particularly in thick composites. Through careful selection of a matrix system (that is fracture energy) it may be possible to design the composite structure for optimum impact resistance.

The consequence of extensive delamination in a loaded

structure is mixed. Under tensile loading delamination has been observed to have little effect on residual strength, indeed, it may even improve it. Under compressive loads however, the problem is more serious. Firstly, delamination renders the composite unsymmetrical in nature resulting in coupling between extensional loads and twisting curvatures. Secondly, delamination reduces the level of support on the main load bearing fibres and may result in a catastrophic failure in buckling. Thirdly, the presence of extensive through-thickness damage permits the ingress of moisture in humid conditions, this process may further degrade the matrix and therefore the composite.

Fibre fracture with its large fracture energy is also a major energy absorbing mechanism. Energies that are dissipated in large areas of delamination may be accommodated in small, localised regions of fibre damage. The effect of such damage on residual properties is equally mixed. Under tensile loading conditions fibre fracture generates large stress concentrations which can sometimes result in substantial reductions in residual strength. In compression, however, the effects of isolated fibre damage may not be as severe (49).

The influence of target geometry on low velocity impact response has been assessed using a variety of target geometries. Under large mass, low velocity impact conditions

where the target responds in its primary mode the geometry of the structure determines its ability to accommodate energy elastically and therfore its impact resistance. This was most marked in the beam coupons. Here, doubling the length of the beam increased its damage threshold energy by up to 230 per cent. However, increasing the target size does not always enhance its impact capability. Consider for example the 150mm long sixteen ply (0,+/-45) beam coupon and the sixteen ply (0,+/-45) 65mm radius plate. Damage in the former initiated between the lower surface fibres after an incident energy of 5.5 Joules, whereas damage in the latter (again between the lower surface fibres) initiated after a much lower energy of 0.7 Joules. This suggests that the practice of evaluating the impact resistance of a large operational structures based on small-scale laboratory tests is incorrect. Small-scale coupon tests do not predict the impact capability of their larger counterparts, nor do they always predict the correct mode of failure, they even fail to rank the composites in terms of increasing impact resistance.

CHAPTER 4. RESIDUAL STRENGTH ASSESSMENT OF IMPACT DAMAGED COMPOSITES

		Page
4.1	Background	88
4.2	Experimental observations	90
4.2.1	Eight ply (+/-45) composite	91
4.2.2	Eight ply (0,+/-45) composite	92
4.2.3	Sixteen ply (0,+/-45) composite	93
4.2.4	Thirty-two ply (+/-45) composite	93
4.2.5	Summary of experimental observations	94
4.3	Prediction of post-impact tensile strength	95
4.3.1	Assessment of composite fracture models	95
4.3.2	Experimental verification of fracture models	99
4.3.3	Comparison of fracture model predictions with experimental data	101
4.4	Summary of residual strength studies	103

CHAPTER 4.

RESIDUAL STRENGTH ASSESSMENT OF IMPACT DAMAGED COMPOSITES

The damage studies presented in chapter 3 clearly showed that low velocity impact loading generates areas of matrix cracking, delamination and fibre fracture, which, at large incident energies frequently extend well away from the point of impact. This chapter considers the effect of such damage on the subsequent load carrying capability of these composites. Attention, in particular, is given to assessing the capability of these damaged composites when subjected to uniaxial tensile loading. On the basis of these findings, attempts are then made to estimate the residual tensile strength of the damaged composites by suitable implementation of a fracture model.

4.1 Background

The present understanding of the factors that affect and control the strength of composite materials containing defects and damage is barely adequate for confident materials selection and structural design. In contrast to metals where failure processes are modelled by self-similar growth of a single (micro) crack and locally high stresses are relieved by the formation of a plastic zone, failure in composites usually occurs as a combination of damage modes and local relief of high stresses can involve processes of matrix cracking, delamination and fibre failure.

Using a variety of damage detection techniques several

workers have observed the growth of damage zones local to regions of high stress concentration. From a strength viewpoint the presence of such localised regions of fracture can be advantageous since they serve to dissipate strain energy and also to redistribute the stress field around the notch or discontinuity. Indeed, it is now generally accepted that composites which encourage the growth of these damage zones offer high fracture toughnesses and good damage tolerance.

The residual tensile strength of a notched or damaged composite is dependent upon many parameters, prominant amongst these being the fibre and matrix properties, fibre surface treatment, notch geometry and laminate stacking configuration. The latter has been investigated in some depth by Lee and Phillips (43). Here it was found that unidirectional composites with their fibres orientated in the zero degree direction and angle ply (+/-45) composites display a notch-insensitive mode of failure where the net section stress at failure attains the overall undamaged strength of the composite. In contrast, most multi-angle composites exhibit notch sensitive fracture behaviour. Here, the composite fails 'prematurely' with the net section stress at failure being below the undamaged strength of the composite. Bishop (48) found that notch sensitivity in carbon fibre composites can be controlled by careful

selection of the fibre stacking sequence. Grouping the zero degree plies together in a (0,+/-45) composite precipitates large shear stresses at the ply interfaces which, at sufficiently high loads, leads to delamination and therefore stress concentration reductions.

4.2 Experimental Observations

The following section details the findings of an experimental programme conducted to examine the effect of impact damage on the residual tensile strength of a number of (+/-45) and (0,+/-45) carbon fibre laminates.

For purposes of continuity, the discussion considers those laminates considered in the previous damage studies programme, their lay-ups being

eight ply (+/-45)
eight ply (0,+/-45)
sixteen ply (0,+/-45)
thirty-two ply (+/-45)

As before, the 150mm x 25mm target geometries were supported on two 12.7mm diameter simple supports positioned 50mm apart and impacted by a 0.75 kg mass with a 6mm diameter hemispherical nose. Uniaxial tensile tests were then conducted on an Instron Universal testing machine with a

crosshead speed of 2mm per minute.

Figures 54 to 57 detail the variation of residual tensile strength with impact energy for the four laminates considered here. Marked on each figure are the observed thresholds for first damage (1), fibre fracture (2) and perforation (3). It is evident that the post-impact capability of these composites is dependent upon the fibre lay-up of the laminate. As a result, the characteristics of these residual strength curves will now be discussed seperately.

4.2.1 Eight ply (+/-45) composite

Damage, in the form of a lower surface matrix crack, was first detected after an impact energy of 0.6 Joules. Examination of the residual strength curve, figure 54, suggests that this localised damage had little or no effect on the residual strength of the laminate. Indeed, appreciable reductions in strength were not observed until 1.2 Joules, this value coinciding with the threshold for fibre fracture. At intermediate impact energies considerable fibre fracture and delamination were incurred in these coupons resulting in significant reductions in tensile strength. The residual strength curve reaches a minimum at the perforation threshold where damage was found to be most severe. At energies above this threshold no further reductions in

tensile strength were incurred, indeed, slight increases are apparent.

4.2.2 Eight ply (0,+/-45) composite

The post-impact characteristics of this one millimetre thick composite are shown in figure 55. Here, unlike the other composites, damage was first incurred by the fibres. The curve indicates that this seemingly innocuous damage precipitated a twenty per cent reduction in tensile strength. This raises serious concerns because this damage was not detected during non-destructive inspection and might therefore pass undetected during a routine in-service inspection programme.

Target perforation occurred after an incident energy of 2.9 Joules and again precipitated the most substantial loss in tensile strength. This fifty five per cent reduction in strength was greater than that incurred by the corresponding (+/-45) composite, reflecting perhaps the greater notch sensitivity of this laminate.

At energies above the perforation threshold a distinct increase in tensile strength is apparent, by 5.0 Joules the residual strength is almost twenty five per cent greater than at perforation.

4.2.3 Sixteen ply (0,+/-45) composite

Damage in this sixteen ply target was first observed after an incident energy of 1.6 Joules. However, this localised region of top surface matrix cracking does not appear to have influenced the tensile strength of the composite, figure 56. Once again, substantial reductions in residual strength were not recorded until the onset of fibre fracture.

The minimum in residual strength occurred at an energy near the perforation threshold. Examination of the C-scans and micrographs again indicated that the damage was considerable at this threshold.

4.2.4 Thirty-two ply (+/-45) composite

The post-impact properties of this four millimetre thick (+/-45) composite are shown in figure 57. As before, at low incident energies where damage is limited to the matrix the residual tensile strength remains unaffected by the impact. However, in contrast to previous observations, no reduction in tensile strength was incurred at the onset of fibre fracture, indeed significant reductions in residual strength reductions were not recorded until 14 Joules.

Once more, the most severe reductions in tensile strength

coincide with the threshold energy for target perforation. Here, the composite has lost approximately eighty per cent of its undamaged tensile strength. This poor post-impact capability is not necessarily an indictment of the fibre stacking sequence but more likely a geometrical effect associated with the low width-thickness ratio of the target coupon.

4.2.5 Summary of Experimental Observations

From this experimental evidence it is clear that carbon fibre composites are extremely sensitive to even low levels of impact damage. In most cases, first reductions in residual strength coincided with the threshold energy for fibre fracture suggesting that this form of damage is perhaps the single most detrimental mechanism to the integrity of a laminated composite when tested in tension. The stress concentrating effect of fibre fracture can be reduced, and sometimes removed, by the presence of local planes of delamination. This was clearly demonstrated in the thirty-two ply composite where the effect of localised top surface fibre fracture was completely removed by the presence of extensive delamination.

It was noted that fibre fracture was always more extensive at or near the perforation threshold and this was reflected in the residual strength curves where the tensile strength was repeatedly a minimum.

The following section outlines an analysis attempting to

predict the residual tensile strength of a damaged composite. Here, the region of fibre fracture is characterized as a sharp notch, permitting the residual strength of the damaged composite to be estimated using a fracture mechanics analysis.

4.3 Prediction of post-impact tensile strength

4.3.1 Assessment of Composite Fracture Models

Mathematical treatments describing the failure characteristics of fibrous composite can be broadly classified into two main categories. Firstly, there exist an number micromechanical analyses where account is taken of the presence of fracture mechanisms such as fibre pull-out and fibre-matrix debonding. The second, more popular approach, is the macroscopic approach. Here only the global response of the composite is considered, effects due to local material heterogeneity are ignored. Within this category lie the notch-insensitive and notch sensitive approaches. The former assumes that structural failure ensues when a uniform stress is developed in the unnotched section is equal to that of the undamaged strength of the material. Notch-insensitive behaviour can therefore be described by the net section relationship (43)

$$\frac{\sigma_r}{\sigma_0} = \left[1 - \frac{2a}{w}\right] \qquad (22)$$

where σ_0 is the plain tensile strength of the composite, 'a' the semi-crack length and 'w' the width of the composite. As previously stated, notch-insensitive behaviour is frequently associated with failure in unidirectional zero degree and angle ply (+/-45) composites where the stress raising effects of the notch are mitigated by the growth of small matrix cracks between the fibres at the notch tip producing a blunting effect.

Notch-sensitive fracture is more common; occurring at stresses below those predicted by the notch-insensitive analysis. There are at present many fracture models available which predict failure in notch-sensitive composites, their level of complexity depending upon the assumptions introduced.

Several workers have applied a simple linear elastic fracture mechanics approach to predict failure in centre-notched composite coupons (74,75). Here, the residual strength of the notched composite 'σ_r' is related to the crack size by the familar relationship

$$\sigma_r = \frac{K_{1c}}{Y[a/w]\sqrt{\pi(a + b_o)}} \qquad (23)$$

where Y(a/w) is the width correction factor which, for a

center-notched coupon, given as

$$Y(a/w) = \sec\left[\frac{\pi a}{W}\right] \qquad (24)$$

and 'K_{1c}' the critical stress intensity factor. The parameter 'b_0' in equation 23 is introduced to account for the effective increase in notch length and can be most easily determined using the approach proposed by Whitney and Browning (76). They assert that this term can be calculated by conducting notched tests on a number of composites and processing the resulting data using the relationship

$$b_o = \frac{1}{n}\sum_{1}^{n}\left[\frac{b_i}{\left[\frac{\sigma_o}{\sigma_{ni}}_{\infty}\right] - 1}\right] \qquad (25)$$

Waddoups et al (77) proposed a fracture mechanics model based on the existence of a hypothetical intense energy region, length α, at the notch tip. This characteristic dimension is assumed to be a material dependent property independent of notch length and notch radii. The Waddoups model states that the notched and unnotched strengths of the composite, σ_r and σ_0 , are related to the crack length by the relationship

$$\frac{\sigma_r}{\sigma_o} = \sqrt{\frac{\alpha}{a + \alpha}} \qquad (26)$$

Based on a knowledge of the stress distribution around a

defect, Nuismer and Whitney (78) developed two fracture models suitable for predicting failure in notched composite structures. The first of these, the point stress failure criterion, assumes that failure occurs when the stress at some distance, 'd_0', ahead of the notch reaches the unnotched strength of the laminate. For a sharp crack, length 'a', in an infinite plate, the point stress model can be written in the form

$$\frac{\sigma_r}{\sigma_o} = \sqrt{\left[1 - \frac{a}{a + d_o}\right]^2} \qquad (27)$$

By extending this analysis, Nuismer and Whitney (78) developed the average stress failure criterion. Here failure is assumed to occur when the stress averaged over some characteristic distance, 'a_0', reaches the unnotched strength of the composite. The average stress criterion is given as

$$\frac{\sigma_r}{\sigma_o} = \sqrt{\frac{1 - {}^{a}/_{(a + a_o)}}{1 + {}^{a}/_{(a + a_o)}}} \qquad (28)$$

In order to assess the suitability of these models for predicting the residual strength of impact damaged composites monotonic tension tests were conducted on a series of centre-notched composite coupons.

4.3.2 Experimental Verification of Fracture Models

Sharp notches between 2mm and 10mm long were introduced into the centre of a number of sixteen ply (+/-45) and (0,+/-45) composites with dimensions 150mm x 25mm using a fine jewellers saw. The residual tensile strengths of the notched composites were then determined by conducting uniaxial tension tests on an Instron Universal testing machine.

The resulting variation of normalised tensile strength with crack length for the sixteen ply (+/-45) composite is presented in figure 58. For purposes of comparison, the predictions yielded by the notch-insensitive model, equation 22, are included in this figure. Although the experimental data is rather limited, it does appear that the simple net sections relationship predicts the residual strength of these composites with some success. The net section failure model was therefore chosen to predict failure in the impact damaged (+/-45) composites

The experimental data for the sixteen ply (0,+/-45) composite is presented for comparison with the Waddoup's model, the LEFM approach and the point and average stress criteria in figures 59a and 59b. These theoretical curves were achieved by fitting equations 23, 26, 27 and 28 to the experimental data, the resulting values for 'a_0', 'd_0', etc are given in table 8.

In all cases, the fracture models appear to conform to the

experimental trends with some success. It is not possible to attach any significance to the characteristic parameters 'a_0' 'α', 'd_0' and 'b_0' other than they appear to lie within the range observed by other workers (43,77,78). The value of 56.1 MPa$\sqrt{m}$ for fracture toughness is also reasonable, and similar to quoted values for composites of this type (49). Previous experimental investigations have suggested that the average stress criterion can be used to predict successfully the residual strength of centrally cracked laminates in both tension (79) and compression (80). Since it is assumed that the characteristic parameter 'a_0' is a material property it should be possible to predict the residual strength of any arbitrary lay-up. Here, the model was compared with experimental data obtained by Kellas (49) following centre notched tests on the following sixteen ply XAS 914C composite

$$((0,+/-45,0)_2)_s$$

Figure 60 shows that agreement between the experimental and theoretical data is reasonable. Therefore, in this programme the average stress criteria was employed to assess the post-impact capability of the impact damaged (0,+/-45) composites.

4.3.3 Comparison of Fracture Model Predictions With Experimental Data

In section 4.2 it was observed that the tensile strength of a carbon fibre composite is particularly sensitive to the presence of fibre fracture. In this analysis the complex region of impact fracture was characterized as a sharp notch with dimensions equal to the maximum lateral extent of fibre fracture as shown schematically in figure 61. The dimensions of the region of fibre fracture were determined by deplying similarly damaged composites.

Figure 62 presents a comparison between the experimental data and the resulting theoretical predictions for the eight ply (+/-45) composite. Disregarding the experimental scatter, it is apparent that the simple notch-insensitive model predicts the experimental trends with some success. Figures 63 and 64 show the corresponding curves for the eight and sixteen ply (0,+/-45) composites. Included in these figures are the predictions yielded by both the average stress criterion and the notch-insensitive model. In each case the scatter in experimental data is much greater than observed in the centre-notched coupons, however, trends are clear. It appears that the failure criterion does not conform to the impact data as impressively as did the results obtained from the centre notched laminates, in this case, the experimental points are shifted towards the notch-insensitive line. This shifting phenomenon is probably due to the presence of extensive delamination around the

region of fibre fracture. This damage reduces the stress concentrating effect of the fibre damage and improves the tensile strength.

Before attempting to predict the variation of residual strength with impact energy it is necessary to understand how the effective crack length varies with incident energy. This was achieved by deplying many damaged coupons and physically measuring the size of the region of fibre damage. Detailed in figures 65 to 67 are the variations of this effective crack size with impact energy for the two eight ply composites and the sixteen ply (0,+/-45) laminate. In each figure there appears to be a rapid growth in fibre damage for energies between the fibre fracture threshold and the perforation threshold. Since this growth in damage is relatively linear with impact energy a least squares curve fit was applied to the data.

By assuming the growth in crack size to be linear between the fibre fracture and perforation thresholds it should therefore be possible to estimate the variation of residual tensile strength with impact energy.

This procedure was applied to predict the post-impact properties of the composites considered here. Again, the notch-insensitive fracture model was employed to predict the behaviour of the (+/-45) composites and the average stress criterion to characterize the failure process in the

(0,+/-45) laminates. It is assumed that for incident energies below the fibre fracture threshold the residual strength remained unaltered equalling at the plain tensile strength of the composite. Also, above the perforation threshold it was assumed that the residual strength remained constant, in this case equalling the value at perforation threshold.

The findings of this analysis are compared with the experimental data in figures 68 to 71.

It appears that the simple fracture models are capable of predicting successfully the variation in residual tensile strength with impact energy in all except the thickest thirty-two ply composite. Agreement in the latter is very poor and is probably a result of excessive delamination around the region of fracture. It must therefore be assumed that these fracture analyses are suited only for predicting the post-impact tensile properties of composites up to and including two millimetres thick.

4.4 Summary of Residual Strength Studies

The experimental evidence presented here clearly indicates that the process of tensile fracture in fibrous composite is complex. In contrast to metals where stress relaxation at the notch occurs by yielding and fracture usually involves the growth of a single microcrack, in laminates stress relaxation and fracture usually result from combinations of splitting parallel to the fibres, delamination and fibre failure.

From these studies it clear that fibre fracture is the single most detrimental damage mechanism to the integrity of a laminated composite when tested in tension. This was most clearly demonstrated in the eight ply (0+/-45) composite where very small regions of rear surface fibre fracture precipitated a twenty per cent reduction in residual tensile strength.

In all the laminates considered here the most substantial reductions in tensile strength coincided with the incident impact energy for target perforation. Examination of the corresponding deplied layers indicated that fibre fracture was extensive at his threshold, spreading to locations well away from the point of impact.

The fracture behaviour of these composites can be broadly classified into two main categories. The first, notch-insensitive failure, was observed in the eight ply (+/-45) composite, where the net section stress at the notch equalled the unnotched tensile strength. In this laminate, failure developed with the initiation and extension of small sub-cracks between the +/-45 fibres. With continued loading these small matrix cracks coalesced, spreading across the entire width of the composite to produce a large damage zone which in turn eliminated the stress concentrating effect of the fibre damage. Final fracture was by macroscopic shearing and was controlled and non-catastrophic.

The second failure phenonenon, notch-sensitive fracture, occurred in the (0+/-45) composites. These composites are sensitive to the presence of notches having strengths

falling below the notch-insensitive line.

A simple fracture mechanics technique was applied with some success to predict the post-impact tensile strength of the (0,+/-45) laminates. Here, the region of fibre fracture was treated as a plain notch of similar transverse dimensions and employed in conjunction with the average stress criterion to predict tensile failure.

It was noted that the impact data generally lay between the notch-sensitive and insensitive curves. This behaviour was attributed to the presence of planes of delamination local to the region of fibre fracture. Such damage has the effect of reducing, or even removing, stress concentrations generated by the fibre damage, thereby resulting in greater than anticipated residual strengths.

The model as it stands is not directly suitable for assessing the variation of tensile strength with impact energy in any arbitrary laminate since it is first necessary to know the relevant variation of crack growth with impact energy. Although these tests indicate that the characteristic crack size increases linearly with impact energy it is first necessary to determine (a) the threshold energy for fibre fracture, (b) that for target perforation and (c) the maximum dimensions of the characteristic crack. The perforation threshold has been predicted successfully in section 3.3.9. Physically determining the fibre fracture threshold proved much more difficult. However, by using the first damage threshold in the analysis (the first damage and fibre fracture thresholds were usually similar) the

post-impact characteristics will still be predicted with some success.

Predicting the maximum dimension of fibre fracture may be possible by considering the perforation model proposed in chapter 3. Here, the geometry of the shear zone was modelled as the curved surface of a frustrum. Consequently, the maximum dimension of the region of fibre fracture is 2(r+t) where 'r' is the projectile radius and 't' the target thickness. Therefore, for the one millimetre targets the maximum extent of fibre fracture should be 8mm and for the 2mm target 10mm. These predictions are realized to some extent in figures 65 to 67.

CHAPTER 5. THE HIGH VELOCITY IMPACT RESPONSE OF CFRP

		Page
5.1	Background	108
5.2	High velocity impact damage studies	111
5.2.1	Eight ply (+/-45) composite	112
5.2.2	Eight ply (0,+/-45) composite	113
5.2.3	Sixteen ply (0,+/-45) composite	114
5.2.4	Thirty-two ply (+/-45) composite	115
5.2.5	Summary of high velocity damage studies	115
5.3	Ballistic perforation of CFRP	118
5.3.1	Background	118
5.3.2	Experimental studies	120
5.3.3	The ballistic perforation model	121
5.3.4	Comparison with experimental data	124
5.3.5	Ballistic perforation of the sixty-four ply (+/-45) composite	125
5.4	The effect of projectile mass on impact response	127
5.5	The influence of impactor diameter on perforation energy	128
5.6	The influence of target geometry impact response	129
5.6.1	The size effect in composite beams	129
5.6.2	The influence of target width	130
5.6.3	High velocity impact of circular composite plates	132
5.7	Summary of high velocity impact studies	133

CHAPTER 5.

THE HIGH VELOCITY IMPACT RESPONSE OF CFRP

This chapter examines the behaviour of a series carbon fibre plastic laminates when subjected to localised high velocity impact loading by a light projectile. Initially, by the extensive use of a range of destructive and non-destructive damage detection techiques, the processes of damage initiation and propagation are monitored in a number of targets. Following this, attention is given to examining and predicting the perforation process in these ballistically impacted laminates. Finally, the effect of high velocity impact damage on residual strength is considered by conducting monotonic tension tests on a range of damaged composites.

5.1 Background

The potential for employing the strong, stiff properties of composite materials in the manufacture of aircraft turbine blades has long been identified. Concerned by the low strain capability and poor transverse properties of composite materials, many aircraft companies have funded large programmes of research with the aim of understanding and, if possible, predicting the ballistic impact response of these materials. Experimental investigations are numerous and the findings of much of this work have been discussed in the literature review presented in chapter 1. Subsequent

attempts to predict ballistic response using either analytical or empirical techniques are somewhat fewer. Kubo and Nelson (81) developed a finite element analysis to model the impact response of a multi-layered orthotropic target. Here, the target displacement field was modelled using a series of harmonic equations and the impact loading condition using a truncated Fourier series. The authors asserted that this analytical approach succesfully modelled the dynamic response of a composite turbine blade. However, no experimental data were presented to verify the range of accuracy of this analysis so it is therefore not possible to fully substantiate these conclusions. The blade impact problem has been further investigated by Sun and Sierakowski (82). Here, the behaviour of a representative blade configuration was modelled by considering the response of a number of discretized masses subjected to an initial velocity condition. Although this analysis yields only qualitative trends the authors suggest that the concepts developed offer designers an initial tool to screen and evaluate those materials most suitable for operational deployment.

In attempting to predict failure in ballistically impacted graphite-epoxy coupons, Preston and Cook (83) combined a Hertzian contact analysis with the solutions to the beam vibration problem. In order to simplify the problem, the authors chose to characterize the flexural properties by defining a term called the equivalent bending modulus for

use in their analysis. Also, the authors accounted for indentation effects by using the composite transverse tensile modulus to characterize the indentation stiffness. However, this assumption may be inaccurate since the stress field in the region of contact is predominantly compressive. It seems more realistic therefore, that the transverse compression properties of the material should be used to describe this process. Indeed, this may in part explain why the authors found that this combined Hertzian-vibration solution over-estimated the impact force and served only to offer an upper bound to the impact problem.

Although arguably effective, these analytical solutions for the impact problem are complex and require considerable computer effort even to model the rather simple beam impact problem. The subsequent cost of extending the capability of these analyses to model the ballistic response of a full scale aeronautical structure would be unjustifiably enormous.

Perhaps a more realistic approach for modelling the high velocity impact problem is to develop a series of semi-empirical models based on the findings of a thorough experimental test programme. By fully evaluating the accuracy and limits of such models it may then be possible to predict the impact behaviour of a full scale aeronautical structure at a fraction of the cost of these complex

analytical tools.

The following sections applies the above rationale to assess the high velocity impact response of carbon fibre reinforced plastic. The first section examines the mechanisms by which damage develops in a series of impacted composite beams. Following this, an energy balance analysis is developed to predict the incident impact energy required to perforate these composite beams. The flexibility of this model is then assessed by conducting impact tests on a series of larger composite structures. Finally, the effect of impact damage on residual strength is considered by conducting tension tests on a series of damaged coupons.

5.2 High Velocity Impact Damage Studies

This section details the processes of damage development in a number of carbon fibre composites. For purposes of continuity, this discussion is limited to the four laminates considered in the low velocity impact programme, their respective lay-ups being

eight ply (+/-45)
eight ply (0,+/-45)
sixteen ply (0,+/45)
thirty-two ply (+/-45)

Since the mechanisms of impact fracture were found to vary

with fibre lay-up the processes of damage development in each lay-up will be discussed in turn.

5.2.1 Eight Ply (+/-45) Composite

The initiation and subsequent development of impact damage in this one millimetre thick target is detailed in figures 72 to 74.

Damage was first detected between the lower surface fibres after an incident energy of 0.4 Joules, figure 73a. Although impossible to verify, this damage may be a result of the local flexural action of the beam, with the lower surface tensile stresses exceeding the fibre-matrix interfacial strength. As would be expected, this damage is not evident in either the resulting C-scan or the X-radiograph, figure 74a.

By 1.33 Joules this damage had extended up through the lowest ply precipitating a plane of delamination at the local ply interface. Now, damage is detected by both the C-scan and the X-radiograph, figure 74b, and can be detected visually, figure 72a.

After an incident energy of 1.46 Joules two top surface matrix cracks extending from locations either side of the impact location were detected, figure 73c. This evidence supports the view that the top surface failure results from the contact-induced tensile stress field.

By 3.0 Joules damage was extensive. The deplied layers of a damaged composite clearly showed that both matrix and fibre damage were incurred in substantial quantities, figure 75. At this energy, many of the rear surface fibres were removed from the composite indicative of stress wave reflection. This will be discussed in more detail at the end of this section.

Target perforation occurred after an incident energy of 3.0 Joules. Here, damage was extensive, spreading well away from the point of impact. Closer examination of the region fracture zone showed that the passage of the projectile through the target precipitated the now familar frustrum-like shear plug, figure 73d.

5.2.2 Eight Ply (0,+/-45) Composite

The processes of damage initiation and development in this (0,+/-45) composite are detailed in figures 76 to 78.

Damage, in the form of lower surface matrix splitting, was first detected after an incident energy of 0.5 Joules.

By 0.9 Joules, figure 77a, this damage had extended up through the lower ply forming a plane of delamination at the lowest interface. Examination of figure 78a indicates that this damage was detected by ultrasonic inspection but not by X-radiography. Again, at intermediate energies damage initiates at the top surface of the target local to the

periphery of the region of contact (see figure 77b). The formative stages of the shear plug are clearly evident in figure 77c leading to full perforation by 4.0 Joules, figure 77d. Once again, damage is extensive at perforation with many of the rear surface fibres having been removed by stress wave effects.

5.2.3 Sixteen ply (0,+/-45) Composite

Damage in this two millimetre thick composite initiated after an incident energy of 0.4 Joules. Interestingly, this damage developed between the uppermost fibres near the perimeter of the area of contact. Again, this initial fracture appears to be a consequence of the contact stress field with failure occurring when the local tensile stresses exceeded the fibre-matrix interfacial strength.

After 1.0 Joules, this top surface matrix crack appears to have generated a plane of delamination near the top surface of the composite, figure 79a.

By 1.9 Joules, figure 79b, damage in the form of matrix cracking and delamination was extensive throughout the thickness of the composite. Interestingly, the distribution of the translaminar matrix cracks is similar to that observed following low velocity impact tests, see figure 26. At incident energies just below the perforation threshold matrix and fibre damage was again extensive, figures 79c

and 80b. Target perforation resulted from an impact energy of 6.9 Joules, again yielding the familiar fracture surface.

5.2.4 Thirty-Two Ply (+/-45) Composite

Damage in this the stiffest target initiated after an incident energy of 0.38 Joules. Once again, this damage developed between the upper surface fibres local to the point of impact. By 0.6 Joules, figure 81a, this damage has spread extensively throughout this top surface ply.

The micrograph of the beam subjected to an incident energy of 3.9 Joules, figure 81b, shows a complex array of matrix cracks extending away from the point of impact. Similar fracture characteristics were observed in this thirty-two ply composite following low velocity impact tests where this process of failure was explained using the model outlined in section 3.2.2.3.

After 11.3 Joules, the formation of the shear plug were observed, figure 81c, and by 20.5 Joules the shear-out process commences, figure 81d. Total shear-out, that is, target perforation, occurred after an incident energy of 24 Joules and resulted in the generation of considerable damage spreading to positions near the target supports.

5.2.5 Summary of High Velocity Damage Studies

From these studies it is becoming clear that the fracture

process in ballistically impacted composites is complex, involving damage propagation by delamination, matrix cracking and fibre fracture.

High velocity impact loading by a light mass induces deformations local to the point of impact leaving much of the target virtually unstressed and undeformed. As a result, most of the energy of an incident projectile is dissipated in the volume of material local to the point of impact. Since the targets capability to accommodate energy in elastic deformations is small, much of the available energy is expended in propagating fracture. This is reflected in the low damage thresholds for high velocity impact loading. For example, under low velocity impact conditions where much energy is accommodated in elastic flexure, damage in the sixteen ply (0,+/-45) composite initiated at 1.61 Joules. Similar tests under high velocity impact conditions, where less energy is accommodated in elastic flexure, yielded a much lower value of 0.4 Joules for the first damage threshold.

Damage in the thick laminates initiated between the fibres in the top surface ply. Close examination of the resulting micrographs suggested that this damage initiated in the resin near the edge of the area of contact. Similar observations were noted in the low velocity impact programme and this was attributed to a contact-induced tensile failure

at the fibre-matrix interface.

At intermediate incident energies, that is, energies between the first damage and perforation thresholds, many fibres were spalled off the rear surface of the target. Fibre spallation is a damage mechanism common to many fibrous composites, resulting from the reflection of stress waves off the rear surface of the target. Although not considered to be a series fracture mechanism in terms of residual strength, several workers have examined methods by which rear surface fibre spallation may be reduced (19,62). Limited success has been achieved by employing a through thickness fibre reinforcement in a laminated composite (19), however, this is impractical from an economic viewpoint. A more feasible approach is to cover the lower surface of the target with a layer of woven fabric, indeed, Demuts (62) has demonstrated the success of this technique.

In all cases, target perforation yielded greatest damage. Interestingly, examination of the micrographs taken from the perforated coupons indicated that both the size and geometry of the shear zones were similar to those observed after drop-weight perforation.

The following section considers the process of perforation in these carbon fibre composites in more detail.

5.3 Ballistic Perforation of C.F.R.P.

Following low velocity impact tests, see chapter 3, it was found that the perforation process generated considerable damage in these multi-layered composite and, from a residual strength standpoint, represented the most severe impact condition. This section examines the high velocity perforation process in more detail and, by use of an energy balance analysis, attempts to model this phenomenon.

5.3.1 Background

The ballistic perforation problem has long been of interest, papers dating back to the early 1800's are not unusual! In more recent years a variety of perforation analyses have been developed, ranging in complexity from simple one dimensional shear-out models (84) to complex three dimensional analytical solutions (85). It is beyond the scope of this survey to discuss all of these models, however, an authoratative and thorough review of this subject has been documented by Backman and Goldsmith (85). Many of these models reduce the complexity of the perforation problem by introducing various assumptions, for example

1. the projectile is rigid and non-deformable
2. the impinging projectile affects only a small region of target local to the point of impact
3. the mass of the penetrating projectile should include

the mass of the target immediately ahead of the projectile

4. the energy dissipated in thermal shock and frictional effects is small

5. the material properties of the target and impactor remain unchanged during the perforation process

6. the target is initially stress free

The majority perforation models are based on the occurance of a single damage mechanism, for example, plugging or hole enlargement. More recently, a number of models have been developed that allow for a combination of damage mechanisms. One example of this is the analysis developed by Awerbuch and Bodner (86). Here, the perforation process is modelled in three stages. In the first stage, the penetrating projectile is resisted by a system of inertial and compressive forces. The second stage of the perforation model accounts for the development of a system of through-thickness shearing forces around the projectile. Finally, stage 3 commences when both the plug and projectile move together as a single body resisted only by the action of a through-thickness shear force. Although in essence simple, this analysis has been applied successfully to predict the post-perforation velocity and impact force-time history in a number of metal targets. However, this analysis is not widely favoured since its semi-empirical nature requires the determination of parameters such as the plug length and the shear zone width.

Few attempts have been made to extend the capability of

these models to predict perforation in multi-layered composite materials. Dorey (45), by equating the incident energy of the projectile to the energy required to shear-out a cylindrical plug, predicted the perforation threshold of a twelve ply carbon fibre composite.

5.3.2 Experimental Studies

Experimental tests were conducted on a wide range of composites in order to determine the minimum impact energy required to achieve perforation. Here, composite beams with dimensions 100mm x 25mm were supported on two 12.7mm diameter steel rollers positioned 50mm apart and impacted by six millimetre diameter, one gram steel balls. Full details of the experimental procedure are given in chapter 2.

Detailed in the left hand column of table 9are the ballistic perforation thresholds of a number of (+/-45) and (0,+/-45) composite beams. The data for the (+/-45) composites is also presented in graphical form in figure 82. The available data suggests that the variation of perforation energy with target thickness is similar to that observed in the low velocity impact programme. Interestingly, similar trends in perforation energy were noted by Shadbolt et al (87) following ballistic impact tests on a series of circular aluminium plates.

From this limited evidence no link between perforation

energy and fibre stacking sequence is evident. The perforation threshold of the eight ply (+/-45) composite was lower than that of the eight ply (0,+/-45) laminate, whereas the perforation threshold of the sixteen ply (+/-45) was considerably greater than that of its (0,+/-45) counterpart. The following section details a model attempting to predict the ballistic perforation threshold of a carbon fibre composite. The accuracy of the model is then assessed by comparing its predictions with the experimental data presented above.

5.3.3 The Ballistic Perforation Model

In the low velocity perforation model developed in chapter 3 account was made for energy dissipation in elastic flexure, contact deformations, delamination and target shear-out. Under high velocity impact conditions other phenomena such as stress wave propagation and local target vibrations are induced. The stress wave problem has been considered in some detail by a number workers (25,26) and an excellent overview of the subject is presented in the book by Kolsky (88). In considering the process of energy dissipation during high velocity impact loading Conrad (89) found that stress wave effects accounted for only a small fraction of the incident energy of the projectile. It also appears that energy dissipation in vibrational effects are small. Backman and

Goldsmith (85) suggest that energy loses due to vibrational behaviour are only significant in very flexible targets where the ratio of impact velocity to target stiffness is large. Based on these findings it was assumed that energy losses due to these effects were small in comparison to those previously mentioned and could therefore be neglected. The energy required for target perforation was determined by accounting for energy dissipation in elastic flexure, contact deformations, delamination and shear-out. The procedure employed for examining these effects was detailed previously in sections 3.3.4, 3.3.91 and 3.3.9.2. Initially, it was assumed that the impinging projectile induced a primary mode of response similar to that shown in figure 83a. The resulting impact load to initiate target failure was determined by examining the local contact and flexural stress fields, see sections 3.3.5 and 3.3.6. Briefly, this critical impact load was substituted into the energy balance equation, (equation 7, section 3.3.4), to yield an estimate for the energy dissipated in contact and flexural deformations. The energy expended in generating delamination was again determined by deplying the composites in a furnace, measuring the visible area of fracture and multiplying this value by the fracture energy for delamination (700 J/M^2). Finally, the energy for shear-out was estimated using the geometrical model presented in

section 3.3.9.1. In this analysis, the shear-out model was modified to account for fibre spallation. Such damage reduces the effective thickness of the composite leaving the projectile to perforate one less ply. The effective thickness of the target is therefore t(n-1)/n where 't' is the original thickness of the composite and 'n' the original number of plies in the composite.

The predicted perforation thresholds for the (+/-45) composite beams are presented for comparison with the relevant experimental data in figure 84. It is immediately clear that the perforation model over-estimates the experimental data for all target thicknesses. This evidence suggests that the assumed primary mode of target response is inaccurate. Other workers (85) investigating the ballistic impact response of metal targets have shown that fast moving, light projectiles induce only deformations local to the point of impact. Further, several workers have identified the ratio of projectile mass to target mass as an important parameter in determining the high velocity impact response of a structure (85,90). Elber (73) suggests that higher, more localised modes of target response are generated when the projectile to target mass ratio approaches unity.

Based on this evidence, the energy balance analysis was modified to take account of a localised target response.

Here, it was assumed that the projectile excited only the volume of material immediate to the point of impact as shown in figure 83b. For simplicity, it was assumed that the mass of this affected region was equal to that of the incident projectile. In the thin four and eight ply targets the subsequent flexural behaviour of this region was modelled using the beam analysis discussed in section 3.3.5. In the thicker composite targets the affected zone will be small in comparison to the dimensions of the beam. Here, target response was modelled by assuming that this region behaved like a circular plate and was therefore analysed using the plate theory discussed in section 3.4.3.2.

5.3.4 Comparison with Experimental Data

The predictions yielded by the perforation analysis are presented for comparison with the experimental data in table 9 and figure 85. Although the model still appears to over-estimate the experimental threshold, agreement is reasonable.

In designing structures for perforation resistance it is necessary to understand how the incident energy of the projectile is dissipated during the impact process. In this programme an energy absorption map was developed to examine impact on the (+/-45) composite beams and this is presented in figure 86. The energy map indicates that shear-out is a

major energy absorbing mechanism in all of the targets. For example, for the two millimetre target approximately seventy per cent of the incident energy of the projectile was dissipated in this shear-out process. As expected, contact and flexural deformations account for less than ten per cent of the incident impact energy in all targets. Delamination, although possessing a relatively low fracture energy (700 J/M^2), appears to be a major energy absorbing mechanism, particularly in the thicker targets. The variation of energy expended in delamination with target thickness is shown in figure 87. The trends in this figure are very similar to those observed during the low velocity impact programme, section 3.3.9. Here, it was suggested that the variation of delaminated area might be estimated by assuming a distribution of delamination similar to that shown in figure 44. Applying this methodology here again gives a reasonable correlation with the experimental data, see figure 87.

5.3.5 Ballistic Perforation of the Sixty-Four Ply Composite

In order to fully assess the validity of the perforation model, a sixty-four ply (+/-45) composite was manufactured and tested. Experimental tests on this eight millimetre thick composite yielded a perforation energy of 40.5 Joules.

The perforation model, however, grossly over-estimated this value, offering an estimate for perforation of 70 Joules, figure 88. The reason behind this substantial departure in agreement was investigated by sectioning one of the perforated coupons and examining the fracture surface under a low power microscope. From this it became clear that two seperate failure modes had been induced by the passage of the projectile, see figure 89. The upper half of the target displayed the now familiar conical-shaped shear zone, whereas the lower half of the target exhibited what appeared to be a local tensile failure. A change in failure mode of this type was explained by considering the impact process in more detail. Upon impact, the incident projectile generated a system of compression stress waves which propagated away from the point of impact at high velocity, see figure 90a. Upon encountering the rear surface of the target, these compression waves were reflected to form tension waves of similar magnitude. As these tension waves propagated through the thickness of the target large tensile stresses were generated at the ply interfaces which, if sufficiently great, generated planes of delamination local to the rear surface of the target, figure 90b. Meanwhile, the incident projectile began to penetrate the upper, so far undamaged

layers of the target resulting in the formation of generating the familiar fracture zone. The mode of failure changed when the projectile encountered the region of extensive delamination in the lower portions of the target. Here, instead of failing in a through-thickness shear mode, the fibres failed as a result of the large tensile stresses generated in front of the penetrating impactor, figure 90c.

5.4 The effect of projectile mass on impact response

In order to examine the effect of varying projectile mass on high velocity impact response impact tests were conducted using projectiles of mass 0.17, 0.6 and 1.0 grams. It was found that the perforation velocity increased with decreasing projectile mass, for example, using the one gram steel ball the perforation velocity of the sixteen ply (+/-45) composite was determined as 125 m/s whereas that for the lighter 0.17 gram projectile was found to be 260 m/s. The resulting variation of perforation energy with impactor mass for the (+/-45) composites is shown in figure 91. Cursory examination of the figure also highlights a mass dependence, with perforation energy decreasing with decreasing projectile mass. Subsequent examination of the C-scans indicated that the area of damage did not vary significantly with projectile mass (this is presented in graphical form in figure 92). Instead, it appears that this

reduction in perforation energy with decreasing impactor mass is a result of less energy being accommodated in local elastic response. Indeed, this supports the assumption introduced in the perforation model.

5.5 The Influence of Impactor Diameter on Perforation Energy

Limited testing was undertaken to assess the suitability of the impact model for predicting perforation by larger radius projectiles. It would be expected that increasing the radius of the incident projectile would increase the amount of energy dissipated in delamination and the local elastic response of the target. Perhaps of greater consequence would be the magnitude of the energy required for shear-out. For example, for a sixteen ply composite the energy required to achieve target shear-out would increase by fifty per cent by changing the projectile radius from three to five millimetres.

In these tests a five millimetre radius steel ball was used to perforate the four, eight and sixteen ply (+/-45) composites. The resulting variation of perforation energy with target thickness for these ten millimetre diameter steel balls is shown in figure 93. The trends in experimental data are similar to those observed using the smaller diameter projectile, however, more energy is now

required to achieve target perforation. Again, it appears that the perforation model predicts adequately perforation in these targets.

5.6 The Influence Of Target Geometry On Impact Response.

This section examines the influence of target geometry on high velocity impact response. This effect is initially assessed by considering the impact response of simple beam coupons. Then, based on the knowledge gained from these tests, the impact respose of a large circular plate is considered.

5.6.1 The Size Effect in Composite Beams

In order to examine the size effect in composite beams, the distance over which the targets were supported was varied between 25mm and 150mm, keeping the beam width fixed at 25mm. As before, impact testing was conducted using six millimetre one gram steel balls.

The geoemtrical effect is most simply assessed by examining the C-scans shown in figure 94. For clarity, this information is also presented in graphical form in figure 95. For these sixteen ply (0,+/-45) laminates it is clear that the area of damage varies little with beam geometry. This is in contrast to the findings of the low velocity impact programme where the target geometry was

found to strongly influence the impact response of the beams.

The incident energy to initiate first damage was determined through the extensive use of the C-scans and micrographs. Figure 96 shows the variation in the damage threshold energy with beam length. Although there is some scatter in these results it is apparent that the damage threshold energy (and velocity) remains independent of beam length. Similar observations were noted following ballistic perforation tests on these sixteen ply beams, figure 97. Here, the perforation energy (and velocity) is seen to vary little with beam geometry. Again, this evidence is contrary to the observations made following drop-weight impact tests where the target geometry determined the strain energy absorbing capability and therefore the target impact resistance.

This experimental evidence suggests that localised high velocity impact loading by a light mass generates a very localised target response thereby leaving much of the target unstressed.

5.6.2 The influence of Target Width

Similar tests were conducted in order to examine the effect of varying the target width on impact response. Here,the length of the target coupons was maintained at 50mm whilst their widths were varied between 25mm and 50mm.

C-scans of several damaged sixteen ply composites are presented for comparison in figure 98. Once again, the overall area of the damage zone exhibits scant dependence upon the target geometry. Similar trends were apparent after conducting perforation tests on these composites. Figures 99 and 100 show that the energy needed to initiate damage and to perforate these sixteen ply (0+/-45) composites remained roughly constant for all geometrical configurations. It is interesting to note however, that the curve in figure 100 tends to a value of approximately 6.3 Joules whereas the corresponding for the beam coupons, figure 96 tends towards the value of 7.0 Joules. This deviation in perforation behaviour probably results from the narrow width of the beam targets, when such small dimensions are involved geometrical effects will result.

Experimental testing on these rather idealized coupons signify that target geometry may not be a significant parameter in determining the response to high velocity impact. However, these geometries are not typical, in order to fully examine this effect it is necessary to extend the test programme to consider the response of a more realistic structure. The following section considers the ballistic impact response of the circular plates considered previously in chapter 3.

5.6.3 High Velocity Impact on Circular Composite Plates

Here, ballistic impact tests were conducted on a series of circular composite plates, radius 65mm, with the aim of assessing damage growth and determining target perforation. The damage threshold energies for a range of composites are given in table 10. It is evident from this data that damage initiates at very low energies in all the composites and that these thresholds are considerably below those recorded following drop-weight impact tests. Data for the (+/-45) targets is presented in graphical form in figure 101. Also included in this figure are the theoretical predictions for first damage yielded by the impact model. It is interesting to note that although the damage model considerably under-estimates the experimental data it does predict the trends in first damage with some success. It again appears that there exists an optimum thickness for first damage although this effect is not as pronounced as that noted in the drop-weight test programme.

For comparative purposes a C-scan of a damaged sixteen ply (0,+/-45) composite is presented with that from a 50mm x 50mm square plate and that from a 50mm x 25mm beam in figure 102. It is interesting to observe that the overall area of damage is approximately the same for all composites. Data from the perforation tests is presented in table 11 and in graphical form in figure 103. These trends in perforation

with target thickness are similar to those recorded during tests on the beam coupons, section 5.3.2. Also, these perforation thresholds are of similar magnitude to those of the simple beam coupons. Included in the table and figure are the perforations energies predicted by the perforation model. Although the model again tends to slightly over-estimate the experimental thresholds it appears that agreement is still reasonable.

5.7 Summary Of High Velocity Impact Studies

From these experimental tests some insight has been gained into the high velocity impact response of CFRP. Whereas low velocity impact by a large mass excites a global mode of target response enabling much energy to be accommodated in elastic flexure, high velocity,low mass impact induces only a local target response permitting little energy to be absorbed in elastic deformations. As a result, the incident energy of a fast moving projectile is dissipated mainly in the volume of material local to the point of impact. This is clearly emphasized by comparing the threshold energies for first damage after low velocity and high velocity impact loading. Consider for example the sixteen ply (0,+/-45) composite. Under low velocity impact conditions damage initiated between the top surface fibres after 1.6 Joules. Under ballistic impact loading similar levels of damage were incurred after the much lower energy of 0.4 Joules. This is

further highlighted by considering the variation of delaminated area with impact energy for low and high velocity impact loading, see figure 115. Here, for a given impact energy daamge was more severe in the ballistically impacted composites.

Interestingly, the damage studies indicated that the processes by which damage initiated and propagated under high velocity impact loading were similar to those involved in the low velocity impact damage development.

In the flexible targets fracture initiated between the fibres at the lower surface. At present, it is not clear which mechanism precipitated this failure, perhaps local flexural stress or maybe some form of rear surface stress wave reflection.

Failure in the thick composites initiated in the matrix at the edge of the area of contact. As before, it appears that this damage occurs as a result of the tensile component of the contact stress field. In the low velocity impact studies it was suggested that the threshold energy for first damage could be enhanced by applying a covering layer of surface treated fibres, that is, a material with a high transverse tensile strength, to the top surface of the composite. From the experimental evidence gathered here it appears that a similar procedure might enhance the damage threshold energy under high velocity impact conditions.

At intermediate energies damage became extensive and was found to be more severe than that incurred after similar low

velocity impact energies. In this region, fibre spallation removed many of the fibres from the rear surface of the target.

In all composites, damage was most extensive at incident energies around the perforation threshold. Here, it was found that the passage of the projectile yielded a shear zone of similiar dimensions and geometry to that observed following drop-weight perforation tests. Attempts to model the ballistic perforation response of these materials have met with some success. Here, it was observed that shear-out is the major energy absorbing mechanism for target thicknesses up to four millimetres.

Above this thickness, delamination takes prominance, accounting for a more than fifty per cent of the incident energy of the projectile. Clearly, efforts to enhance the ballistic perforation resistance of these composites must centre on optimizing the transverse fracture energy, the fracture energy for delamination or both.

The influence of target geometry on high velocity impact response has been examined by conducting tests on a variety of target geometries. It appears that if the dimensions of the target are greater than the size of the 'impact affected zone' geometrical effects are very small. This suggests therefore that tests on small laboratory test coupons are suitable for assessing the ballistic impact capability of a full scale operational structure.

CHAPTER 6. RESIDUAL STRENGTH AFTER HIGH VELOCITY IMPACT LOADING

		Page
6.1	Introduction	137
6.2	Experimental studies	139
6.2.1	Eight ply (+/-45) composite	139
6.2.2	Eight ply (0,+/-45) composite	140
6.2.3	Sixteen ply (0,+/-45) composite	141
6.2.4	Thirty-two ply (+/-45) composite	141
6.3	Prediction of residual tensile strength after high velocity impact	141
6.3.1	Comparison with experimental data	142
6.4	Summary of residual strength studies	144

CHAPTER 6

RESIDUAL STRENGTH AFTER HIGH VELOCITY IMPACT LOADING

In chapter 4 it was observed that low velocity impact damage seriously degraded the residual load carrying capability of a composite when tested in tension. This chapter examines the effect of high velocity impact damage on the residual tensile strength of a carbon fibre composite.

6.1 Background

Mathematical treatments predicting failure in impact damaged composites are scarce, probably due to the inherent difficulties involved in modelling the complex region of impact fracture. Husman et al (36) proposed an analogy, in the terms of residual strength, between the damage inflicted by a small hard particle and the damage inflicted by implanting a crack of known dimensions in a static tensile coupon. It was assumed that the difference between the energy density required to break an undamaged coupon and that required to break a similar impacted coupon is directly proportional to the kinetic energy imparted to the specimen. It was further assumed that the incident energy of the projectile is dissipated over some characteristic surface area the size of which is independent of incident energy. The resulting relationship for residual strength in terms of the incident kinetic energy of the projectile is

$$\frac{\sigma_r}{\sigma_o} = \sqrt{\frac{W_s - KW_{ke}}{W_s}} \qquad (29)$$

where ' σ_o ' is the undamaged strength, 'Ws' the work per unit volume to break the specimen, 'Wke' the kinetic energy per unit thickness imparted to the specimen and 'K' an effective damage constant.

Although agreement between the theoretical predictions and experimental data appears impressive, the overall applicability of the Husman model is questionable since the damage constant, 'K', varies with fibre lay-up and support conditions requiring its determination for each impact situation.

Avery (6) employed a similar fracture mechanics methodology to assess the survivability of a ballistically impacted composite structure. In this approach the residual fracture stress of the composite target was related to the impact damage size by defining an equivalent stress intensity factor for gun fire. Based on observations noted in impacted metal targets the region of impact damage was modelled as a circular hole with two 2.5mm cracks extending from either side. The resulting fracture model relates the equivalent stress intensity factor, Λ_c , to the fracture stress, σ_r , by the equation

$$\Lambda_c = \sigma_r \sqrt{\frac{\pi TLD_{eff}}{2}} \qquad (30)$$

Before attempting to predict the post-impact capability of

an impact damaged composite it is first necessary to examine experimentally the effect of impact damage on residual strength.

6.2 Experimental Observations

As before, this chapter commences by examining the experimental evidence gathered from tests on the following four laminates

eight ply (+/-45)
eight ply (0,+/_45)
sixteen ply (0,+/_45)
thirty-two ply (+/-45)

Figures 104 to 107 show the variation of residual tensile strength with impact energy for these composites. Marked on each figure are the experimentally determined thresholds for first damage (1), fibre fracture (2) and perforation (3). The post-impact properties of each of these laminates will now be discussed in turn.

6.2.1 Eight Ply (+/-45) Composite

At low incident impact energies damage in this one millimetre thick composite was limited to the matrix. Figure 104 indicates that such low levels of damage had little effect upon the load carrying capability of this composite in tension. First reductions in tensile strength

coincided with the threshold energy for fibre fracture. However, this loss in strength was not great, the region of fibre fracture was probably isolated by the presence of local delamination. The residual strength curve drops off rapidly with increasing impact energy until it reaches a minimum value at the perforation threshold. At energies above perforation, the residual strength does not appear to vary significantly from this value.

6.2.2 Eight Ply (0,+/-45) Composite

The variation of residual tensile strength with impact energy in this eight ply composite is shown in figure 105. Here, unusually, no reductions in tensile strength were recorded in laminates displaying low levels of fibre fracture, once again the deleterious effects of such fracture appear to be mitigated by the presence of delamination.

As before, strength reductions were greatest at the threshold energy for target perforation, approximately 3.2 Joules. Here damage was extensive.

In this case slight improvements in residual strength were noted in those laminates impacted at energies in excess of the perforation threshold.

6.2.3 Sixteen Ply (0,+/-45) Composite

As in the previous case, low levels of localised fibre fracture do not precipitate reductions in tensile strength, figure 106. Indeed, significant reductions were not recorded until energies equivalent to approximately twice that of the fibre fracture threshold. At target perforation, this again representing the most severe impact condition, a sixty per cent loss in tensile strength was incurred.

6.2.4 Thirty-Two Ply (+/-45) Composite.

The post-impact properties of this four millimetre thick laminate are depicted in figure 107. The figure indicates that strength reductions were incurred at energies above 10 Joules, this again being considerably above the fibre damage threshold. At perforation, the damage studies indicated that fracture was extensive with this being reflected in the figure where a seventy per cent loss in strength is apparent.

6.3 Prediction of Residual Tensile Strength Afte High Velocity Impact Loading

In attempting to predict the residual tensile strength afte low velocity impact, chapter 4, four failure models wer examined,these were as follows:

1. classical LEFM
2. Waddoup's fracture model
3. point stress failure criterion
4. average stress failure criterion

Following tests on a series of centre-notched sixteen ply (0,+/-45) composites it was found that the average stress failure criterion was best suited for predicting residual tensile strength. Consequently, the average stress failure criterion was employed to predict the tensile strength of these ballistically impacted composites.

As before, the crack length 'a' was assumed to be equal to the dimensions of the maximum transverse length of fibre fracture, see figure 61. The value for the characteristic distance 'a_0' was taken as 1.95 mm, that is, the value determined during tension tests on pre-notched composites.

Before being able to predict the variation of tensile strength with impact energy it is first necessary to know how the dimensions of the impact fracture zone vary with incident energy. This was achieved, as before, by deplying similarly damaged composites in a furnace and measuring the extent of damage. The variation of this damage size with impact energy for the two eight ply and the sixteen ply composites is shown in figures 108 to 110.

It is apparent that the scatter in experimental data is more considerable than that observed under low velocity impact conditions. However, in order to simplify the fracture analysis a least squares fit was again applied to the data. By assuming this linear variation of damage size (effective crack length) with impact energy and employing the average stress criterion it is possible to estimate how the residual tensile strength will vary with impact energy. This was undertaken for

the four laminates mentioned earlier and the resulting predictions are compared with the experimental data in figures 111 to 114.

First consider the eight ply (+/-45) composite shown in figure 111. Here it is evident that the simple net section fracture model over-estimates the post-impact capability, particularly at energies equal to and above the perforation threshold. This considerable departure between theory and experiment was attributed to the presence of extensive delamination in these composites. Since such delamination uncouples the composite into individual laminae shear failure at the fibre matrix interface results at low tensile loads.

Contradicting trends were observed in the failure of the eight ply (0,+/-45) composite, figure 112. Here, the average stress failure criterion under-estimated the experimental data. Again, this was attributed to the presence of extensive delamination around the notch. In these laminates delamination serves to isolate the stress concentrating effects of the impact damage leaving the main load-bearing fibres to fail in a 'quasi' notch-insensitive mode.

Suprisingly, agreement is reasonably good in the two thicker composites, figures 113 and 114. Here, although the scatter in experimental data is more considerable the two fracture models provide a reasonable level of agreement with the experimental data.

6.4 Summary Of Residual Strength Studies.

In chapter 5 it was observed that high velocity impact generated extensive matrix and fibre fracture. In these studies such damage has been seen to precipitate significant reductions in residual tensile strength. In contrast to the low velocity residual strength studies, the scatter in experimental data is more pronounced, this probably being a legacy of the poorer accuracy of the gas gun. However, trends are clear.

In each composite, initial reductions in tensile strength occurred at energies considerably above the threshold for fibre fracture. It appears that the presence of considerable delamination around the region of fibre damage has reduced local stress concentrations.

As before, the greatest reductions in tensile strength occurred at energies around the perforation threshold where impact damage was most severe.

Attempts to predict the residual tensile strength have been less successful than in the low velocity impact programme. Here again, it was assumed that the stress concentrating effect of the damage has been reduced by local interlaminar fracture.

A Comparison of the Low and High velocity Impact Response of CFRP.

From the experimental evidence presented here it is now possible to compare the low and high velocity impact response of this carbon fibre composite system.
In most laminates the processes of damage initiation were similar for both loading extremes, however, the incident impact energies necessary to initiate first damage depended strongly upon the impact conditions. Under low velocity impact loading the contact time between the impactor and target is long and the target responds in global flexure frequently allowing considerable energy to be accommodated elastically. The response under high velocity impact loading was quite different. Here, it appears that the projectile excites a local target response leaving much of the target effectively unstressed. As a result, the elastic energy stored is small. This is clearly demonstrated when the damage threshold energies for low and high velocity impact are compared, see table 12. The incident energy to initiate damage under low velocity impact conditions is up to four hundred per cent greater than that for high velocity impact.

At energies above the damage threshold similar observations were made. Figure 115 compares the variation of delaminated area with impact energy for the sixteen ply (0,+/-45) laminate under both low and high velocity impact loading.

Again, it appears that ballistic impact represents the more severe loading condition.

The incident energies for low velocity and ballistic perforation of the beam coupons did not differ significantly, see table 13, however, it appears that the processes of energy absorption did. For low velocity impact a significant percentage of the incident energy is accommodated elastically whereas under high velocity impact more energy is dissipated in delamination.

The differences between the low and high velocity impact response of this material were most pronounced when considering the effect of geometry on impact response. Under low velocity impact loading the target geometry determined its ability to accommodate energy elastically and therefore its impact resistance. For high velocity impact, where the response is localised, the target dimensions appear to be unimportant. Here, the damage threshold of the 150mm long sixteen ply (0,+/-45) beam was 5.5 Joules whereas the threshold under high velocity impact was only 0.4 Joules.

CONCLUSIONS

Through an extensive test programme some insight has been yielded into the low and high velocity impact response of a laminated fibrous composite. It is becoming clear that the impact process in composite materials is complex with the incident energy of the projectile being dissipated in a variety of elastic and fracture mechanisms.

Up to the point of initial fracture composites present few problems, displaying specific strengths considerably in excess of those offered by conventional metallic materials. At energies above this damage threshold, planes of fracture are generated which, at large energies, frequently extend well away from the point of impact. Closer examination of these damaged coupons highlighted a number of individual fracture processes. On a microscopic level damage mechanisms such as fibre pull-out and fibre-matrix debonding have been observed. At the other extreme,energy has been dissipated in forming planes of delamination, matrix cracking and fibre fracture.

It has been shown that the low velocity impact resistance of a composite structure is governed by its ability to accommodate energy elastically. This was clearly demonstrated during tests on a series of sixteen ply (0,+/-45) composite beams. Here, it was found that doubling the length of the target structure increased the energy for first damage by over two hundred per cent.

In almost every laminate, damage initiated either in the matrix or at the fibre matrix interface. For the spherical impact problem the location of this first failure has been shown to depend strongly upon the target stiffness and projectile diameter. In the flexible targets impacted by both small and large diameter projectiles, damage initiated at the lower surface of the target as a result of the locally large flexural stress field. Such damage proved difficult to detect using conventional non-destructive techniques and may therefore pass undetected during a routine inspection procedure.

Failure in the thick targets impacted by a small diameter projectile initiated at the top surface of the composite local to the point of contact. Here, it has been shown that fracture is initiated by the tensile component of the contact stress field. As a result, it has been suggested that the damage threshold energy of a thick composite structure can be enhanced by applying a top layer of material exhibiting superior properties transverse to the fibres. A ply containing heavily surface treated fibres is a distinct possibility.

The variety of damage assessment techniques used indicated that damage was most extensive at the threshold energy for target perforation. Here, the passage of the projectile through the composite removed much of the material from

around the point of impact yielding a characteristic frustrum-shaped fracture surface.

High velocity impact by a light mass excites a mode of response entirely different from that of low velocity impact. Here, a local mode of target response is induced resulting in much of the incident energy of the impactor being dissipated in the volume of material immediate to the impact location.

As a result, less energy is accommodated in elastic mechanisms and more in fracture processes. This was clearly emphasized by the low damage threshold energies exhibited by the wide range of composites considered. For example, under low velocity impact loading damage in the sixteen ply (0,+/-45) composite initiating at an incident energy of 1.6 Joules. High velocity impact tests on this two millimetre thick target yielded a much lower damage threshold of 0.4 Joules.

By determining an energy balance for both the low and high velocity impact process considerable success has been achieved in modelling the impact capability of the range of carbon fibre composites. The energy model suggests that at perforation, through thickness shear-out is the principal energy absorbing mechanism in thin composite targets.

In the thicker targets delamination, although exhibiting a low fracture energy, proved to be dominant, accounting for

more than fifty per cent of the incident energy of the projectile.

The influence of target geometry on impact response is varied. Under low velocity impact conditions where a primary mode of target response is induced, the target geometries determines the energy absorbing capability of the composite and therefore its resistance to impact loading. However, increasing the volume of the target structure does not always increase its impact resistance. This was most marked in the sixteen ply (0,+/-45) composites where the damage threshold for a 150mm X 25mm beam (5.5 Joules) was considerably above that of the larger 65mm radius plate (0.7 Joules), This evidence suggested that the technique of assessing the low velocity impact response of a composite structure by conducting small-scale coupon tests is misleading, such tests neither predict the impact capability of the composites nor do they highlight the mode of failure. The influence of target geometry on high velocity impact response is small.

Here, it was found that no geometrical effect exists as long as the dimension of the target structure is greater than that of the impact affected zone. For the light six millimetre diameter projectiles considered here a target with dimensions 50mm x 50mm was suitable for assessing the impact behaviour of any larger geometry.

The detrimental effect of localised impact loading on residual strength has been highlighted by conducting monotonic tension tests on a range of carbon fibre laminates. It has been observed that the tensile strength of these composites is particularly sensitive to even small amounts of fibre damage. The stress concentrating effect of such fibre fracture can be reduced,or even removed by the presence of local planes of delamination.

By treating the region of fibre fracture as a simple notch of similar dimensions and by using the Nuismer and Whitney average stress failure criterion it has been possible to predict the residual tensile strength of the low velocity impact damaged coupons with some success.

Predicting the residual tensile strength after high velocity impact loading has not been as successful. Here, the presence of such extensive delamination around the region of fibre fracture effectively isolates the crack and shifts the mode of failure closer to that notch-insensitive fracture.

REFERENCES

1. Sharples T. Application of carbon fibre composites to military aircraft structures. AGARD CP283 (1980), pp11-17.

2. 'Composites'. Advertising supplement. Flight International, vol. 124 (1983), pp1735-1738.

3. Zweben C. Advanced composites for aerospace applications. Composites, vol. 12 (1981), pp235-240.

4. Warwick. G. Forward sweep technology. Flight International, vol. 125, (1984), pp1563-1568.

5. Rhodes M.D. and Wiliams J.G. Effect of resin on impact damage tolerance of graphite-epoxy laminates. NASA TND 8411 (1977).

6. Avery J.G. and Porter T.R. Comparisons of the ballistic impact response of metals and composites for military aircraft applications. ASTM STP 568 (1975), pp3-29.

7. Cristescu N. Malvern L.E. and Sierakowski R.L. Failure mechanisms in composite plates impacted by blunt-ended penetrators. ASTM STP 568 (1975), pp159-172.

8. Cantwell W.J. and Morton J. Low velocity impact damage in carbon fibre reinforced plastic laminates. Proc. of the fifth International Congress on Experimental Mechanics. Montreal 1984, pp314-319.

9. Baker A.A. Jones R. and Callinan R.J. Australian views and programmes on damage tolerance of graphite/epoxy composites. To be published in J.Composite Structures.

10. Austin C.D. Johnson W. and Walters B.J. Bursting and bulging of carbon fibre composite discs. Composites, 13 (1982), pp383-388.

11. Takeda N. Sierakowski R.L. Ross C.A. and Malvern L.E. Delamination-crack propagation in ballistically impacted glass/epoxy laminates. Experimental Mechanics, 22 (1982), pp19-25.

12. Butcher B.R. and Fernback P.J. Impact resistance of unidirectional CFRP under tensile stress: further experimental variables. Fibre Science and Technology, 14 (1981), pp41-58.

13. Ross C.A. Cristescu N. and Sierakowski R.L. Experimental studies on failure mechanisms of impacted composite plates. Fibre Science and Technology, 9 (1976), pp177-188.

14. Adams D.F. and Miller A.K. An analysis of the impact behaviour of hybrid composite materials. Material Science and Engineering, 19 (1975) pp245-260.

15. Wrzesien A. Improving the impact resistance of glass fibre composites. Composites, vol3 (1982), pp172-174.

16. Favre J.P. Improving the fracture energy of CFRP by delamination promoters. J. Materials Science, 12 (1977), pp43-50.

17. Bishop S.M. and Morton J. Fatigue of notched (0,+/-45) CFRP with woven and non-woven (+/-45) layers. Advances in Fracture Research, Valluri S.R et al (Eds.). Pergamon Press Oxford, vol. 4, 1984.

18. Cantwell W.J. Curtis P.T. and Morton J. Post-impact fatigue performance of carbon fibre laminates with non-woven and mixed-woven layers. Composites, 14 (1983), pp301-305.

19. Garrett R.A. Effect of defects on aircraft composite structures. AGARD CP355 (1983), paper 3.

20. Dorey G. Fracture behaviour and residual strength of carbon fibre composites subjected to impact loads. AGARD CP163 (1974), paper B3.

21. Wilkins D.J. The engineering significance of defects in composite structures. Presented at the symposium on Environmental effects in Composite Materials, London 1983.

22. Harris B. Beaumont P.W.R. and Moncuilli de Ferran E. Strength and fracture toughness of carbon fibre polyester composites. J. Materials Science, 6 (1971), pp238-251.

23. Cantwell W.J. Curtis P.T. and Morton J. Impact and subseqent fatigue damage in carbon fibre laminates. Int. J. of Fatigue, 6 (1984), pp113-117.

24. Bradshaw F.J. Dorey G. and Sidey G.R. Impact resitance of C.F.R.P. RAE TR 72240 (1972).

25. Shen Le-tian, Zhao Shi-da and Bai Yi-long. Threshold and some microscopic observations of spallation of phenolic-resin based woven roving glass fibre reinforced composite materials. Int.J. of Impact Engineering, 2 (1985), pp169-178.

26. Roylance D. Stress wave damage in graphite-epoxy laminates. J. of Composite Materials, 14 (1980), pp111-119.

27. Adams D.F. and Perry J.L. Low level impact response of graphite-epoxy hybrid composites. J. of Engineering Materials and Technology, 20 (1977), pp257-263.

28. Adams D.F. and Perry J.L. The static and impact behaviour of graphite-epoxy laminates containing third phase reinforcement materials. J. Testing and Evaluation, 5 (1977), pp114-123.

29. Beaumont P.W.R. Fracture mechanisms in fibrous composites. Proc. of Fracture Mechanics Conf. Cambridge 1979, paper 9.

30. Phillips D.C. The fracture energy of carbon fibre reinforced glass. J. of Materials Science, 7 (1972), pp1175-1191.

31. Beaumont P.W.R. and Server W.L. Some observations on the dynamic fracture behaviour of carbon-fibre strengthened epoxy resin. ASTM STP 580 (1976), pp443-457.

32. Toland R.H. Impact testing of carbon-epoxy composite materials. ASTM STP 563 (1975), pp133-145.

33. Chamis C.C. Hanson P. and Serafini T.T. Impact resistance of unidirectional fibre composites. NASA TN-D 6463 (1971).

34. Phillips D.C. and Tetelman A.S. The fracture toughness of fibre composites. Composites, Vol 3 (1972), pp216-223.

35. Suarez J.A. and Whiteside J.B. Comparison of residual strength of composite and metal structures after ballistic damage. ASTM STP 568 (1975), pp72-91.

36. Husman G.E. Whitney J.M. and Halpin J.C. Residual strength characterization of laminated composites subjected to impact loading. ASTM STP 568 (1975), pp92-113.

37. Butcher B.R. The dynamic notch toughness of fibre composites, part 2. Composites, 7 (1976), pp81-87.

38. Oplinger D.W. and Slepetz J.M. Impact damage tolerance of graphite-epoxy sandwich panels. ASTM STP 568 (1975), pp30-48.

39. Cantwell W.J. Curtis P.T. and Morton J. An assessment of the impact performanace of CFRP reinforced with high strain carbon fibres. To be published in Composite Science and Technology.

40. Curtis P.T. An initial evaluation of a high strain carbon fibre reinforced epoxy. RAE TR 84004 (1984).

41. Rich G. and Bunsell A.R. The behaviour of boron-aluminium composites during and after impact. J. Materials Science, 14 (1979), pp2373-2383.

42. Rogers K.F. Sidey G.R. and Kingston-Lee D.M. Ballistic impact resistance of carbon fibre laminates. Composites, 2 (1971), pp237-241.

43. Lee R.J. and Phillips D.C. The damage tolerance of high performance composites, Composite Structures 1, Marshall I H. (Ed.), Elsevier Applied Science Publishers, pp536-554, (1981).

44. Williams J.G. Rhodes M.D. and Starnes J.H. Effect of resin on impact tolerance of graphite-epoxy laminates. ASTM STP 787 (1982), pp450-480.

45. Dorey G. Impact and crashworthiness of composite structures. In Structural Impact and Crashworthiness 1, G.A.O. Davies (Ed.). Elsevier Applied Science Publishers (1984).

46. Cantwell W.J. An investigation into the impact resistance of CFRP. M.Sc. thesis, Imperial College, London 1982.

47. Ross C.A. and Sierakowski R.L. Studies on the impact resistance of composite plates. Composites, 4 (1973), pp157-161.

48. Bishop S.M. The significance of defects on the failure of fibre composites. Presented to the Structures and Materials Panel, AGARD, 1983.

49. Kellas. S. Tension-compression fatigue performance of notched orthotropic CFRP laminates. M.Sc. thesis, Imperial College, London 1984.

50. Harris B. and Bunsell A.R. Impact properties of glass/carbon fibre hybrid composites. Composites, 6 (1975), pp197-201.

51. Helfinstine J. Charpy impact of unidirectional graphite aramid epoxy hybrid composites. ASTM STP 617 (1977), pp375-388.

52. Stellbrink K.K. On the behaviour of impact damaged CFRP laminates. Fibre Science and Technology, 18 (1983), pp95-108.

53. Dorey G. Sidey G.R. and Hutchings J. Impact properties of carbon fibre/kevlar hybrid composites. Composites, 9 (1978), pp25-32.

54. Stellbrink K.K. and Aoki R.M. Effect of defects on the behaviour of composites. Proc. ICCM 4, Tokyo 1982, pp853-860.

55. Olster E.F. and Roy P.A. Tolerance of advanced composites to ballistic impact damage. ASTM STP546 (1974), pp583-603.

56. Butcher B.R. The dynamic notch toughness of fibre composites, part 1. Composites, 7 (1976), pp12-16.

57. Sarma A.V. Low velocity impact tests on fibrous composite sandwich structures. ASTM STP 734 (1981), pp54-70.

58. Rhodes M. Impact tests on fibrous composite sandwich structures. NASA TM 78719 (1978).

59. Cantwell W.J. Curtis P.T. and Morton J. A study of the impact resistance and subsequent 0-compression fatigue performance of non-woven and mixed-woven composites. Structural Impact and Crashworthiness 2, J. Morton (Ed.), Elsevier Applied Science Publishers, pp521-531, 1984.

60. Adams D.F. and Perry J.L. Instrumented Charpy impact tests of several unidirectional composite materials. Fibre Science and Technology, 8 (1983), pp275-302.

61. Broutman L.J. and Rotem A. Impact strength and toughness of fibre composite materials. ASTM STP 568 (1975), ppl14-133.

62. Demuts. E. Whitehead D.S. and Deo R.B. Assessment of the damage tolerance in composites. Presented at the Conf. on Structural Impact and Crashworthiness, London, 1984.

63. Avery J.G. Fracture control in ballistically damaged graphite-epoxy wing structures. ASTM STP 743 (1981), pp338-359.

64. Dorey G. Damage tolerance in advanced composite materials. Presented at the AHS/NASA conf. on helicopter structures, paper 13, 1972.

65. Freeman S.M. Damage propagation in graphite-epoxy by a deplying technique. AFWAL TR 81 3157 (1981).

66. Greszczuk L.B. Response of composite materials to particle impact. ASTM STP 568 (1975), ppl83-209.

67. McQuillen E. Gause L. and Llorens R. Low velocity transverse normal impact of graphite composite laminates. J. Composite Materials, 10 (1976), pp79-91.

68. Caprino G. Crivelli I. and Di Ilio A. Elastic behaviour of composite structures under low velocity impact. Composites, 15 (1984), pp231-234.

69. Harding J. and Welsh L.M. A tensile testing technique for fibre reinforced composites at impact rates of strain. J. Materials Science, 18 (1983), pp1810-1826.

70. Buskell N. The post-buckling behaviour of carbon fibre reinforced plastic. Ph.D. thesis in preparation, Imperial College, London 1985.

71. High temperature prepregs of unidirectional carbon, glass and aramid fibre. Ciba Geigy Inf. sheet FTA49D (1981).

72. Love A.E.H. The stress produced in a semi-infinite body by pressure on part of the boundary. Proc. of the Royal Society, 118 A667 (1929), pp377-420.

73. Elber W. Failure mechanics in low velocity impacts on thin composite plates. NASA TP2152 (1983).

74. Owen M.J. and Bishop P.T. Critical stress intensity factor applied to glass reinforced polyester resin. J. Composite Materials, 5 (1971), pp146-159.

75. Kellas S. Morton J. and Bishop S.M. Fatigue damage development in a notched carbon fibre composite. Proc. of ICCM 5, San Diego 1985.

76. Whitney J.M. and Browning C.E. Materials characterization for matrix dominated failure modes. ASTM STP 836 (1984), pp104-124.

77. Waddoups M.E. Eisenmann J.R. and Kaminski B.E. Macroscopic fracture mechanisms of advanced composite materials. J. Composite Materials, 5 (1981), pp446-454.

78. Nuismer R.J. and Whitney J.M. Uniaxial failure of composites containing stress concentrations. ASTM STP 593 (1975), pp117-142.

79. Nuismer R.J. and Labor J.D. Applications of the average stress failure criterion: Part 1 tension. J. Composite Materials, 12 (1978), pp238-252.

80. Nuismer R.J. and Labor J.D. Applications of the average stress criterion: Part 2 compression. J. Composite Materials, 13 (1979), pp49-60.

81. Kubo T. and Nelson R.B. Analysis of impact stresses in composite plates. ASTM STP 568 (1975), pp228-244.

82. Sun C.T. and Sierakowski R.L. Studies on impact structural damage of composite blades. ASTM STP 568, pp212-227.

83. Preston J.L. and Cook T.S. Impact response of graphite-epoxy flat laminates using projectiles that simulate aircraft engine encounters. ASTM STP 568 (1975), pp49-71.

84. Recht R.F. and Ipson T.W. Ballistic perforation dynamics. J. Applied Mechanics, 30 (1963), pp384-390.

85. Backman M.E. and Goldsmith W. The mechanics of perforation of projectiles into targets. Int. J. Engineering Science, 16 (1978), pp1-99.

86. Awerbuch A. and Bodner S.R. Analysis of the mechanics of perforation of projectiles in metallic plates. Int. J. Solids and Structures, 10 (1974), pp671-684.

87. Shadbolt R.J Corran R.S.J. and Ruiz C. A preliminary investigation of plate perforation in the sub-ordnance range, 1. single layer taregts. Univ. of Oxford Engineering Sciences report.

88. Kolsky H. Stress waves in solids-new edition. Dover publications 1963.

89. Conrad H. A method of calculating energy losses during impact. J. Applied Mechanics, 6 (1939).

90. Djahansouzi B. Private communication.

Table 1.

Details of Laminates Used in Test Programme

Laminate	No. of plies	Thickness (mm)
$(+/-45)_2$	4	0.5
$((+/-45)_2)_s$	8	1.0
$((+/-45)_4)_s$	16	2.0
$((+/-45)_8)_s$	32	4.0
$(0,+/-45,0)_s$	8	1.0
$((0,0,+/-45)_2)_s$	16	2.0

Table 2.

Material Properties for the XAS-914C System

Longitudinal tensile modulus	135 GPa
Transverse tensile modulus	8 GPa
Major Poissons ratio ν_{12}	0.31
Shear modulus G_{12}	5.9 GPa
Longitudinal tensile strength	1300 MPa
Transverse tensile strength	78 MPa
Longitudinal tensile failure strain	0.012
Transverse tensile failure strain	0.007
Longitudinal compression failure strain	0.011

Table 3.

Prediction of first damage in beam coupons.

Drop-weight Impact.

Laminate	Predicted damage Threshold (Joules)	Location	Experimental Threshold (Joules)	Location
4 ply (+/-45)	0.29	L/S	0.22	L/S
8 ply (+/-45)	0.58	L/S	0.63	L/S
16 ply (+/-45)	1.6	L/S	1.20	L/S
32 ply (+/-45)	0.62	T/S	0.87	T/S
64 ply (+/-45)	0.18	T/S	0.48	T/S
8 ply (0,+/-45)	0.9	T/S	1.00	L/S
16 ply (0,+/-45)	1.48	T/S	1.61	T/S
32 ply (0,+/-45)	0.37	T/S	0.51	T/S

T/S = Top surface L/S = Lower surface

Table 4.

Fibre fracture thresholds for composite beams

Laminate	Predicted (Joules)	Experimental (Joules)
4 ply (+/-45)	1.1	0.6
8 ply (+/-45)	2.45	1.25
16 ply (+/-45)	3.04	1.28
8 ply (0,+/-45)	0.96	1.00
16 ply (0,+/-45)	2.01	1.71

Table 5.

Drop-Weight Perforation thresholds of composite beams

Laminate	Predicted (Joules)	Experimental (Joules)
4 ply (+/-45)	1.33	1.50
8 ply (+/-45)	3.66	3.22
16 ply (+/-45)	7.83	7.35
32 ply (+/-45)	29.9	25.50
8 ply (0,+/-45)	3.5	2.9
16 ply (0,+/-45)	7.48	6.6

Table 6

Drop-Weight Damage Thresholds in Circular Composite Plates.

Laminate	Experiment (Joules)	Theoretical (Joules)
4 ply (+/-45)	0.24	0.29
8 ply (+/-45)	0.46	0.54
16 ply (+/-45)	1.30	1.50
8 ply (0,+/-45)	0.37	0.42
16 ply (0,+/-45)	0.75	1.24

Table 7.

Drop-Weight Perforation Thresholds in Circular Composite Plates.

Laminate	Experiment (Joules)	Theoretical (Joules)
4 ply (+/-45)	0.91	0.7
8 ply (+/-45)	3.1	2.55
16 ply (+/-45)	8.25	8.0
32 ply (+/-45)	-	-
8 ply (0,+/-45)	3.0	2.6
16 ply (0,+/-45)	7.45	8.15

Table 8.

Damage Constants Used in the LEFM, Waddoup's, Point Stress and Average stress Failure Models

L.E.F.M.	K_{1c}	56.1 MPa$\sqrt{m}$
	b_0	0.75 mm
Waddoup's	α	0.80 mm
Average Stress	a_0	1.95 mm
Point Stress	d_0	2.40 mm

Table 9.

Ballistic Perforation Thresholds in Composite Beams

Laminate	Experiment (Joules)	Predicted (Joules)
4 ply (+/-45)	1.2	1.47
8 ply (+/-45)	2.7	3.2
16 ply (+/-45)	7.8	7.45
32 ply (+/-45)	24.2	28.5
8 ply (0,+/-45)	3.2	3.85
16 ply (0,+/-45)	6.7	7.45

Table 10.

Ballistic Damage Thresholds in the Circular Composite Plates

Laminate	Experiment (Joules)	Location
4 ply (+/-45)	0.13	L/S
8 ply (+/-45)	0.14	L/S
16 ply (+/-45)	0.36	L/S
32 ply (+/-45)	0.26	T/S
8 ply (0,+/-45)	0.16	L/S
16 ply (0,+/-45)	0.30	T/S

Table 11.

Ballistic Perforation Thresholds in Circular Composite Plates

Laminate	Experiment (Joules)	Predicted (Joules)
4 ply (+/-45)	1.4	1.6
8 ply (+/-45)	2.6	3.1
16 ply (+/-45)	6.05	7.2
32 ply (+/-45)	-	-
8 ply (0,+/-45)	2.5	2.42
16 ply (0,+/-45)	6.8	7.3

Table 12

Comparison of the Damage Thresholds in Composite Beams After Low and High Velocity Impact

Laminate		L.V. (Joules)	H.V. (Joules)
4 ply	(+/-45)	0.22	0.17
8 ply	(+/-45)	0.63	0.40
16 ply	(+/-45)	1.20	0.61
32 ply	(+/-45)	0.87	0.37
8 ply	(0,+/-45)	1.00	0.36
16 ply	(0,+/-45)	1.61	0.40

L.V. = Low Velocity H.V. = High Velocity

Table 13

Comparison of the Perforation Thresholds in Composite Beams After Low and High Velocity Impact

Laminate		L.V. (Joules)	H.V. (Joules)
4 ply	(+/-45)	1.50	1.2
8 ply	(+/-45)	3.22	2.7
16 ply	(+/-45)	7.35	7.8
32 ply	(+/-45)	25.50	24.2
8 ply	(0,+/-45)	2.9	3.2
16 ply	(0,+/-45)	6.6	6.7

L.V. = Low Velocity H.V. = High Velocity

STRENGTH COMPARISON WITH CONVENTIONAL AIRCRAFT MATERIALS
FROM SHARPLES (1)

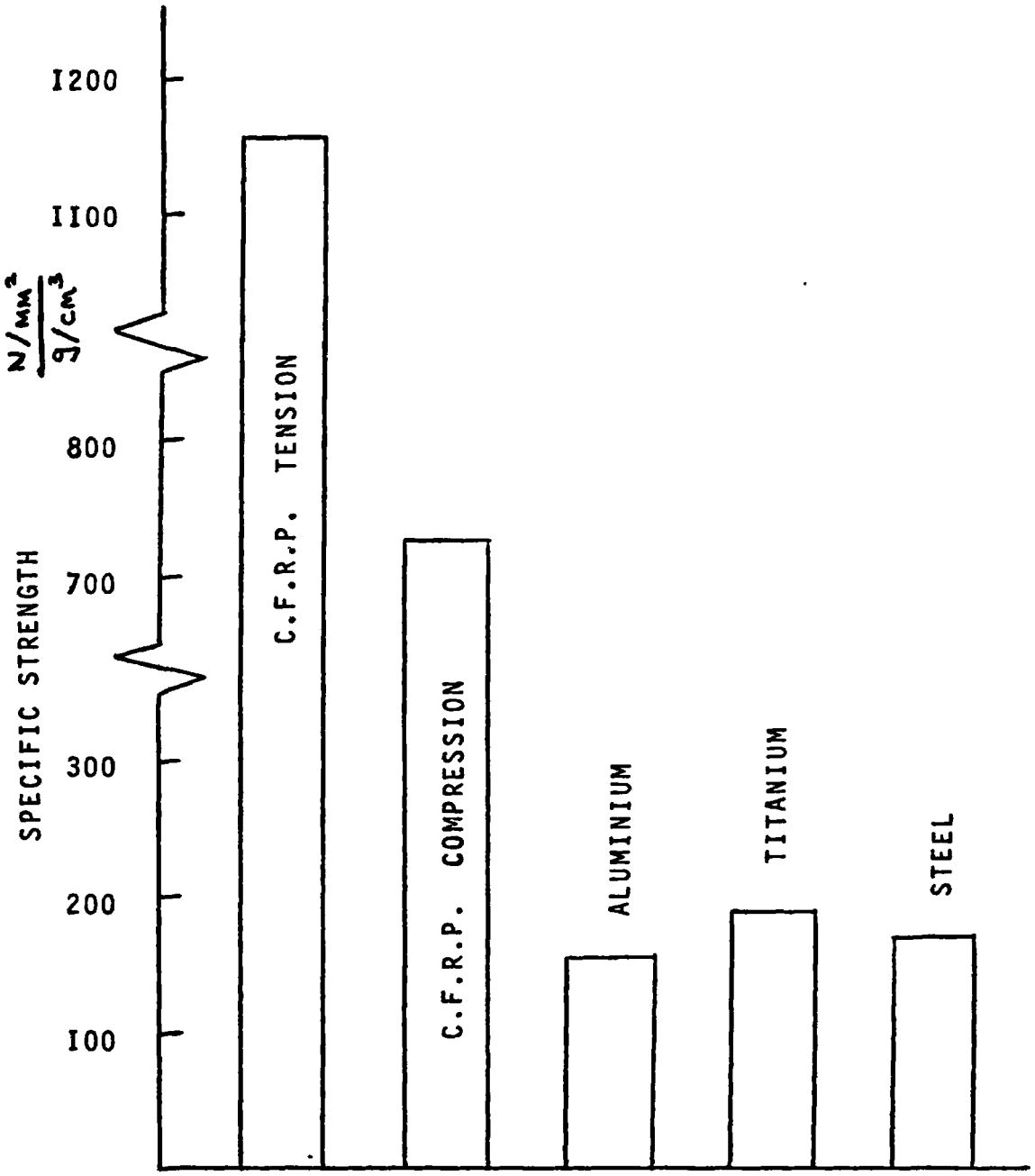
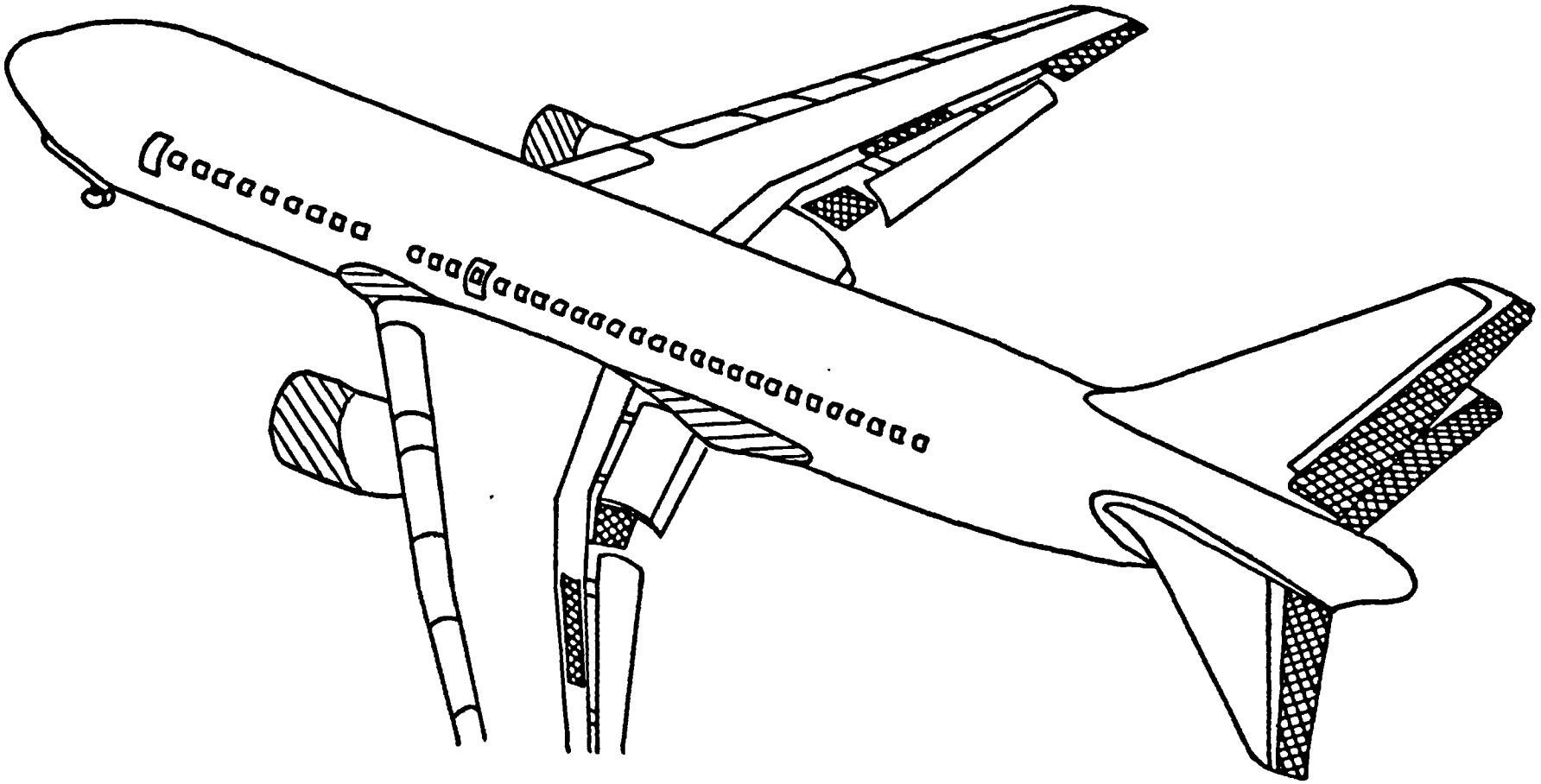


Figure 1

Figure 2



C.F.R.P.

HYBRID

BOEING 767 EMPLOYS COMPOSITES EXTENSIVELY IN ITS STRUCTURE

THE VARIATION OF RESIDUAL COMPRESSIVE STRENGTH WITH IMPACT ENERGY

SIXTEEN PLY $(+/-45,0_2,-/+45,0_2)$ (18)

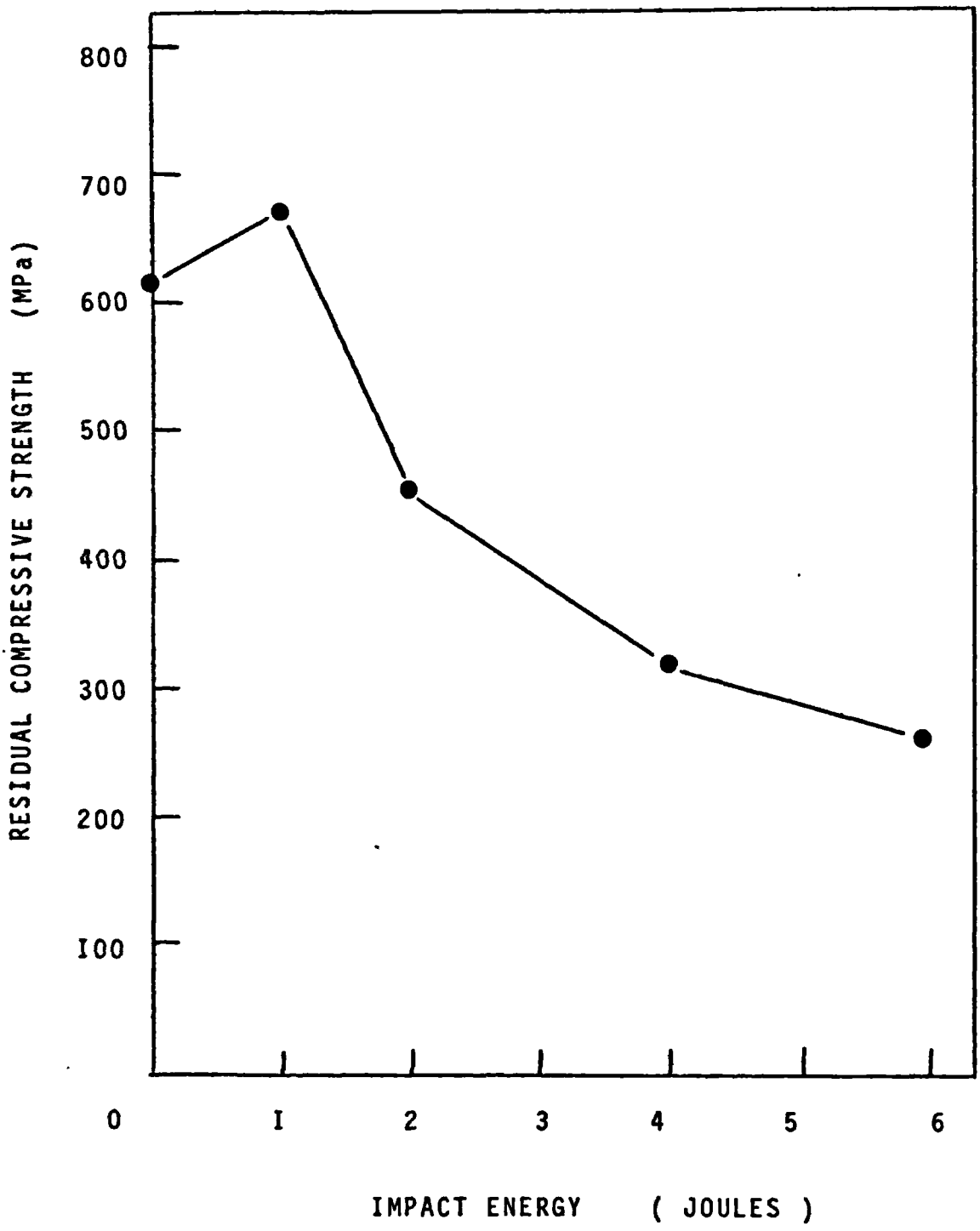


Figure 3

THE VARIATION OF RESIDUAL TENSILE STRENGTH WITH IMPACT ENERGY

SIXTEEN PLY $(+/-45,0_2,-/+45,0_2)$ (23)

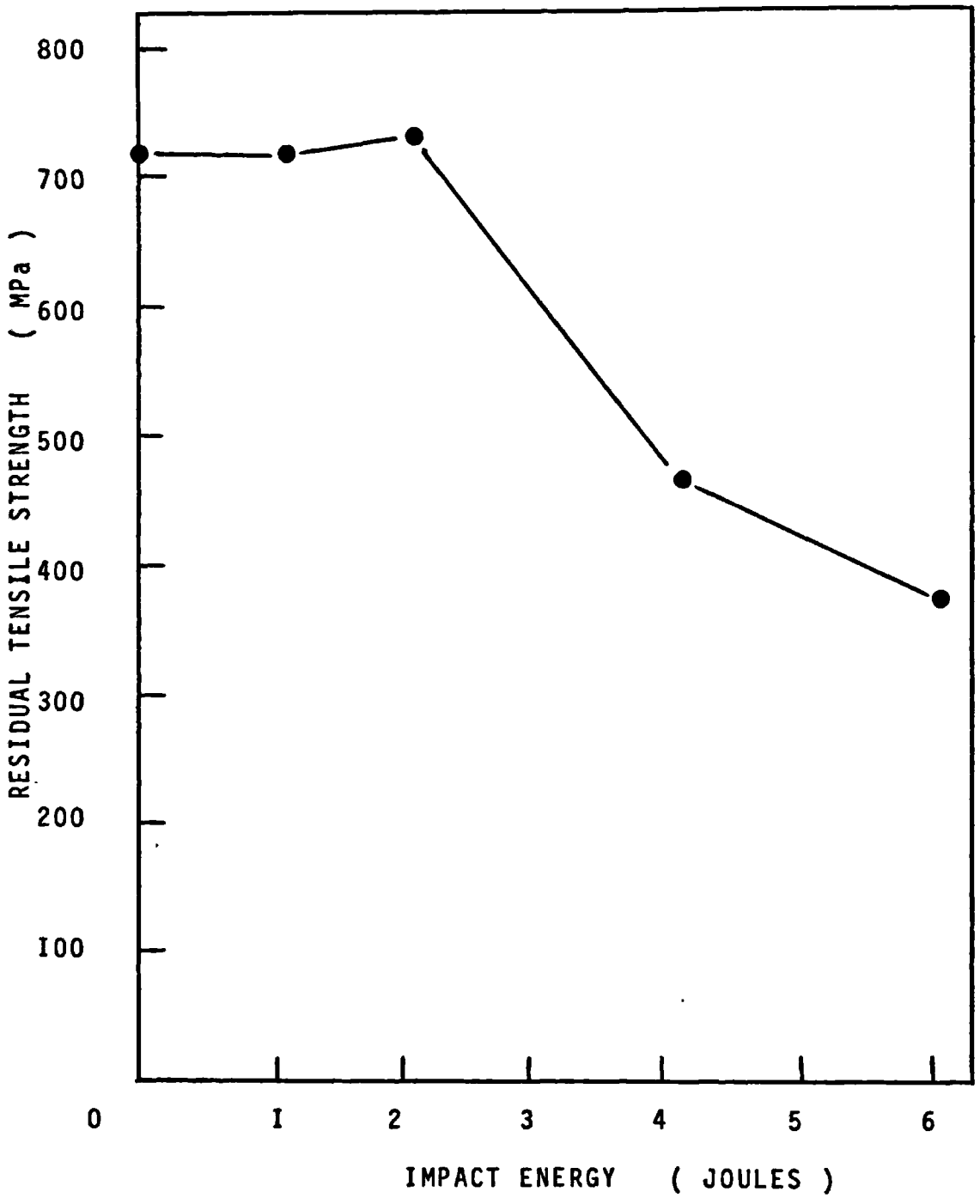


Figure 4

A COMPARISON OF THE RESIDUAL TENSILE STRENGTHS OF HIGH STRAIN TO FAILURE COMPOSITES WITH A CONVENTIONAL LAMINATE

SIXTEEN PLY (0,+/-45) COMPOSITE (39)

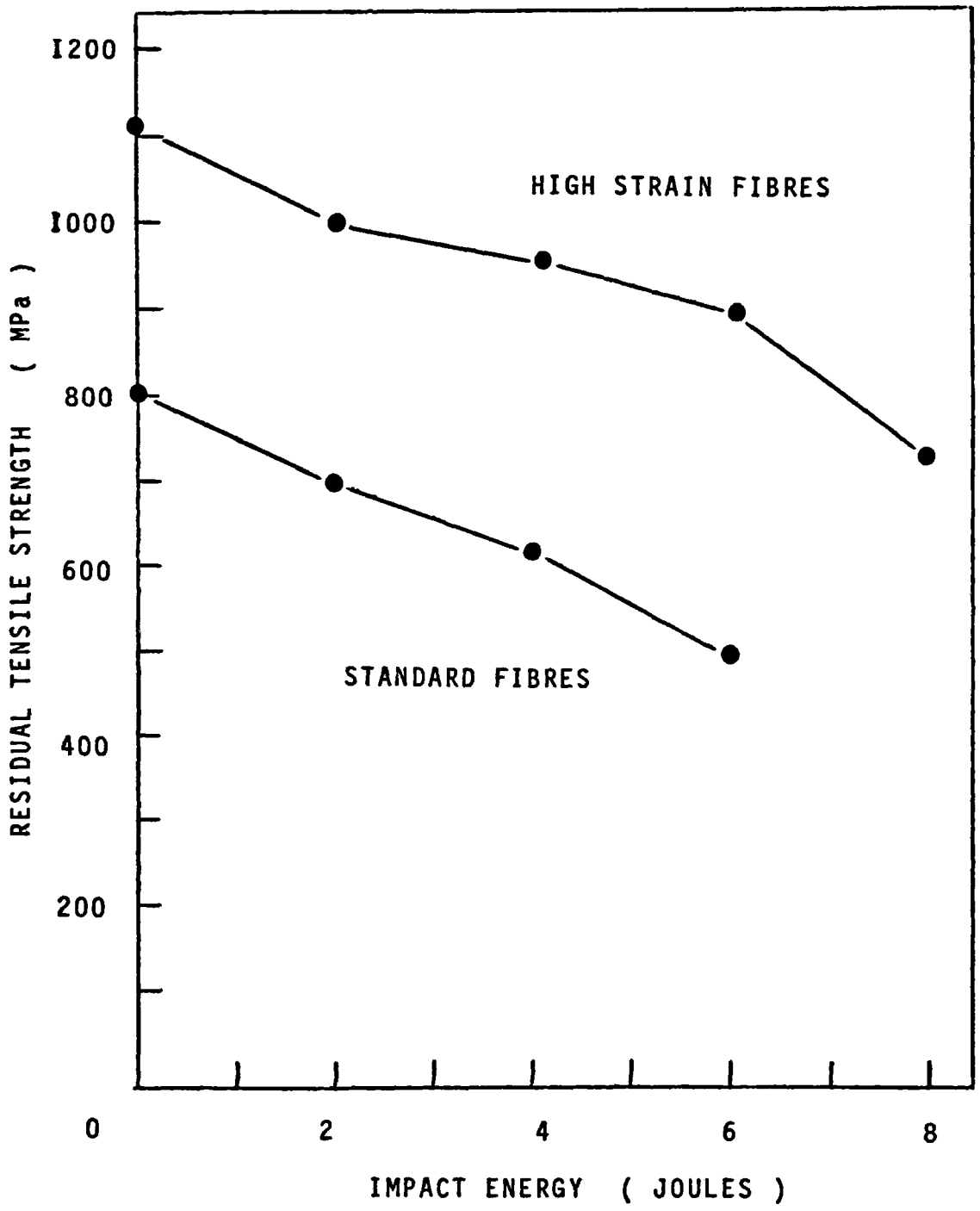


Figure 5a

A COMPARISON OF THE RESIDUAL COMPRESSIVE STRENGTHS OF A HIGH STRAIN TO FAILURE COMPOSITE WITH A CONVENTIONAL LAMINATE

SIXTEEN PLY (0,+/-45) COMPOSITE (39)

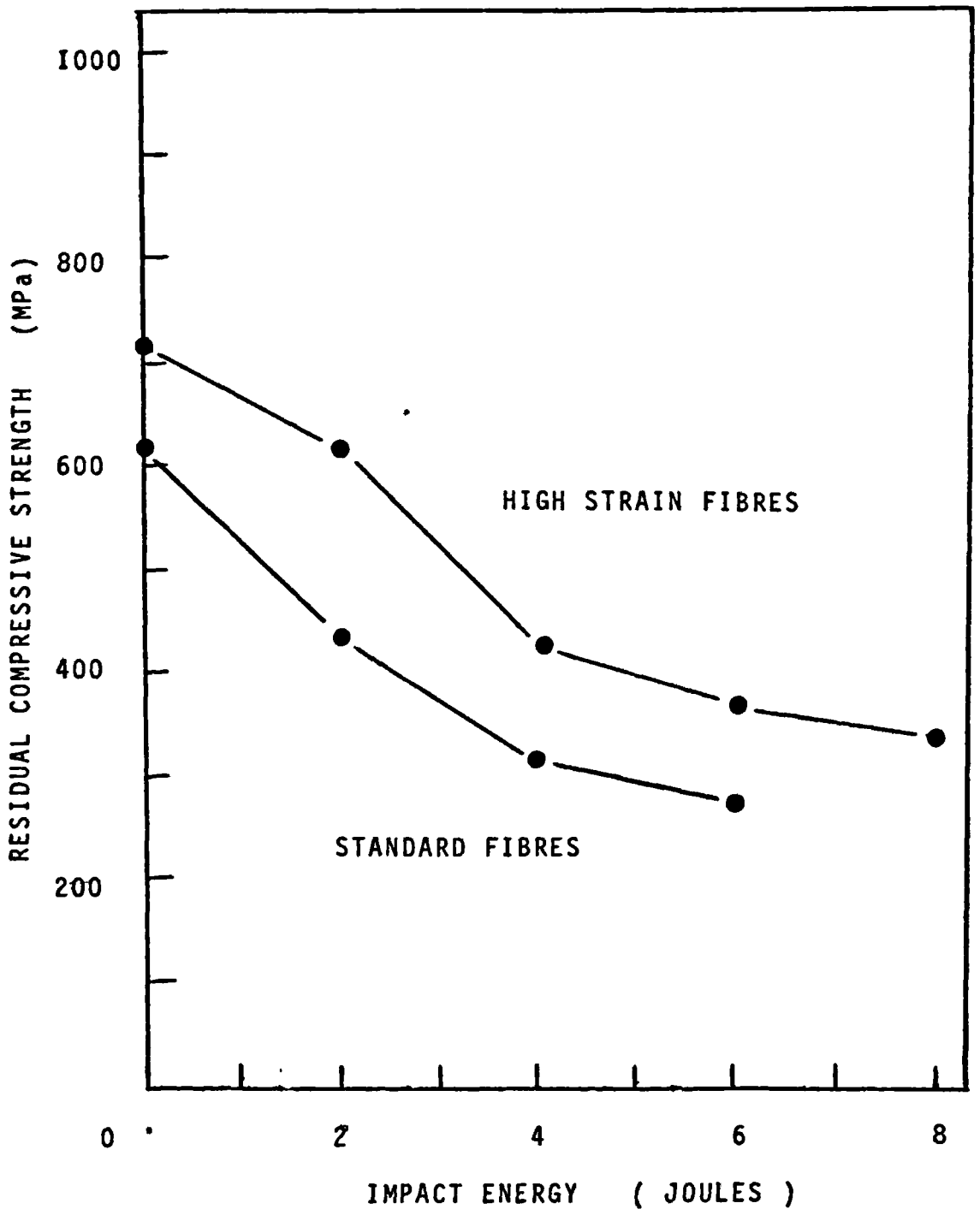


Figure 5b

ULTRASONIC C-SCANS SHOWING THE EFFECT OF INCREASING THE STRAIN TO FAILURE OF THE COMPOSITE MATRIX ON IMPACT RESISTANCE (5)

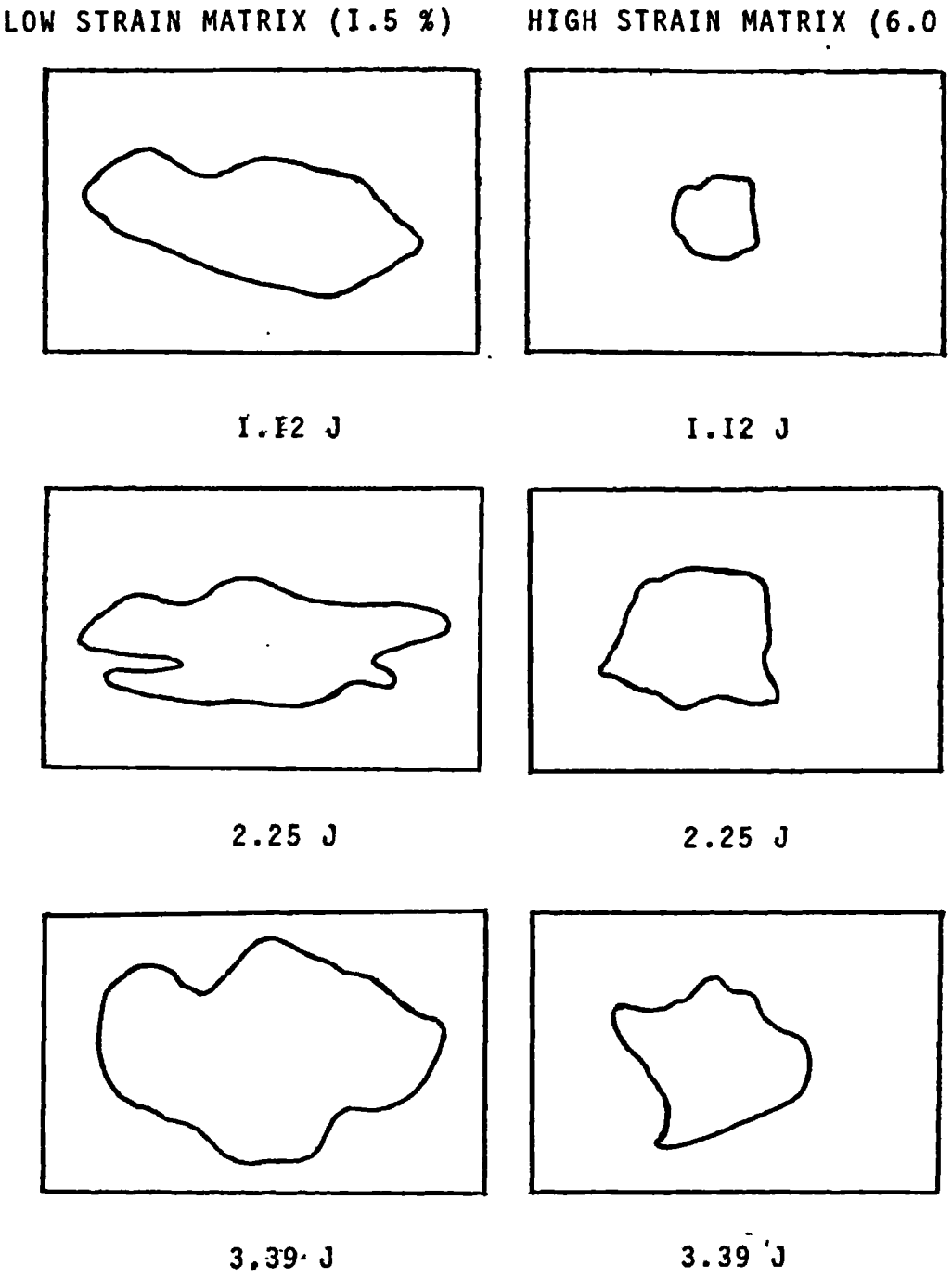


Figure 6

FIGURE SHOWING THE EFFECT OF FIBRE STACKING SEQUENCE ON POST DROP WEIGHT IMPACT RESIDUAL STRENGTH. (46)

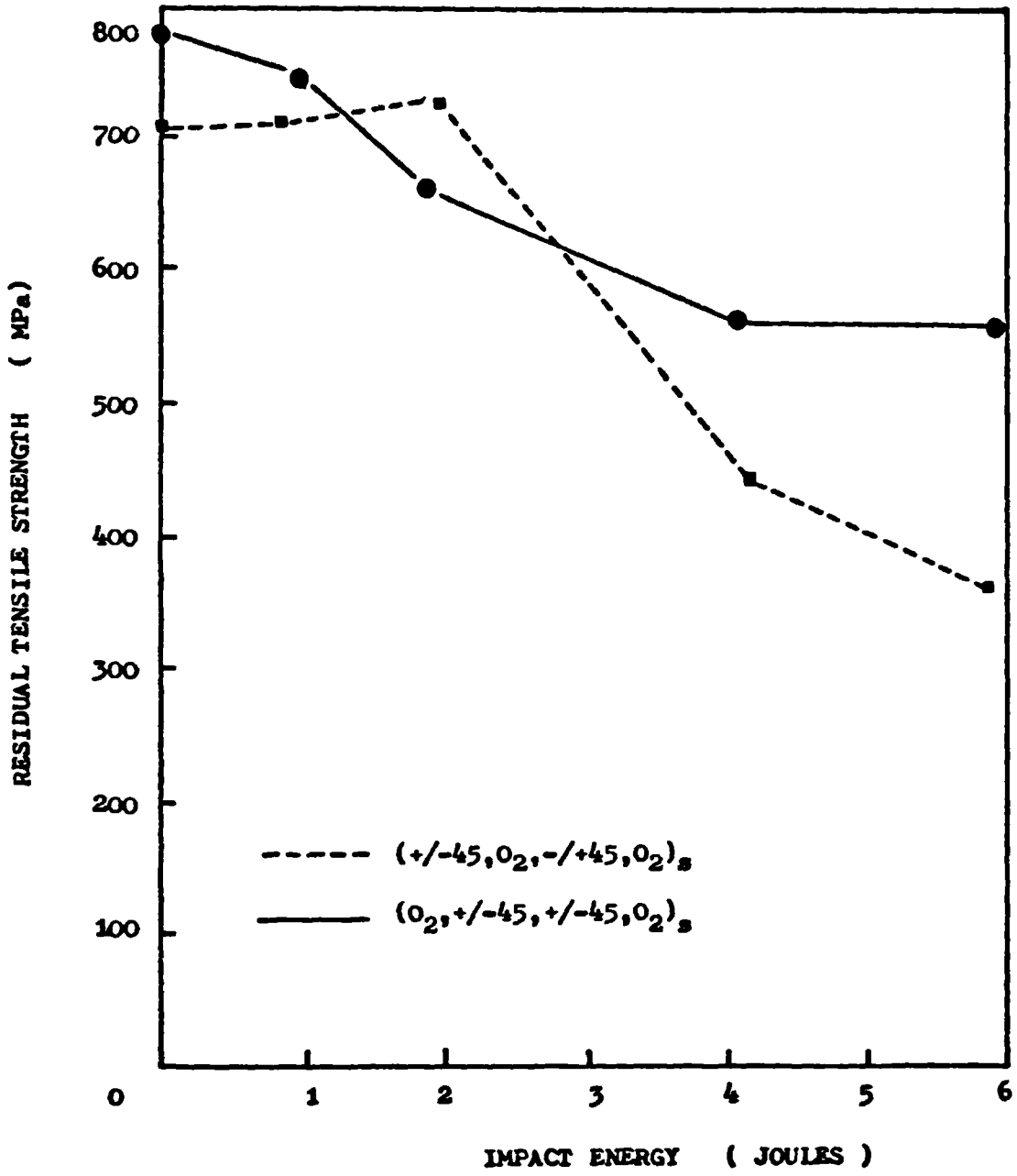
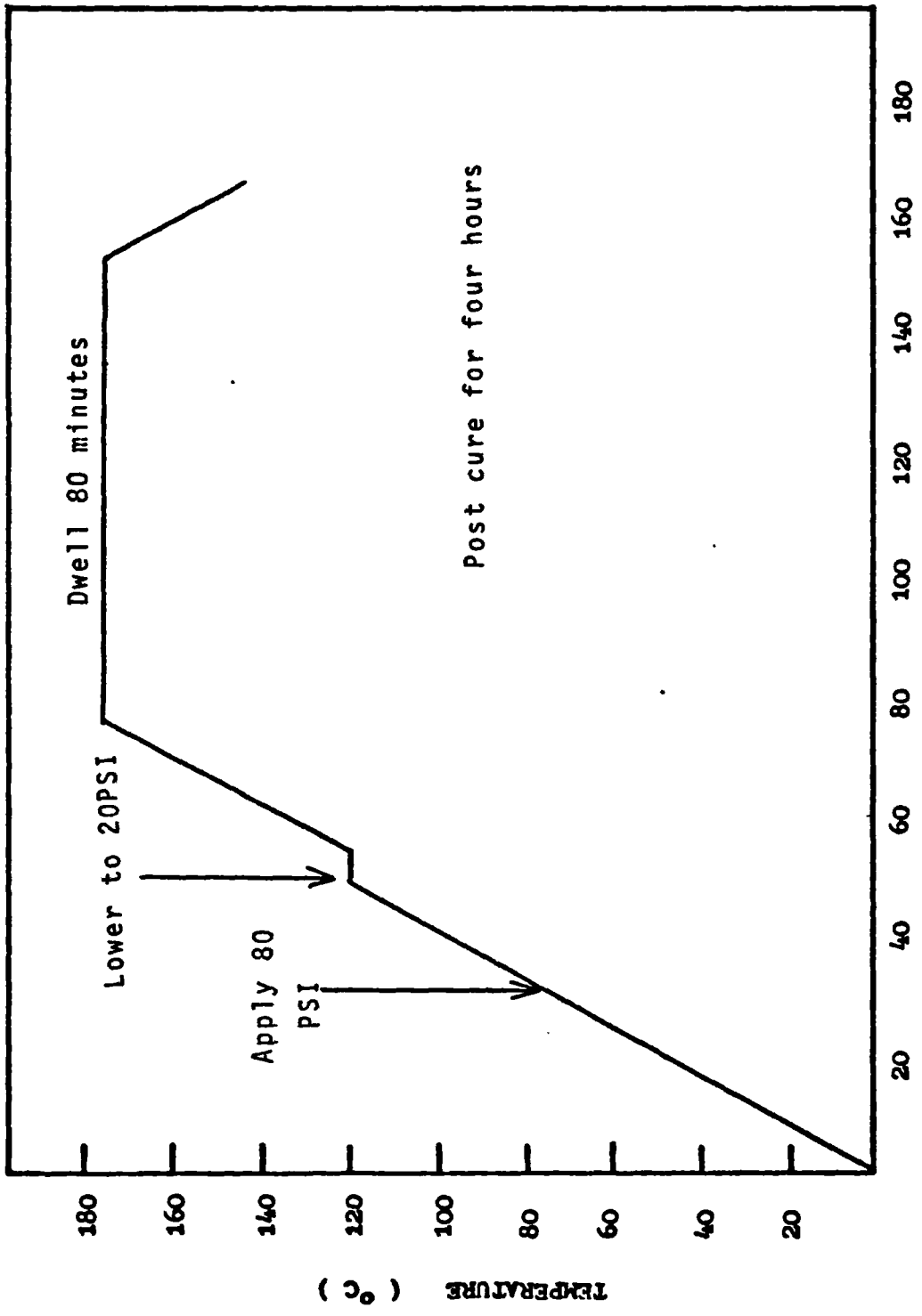
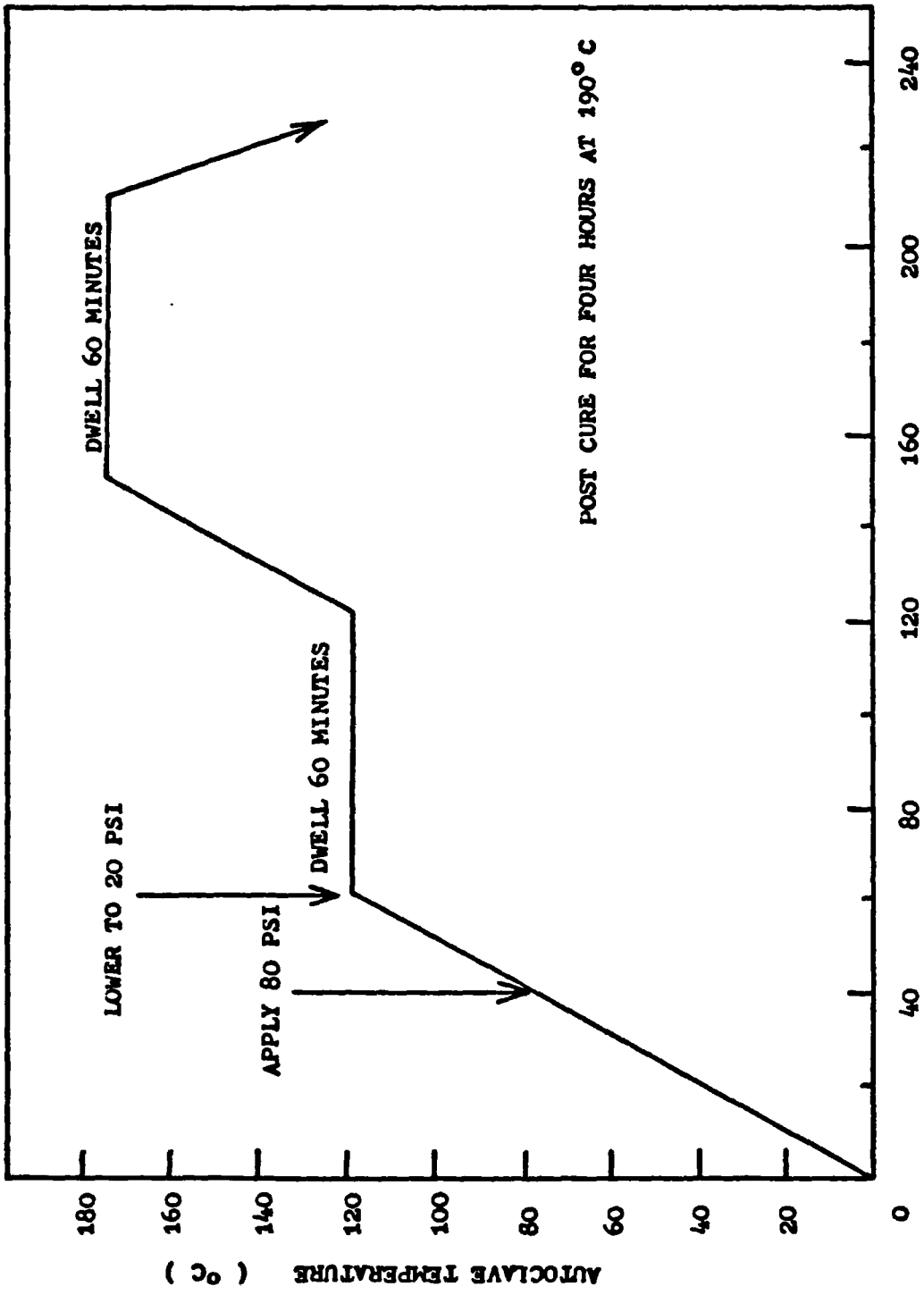


Figure 7



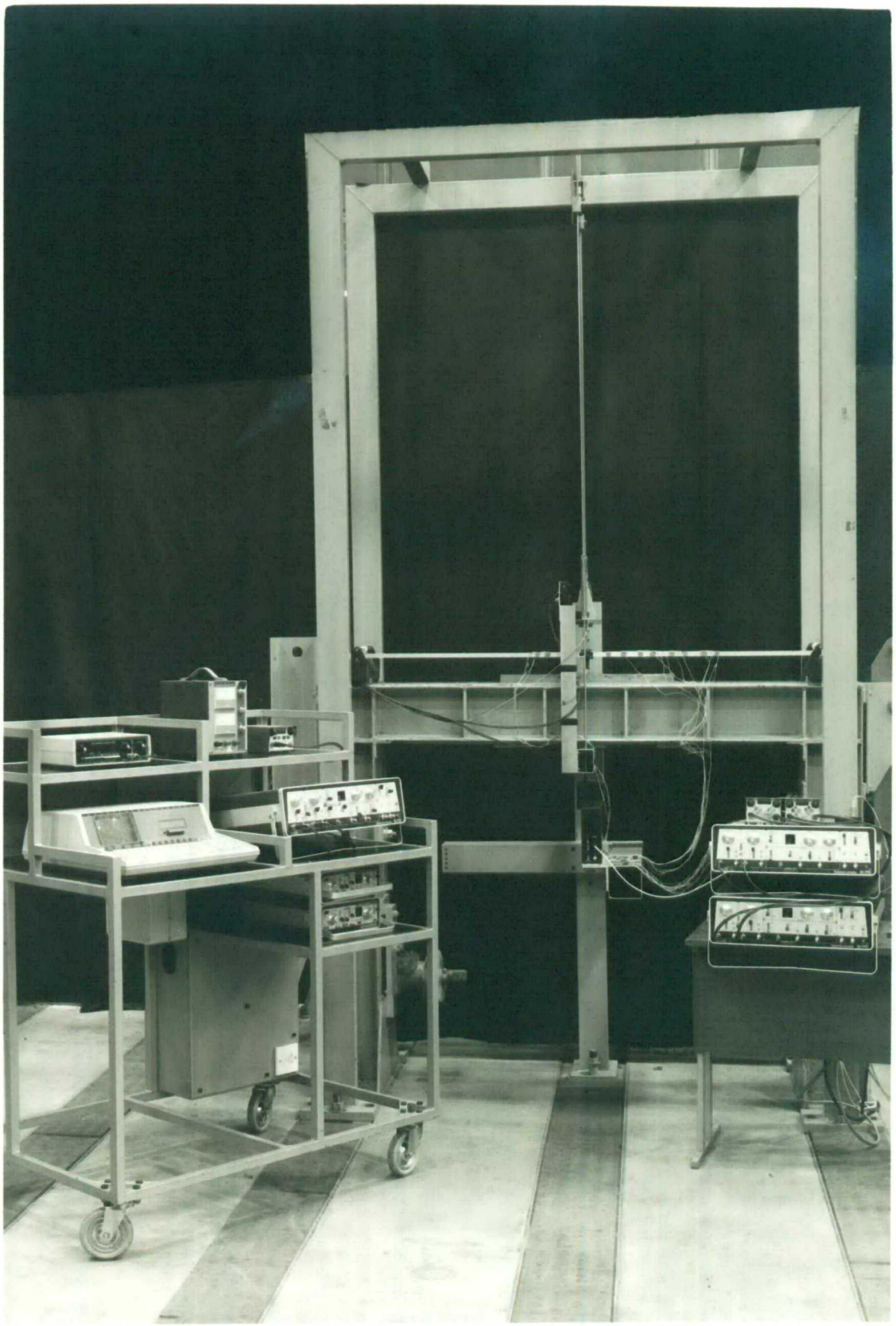
DETAILS OF THE CURE CYCLE FOR THE XAS 914C SYSTEM

Figure 8



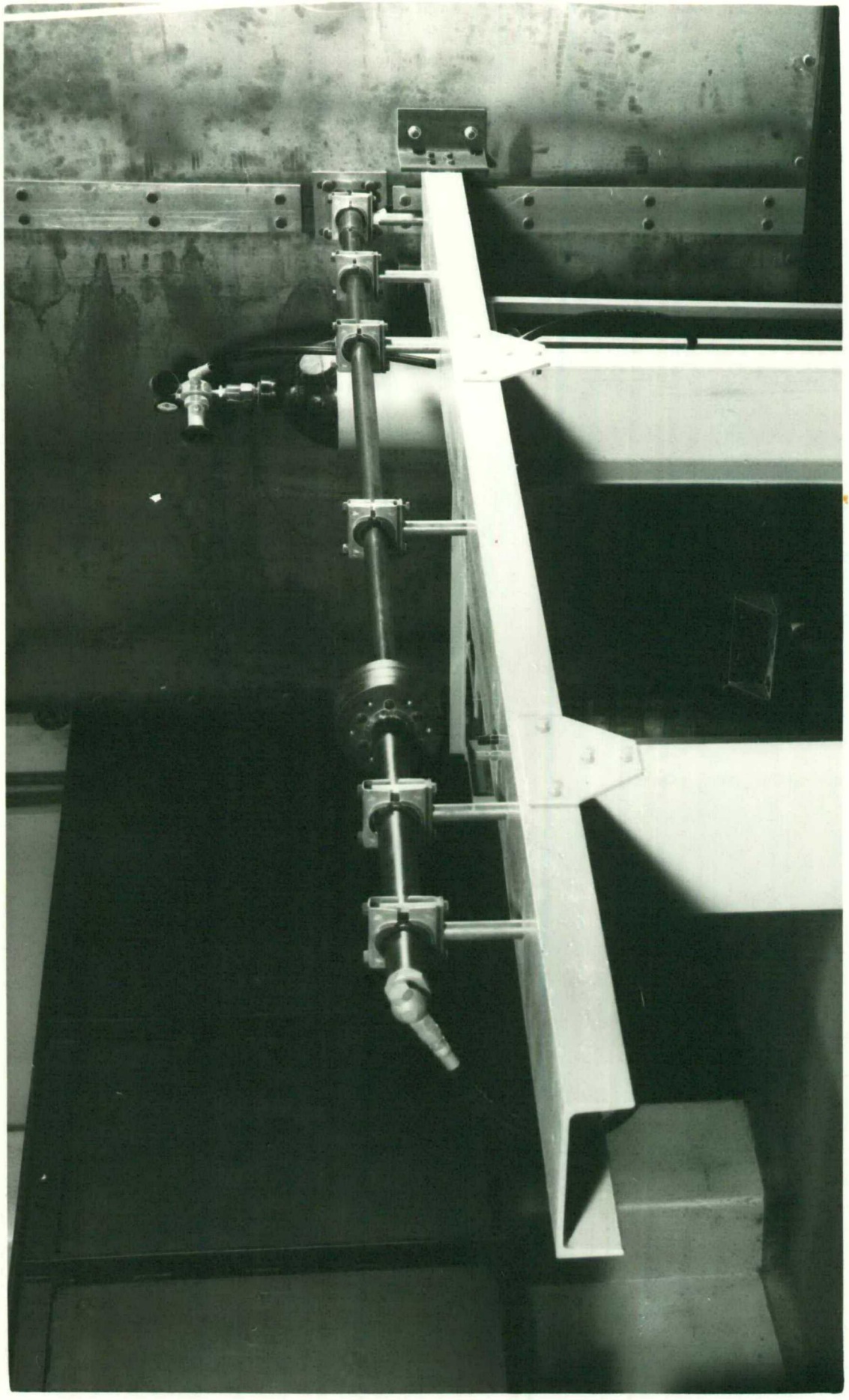
THE CURE CYCLE FOR THE SIXTY FOUR PLY (+/-45) COMPOSITE

Figure 9



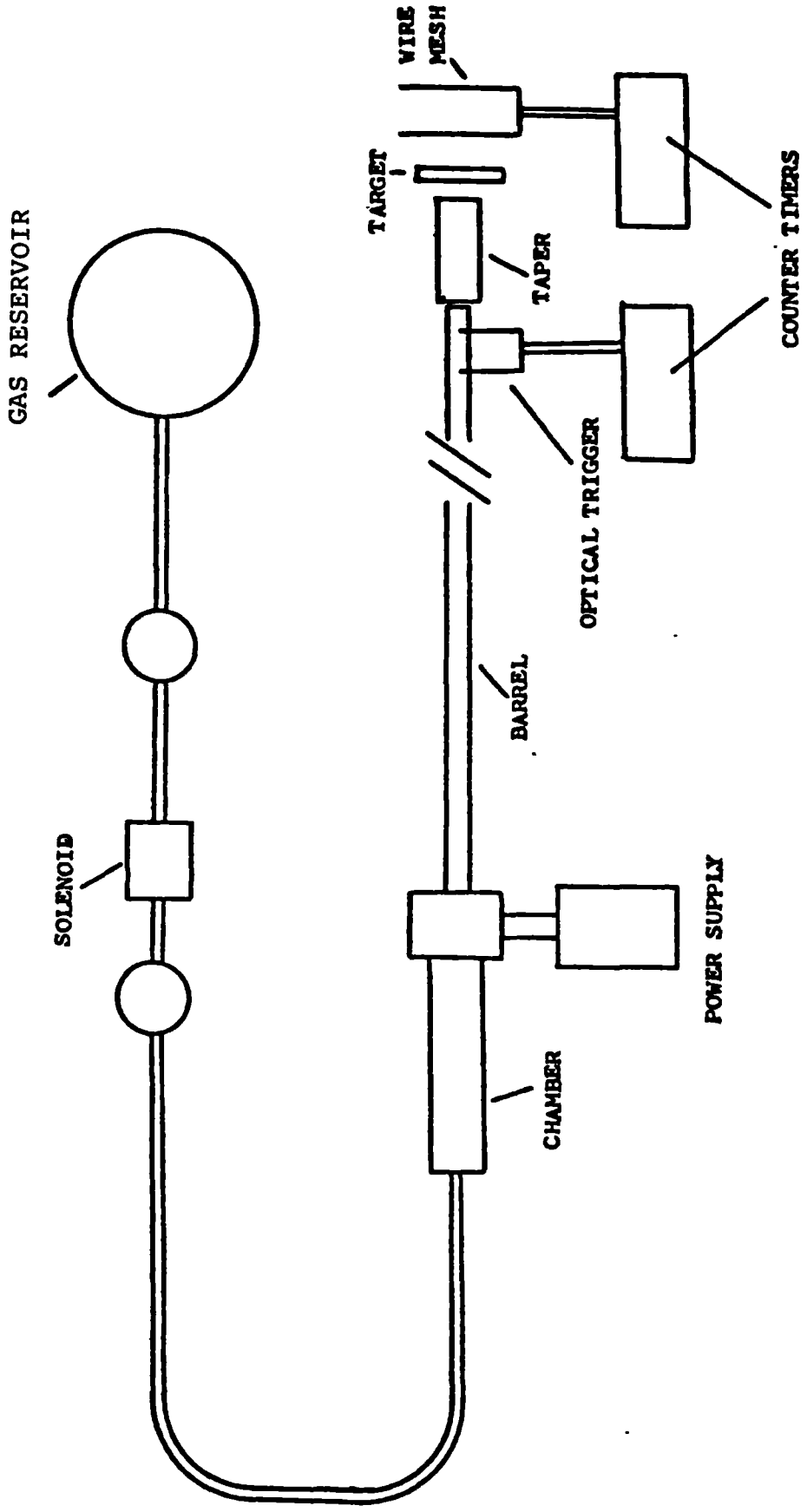
THE DROP-WEIGHT IMPACT RIG

Figure 10



THE HIGH VELOCITY GAS GUN

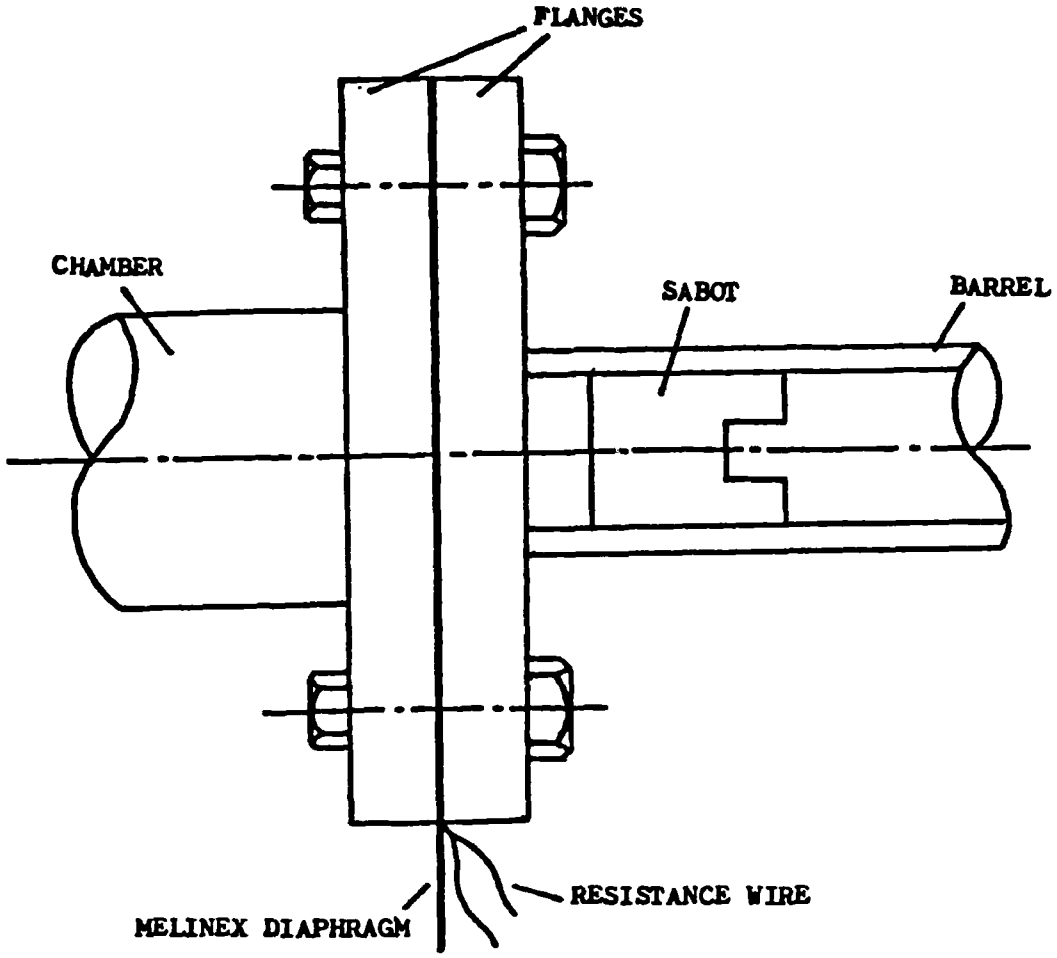
Figure 11



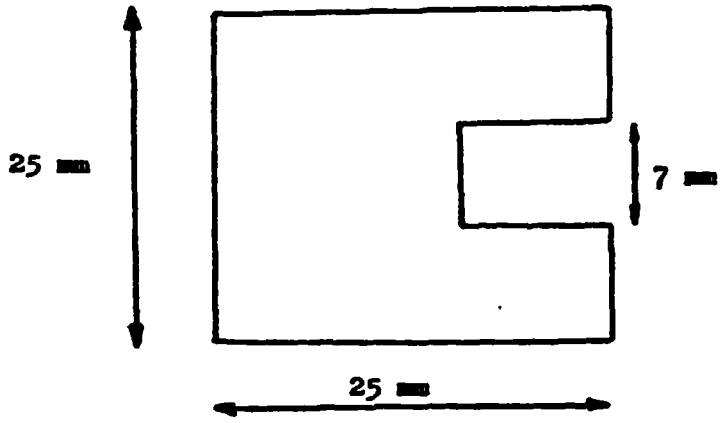
SCHEMATIC REPRESENTATION OF THE GAS GUN AND ACCESSORIES

Figure 12

DETAILS OF THE GAS GUN.

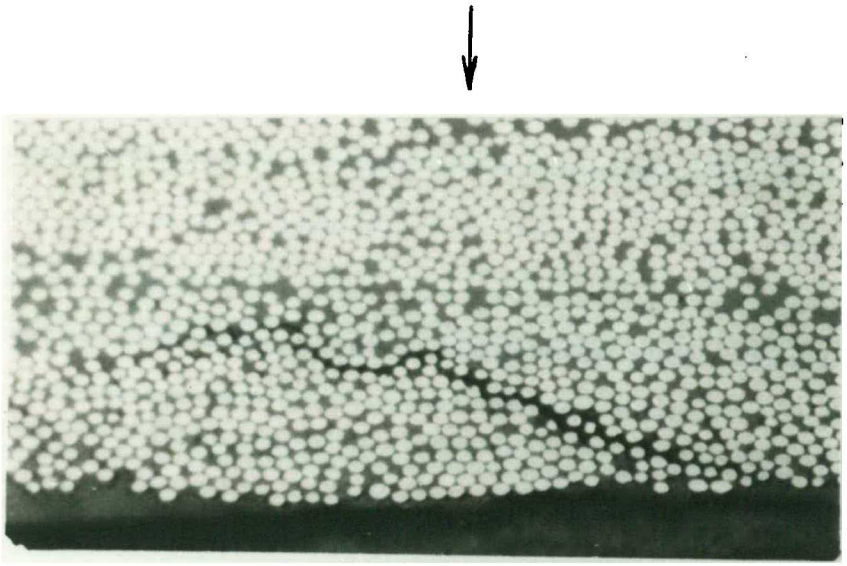


(a) SABOT LOCATION IN THE GAS GUN

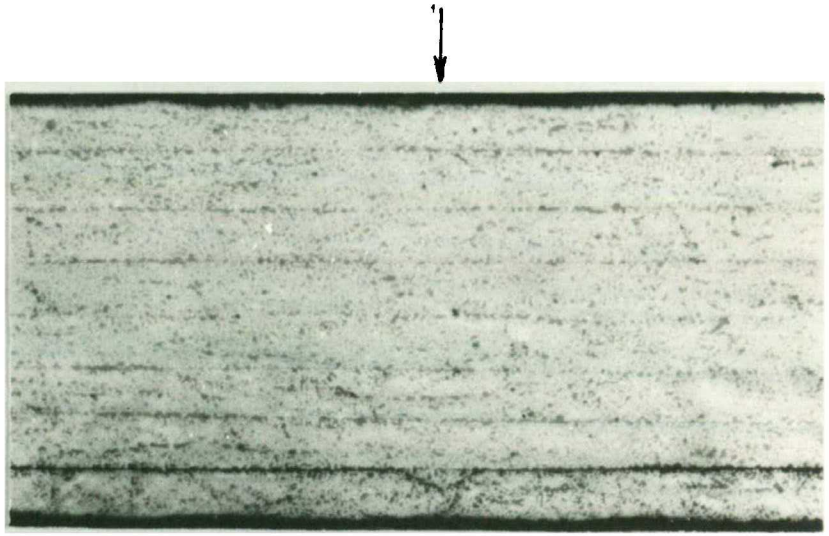


(b) SABOT GEOMETRY

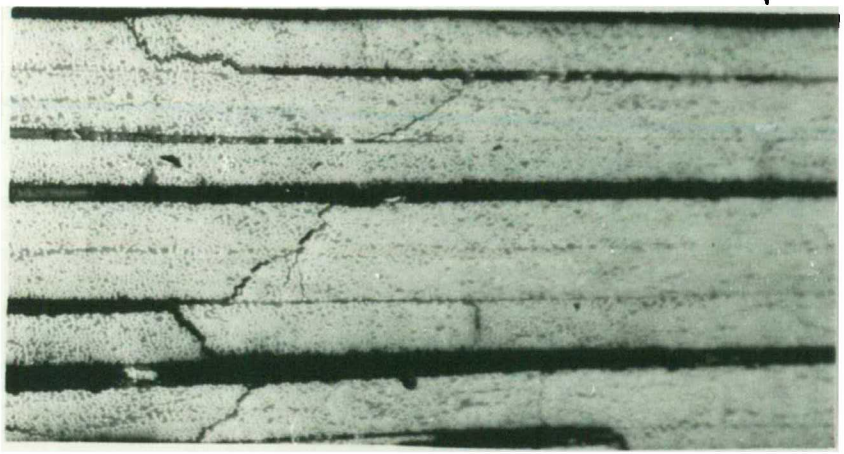
Figure 13



(a) 0.63 JOULES



(b) 0.81 JOULES



(c) 1.2 JOULES



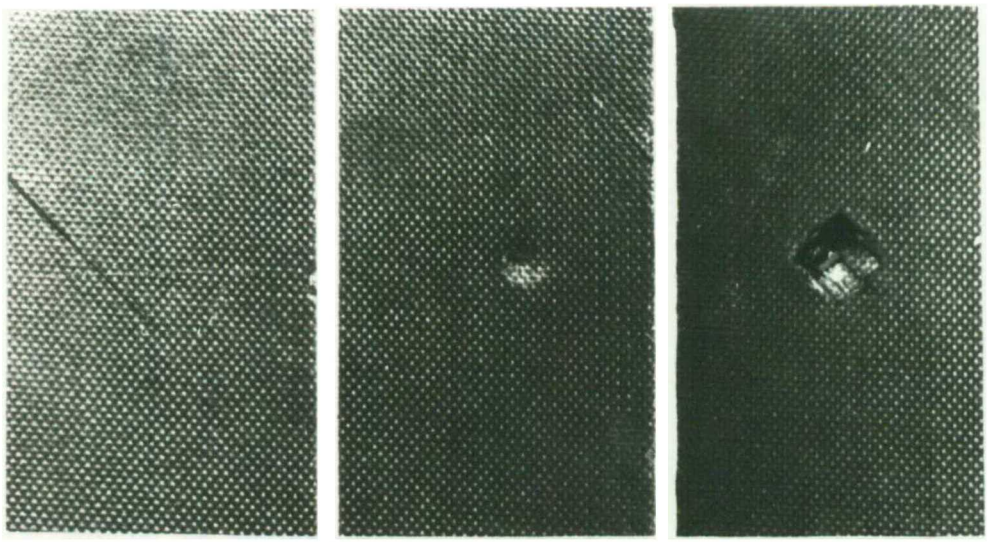
(d) 3.3 JOULES

Figure 14

DAMAGE GROWTH IN THE EIGHT PLY (+/-45) COMPOSITE

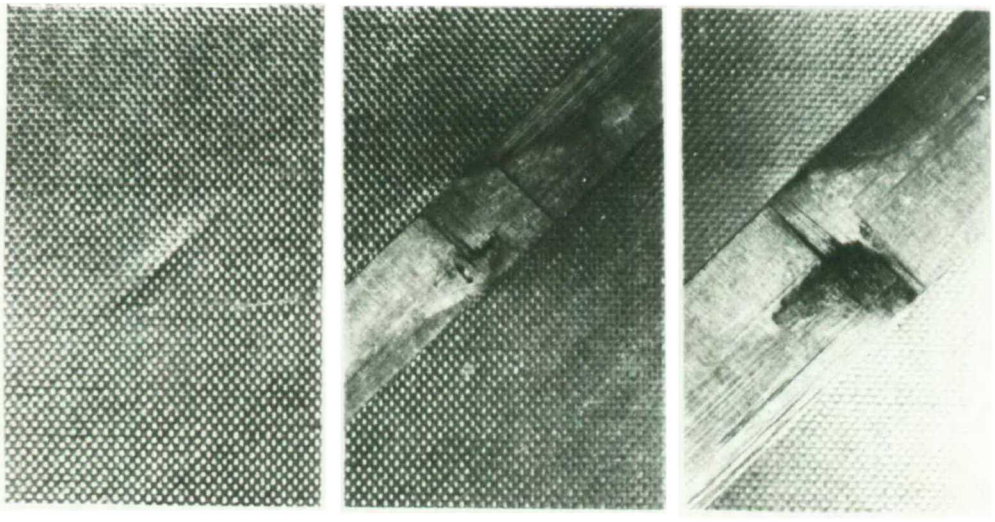
DROP WEIGHT IMPACT

PHOTOGRAPHS DETAILING THE DAMAGE INCURRED BY THE EIGHT PLY (+/-45) COMPOSITE AFTER LOW VELOCITY IMPACT.



TOP SURFACE

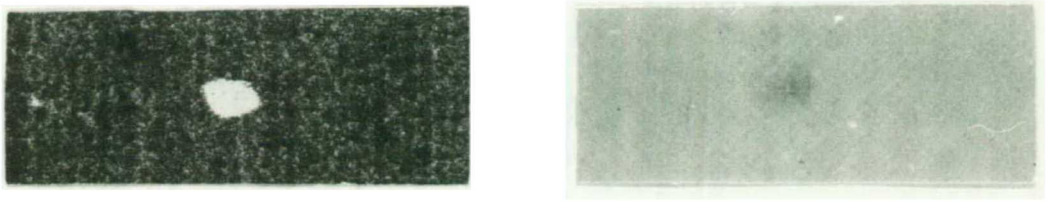
0.81 J	1.2 J	3.3 J
A	B	C



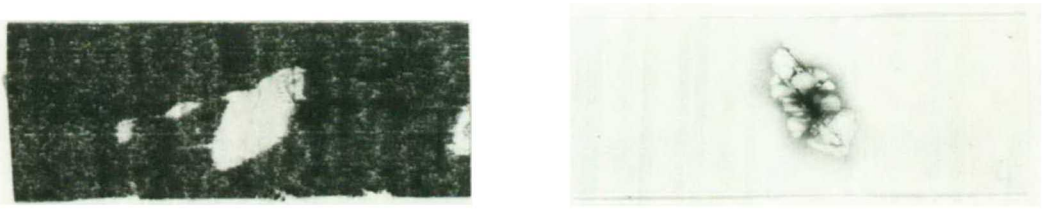
BACK SURFACE

Figure 15

RADIOGRAPHS AND ULTRASONIC C-SCANS OF DAMAGED EIGHT PLY (+/-45) COMPOSITE TAKEN AFTER LOW VELOCITY IMPACT.



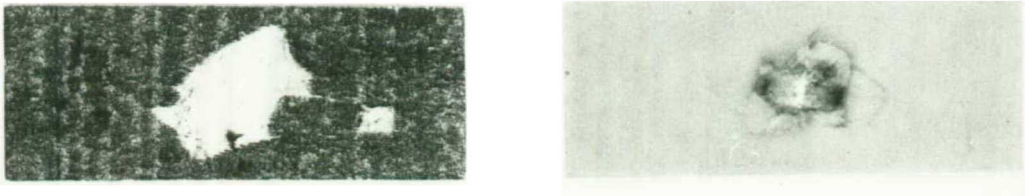
A 0.81 JOULES



B 1.2 JOULES



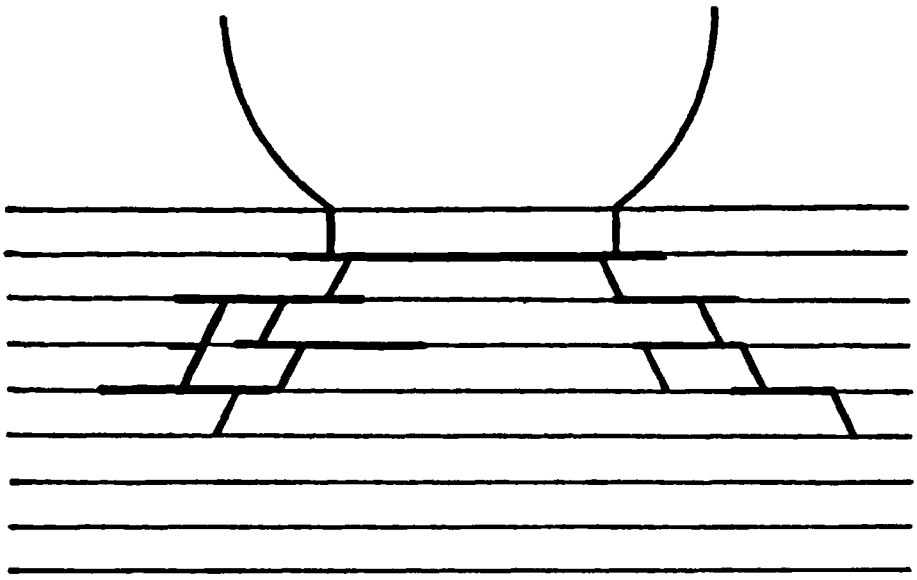
C 2.5 JOULES



D 3.3 JOULES

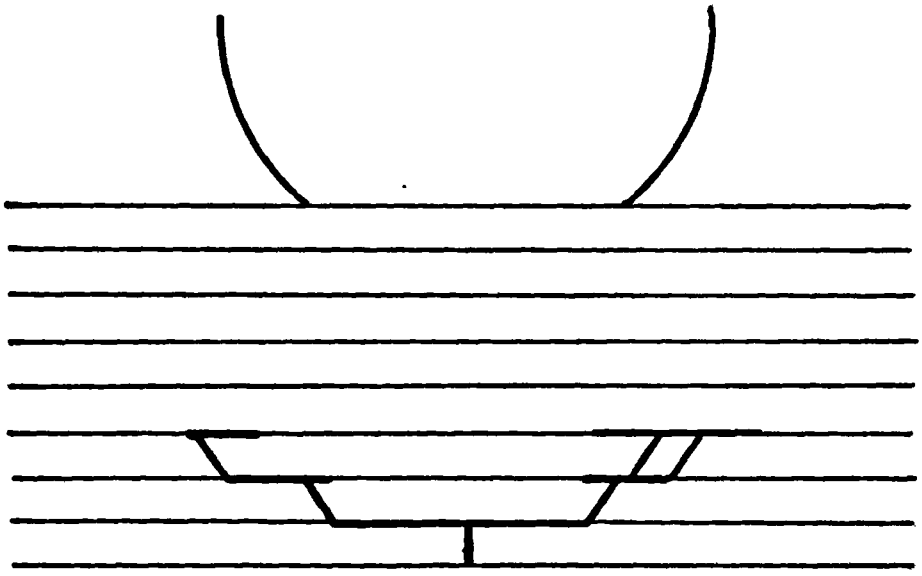
Figure 16

SCHEMATIC REPRESENTATIONS OF IMPACT DAMAGE



(a)

SCHEMATIC REPRESENTATION OF CONTACTOR INDUCED DAMAGE.



(b)

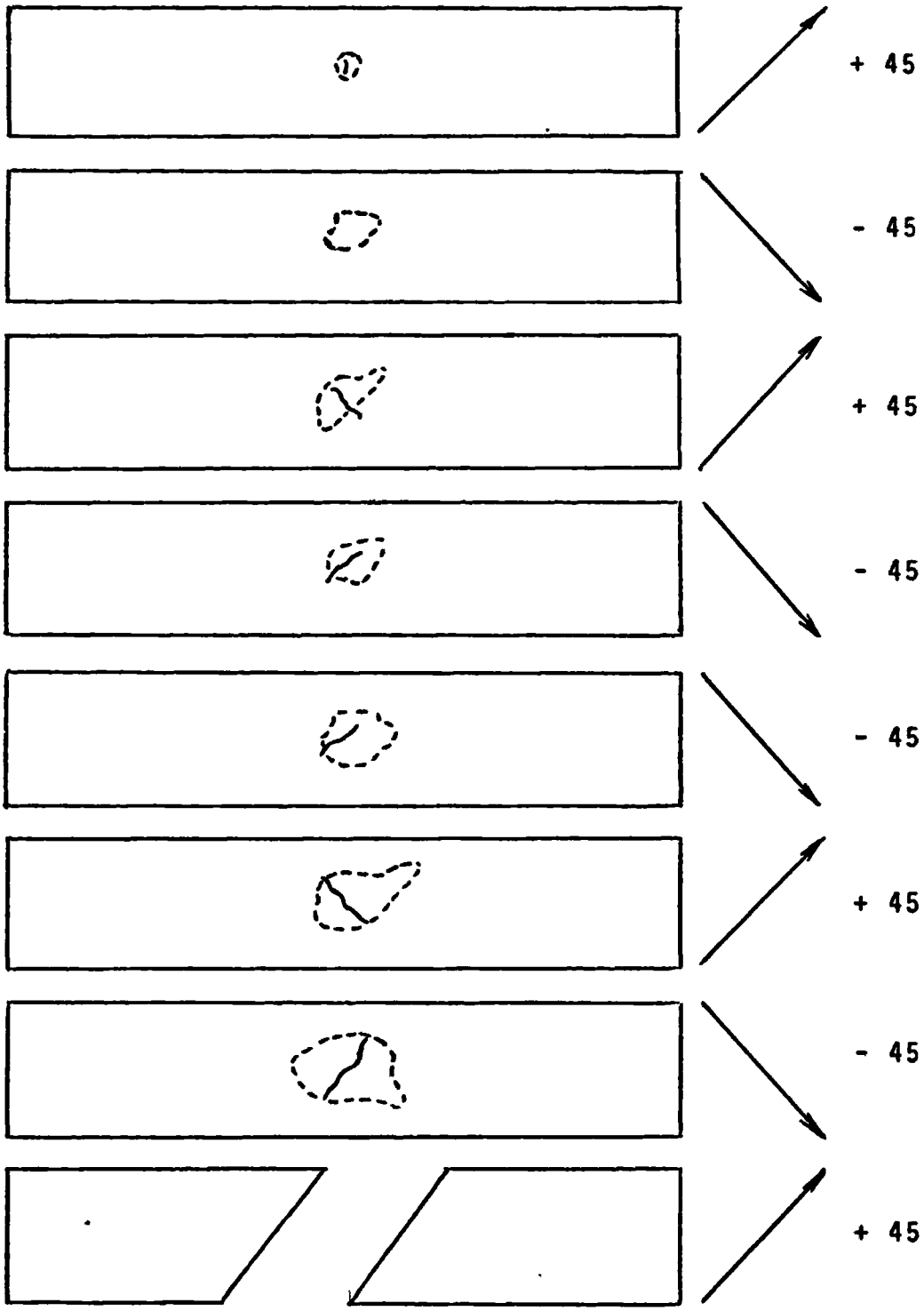
SCHEMATIC REPRESENTATION OF FLEXURE INDUCED DAMAGE.

Figure 17

DEPLIED LAYERS OF AN EIGHT PLY (+/-45) COMPOSITE

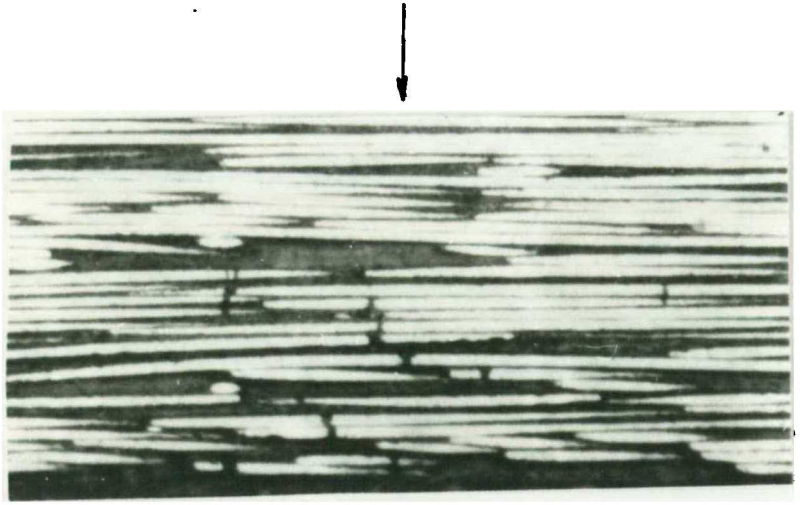
DROP-WEIGHT IMPACT

2.7 JOULES

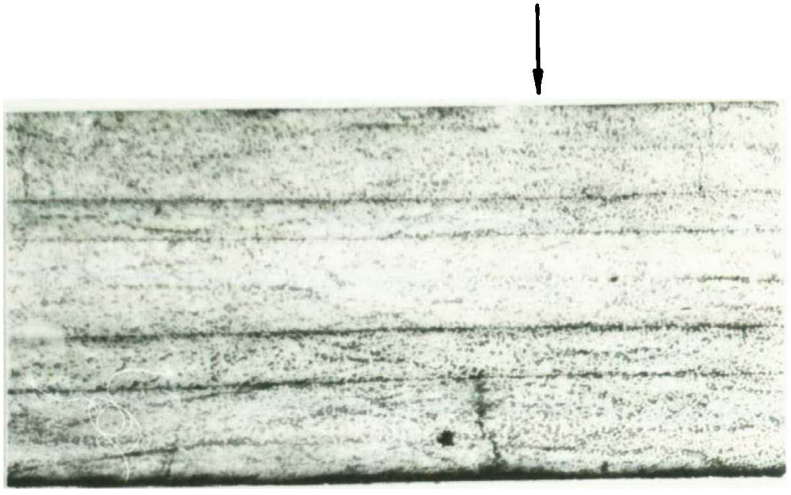


DELAMINATION FIBRE FRACTURE

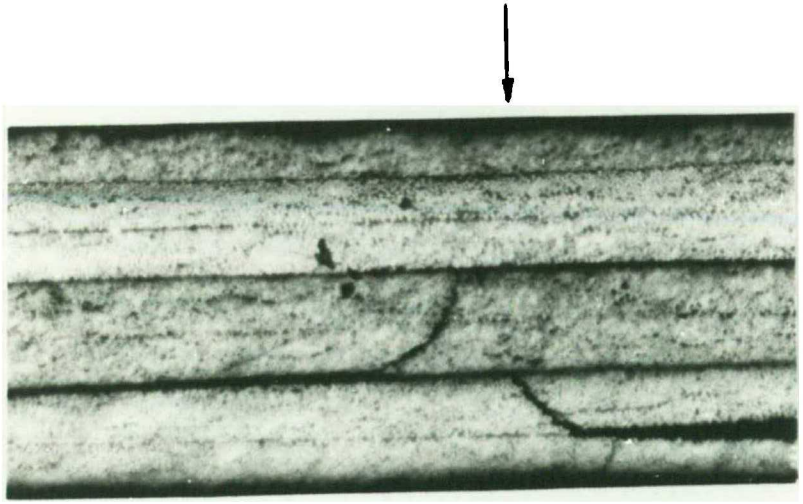
Figure 18



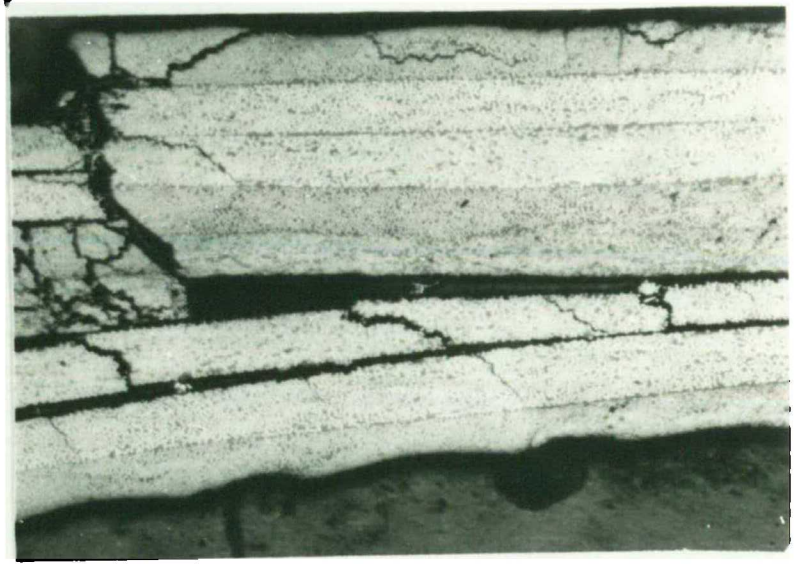
A 1.0 JOULES



B 1.2 JOULES



C 1.6 JOULES



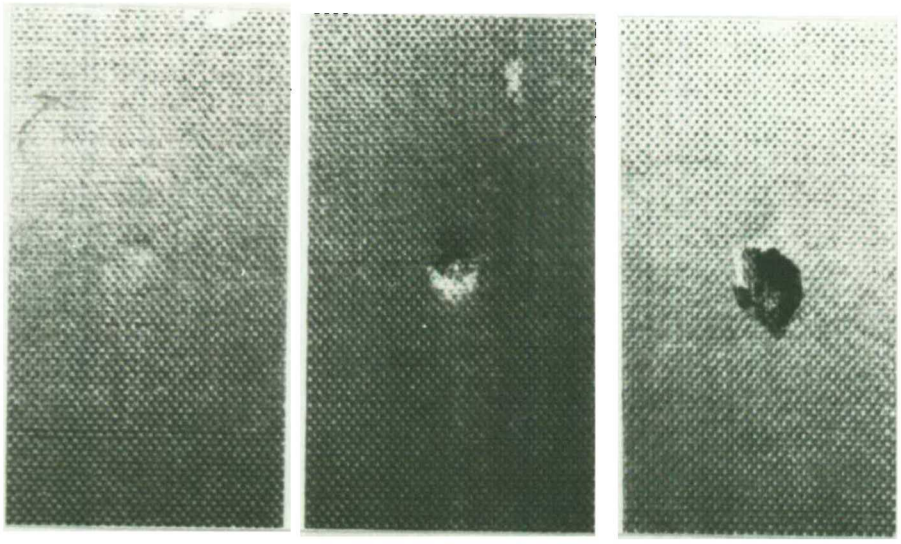
D 2.75 JOULES

Figure 19

DAMAGE GROWTH IN EIGHT PLY (0,+/-45) COMPOSITE .

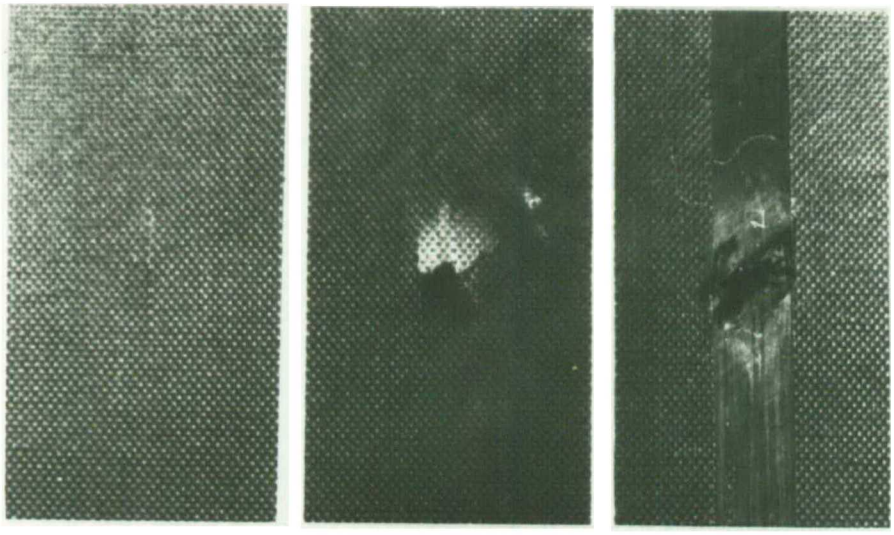
LOW VELOCITY IMPACT

PHOTOGRAPHS DETAILING THE DAMAGE INCURRED BY THE EIGHT PLY $(0_2, +/-45)$ COMPOSITE AFTER LOW VELOCITY IMPACT.



TOP SURFACE

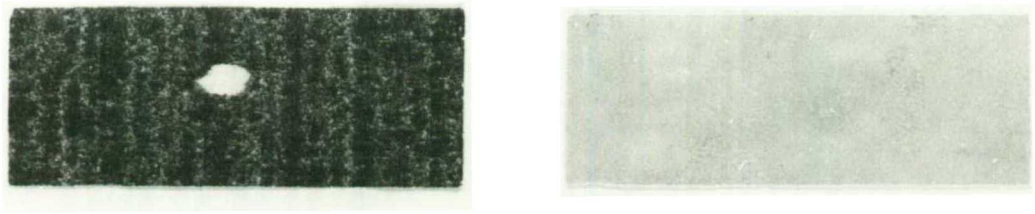
1.0 J	2.5 J	2.9 J
A	B	C



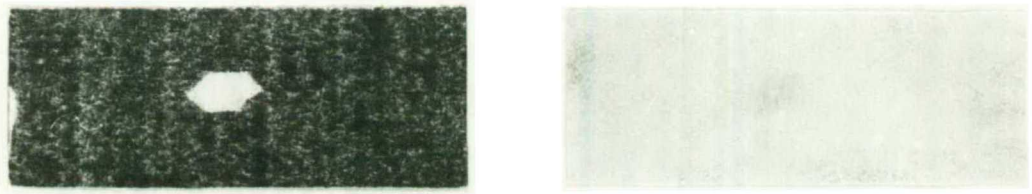
BACK SURFACE

Figure 20

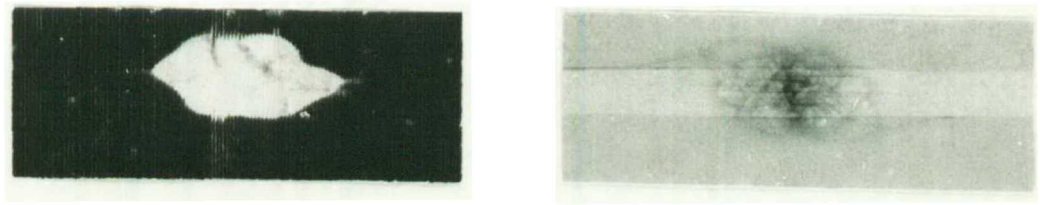
RADIOGRAPHS AND ULTRASONIC C-SCANS OF DAMAGED EIGHT PLY (0,+/-45) COMPOSITE TAKEN AFTER LOW VELOCITY IMPACT LOADING.



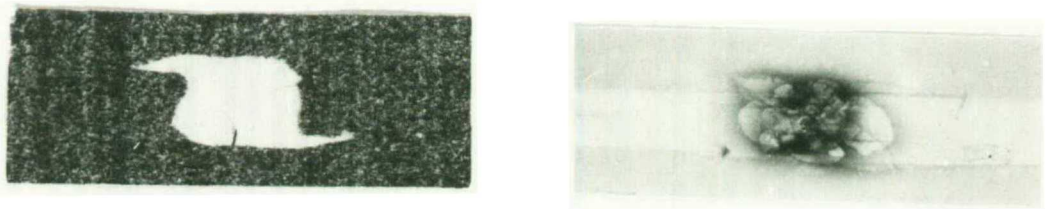
A 1.2 JOULES



B 1.6 JOULES



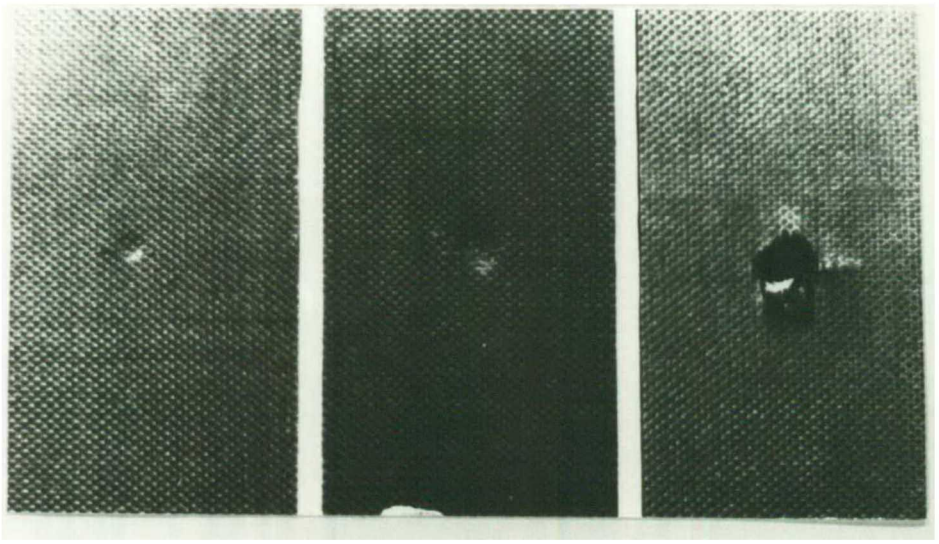
C 2.75 JOULES



D 2.9 JOULES

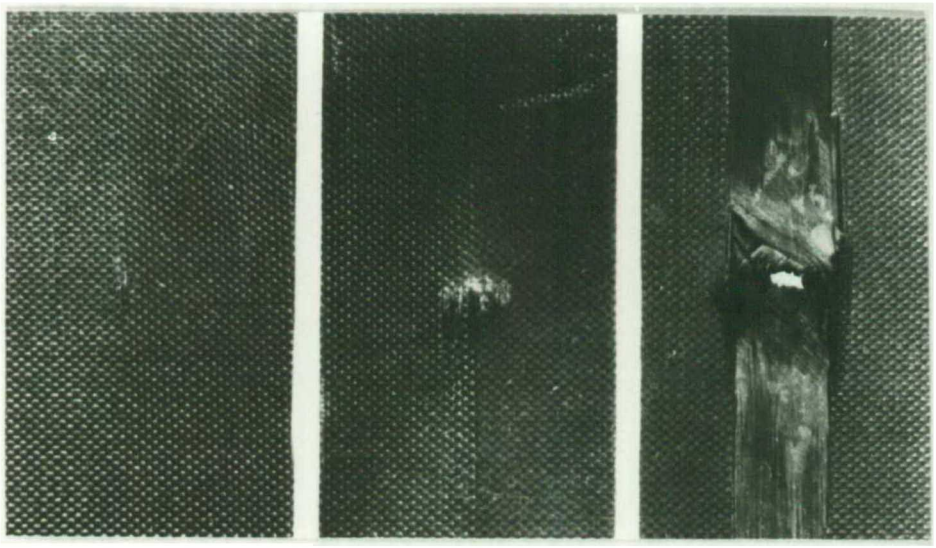
Figure 21

PHOTGRAPHS DETAILING THE DAMAGE INCURRED IN THE SIXTEEN PLY (0,+/-45) COMPOSITE AFTER LOW VELOCITY IMPACT



TOP SURFACE

1.9 J	4.8 J	6.6 J
A	B	C

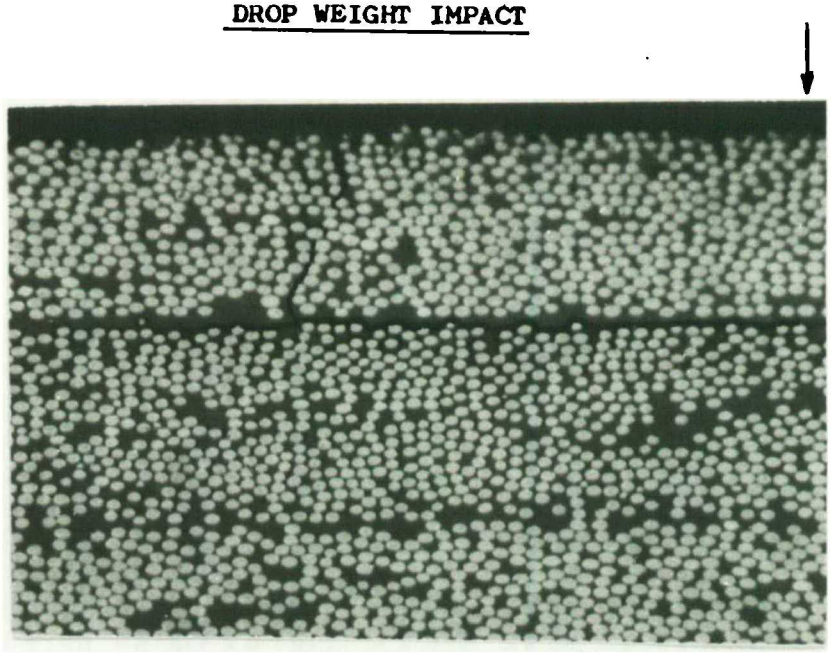


BACK SURFACE

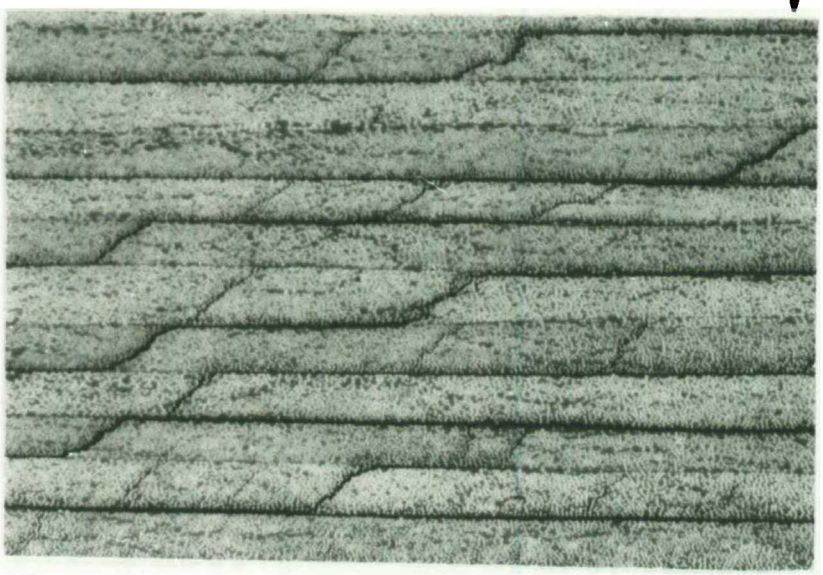
Figure 22

DAMAGE GROWTH IN SIXTEEN PLY (0,+/-45) COMPOSITE

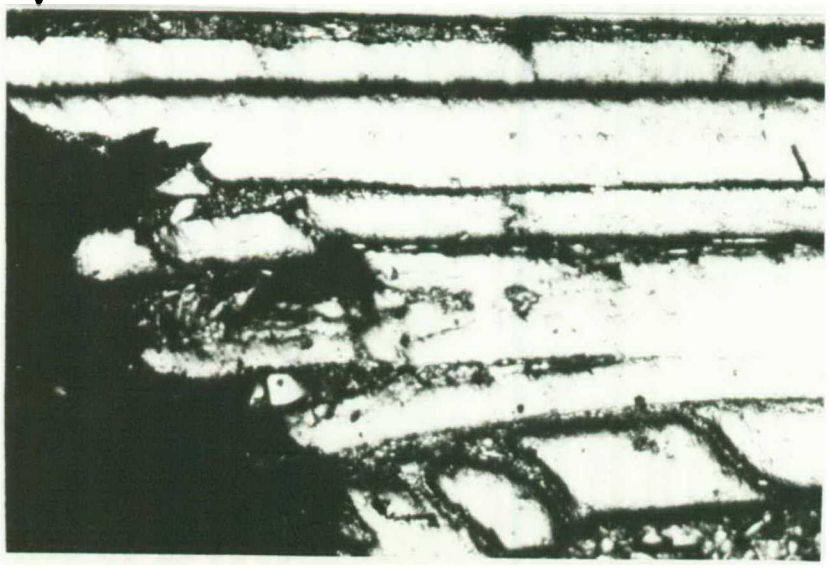
DROP WEIGHT IMPACT



A 1.6 JOULES



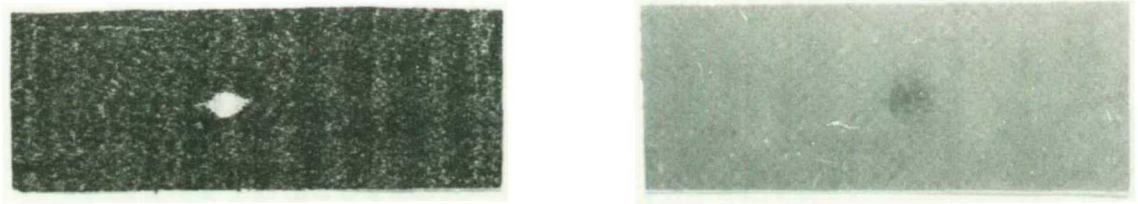
B 2.4 JOULES



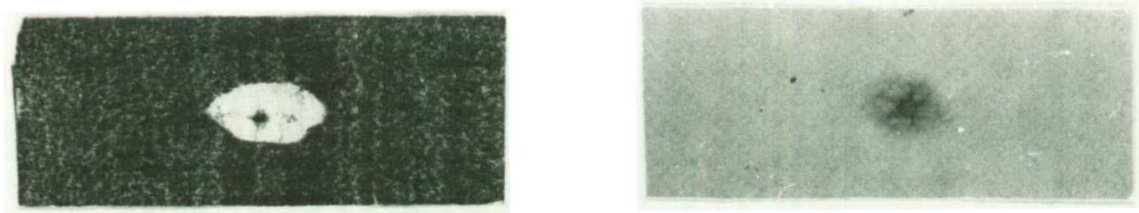
C 6.6 JOULES

Figure 23

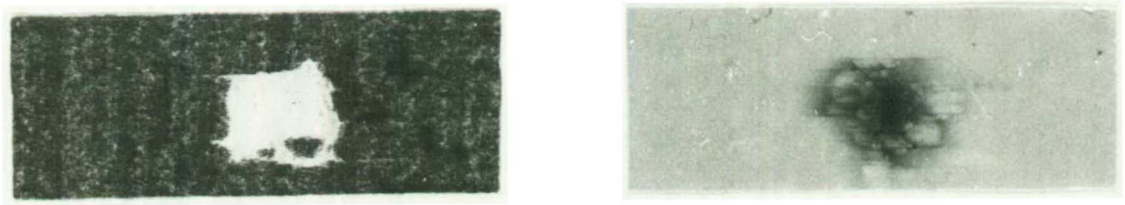
RADIOGRAPHS AND ULTRASONIC C-SCANS OF DAMAGED SIXTEEN PLY (0,+/-45) COMPOSITE AFTER LOW VELOCITY IMPACT LOADING.



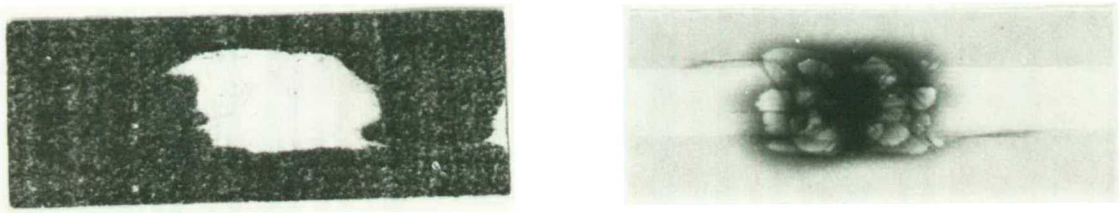
A 1.6 JOULES



B 2.4 JOULES



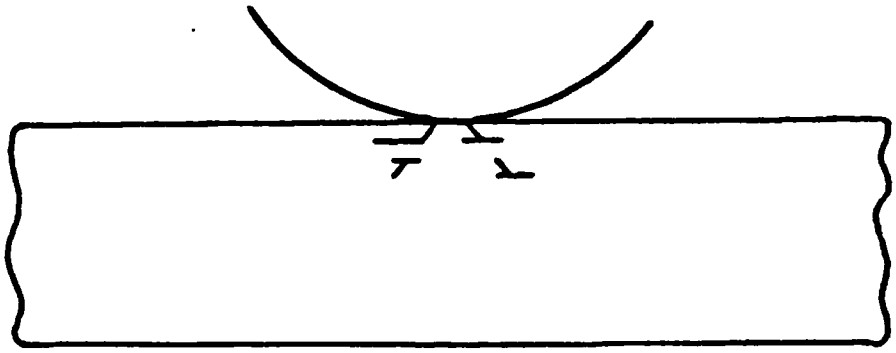
C 4.5 JOULES



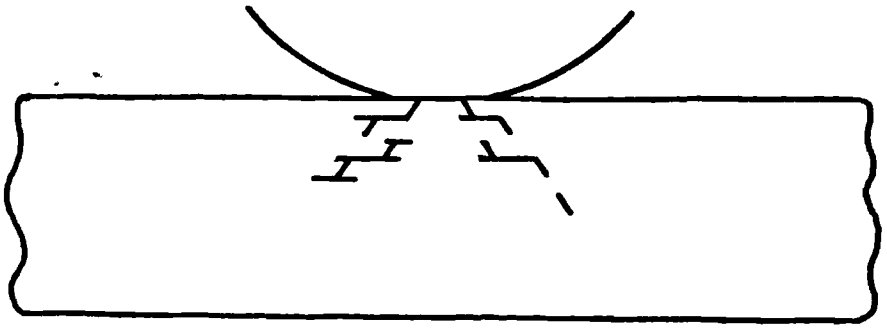
D 6.6 JOULES

Figure 24

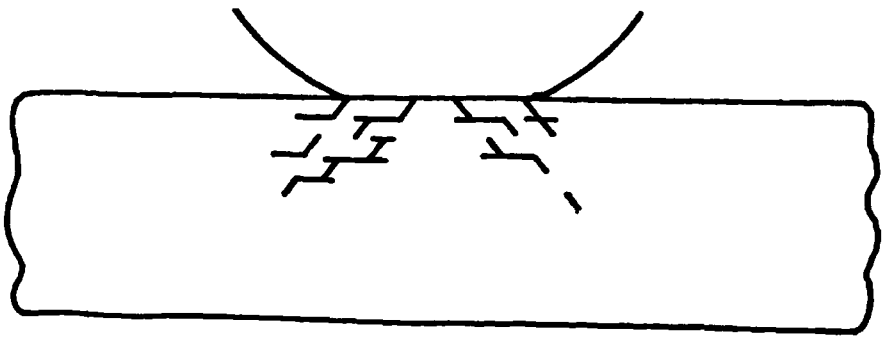
DEVELOPMENT OF TOP SURFACE DAMAGE IN STIFF TARGETS SUBJECTED TO LOW VELOCITY IMPACT.



STAGE 1.



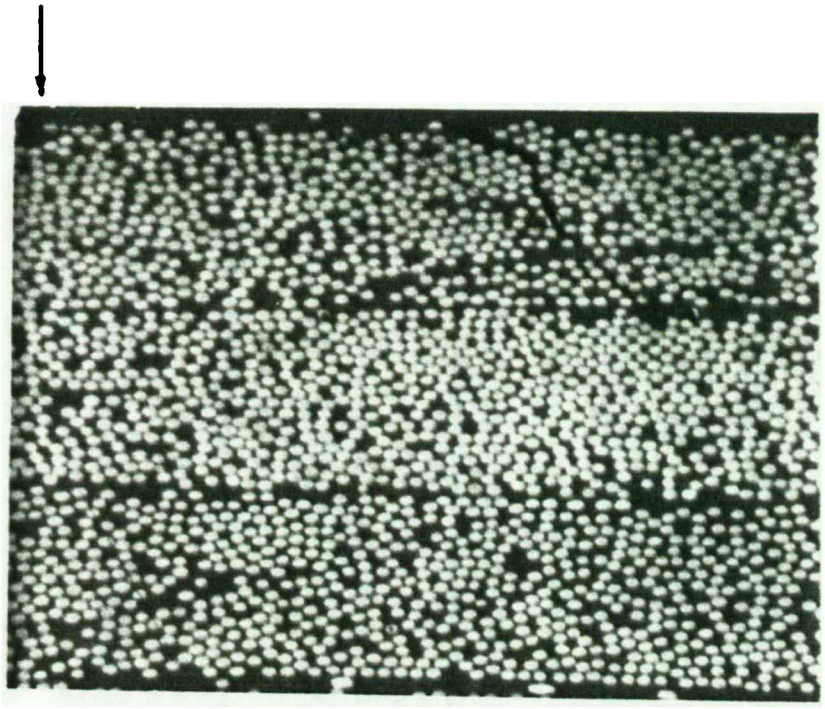
STAGE 2.



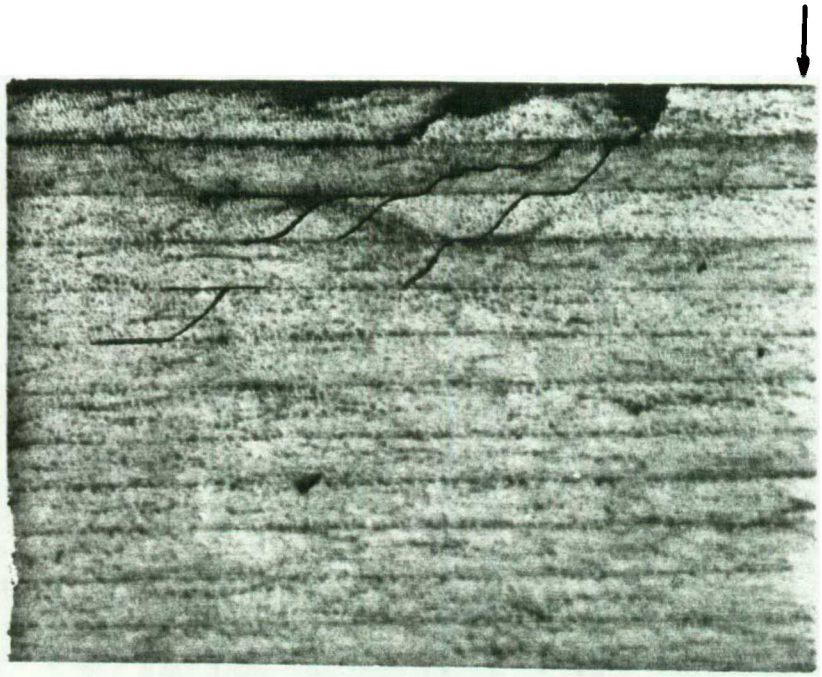
STAGE 3.

Figure 25

DAMAGE GROWTH IN THE THIRTY-TWO PLY (+/-45) COMPOSITE DURING LOW VELOCITY IMPACT



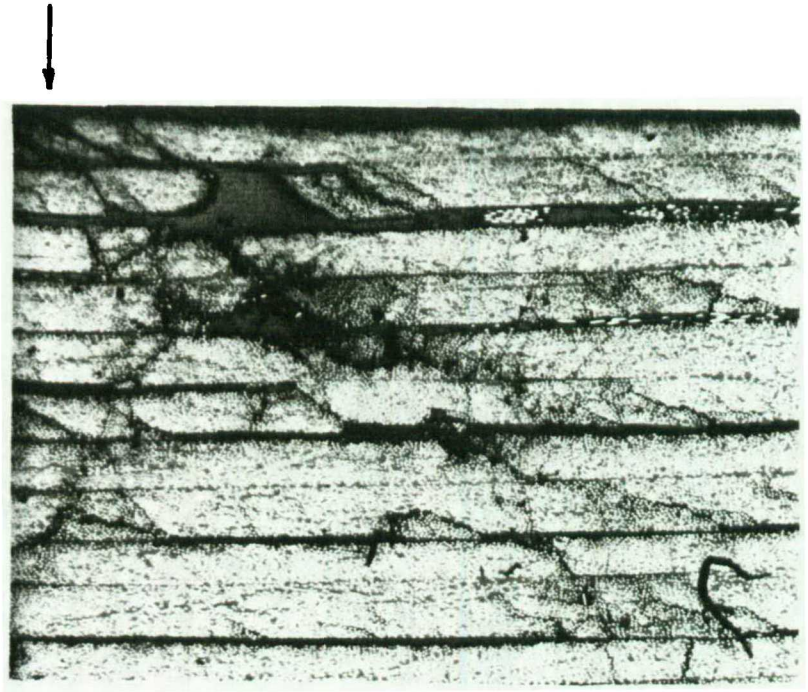
(a) 0.4 JOULES



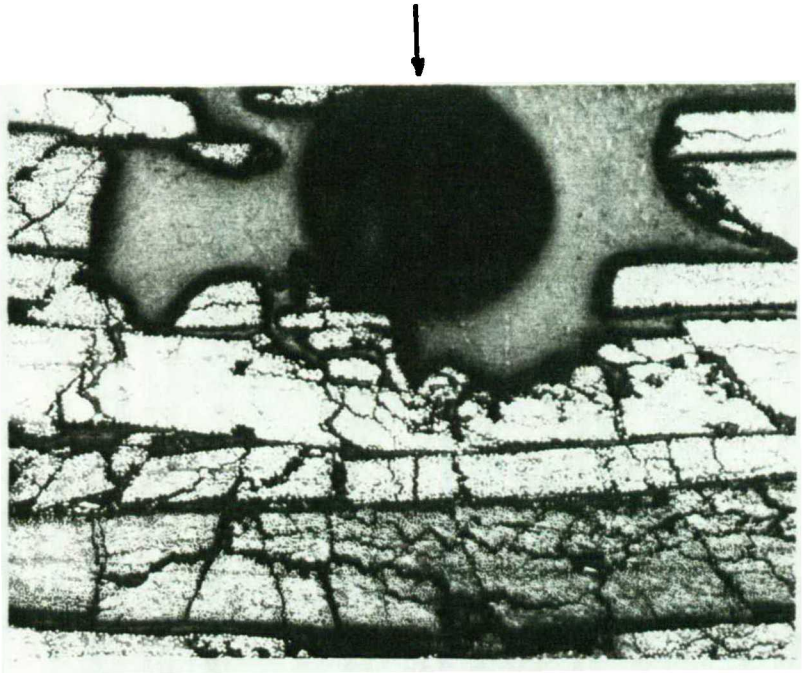
(b) 0.8 JOULES

Figure 26

DAMAGE GROWTH IN THE THIRTY-TWO PLY (+/-45) COMPOSITE DURING LOW VELOCITY IMPACT



(c) I5.0 JOULES



(d) 22.3 JOULES

Figure 26

THE VARIATION OF BEAM DISPLACEMENT WITH APPLIED LOAD FOR THE SIXTEEN PLY (0,+/-45) COMPOSITE.

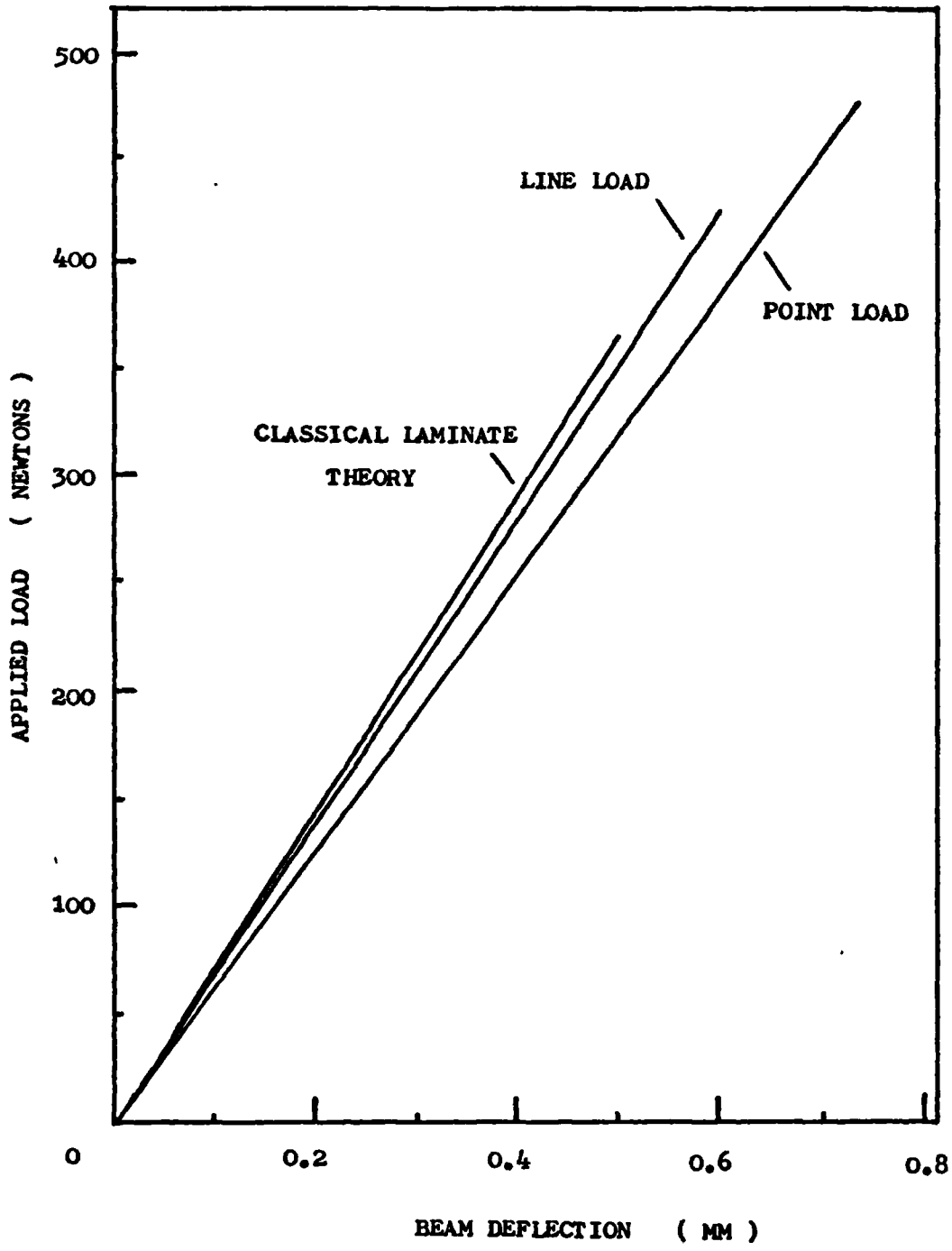


Figure 27

SCHEMATIC REPRESENTATION OF THE STATIC INDENTATION TEST FIXTURE

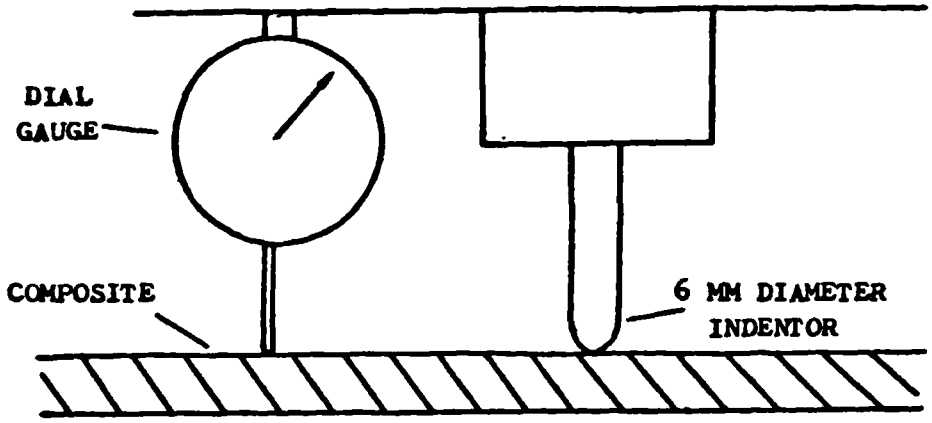


Figure 28

THE VARIATION OF CONTACT FORCE WITH CONTACT DEFORMATION .

PROJECTILE DIAMETER = 6 MM. LAMINATE, 16 PLY $(0,\pm 45)$

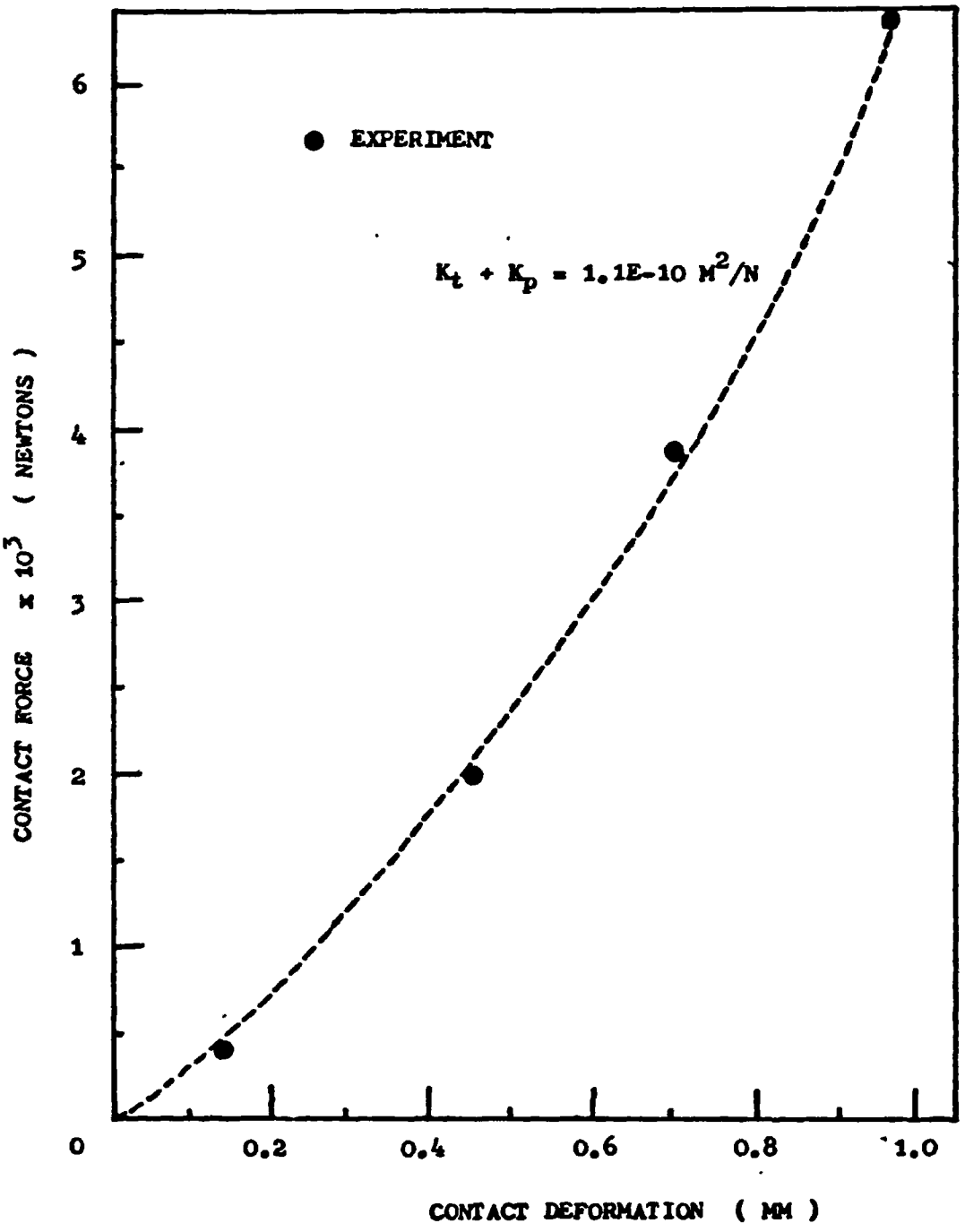


Figure 29

THE PREDICTED VARIATION OF IMPACT FORCE WITH IMPACT VELOCITY FOR THE (+/-45) COMPOSITES. DROP WEIGHT IMPACT.

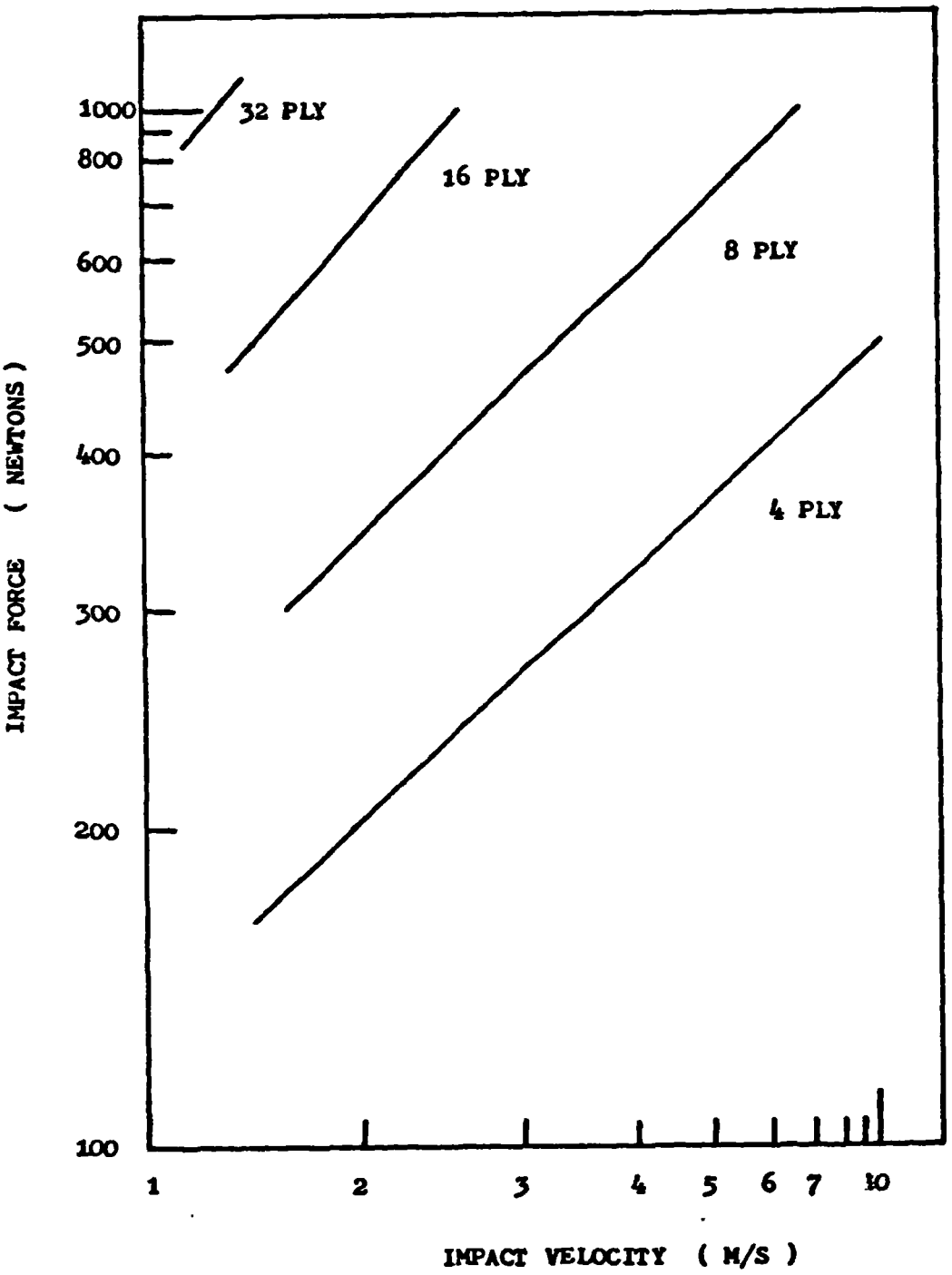


Figure 30

COMPARISON OF THE PREDICTED AND EXPERIMENTAL IMPACT FORCE VARIATION WITH IMPACT VELOCITY DROP WEIGHT IMPACT.

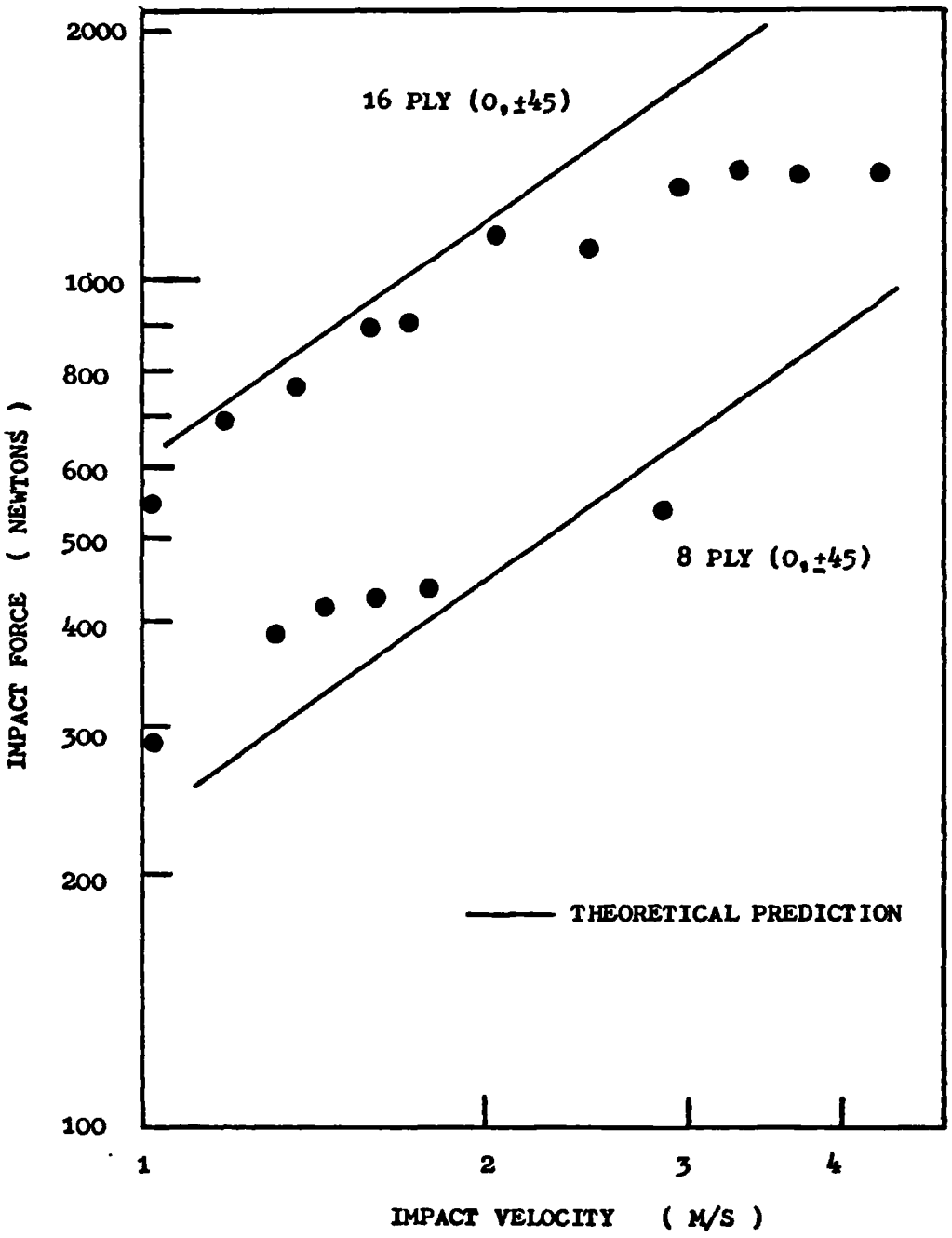
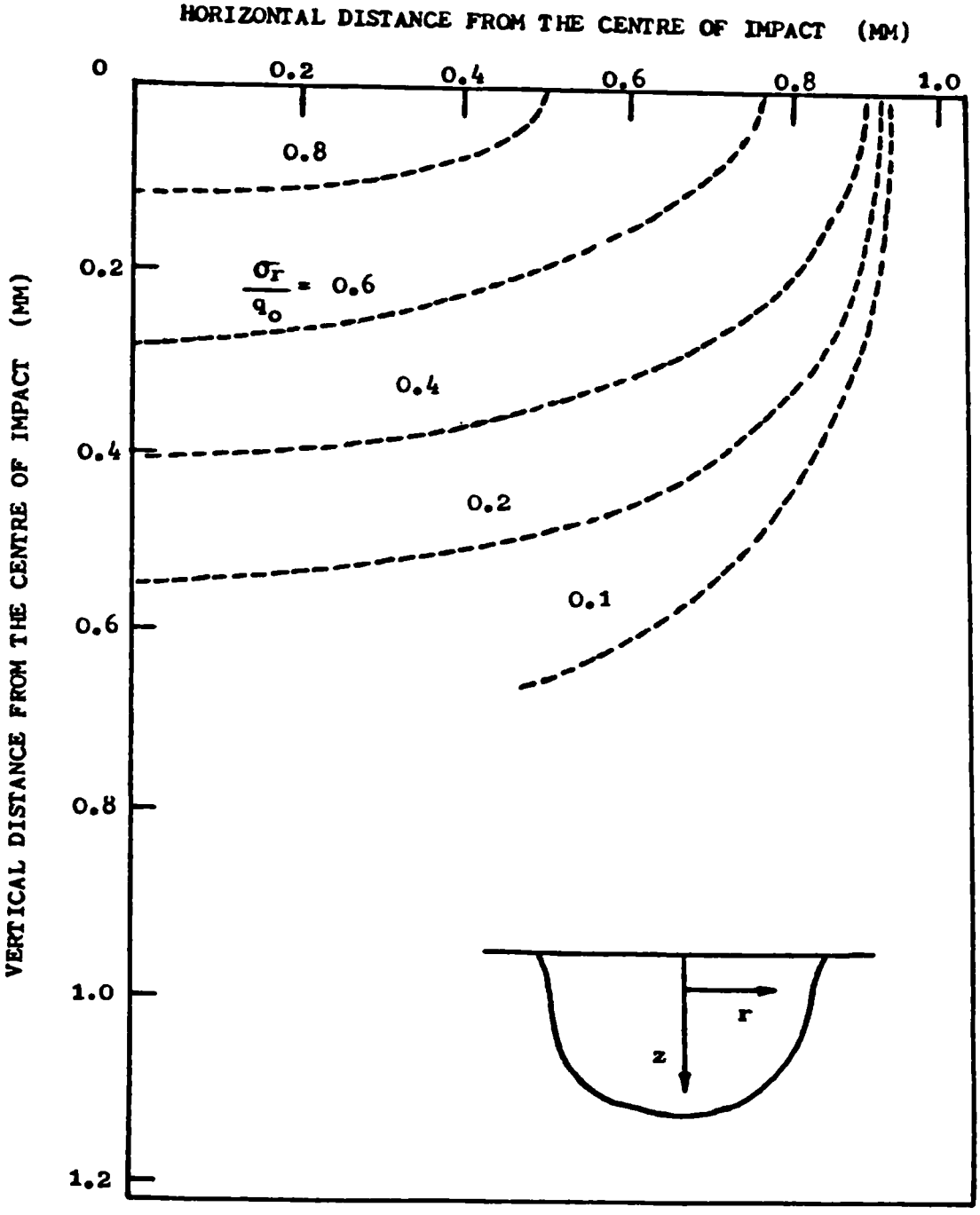


Figure 31

PREDICTED STRESS DISTRIBUTION IN AN ISOTROPIC TARGET SUBJECTED TO IMPACT LOADING



RADIUS OF AREA OF CONTACT = 0.95 MM

Figure 32

PREDICTED STRESS DISTRIBUTION IN AN ISOTROPIC TARGET SUBJECTED TO IMPACT LOADING

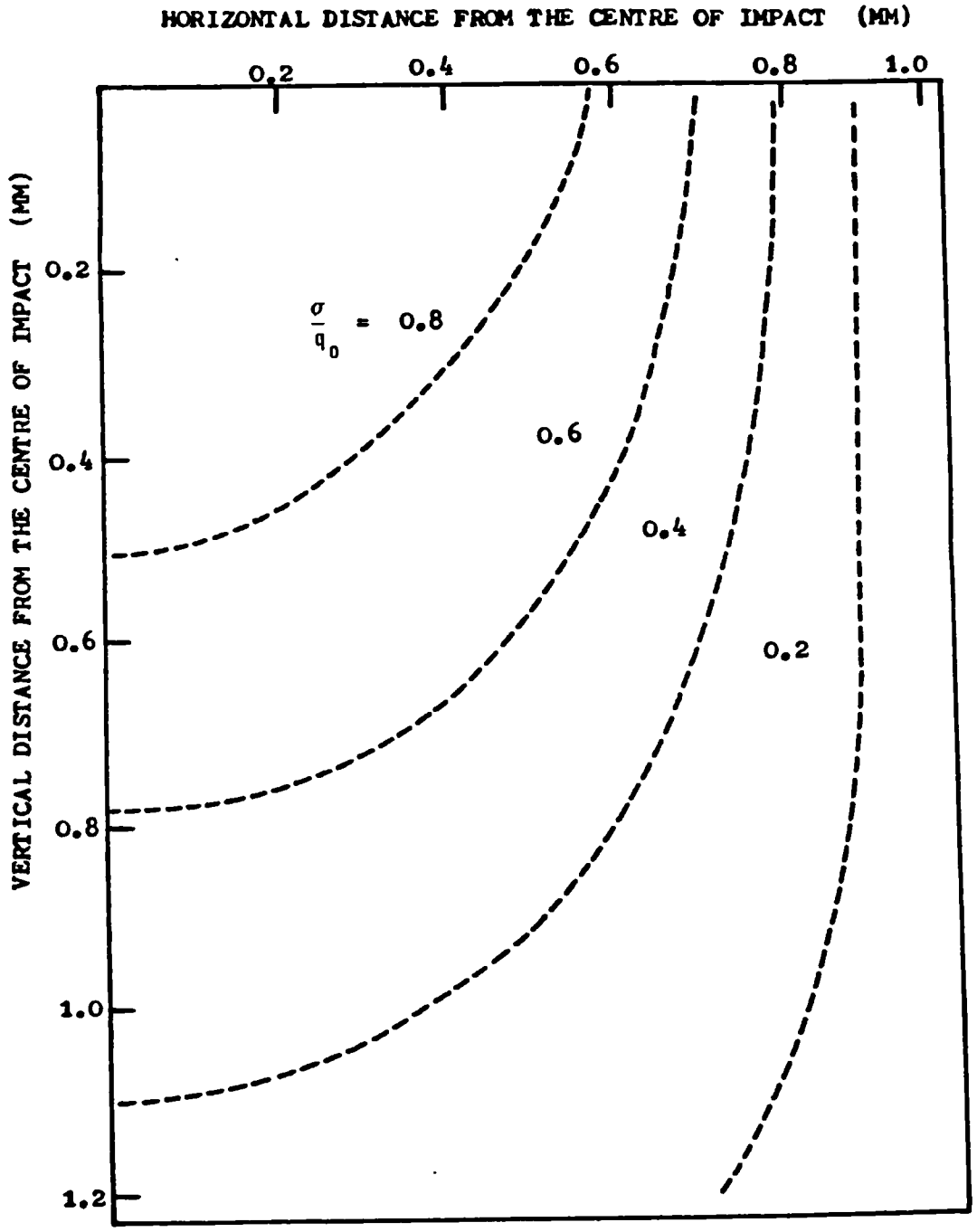
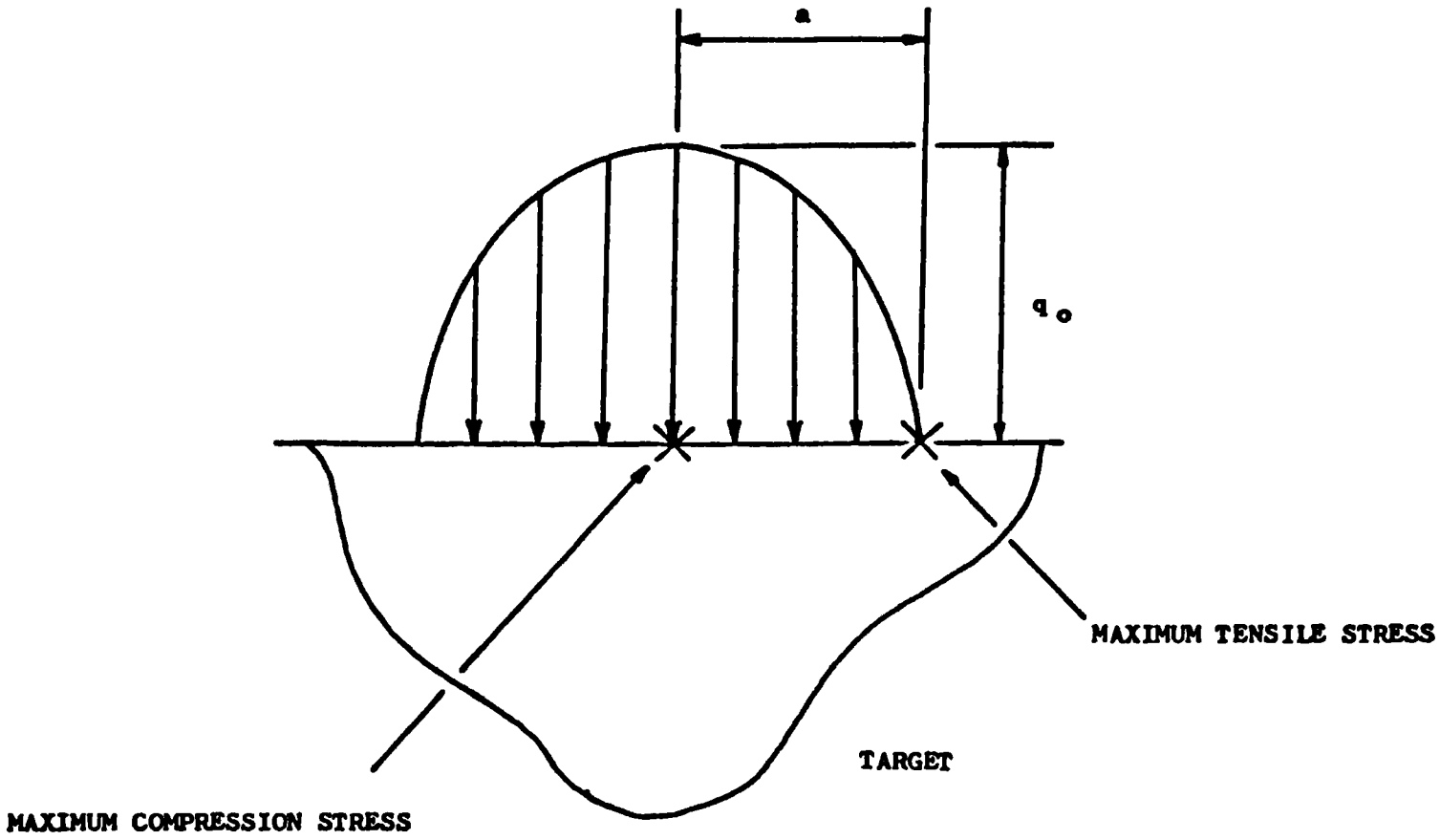


Figure 33

Figure 34



THE LOCATIONS OF THE MAXIMUM TENSILE AND COMPRESSIVE STRESSES IN AN IMPACTED TARGET.

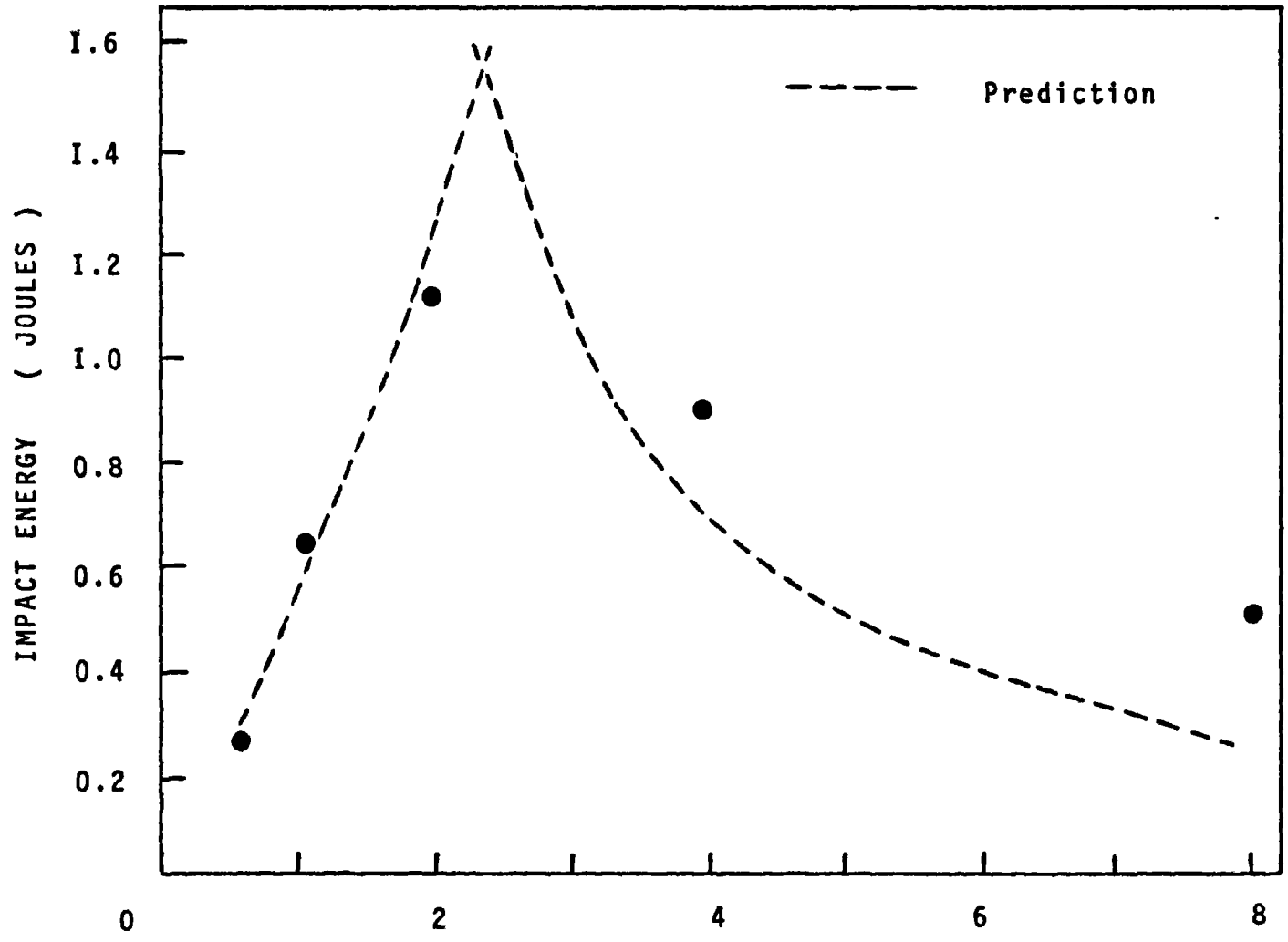


Figure 35

THE VARIATION OF IMPACT ENERGY FOR FIRST DAMAGE WITH TARGET THICKNESS

INCIDENT ENERGY TO CAUSE FIRST DAMAGE IN THE (0,+/-45) COMPOSITE BEAMS. DROP WEIGHT IMPACT.

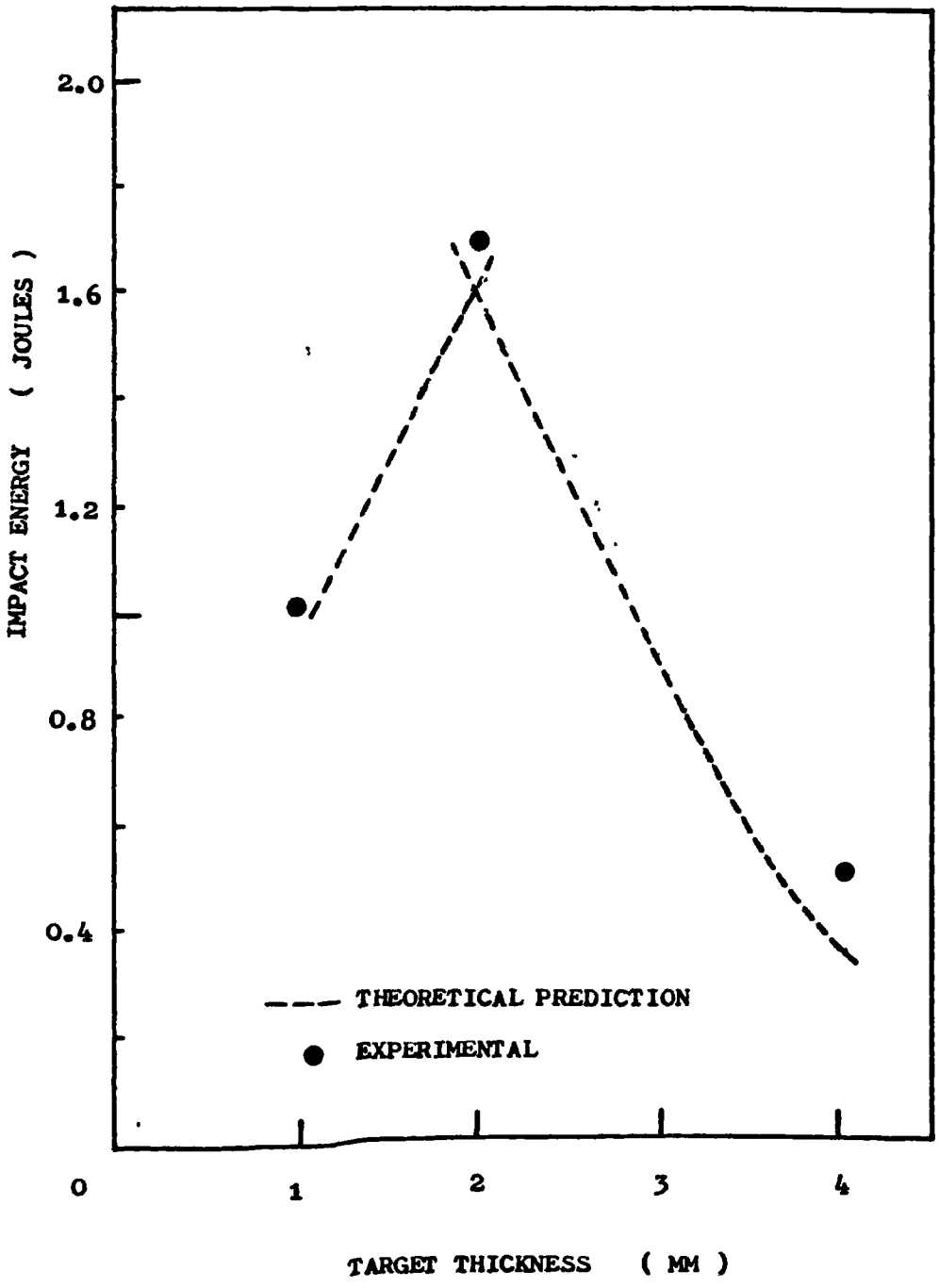


Figure 36

THE VARIATION OF NORMALISED FLEXURAL STIFFNESS WITH IMPACT ENERGY

EIGHT PLY (+/-45) COMPOSITE. DROP WEIGHT IMPACT.

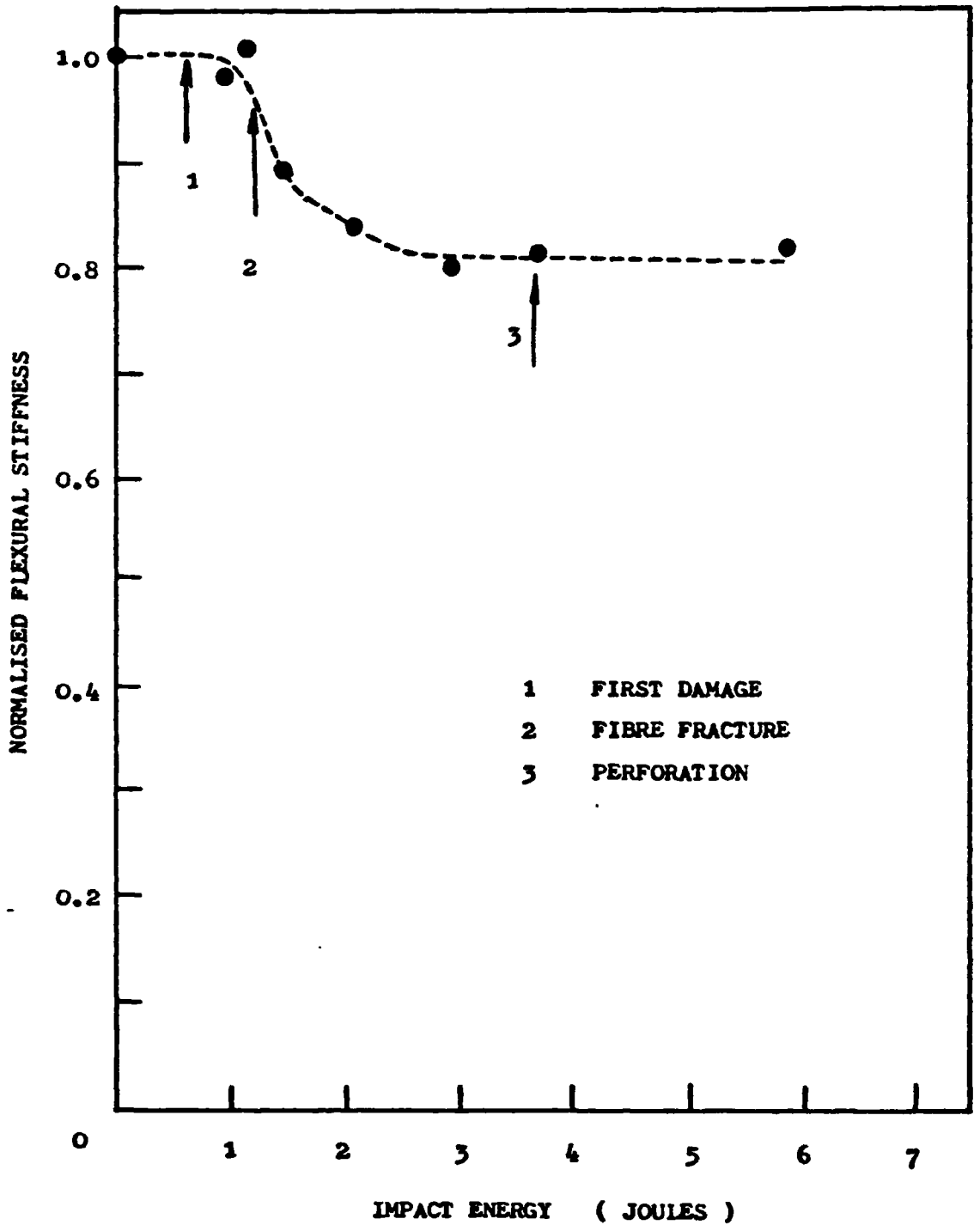


Figure 37

THE VARIATION OF NORMALISED FLEXURAL STIFFNESS WITH IMPACT ENERGY

SIXTEEN PLY (0,+/-45) COMPOSITE. DROP WEIGHT IMPACT.

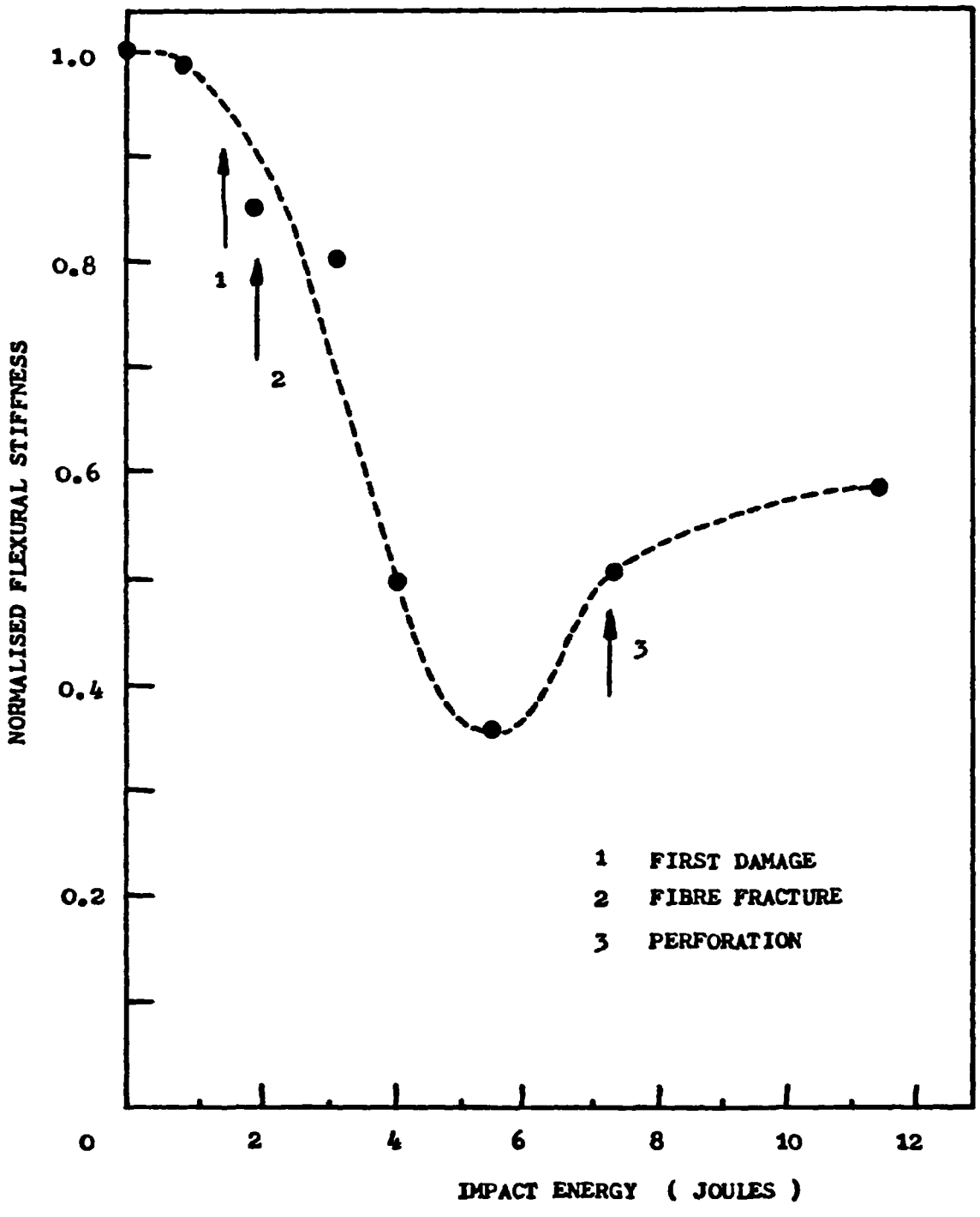
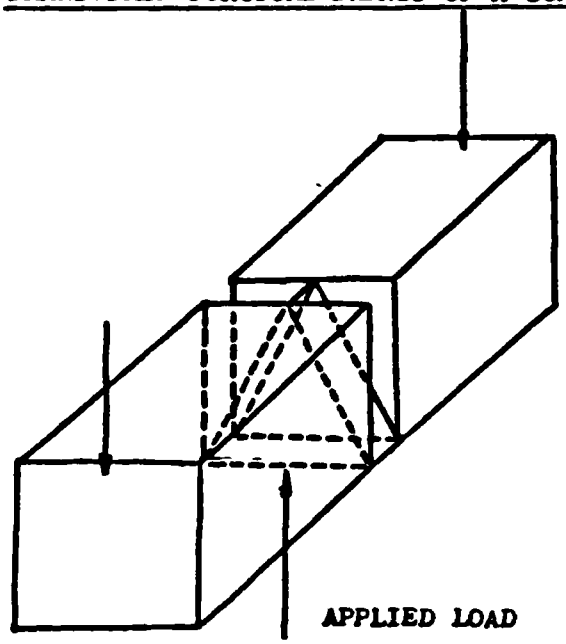


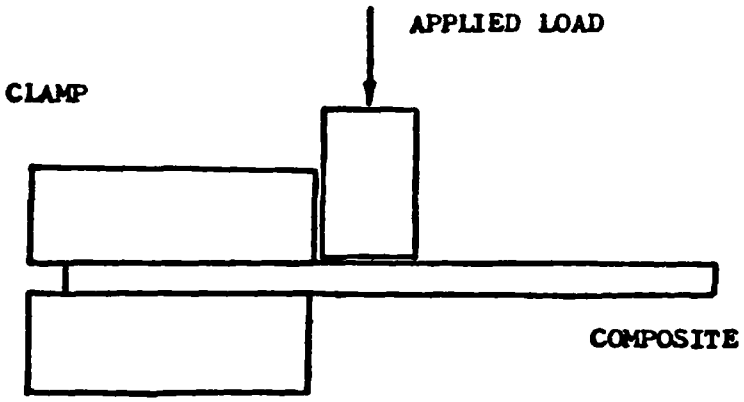
Figure 38

SCHEMATIC DIAGRAMS SHOWING TECHNIQUES FOR MEASURING THE TRANSVERSE FRACTURE ENERGY OF A COMPOSITE.



(a)

The 'V' Notched Beam Test



(b)

THE TECHNIQUE EMPLOYED FOR MEASURING THE TRANSVERSE FRACTURE ENERGY OF THE COMPOSITE PANELS

Figure 39

CURVES FOR THE DETERMINATION OF THE FRACTURE ENERGIES OF THE FOUR PLY COMPOSITES.

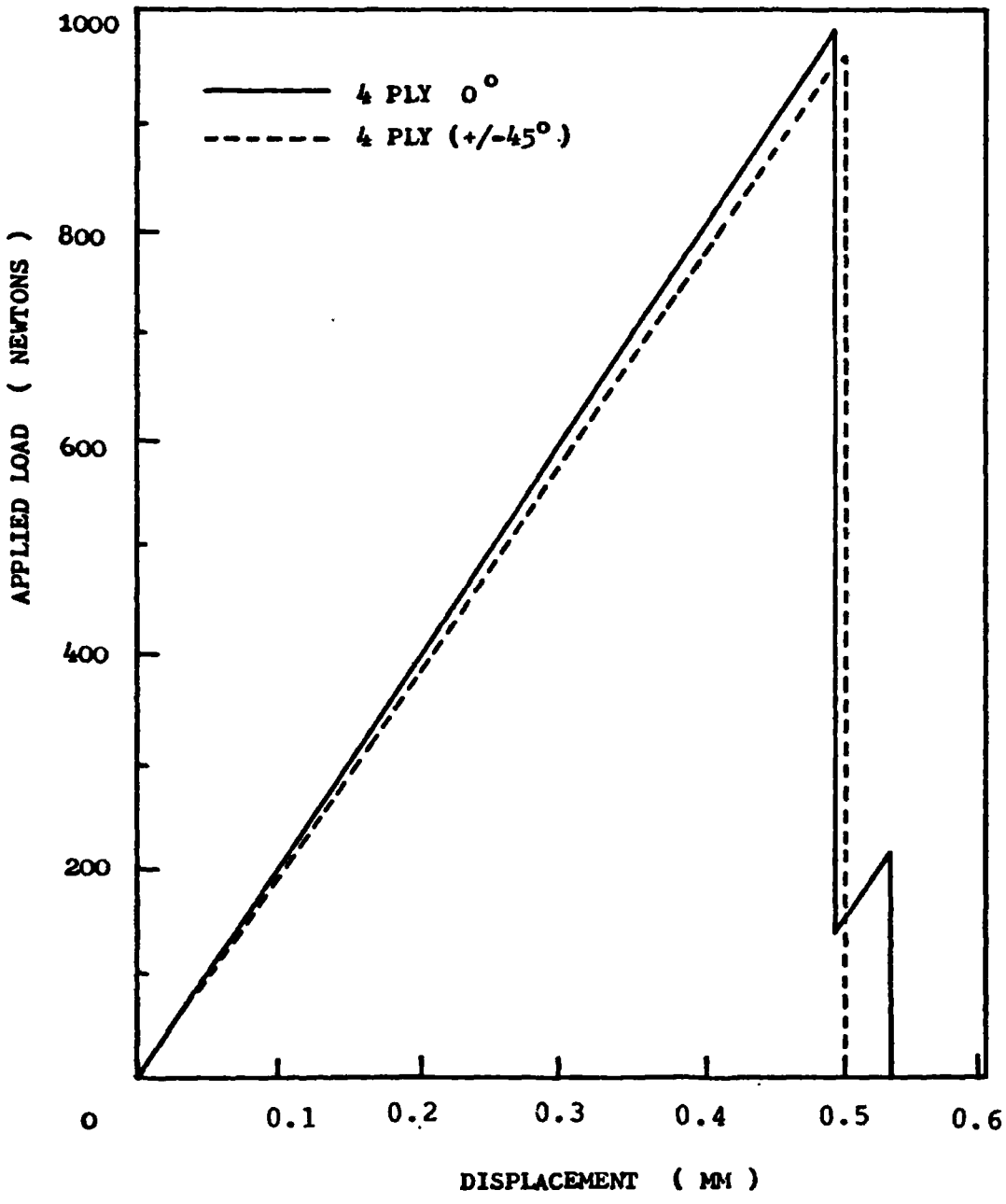


Figure 40

THE VARIATION OF THE DROP-WEIGHT PERFORATION ENERGY WITH TARGET THICKNESS FOR THE (+/-45) COMPOSITES.

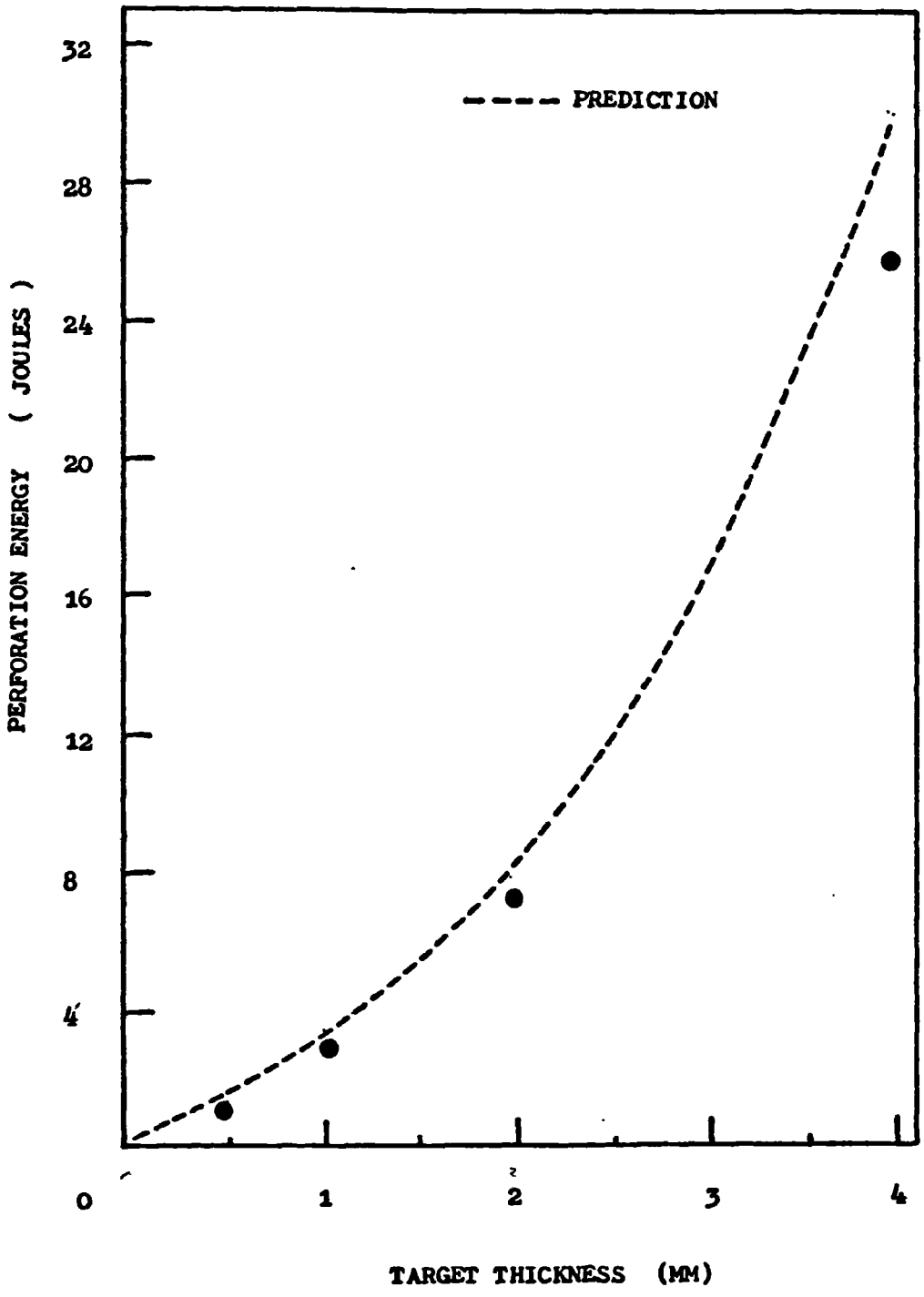


Figure 41

THE ABSORPTION OF ENERGY IN THE (+/-45) COMPOSITES.

DROP WEIGHT IMPACT.

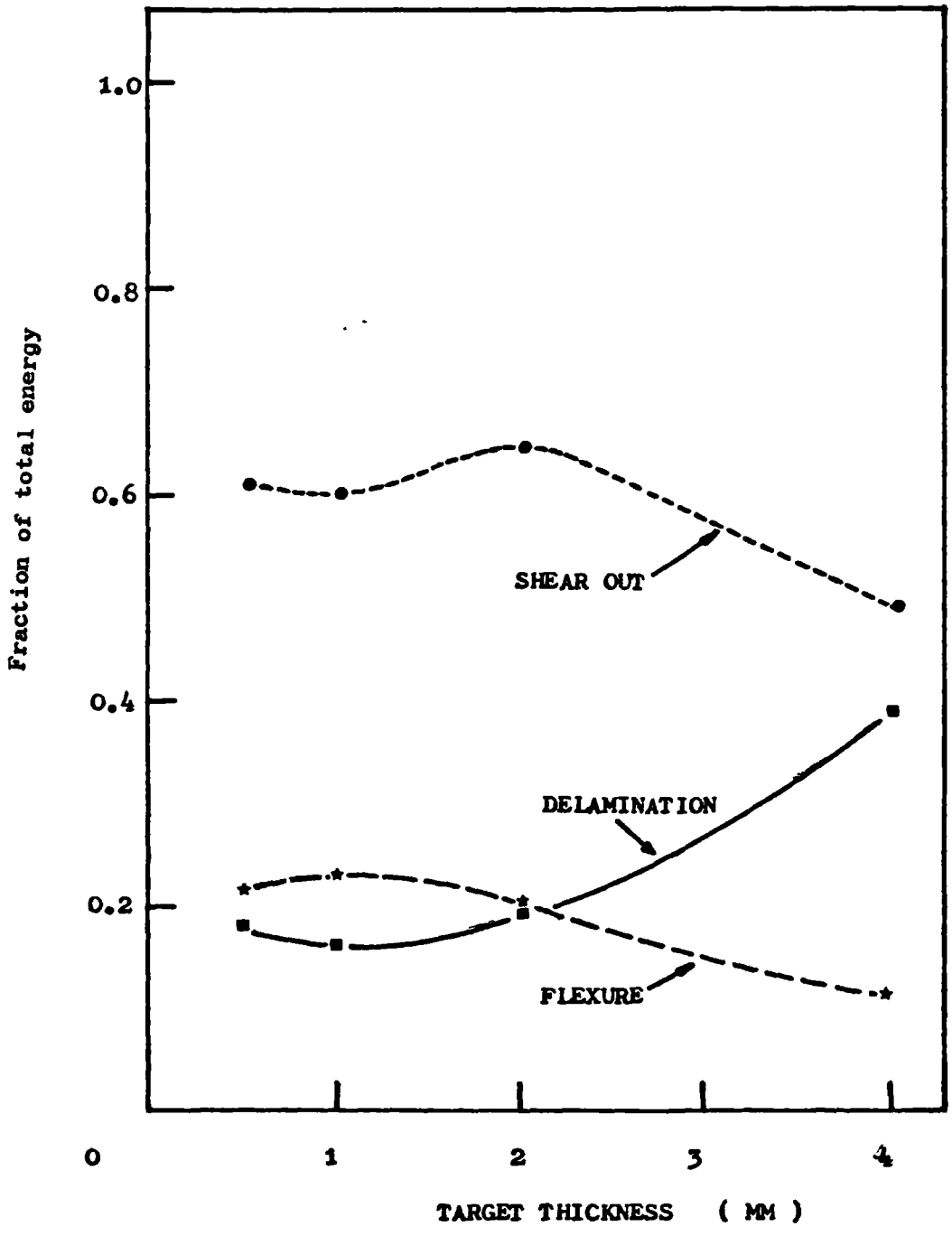


Figure 42

THE VARIATION OF ENERGY DISSIPATED IN DELAMINATION WITH TARGET THICKNESS

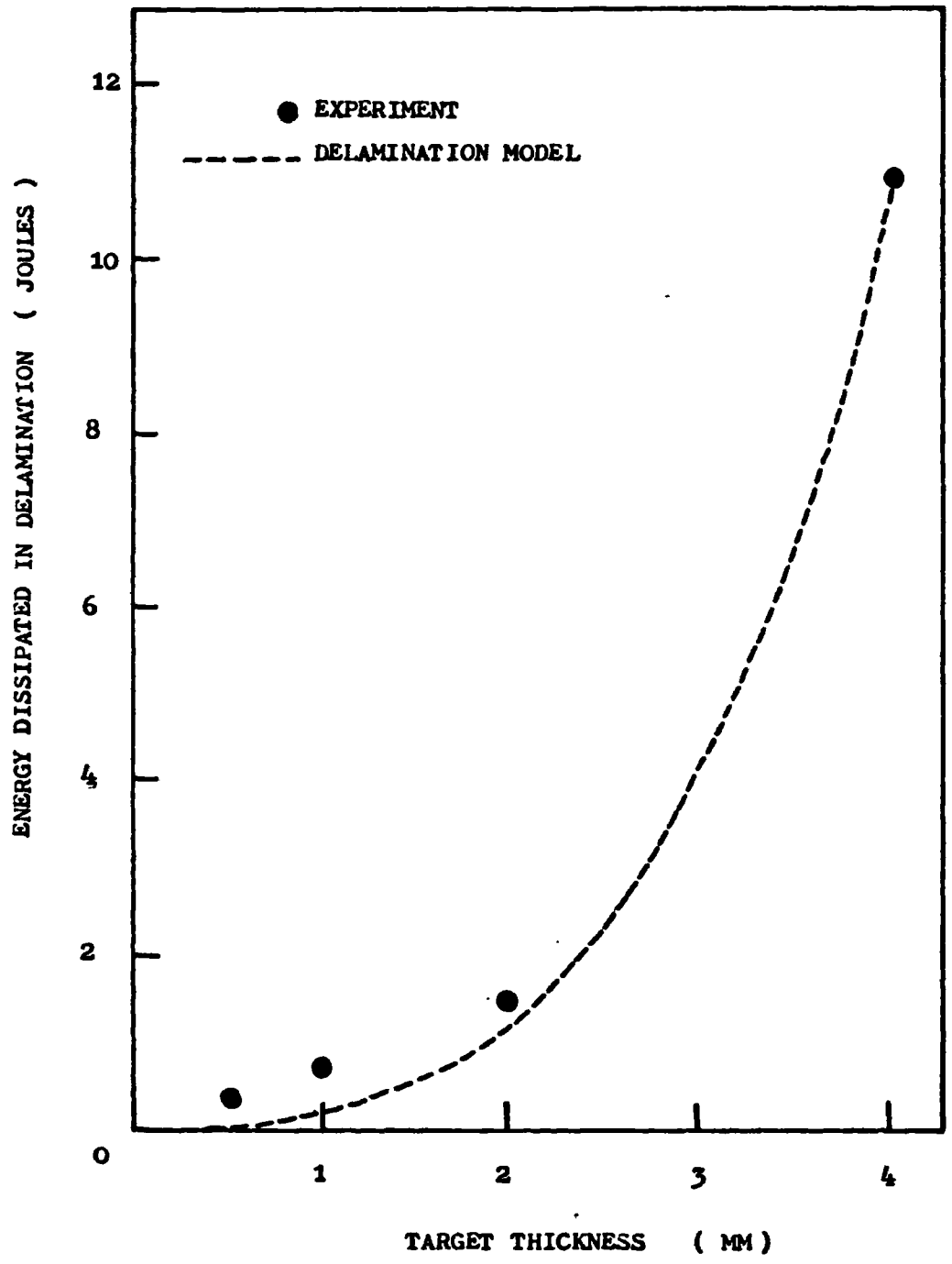
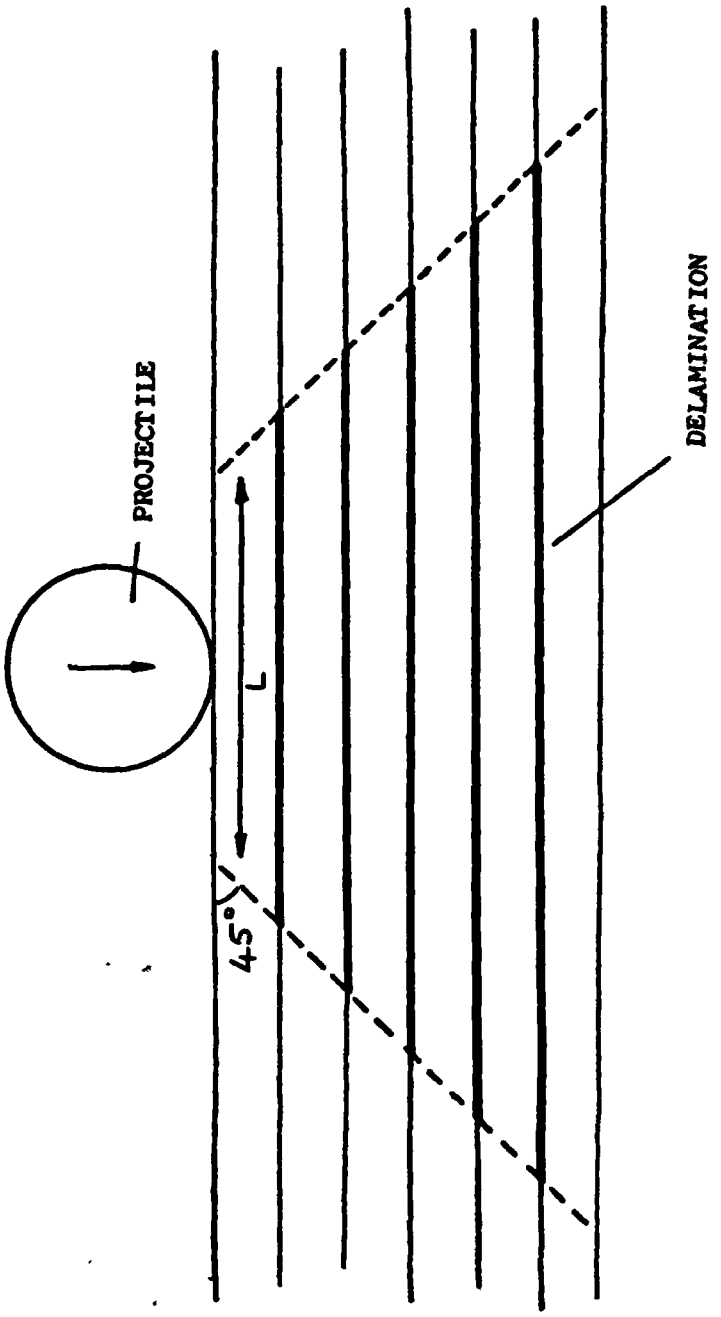


Figure 43



SCHEMATIC REPRESENTATION OF DELAMINATION DAMAGE

Figure 44

THE VARIATION OF THE DROP-WEIGHT PERFORATION ENERGY WITH TARGET THICKNESS FOR THE (+/-45) COMPOSITES.

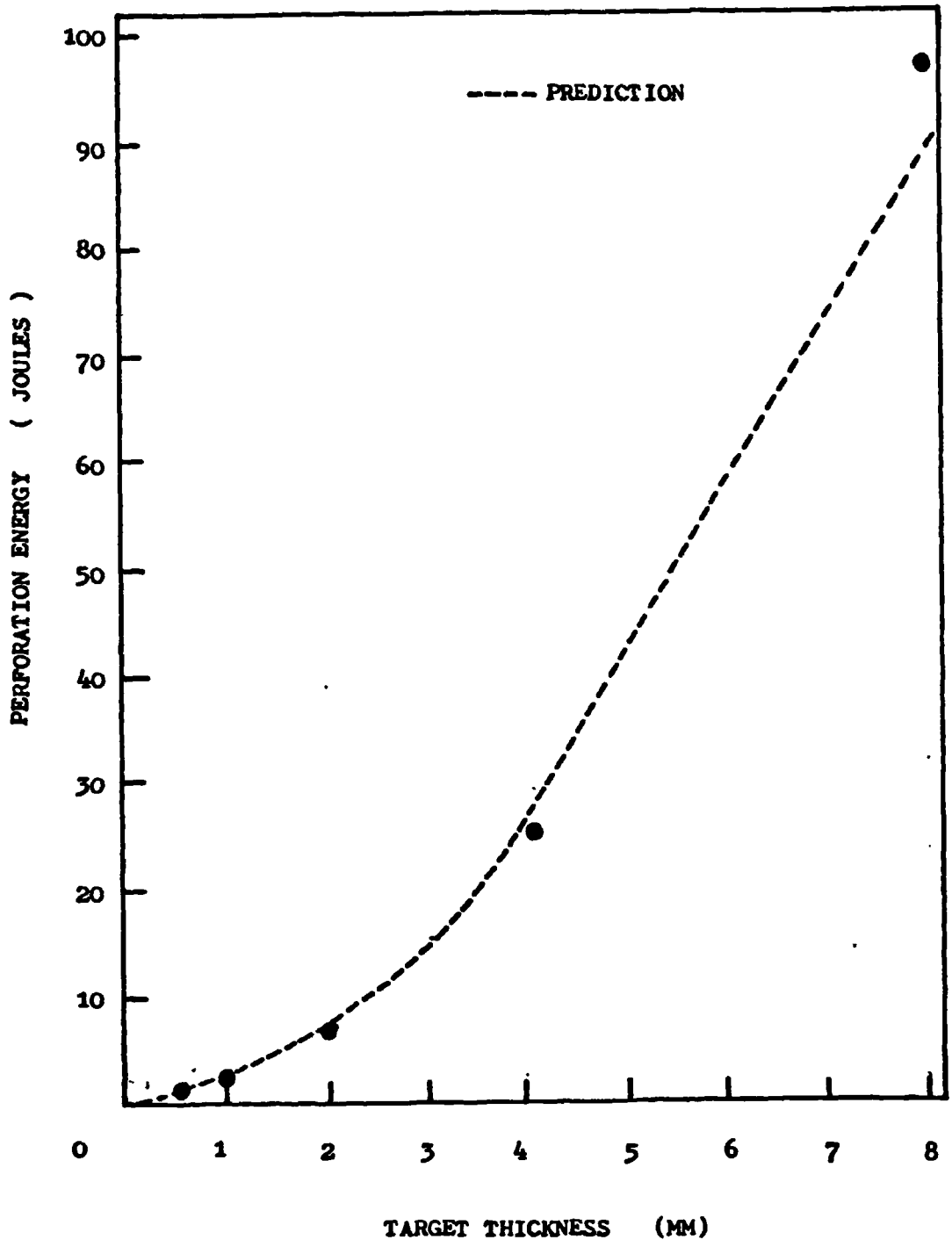
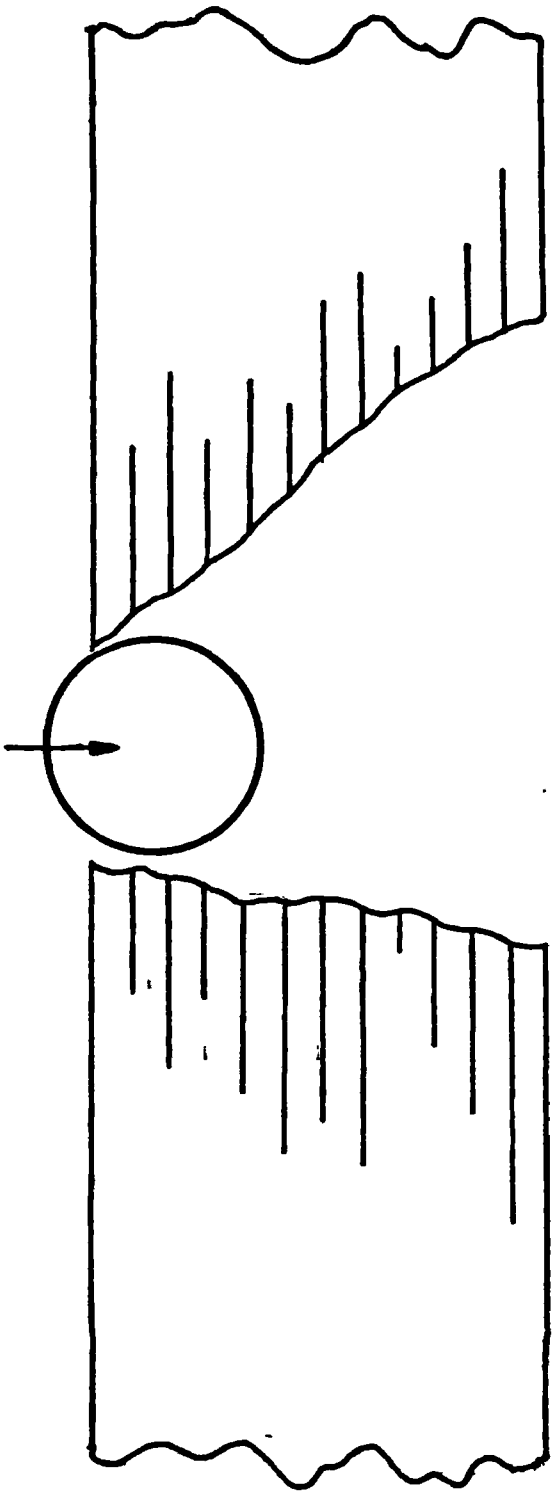


Figure 45



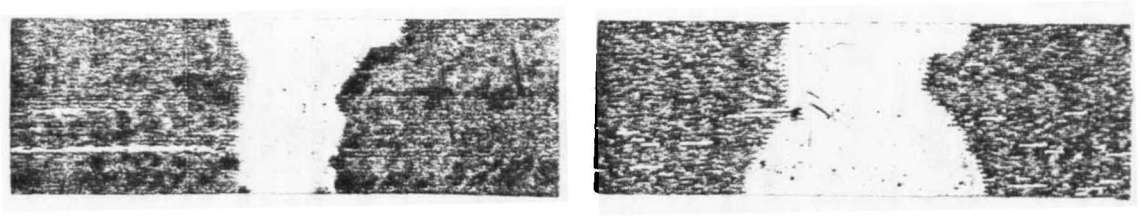
SCHEMATIC REPRESENTATION OF THE SHEAR ZONE IN THE SIXTY FOUR PLY (+/-45) COMPOSITE SUBJECTED TO LOW VELOCITY IMPACT.

Figure 46

ULTRASONIC C-SCANS SHOWING THE EFFECT OF BEAM LENGTH ON LOW VELOCITY IMPACT DAMAGE

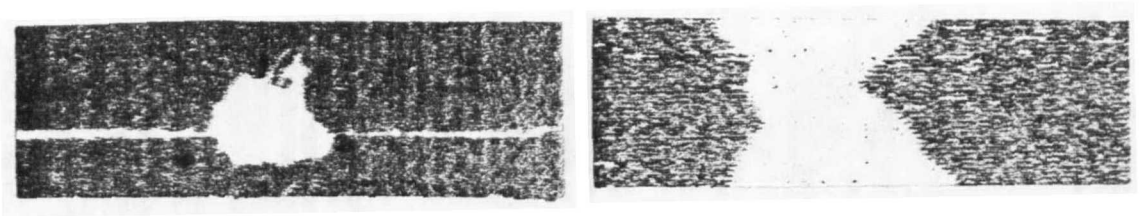
IMPACT ENERGY = 4.2 JOULES

IMPACT ENERGY = 6.0 JOULES



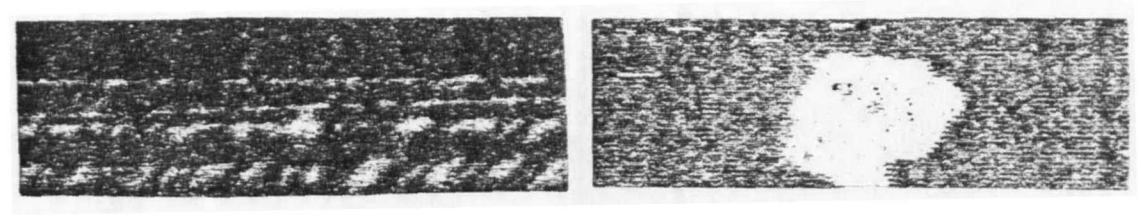
LENGTH = 50 MM

LENGTH = 50 MM



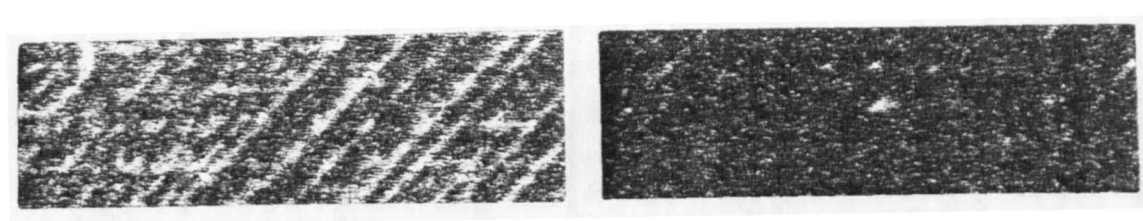
LENGTH = 75 MM

LENGTH = 75 MM



LENGTH = 100 MM

LENGTH = 100 MM



LENGTH = 150 MM

LENGTH = 150 MM

Figure 47

THE VARIATION OF INCIDENT TO CAUSE FIRST DAMAGE WITH BEAM LENGTH.

SIXTEEN PLY (0_s,+/-45) COMPOSITE. LOW VELOCITY IMPACT

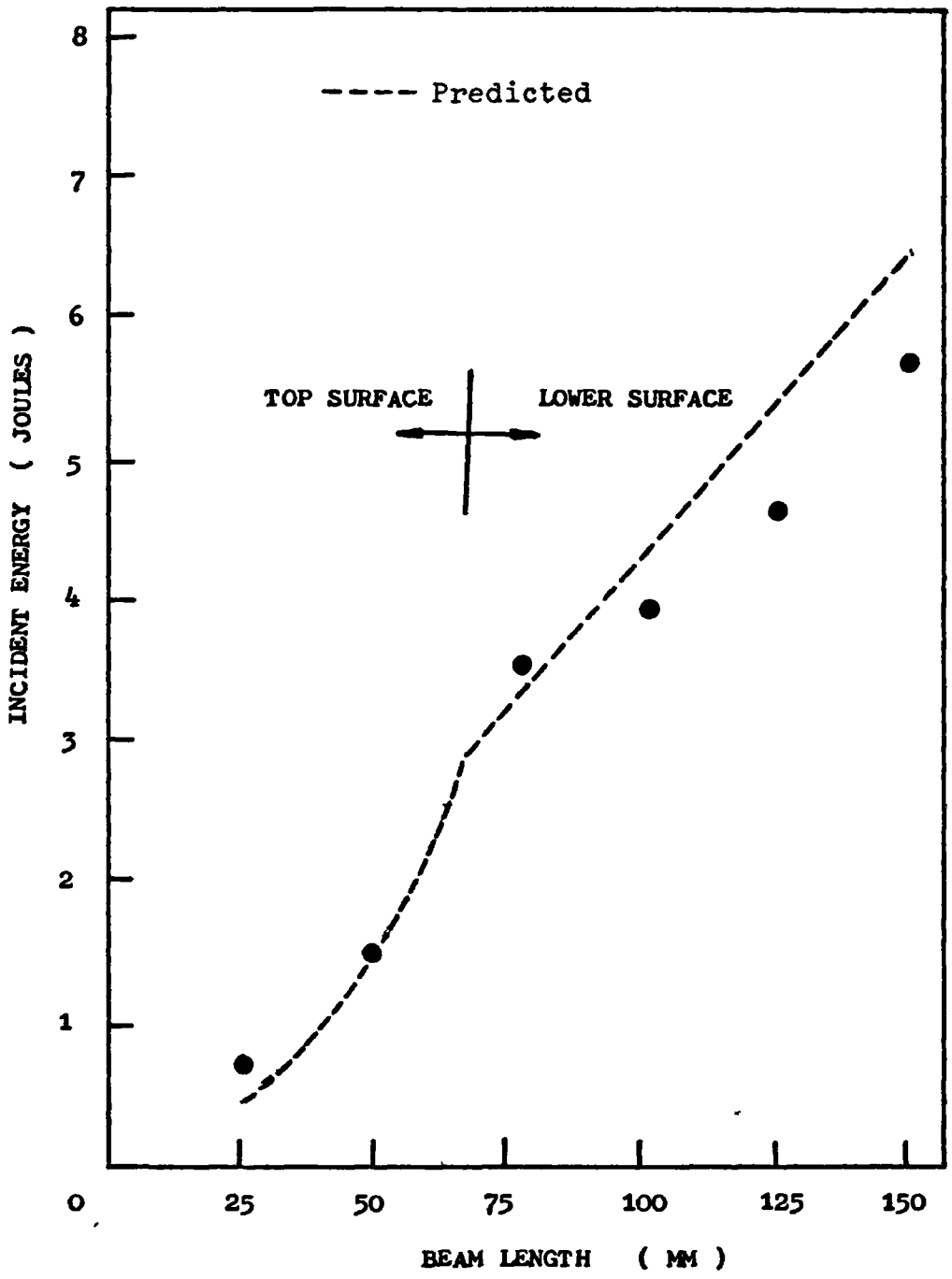


Figure 48

THE VARIATION OF IMPACT ENERGY TO INITIATE FIBRE FRACTURE WITH IMPACT ENERGY. SIXTEEN PLY (0,+/-45) COMPOSITE. DROP WEIGHT IMPACT.

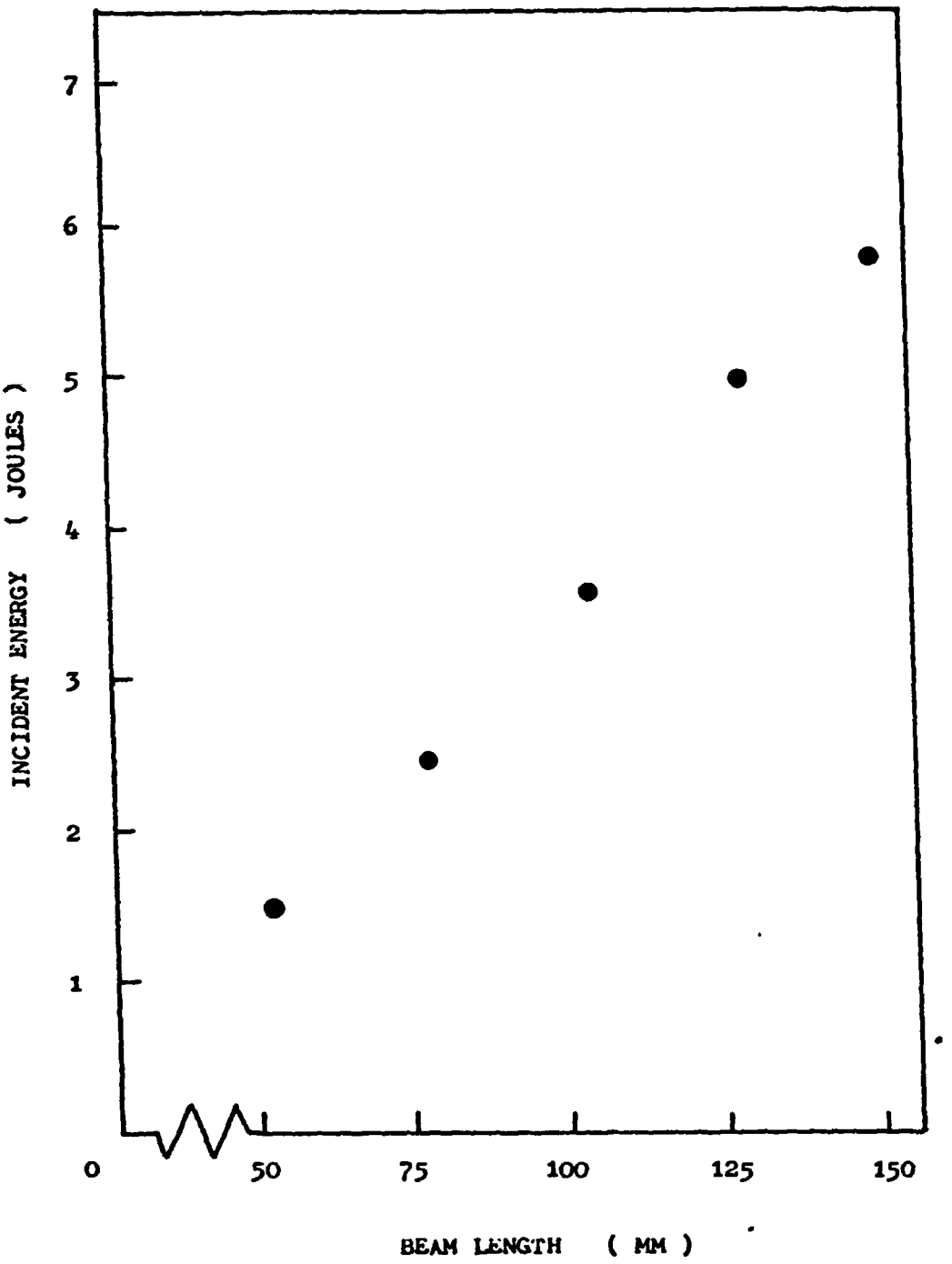


Figure 49

THE EFFECT OF BEAM LENGTH ON THE VARIATION OF DROP-WEIGHT PERFORATION ENERGY WITH BEAM LENGTH.
SIXTEEN PLY (0,+/-45) COMPOSITE.

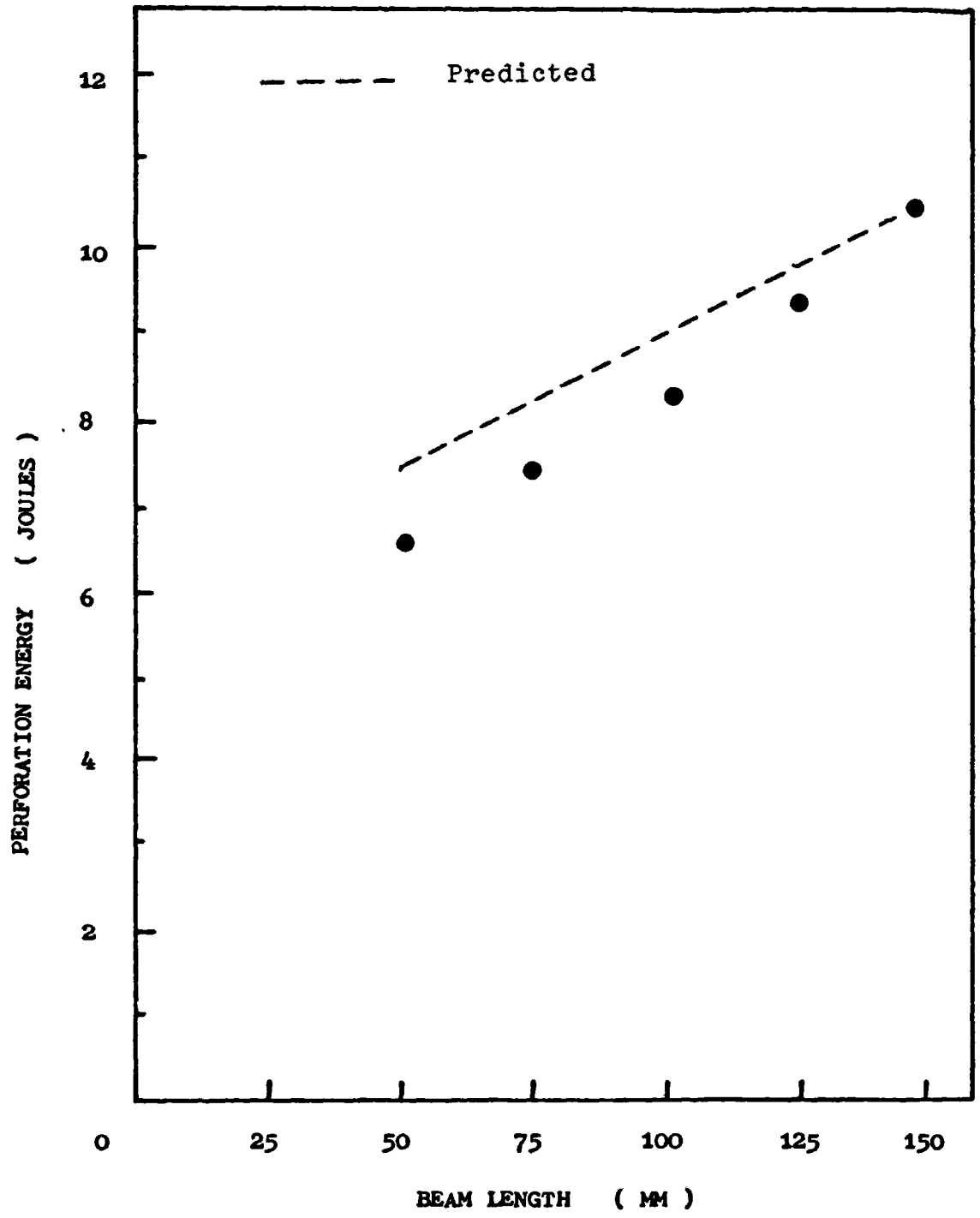
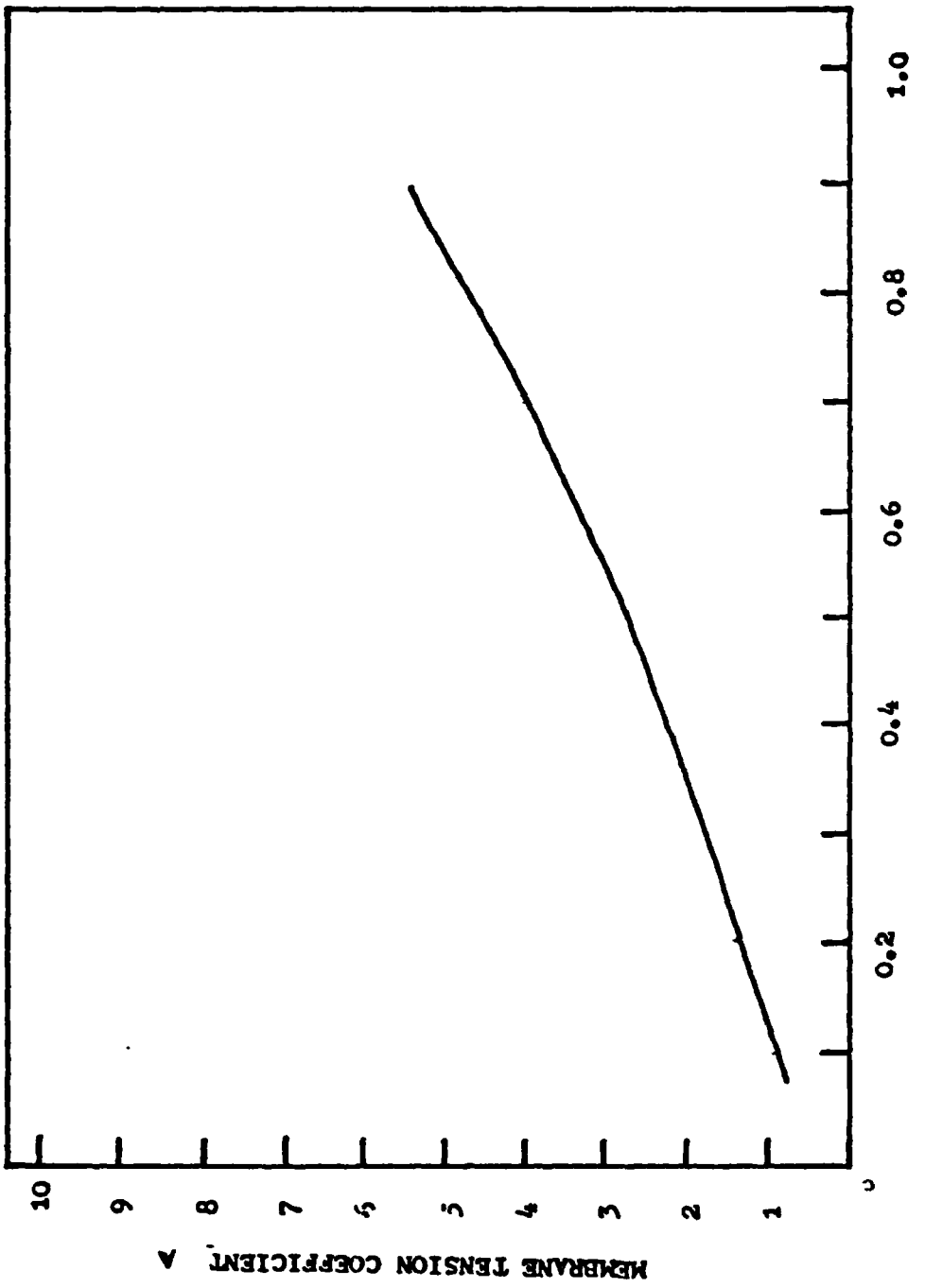


Figure 50



THE VARIATION OF THE MEMBRANE TENSION COEFFICIENT

Figure 51

THE VARIATION OF INCIDENT ENERGY TO INITIATE FIRST DAMAGE WITH TARGET THICKNESS FOR THE (+/-45) CIRCULAR PLATES

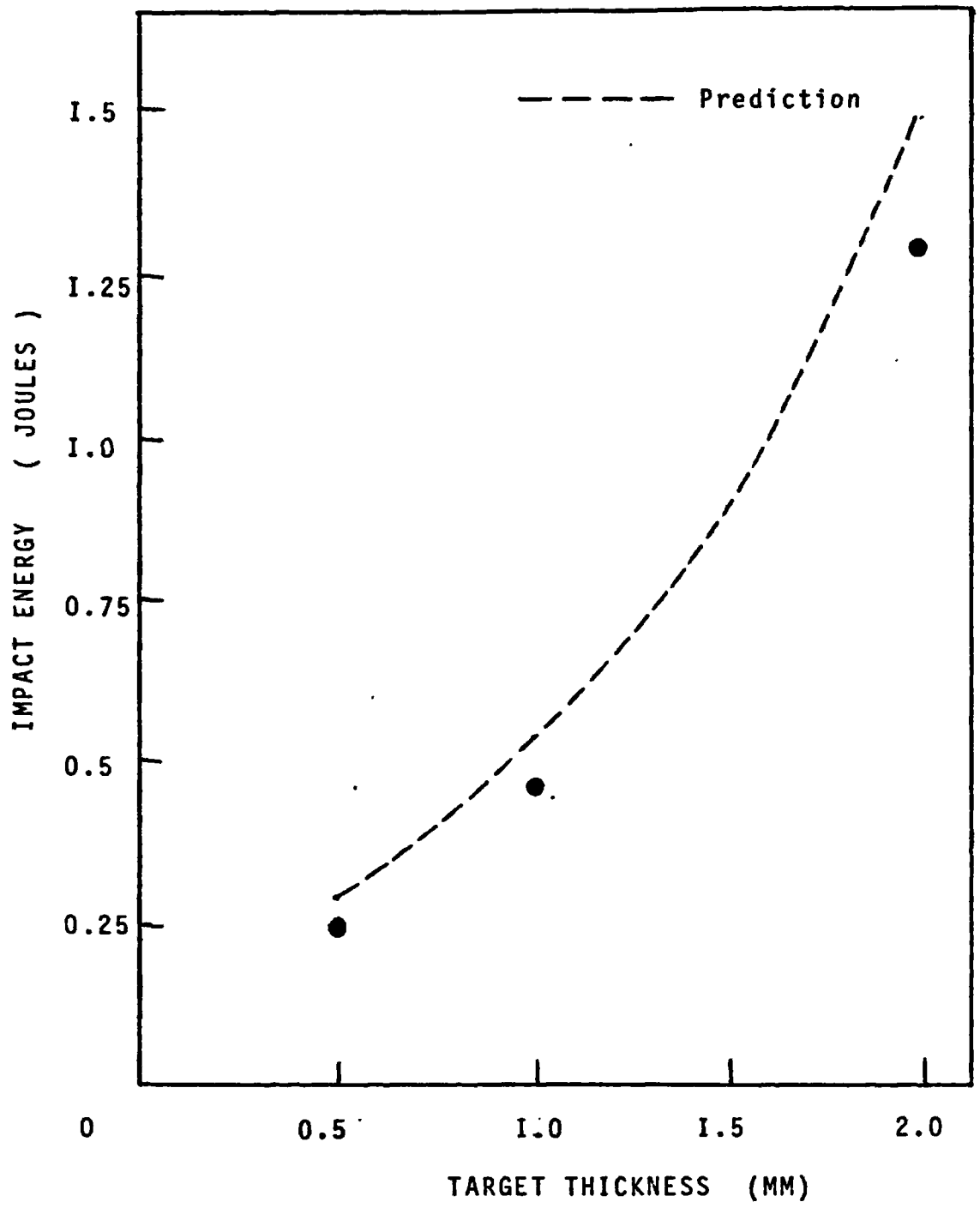


Figure 52

THE VARIATION OF PERFORATION ENERGY WITH TARGET THICKNESS FOR THE (+/-45) CIRCULAR PLATES

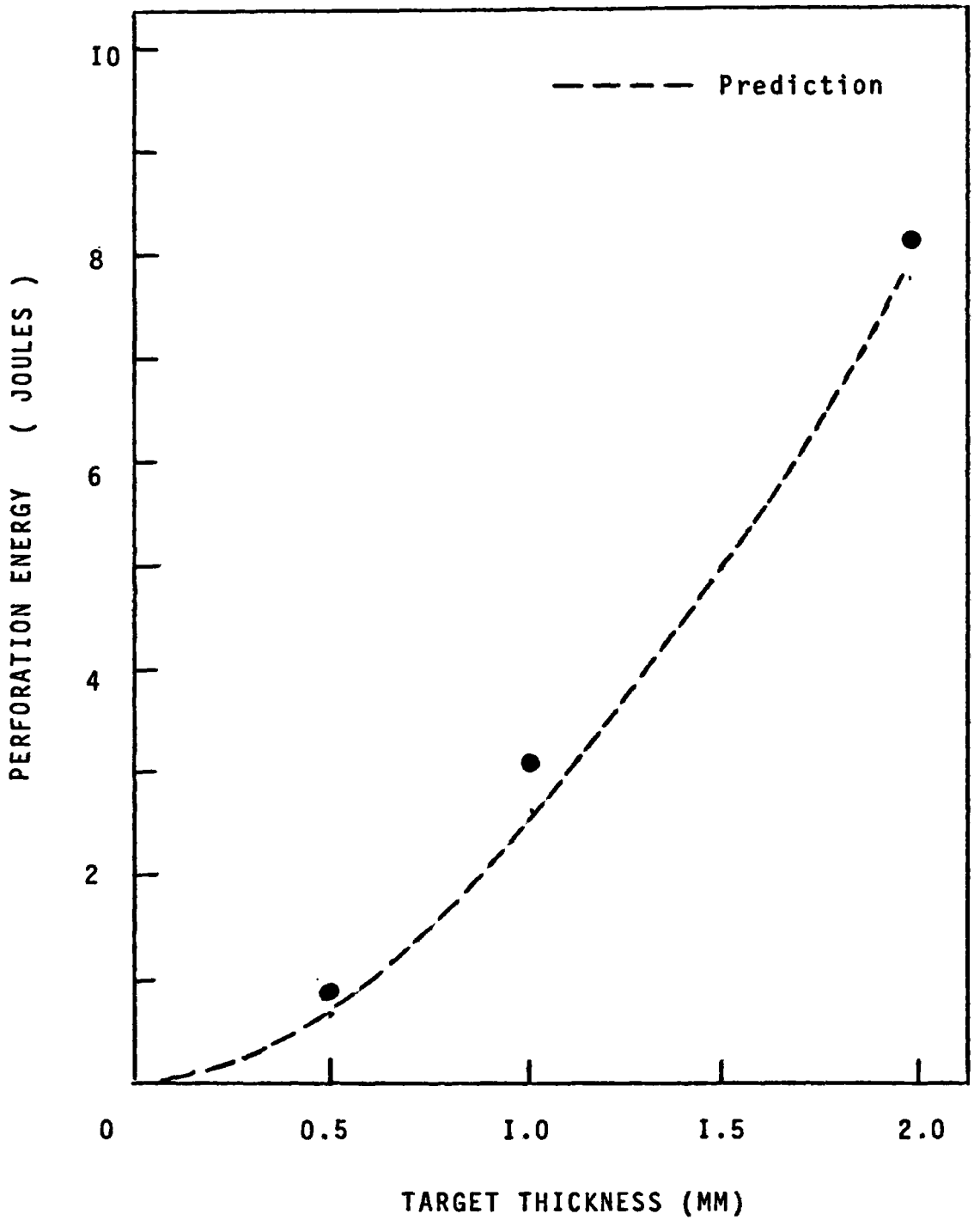


Figure 53

THE VARIATION OF RESIDUAL TENSILE STRENGTH WITH IMPACT ENERGY FOR THE EIGHT PLY (+/-45) COMPOSITE.

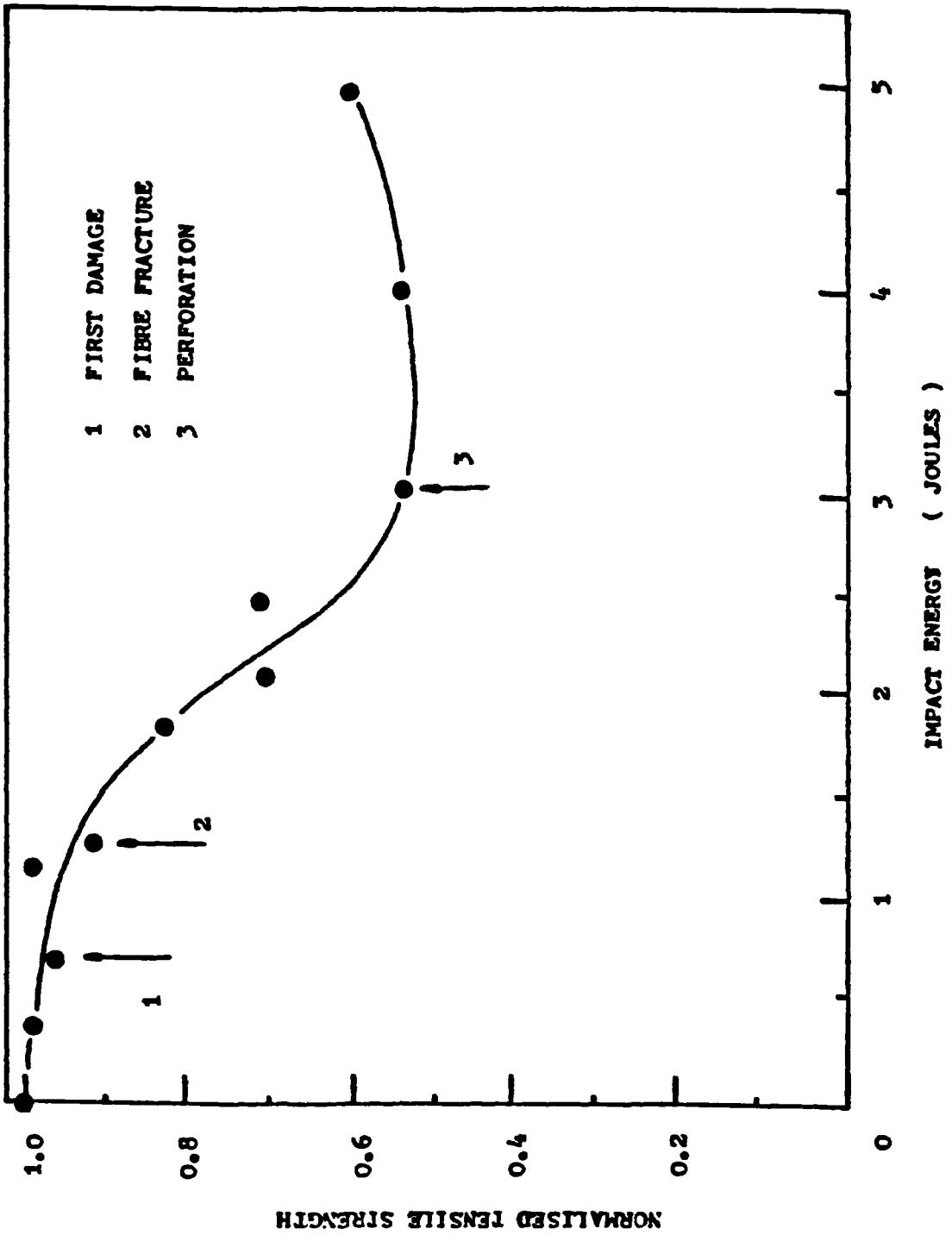
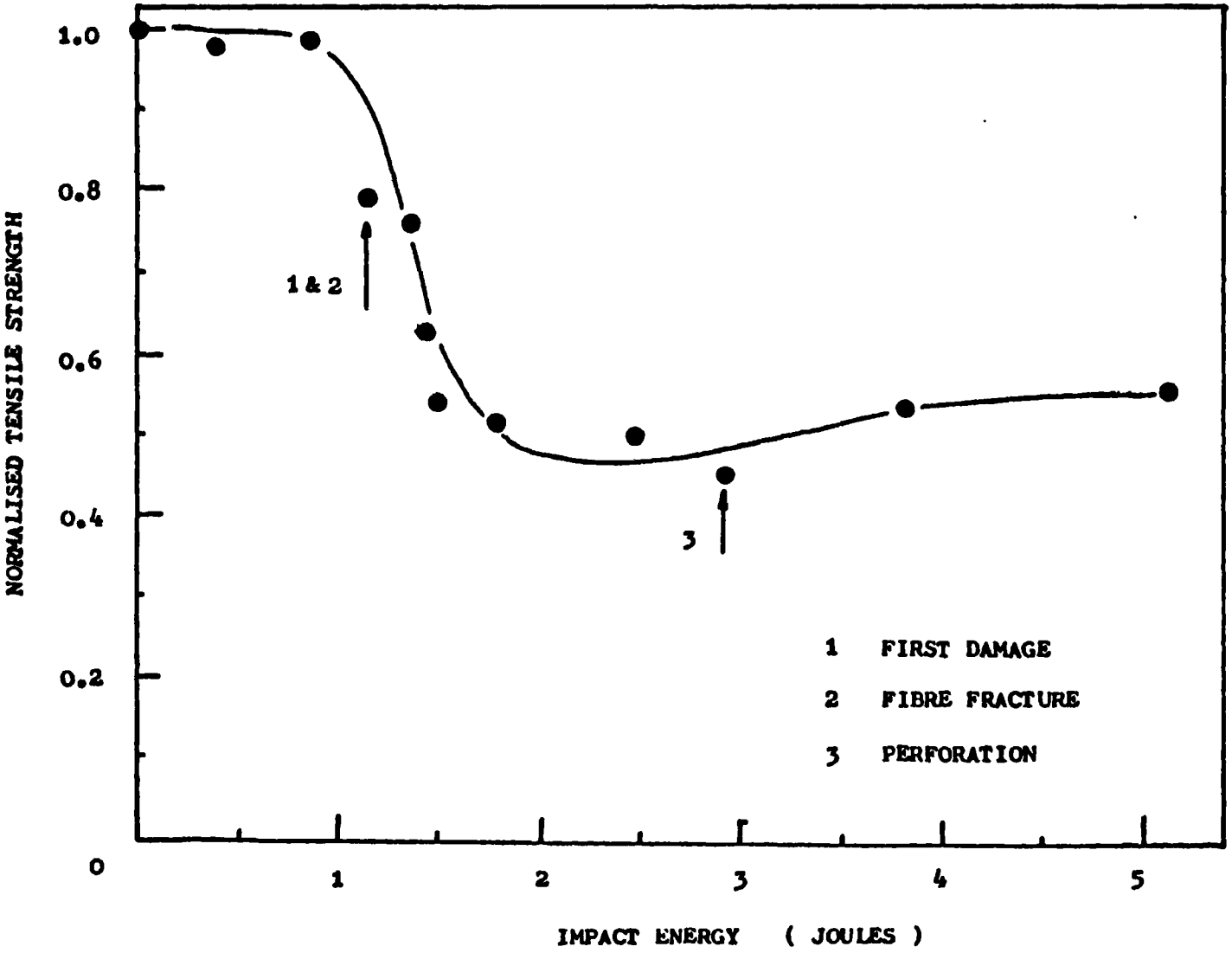


Figure 54

Figure 55



DROP WEIGHT IMPACT

THE VARIATON OF THE NORMALISED TENSILE STRENGTH WITH IMPACT ENERGY

EIGHT PLY (0,+/-45)

THE VARIATION OF RESIDUAL TENSILE STRENGTH WITH IMPACT ENERGY FOR THE SIXTEEN PLY (0,+/-45) COMPOSITE.

DROP WEIGHT IMPACT

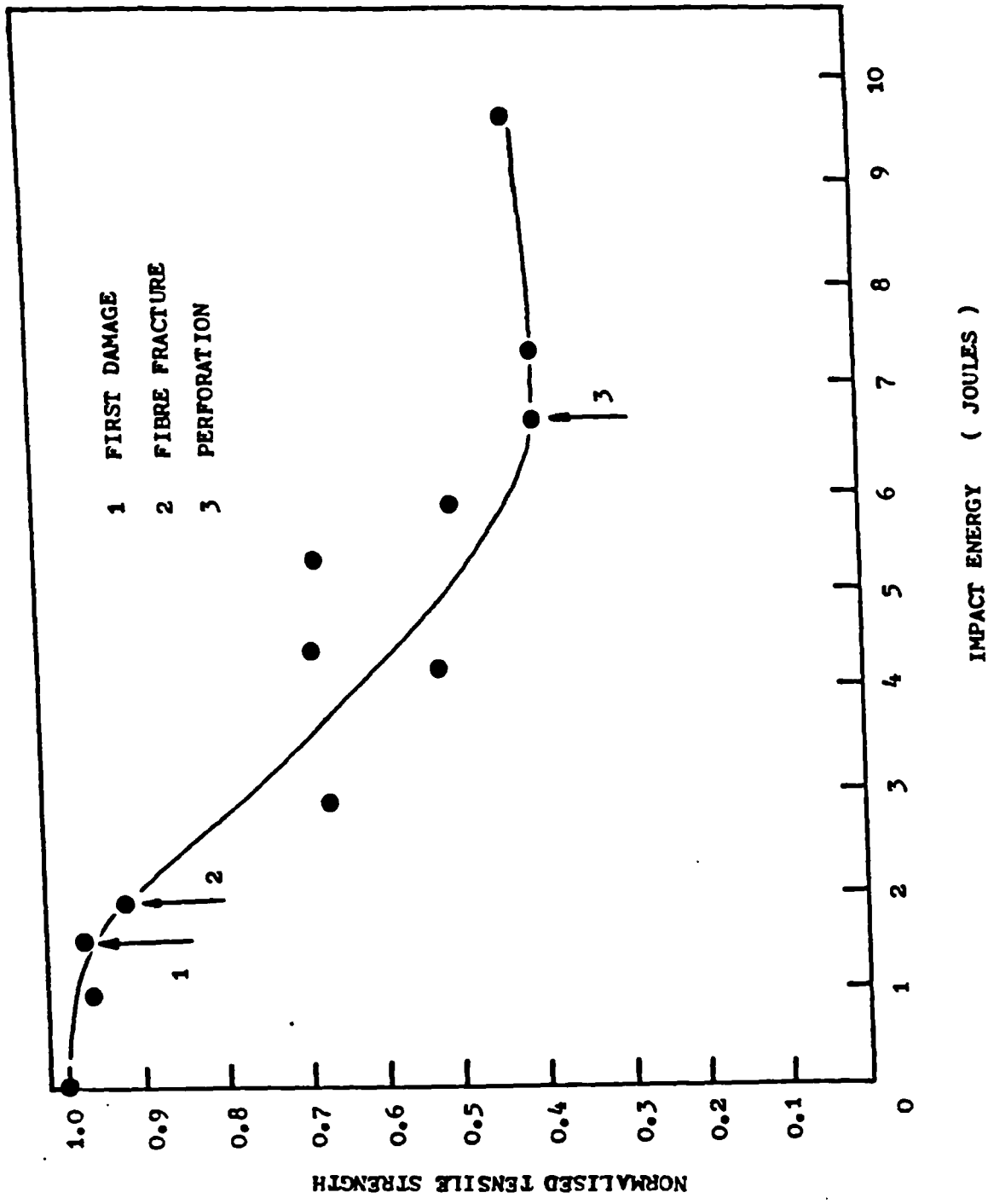


Figure 56

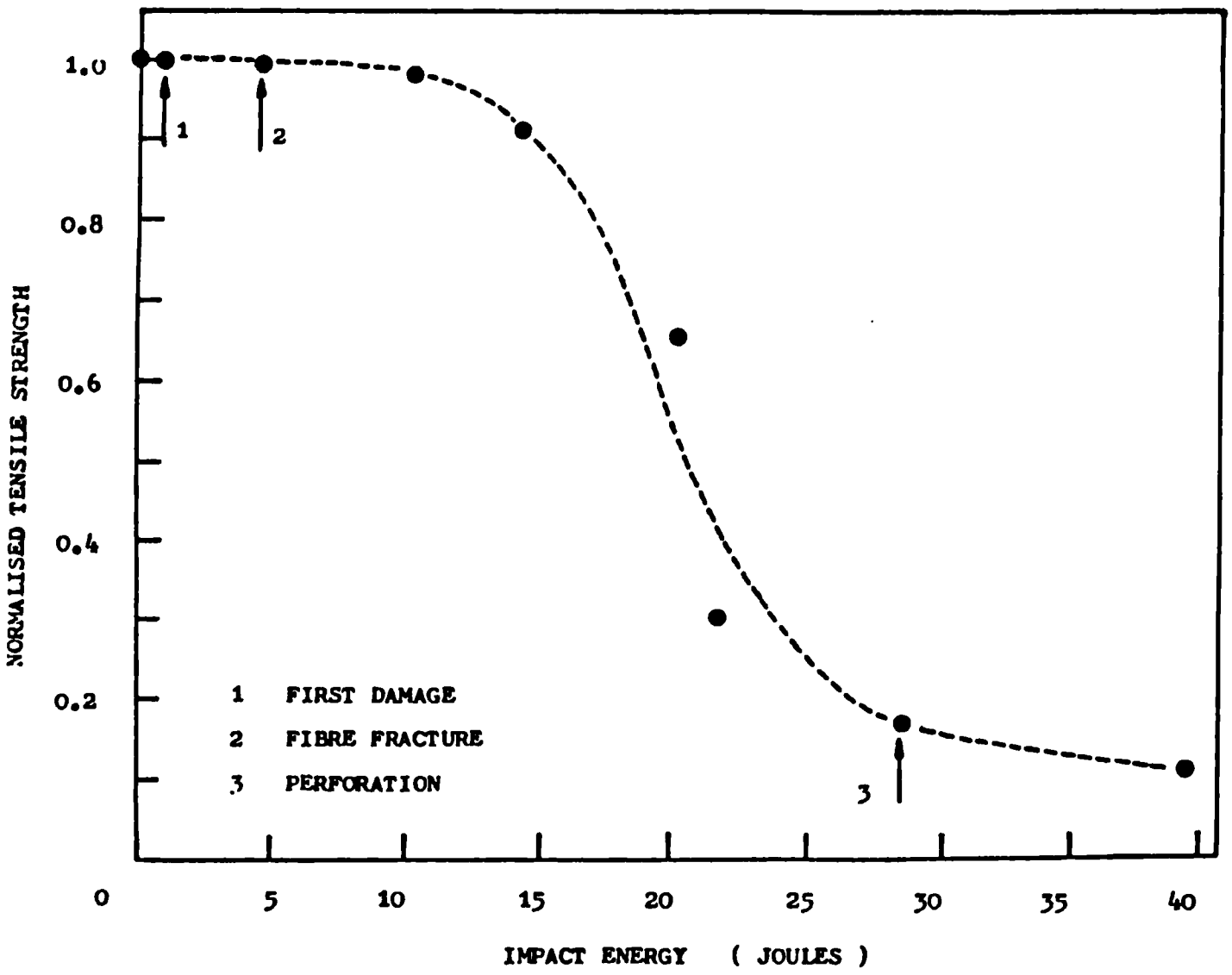


Figure 57

THE VARIATION OF NORMALISED TENSILE STRENGTH WITH IMPACT ENERGY

COMPARISON OF NOTCH INSENSITIVE MODEL WITH DATA FROM CENTRE NOTCHED SIXTEEN PLY (+/-45) COMPOSITE.

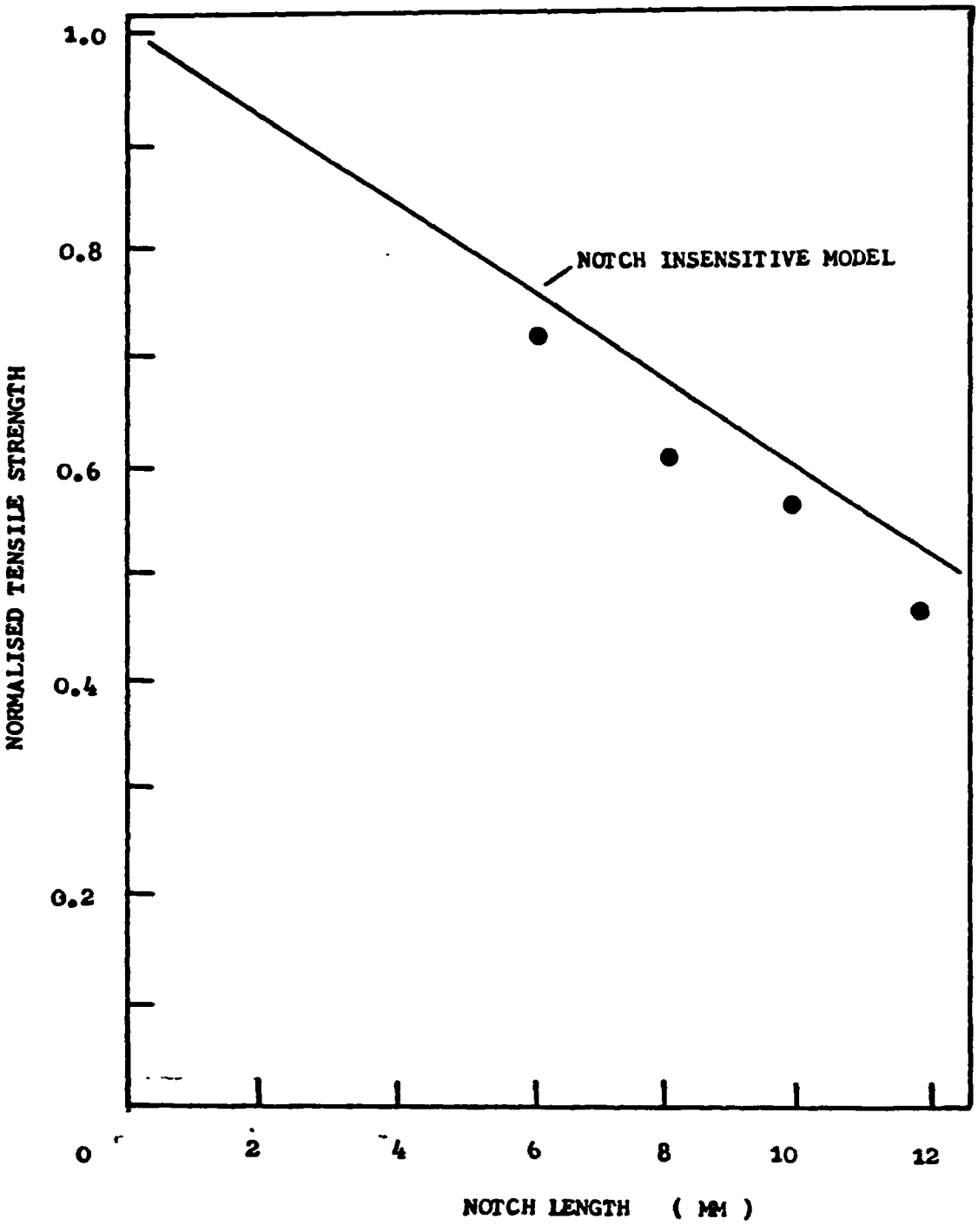


Figure 58

COMPARISON OF WADDOUPS FRACTURE MODEL AND LEFM WITH CENTRE NOTCHED SIXTEEN PLY (0,+/-45) COMPOSITES.

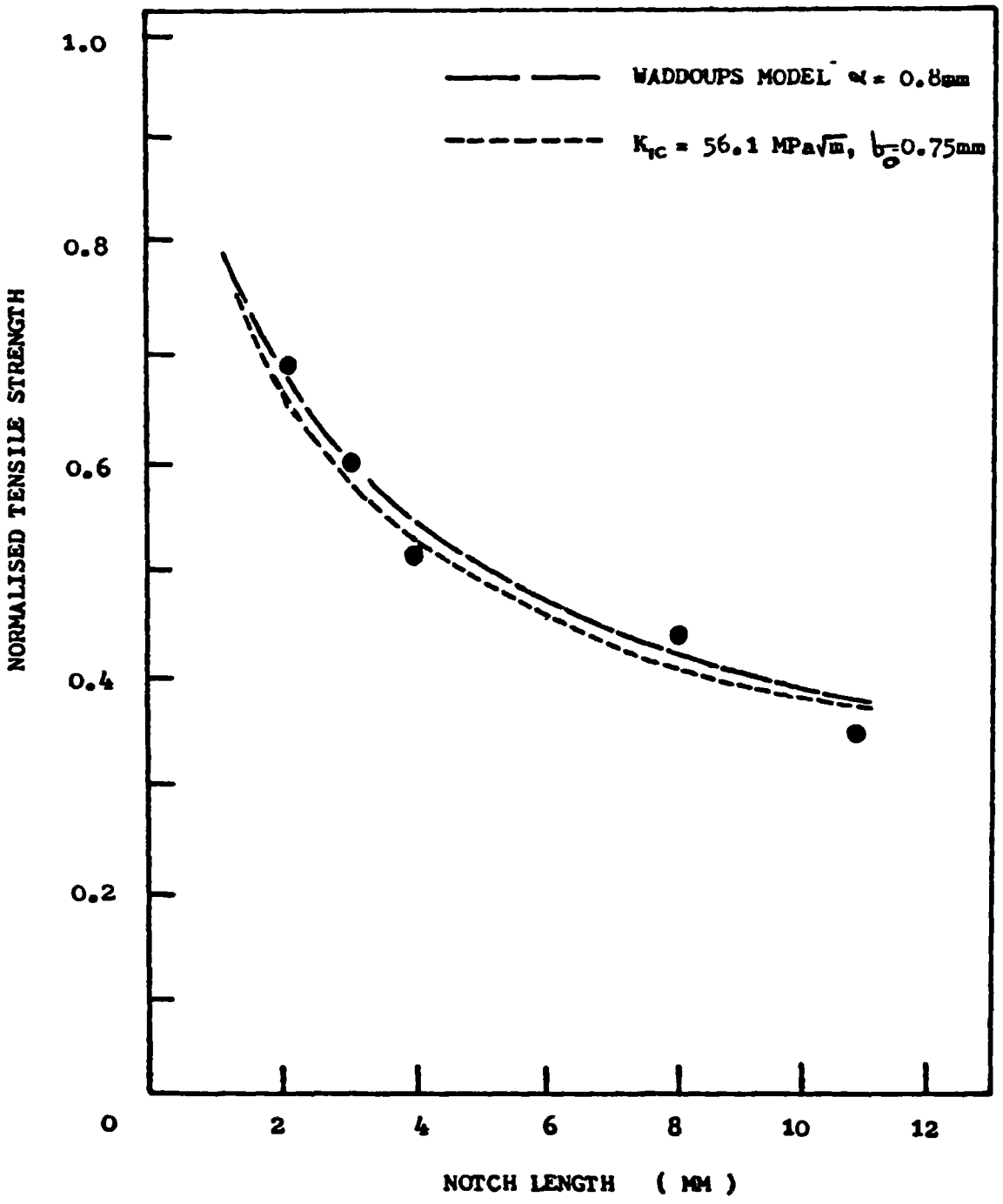


Figure 59a

COMPARISON OF AVERAGE STRESS CRITERION AND POINT STRESS CRITERION WITH CENTRE NOTCHED SIXTEEN PLY (0,+/-45) COMPOSITES.

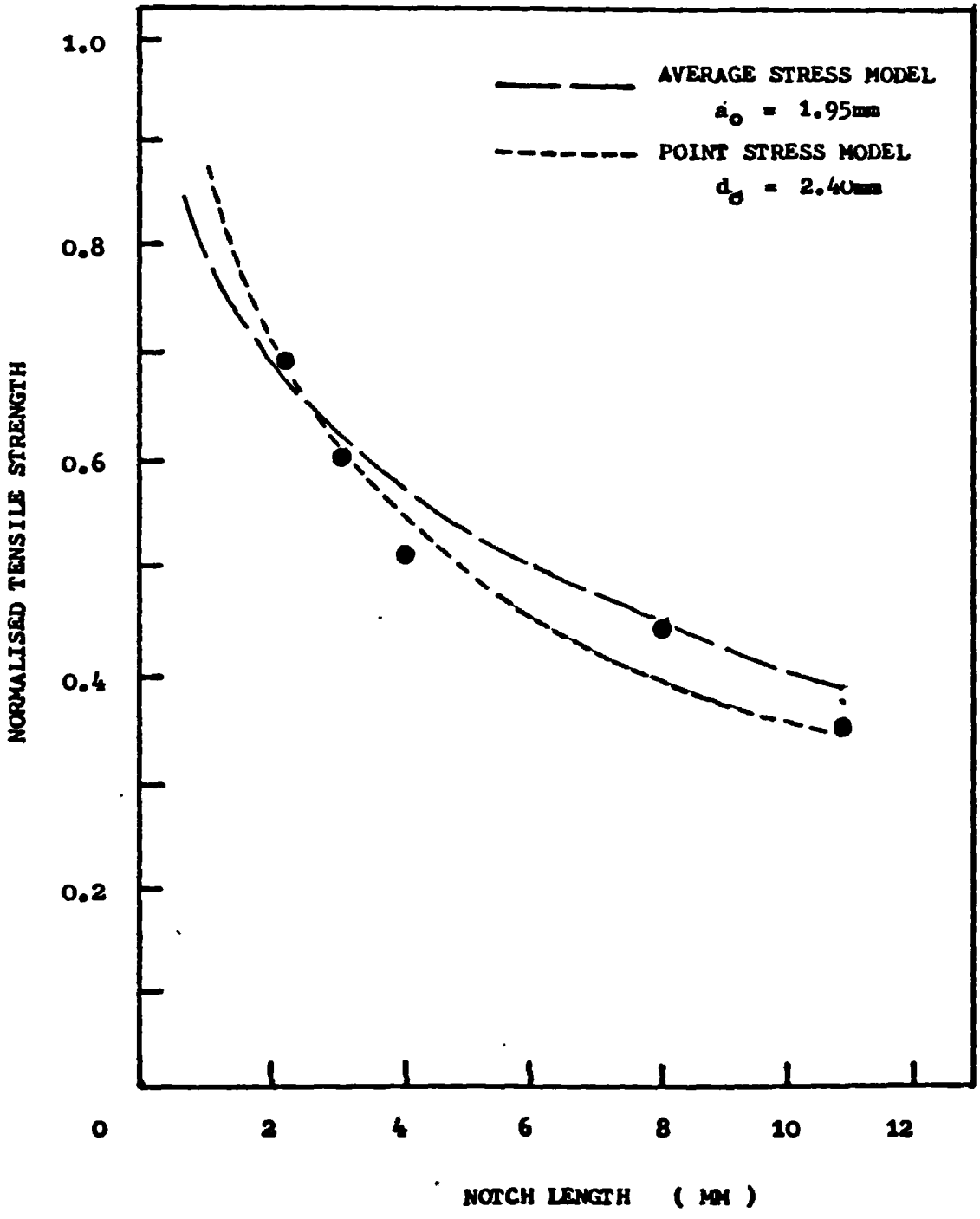


Figure 59b

THE VARIATION OF NORMALISED TENSILE STRENGTH WITH CRACK LENGTH FOR $\left[\left[0,+/-45,0\right]_2\right]_s$ COMPOSITE.

DATA TAKEN FROM KELLAS (49)

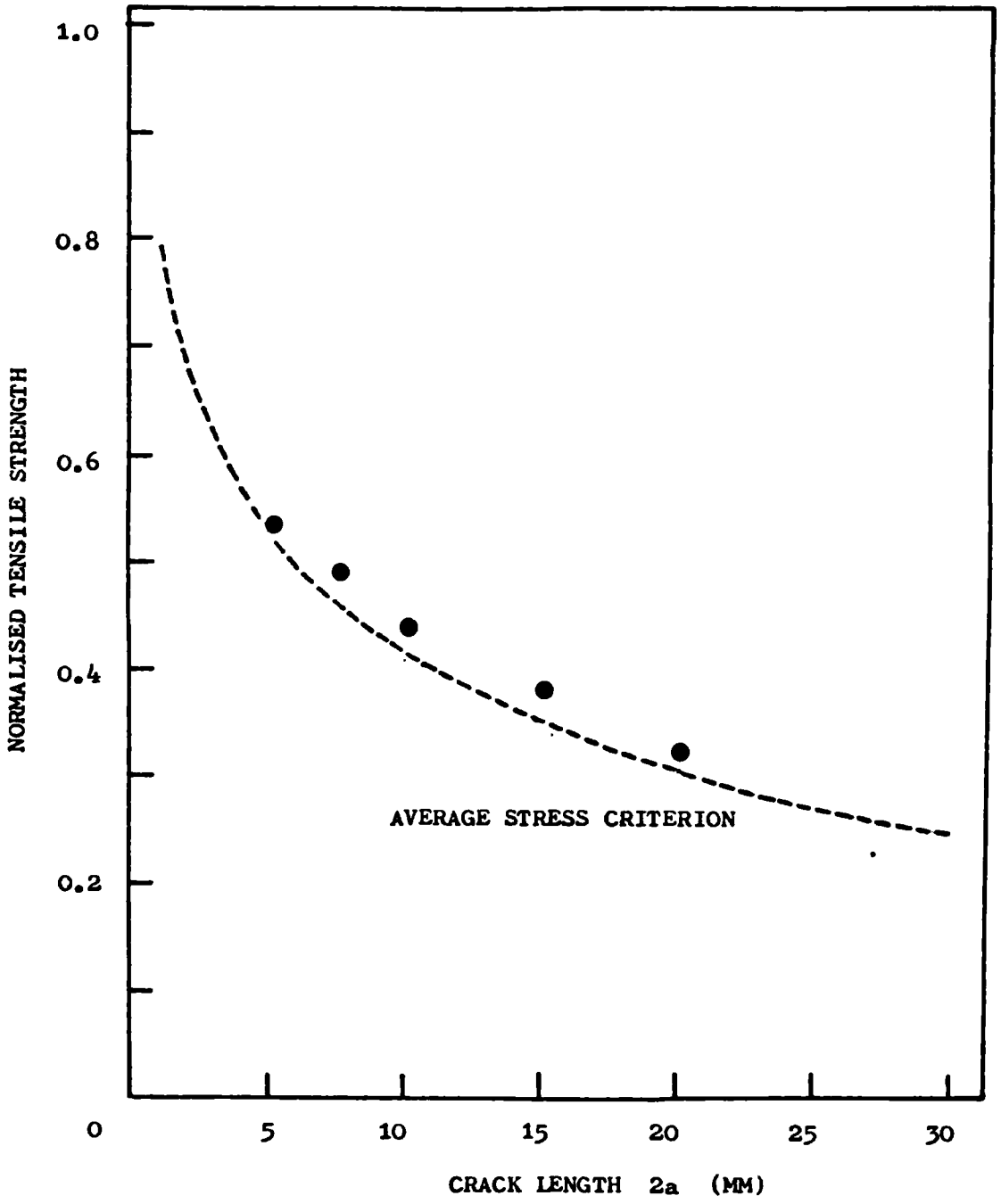
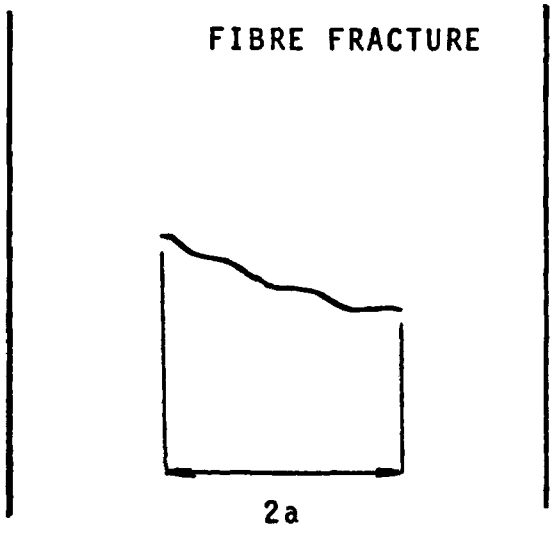


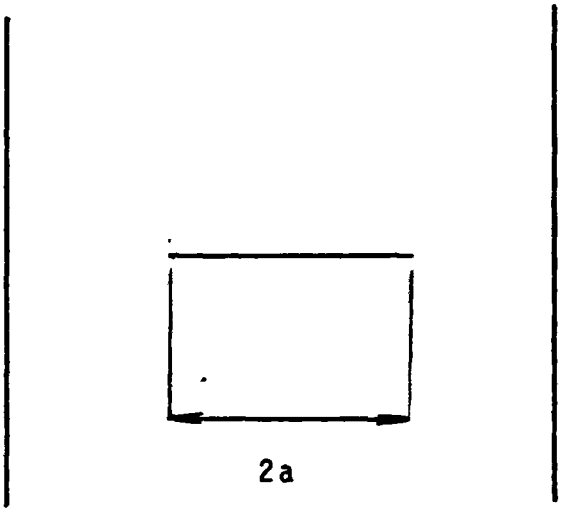
Figure 60

SCHEMATIC REPRESENTATIONS SHOWING HOW IMPACT DAMAGE IS IDEALISED AS A SIMPLE CRACK FOR THE FRACTURE MECHANICS ANALYSIS



IMPACT DAMAGE

(a)



EQUIVALENT CRACK

(b)

Figure 61

THE VARIATION OF NORMALISED TENSILE STRENGTH WITH CRACK LENGTH FOR TH

EIGHT PLY (+/-45) COMPOSITE SUBJECTED TO DROP WEIGHT IMPACT

LOADING

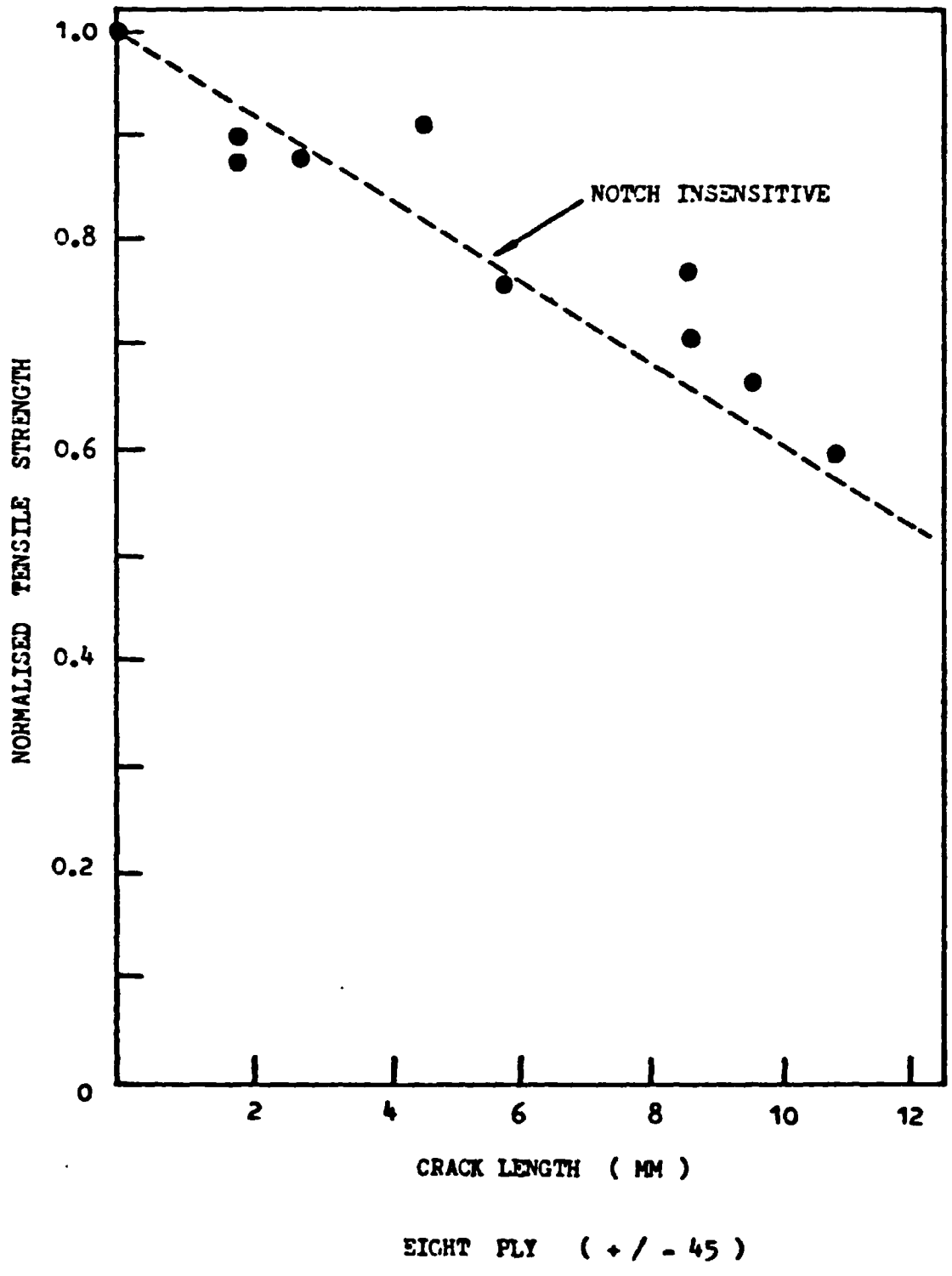


Figure 62

THE VARIATION OF NORMALISED TENSILE STRENGTH WITH CRACK LENGTH FOR THE EIGHT PLY (0,+/-45) COMPOSITE SUBJECTED TO DROP WEIGHT IMPACT LOADING

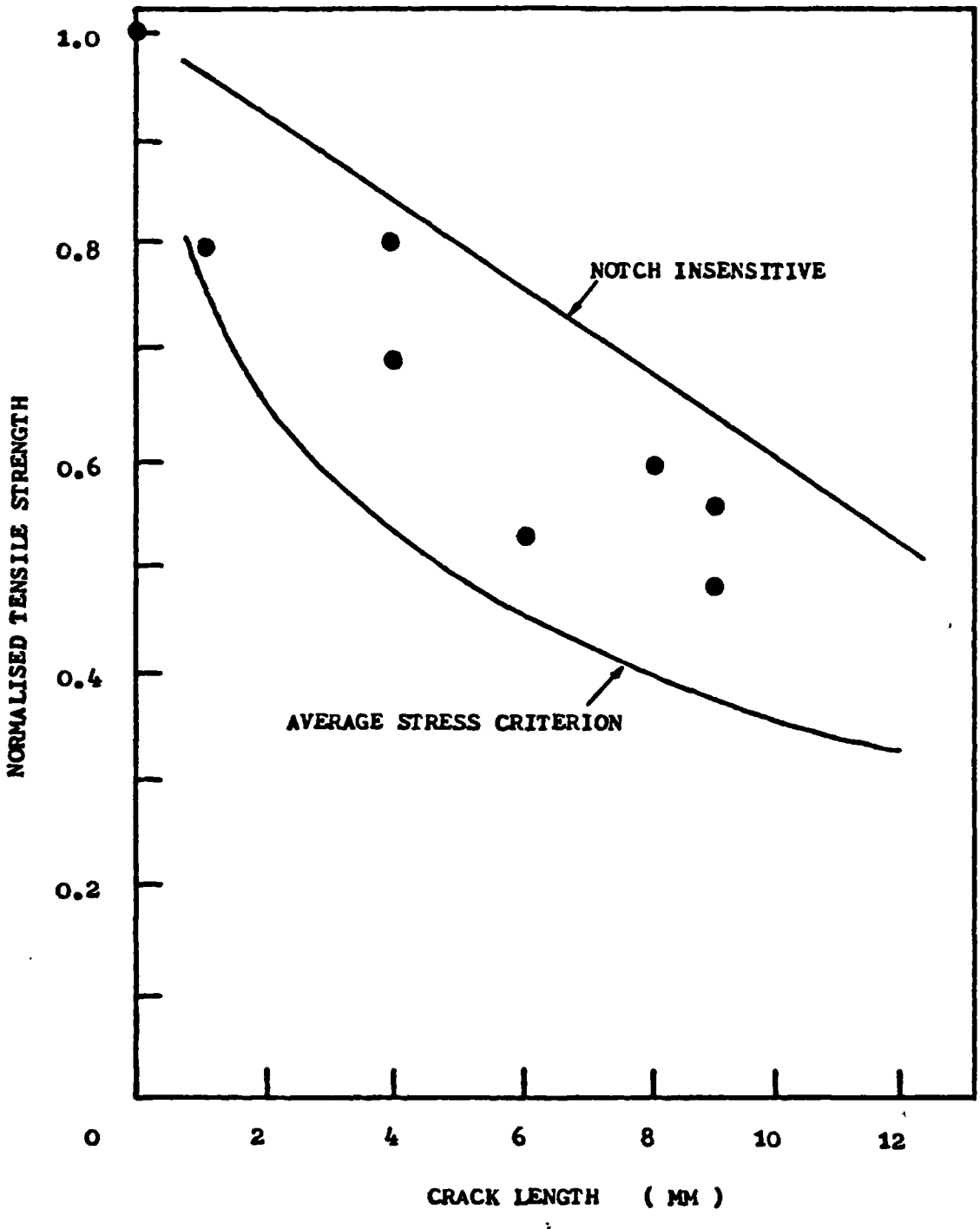


Figure 63

THE VARIATION OF NORMALISED TENSILE STRENGTH WITH CRACK LENGTH FOR THE SIXTEEN PLY (0,+/-45) COMPOSITE SUBJECTED TO DROP WEIGHT IMPACT LOADING.

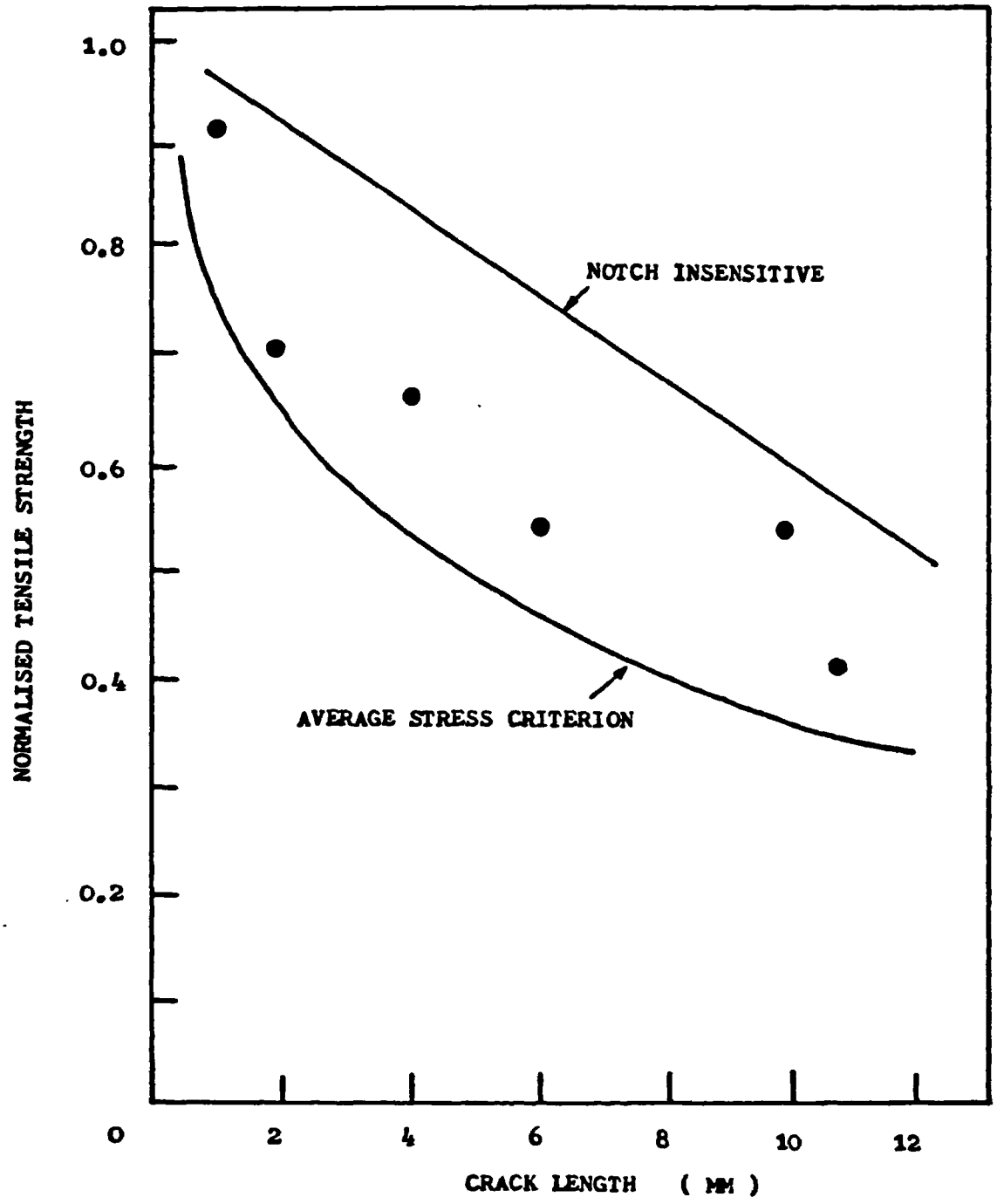


Figure 64

DAMAGE DEVELOPMENT IN THE EIGHT PLY (+/-45) COMPOSITE SUBJECTED TO DROP WEIGHT IMPACT LOADING.

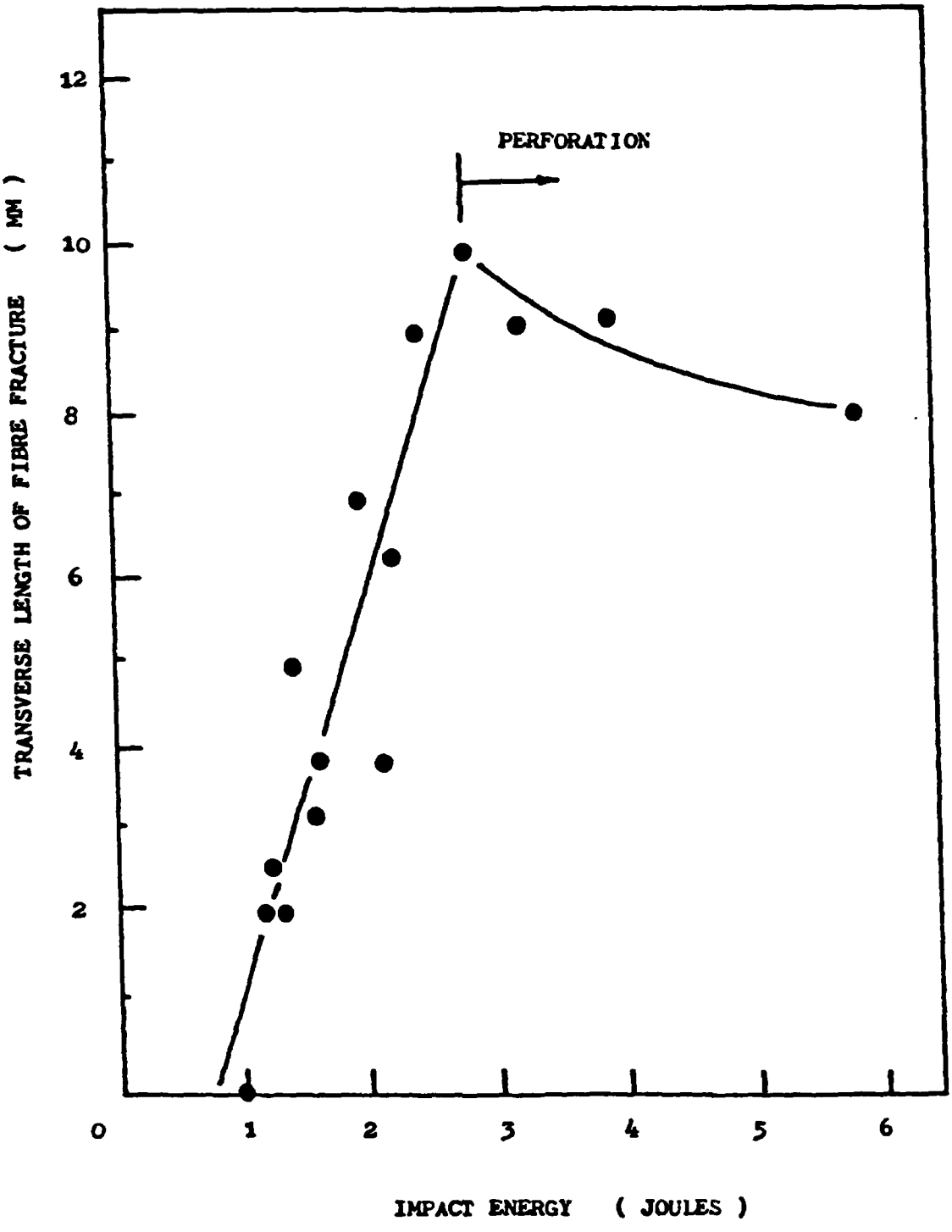


Figure 65

DAMAGE DEVELOPMENT IN THE EIGHT PLY (0, +/-45) COMPOSITE SUBJECTED TO DROP WEIGHT IMPACT LOADING

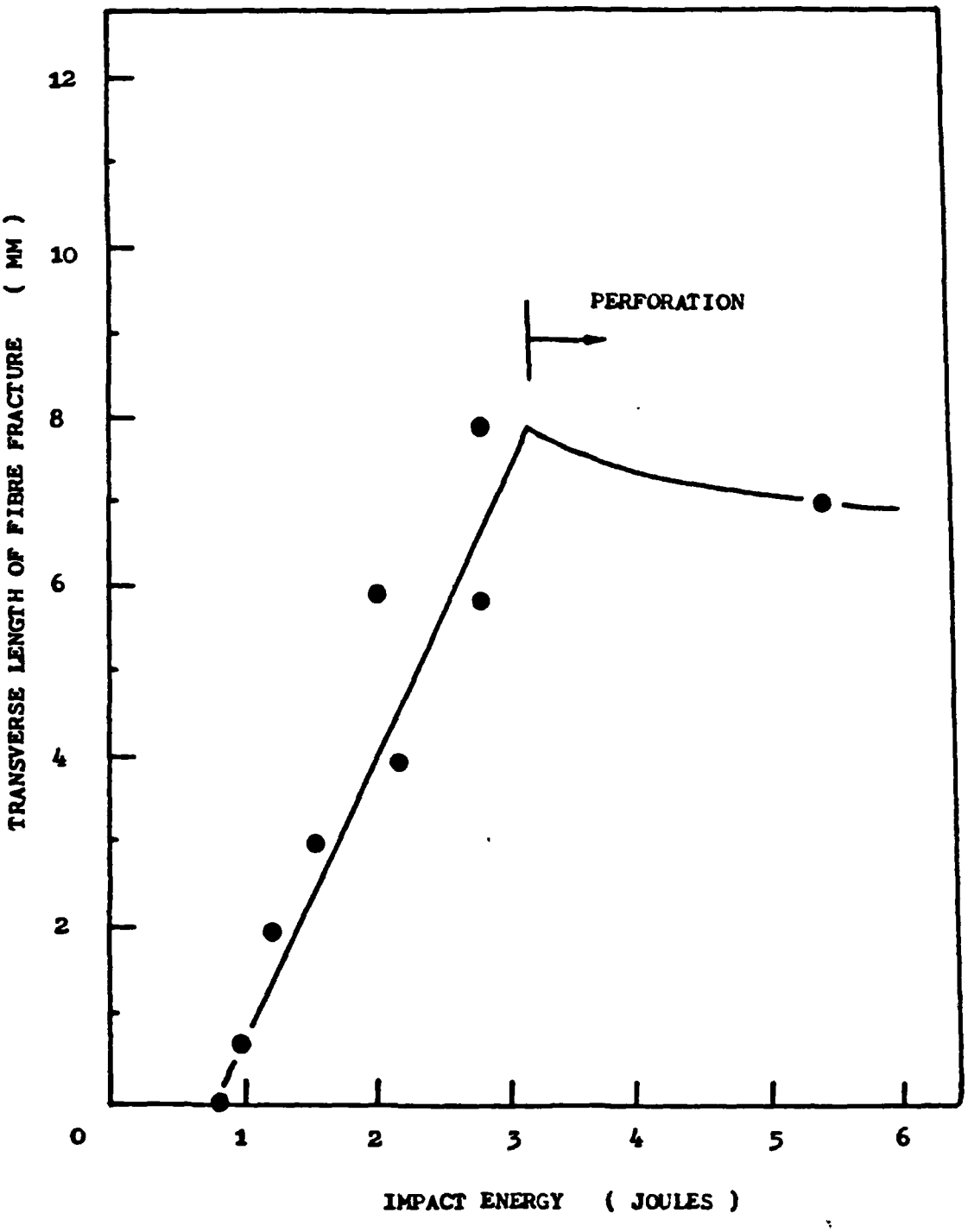


Figure 66

DAMAGE DEVELOPMENT IN THE SIXTEEN PLY (0,+/-45)COMPOSITE SUBJECTED TO DROP WEIGHT IMPACT LOADING.

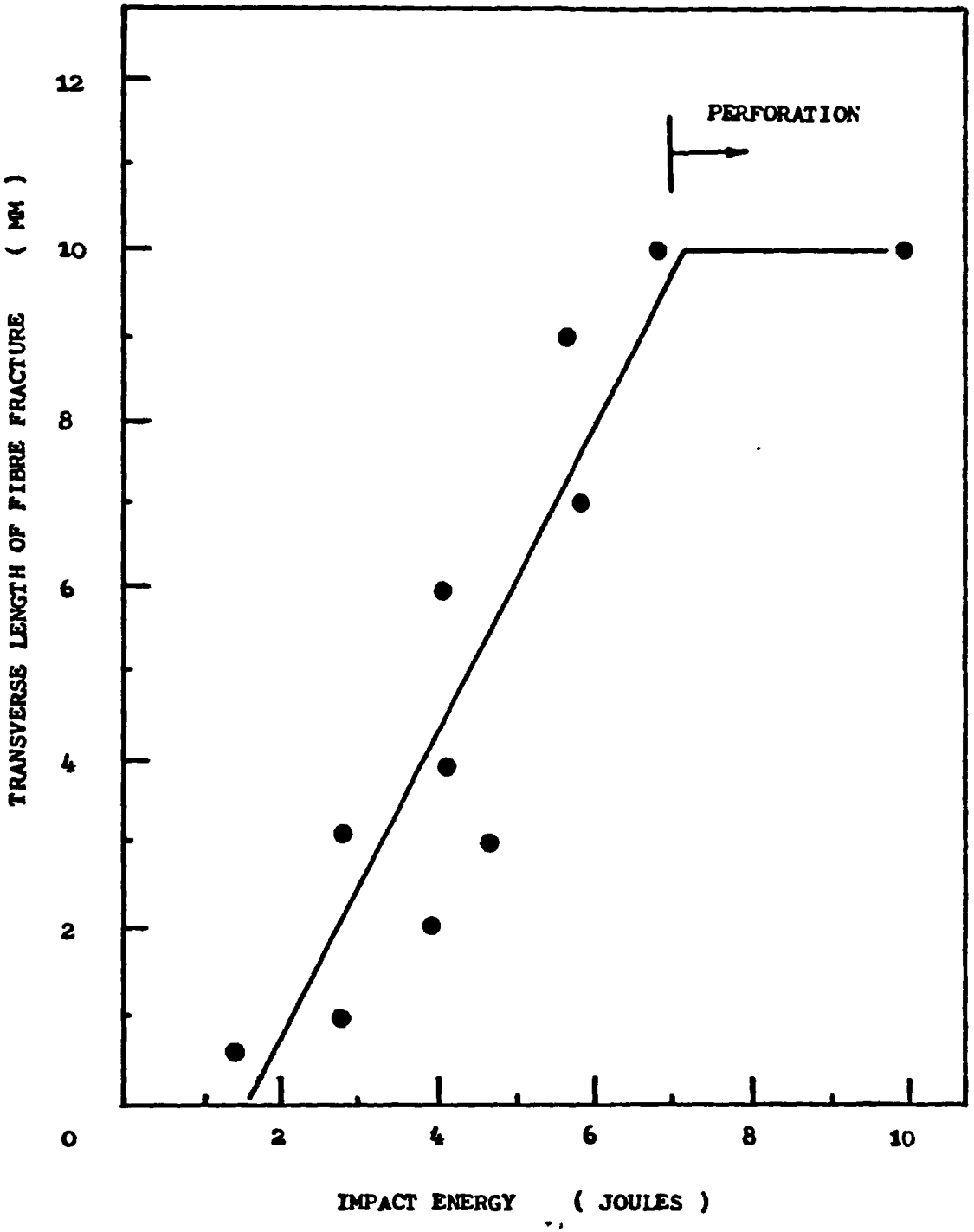
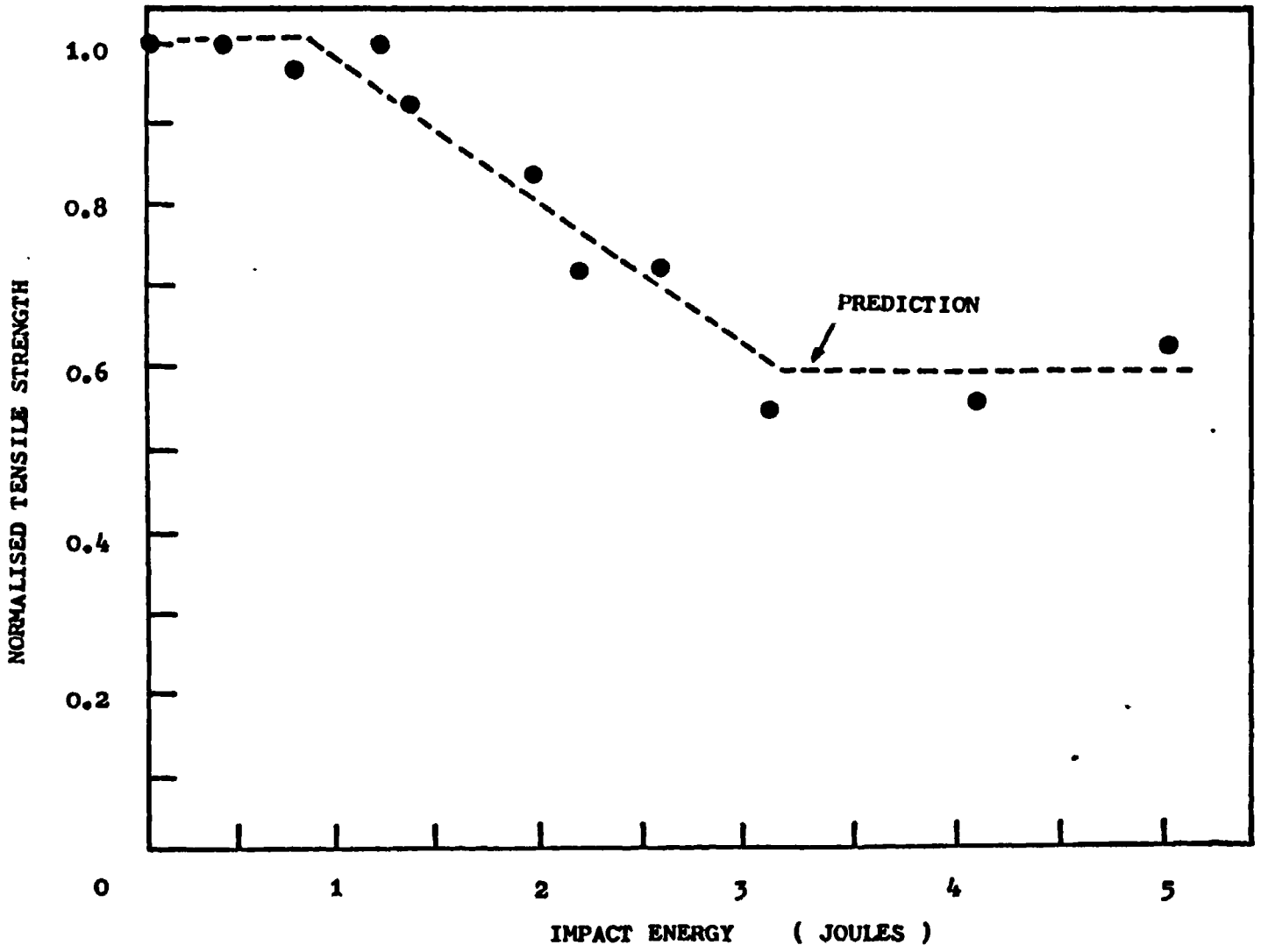


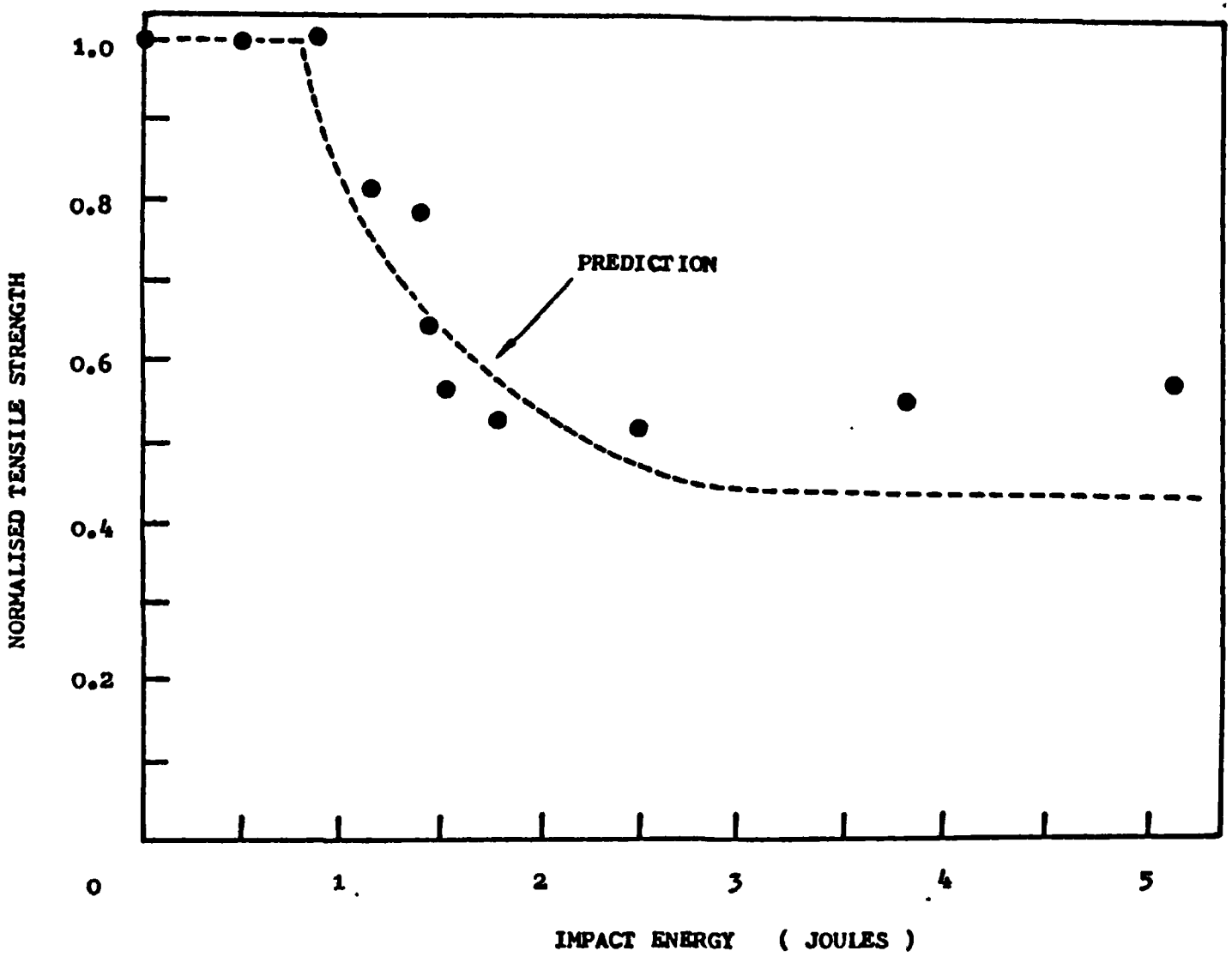
Figure 67



PREDICTION OF RESIDUAL TENSILE STRENGTH OF EIGHT PLY (+/-45) COMPOSITE

Figure 68

Figure 69



PREDICTION OF RESIDUAL TENSILE STRENGTH OF EIGHT PLY (0.+/-45) COMPOSITE

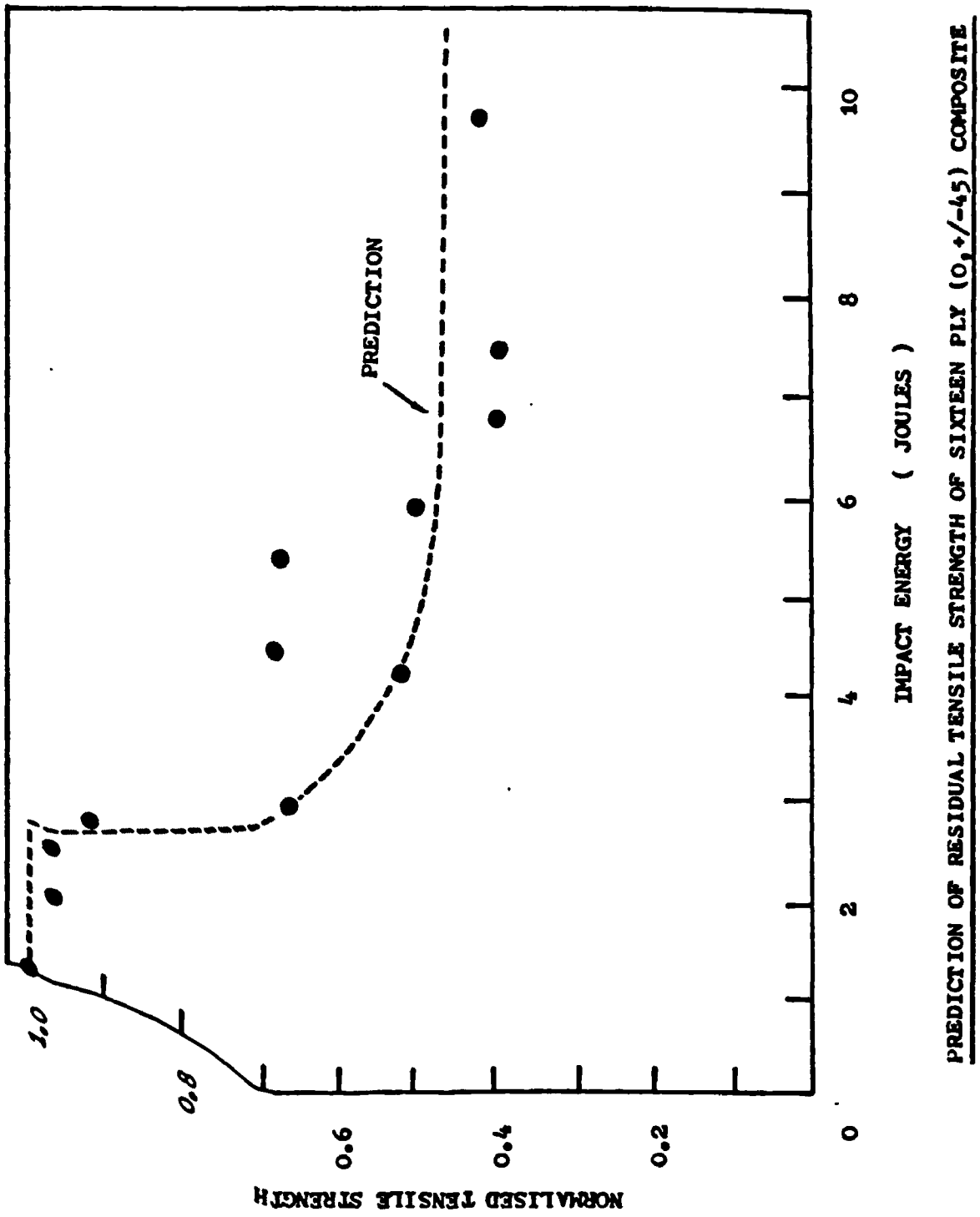

PREDICTION OF RESIDUAL TENSILE STRENGTH OF SIXTEEN PLY (0,+/-45) COMPOSITE
NORMALISED TENSILE STRENGTH
1.0
0.8
0.6
0.4
0.2
0
2
4
6
8
10
IMPACT ENERGY (JOULES)
PREDICTION

Figure 70

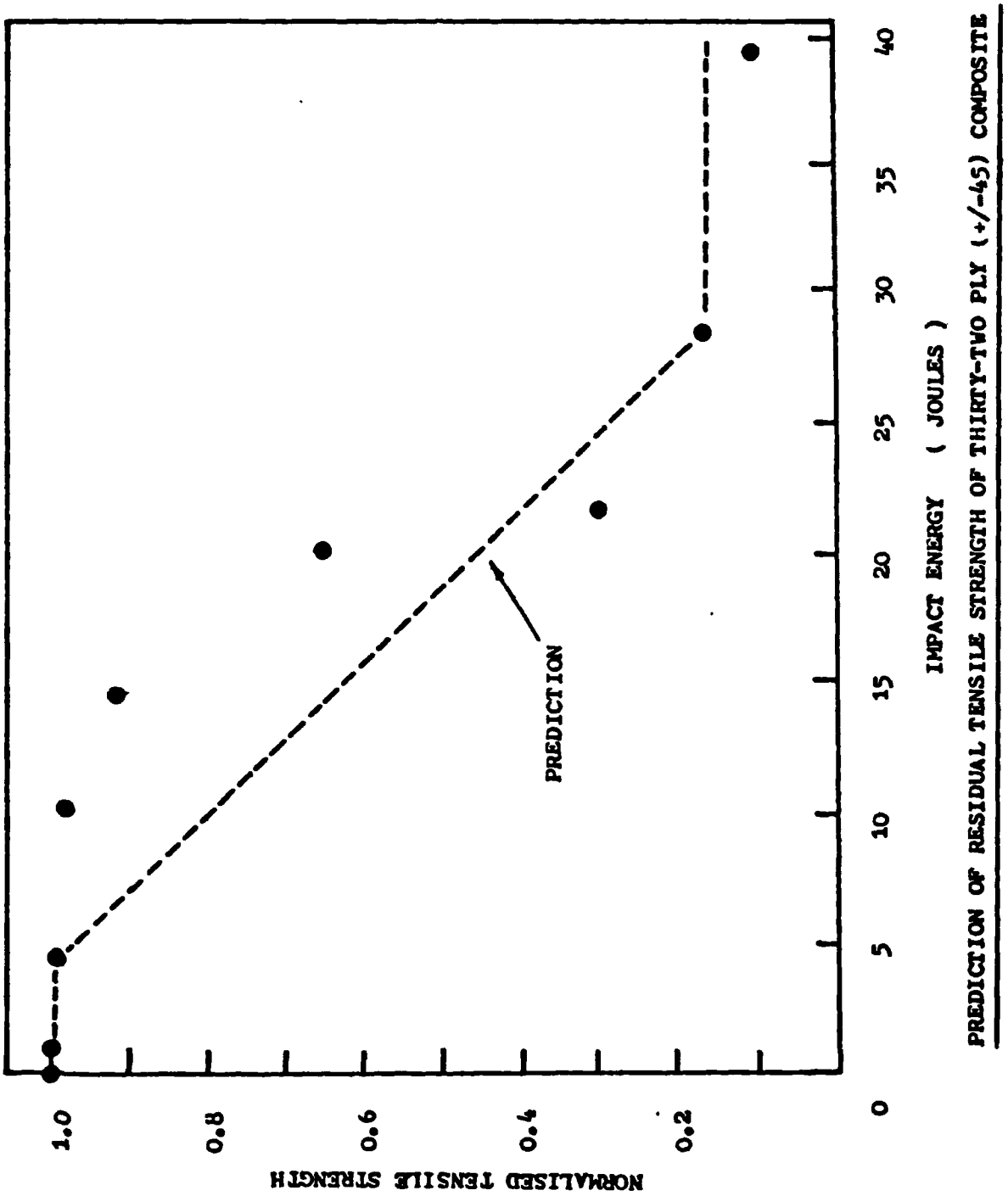
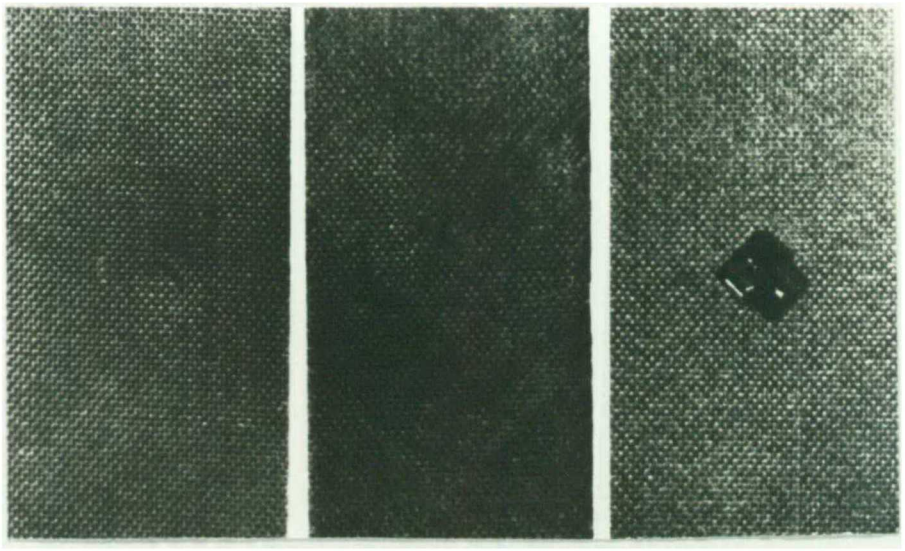

PREDICTION OF RESIDUAL TENSILE STRENGTH OF THIRTY-TWO PLY (+/-45) COMPOSITE
NORMALISED TENSILE STRENGTH
1.0
0.8
0.6
0.4
0.2
0
5
10
15
20
25
30
35
40
IMPACT ENERGY (JOULES)
PREDICTION

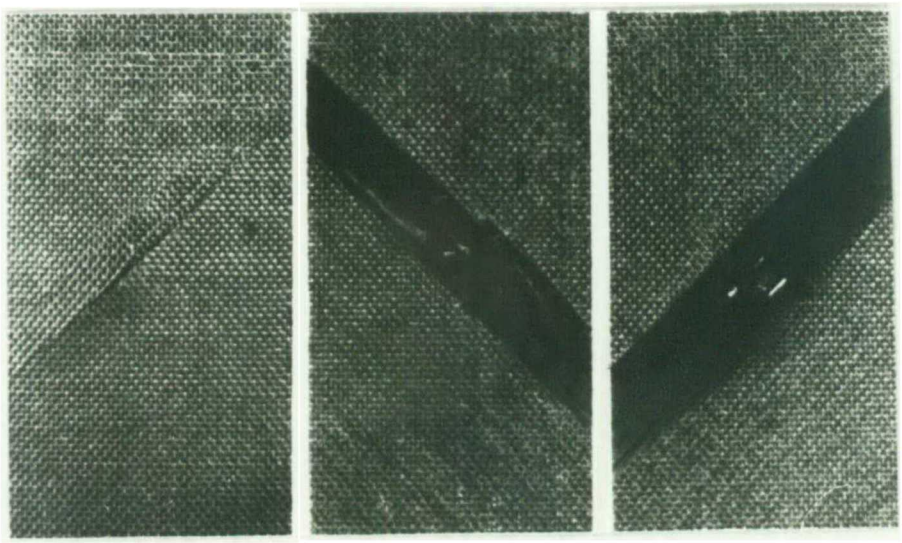
Figure 71

PHOTOGRAPHS DETAILING THE DAMAGE INCURRED BY THE EIGHT PLY (+/-45) COMPOSITE AFTER HIGH VELOCITY IMPACT.



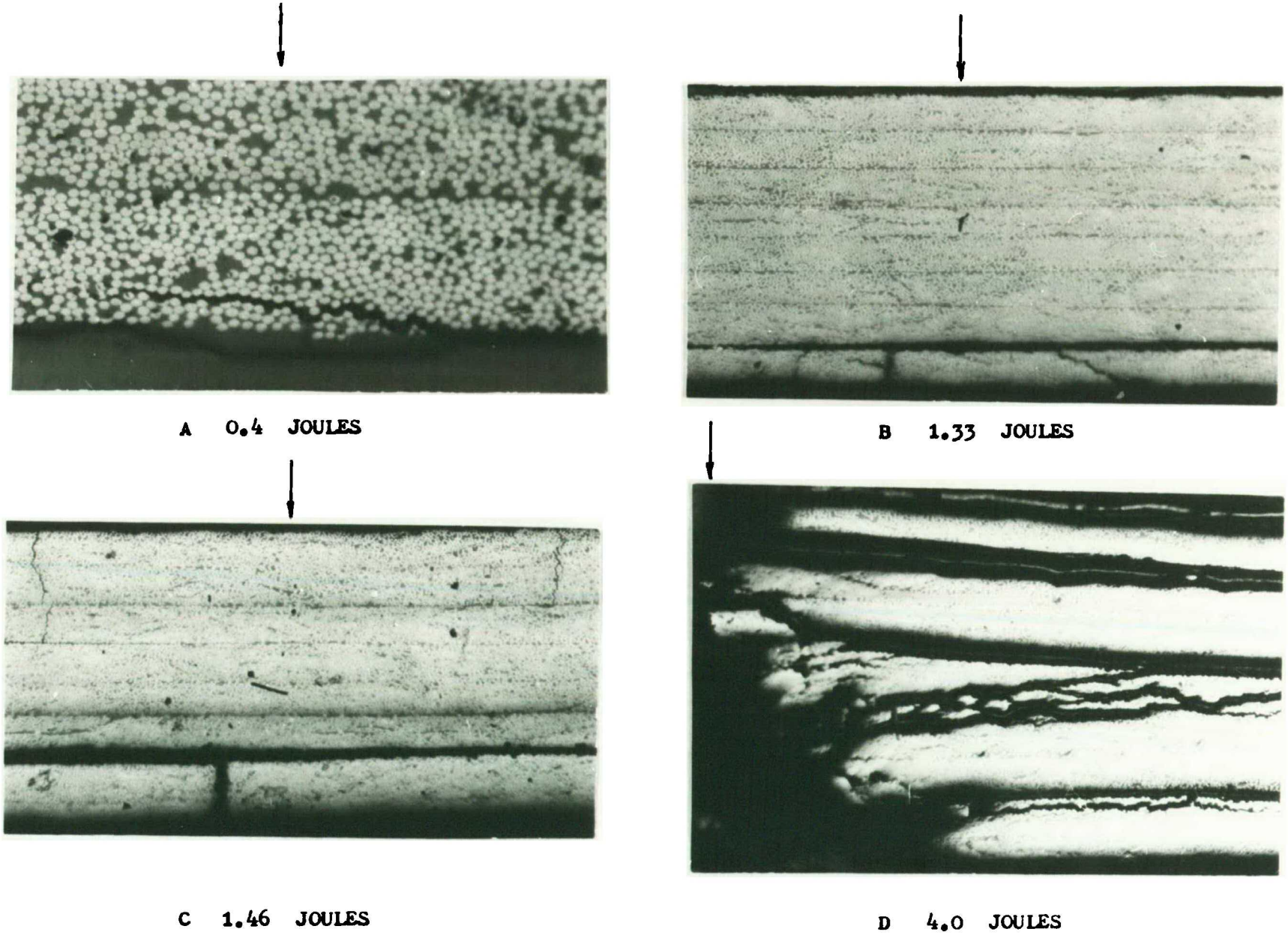
TOP SURFACE

1.35 J	2.7 J	3.5 J
A	B	C



BACK SURFACE

Figure 72



A 0.4 JOULES

B 1.33 JOULES

C 1.46 JOULES

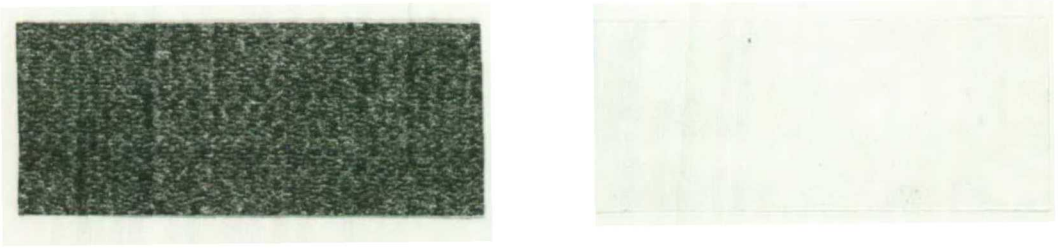
D 4.0 JOULES

Figure 73

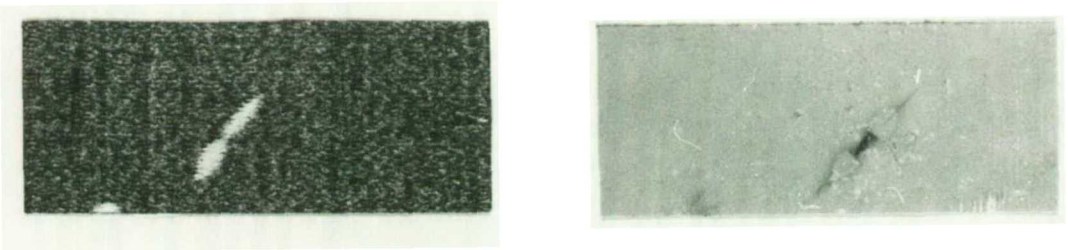
DAMAGE GROWTH IN EIGHT PLY (+/-45) COMPOSITE

HIGH VELOCITY IMPACT

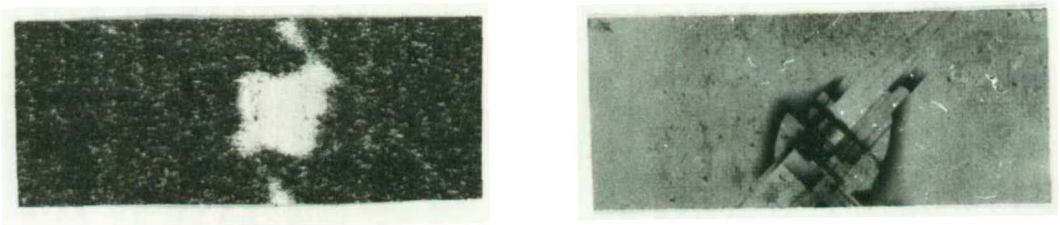
RADIOGRAPHS AND ULTRASONIC C-SCANS OF DAMAGED EIGHT PLY (+/-45) COMPOSITES AFTER HIGH VELOCITY IMPACT.



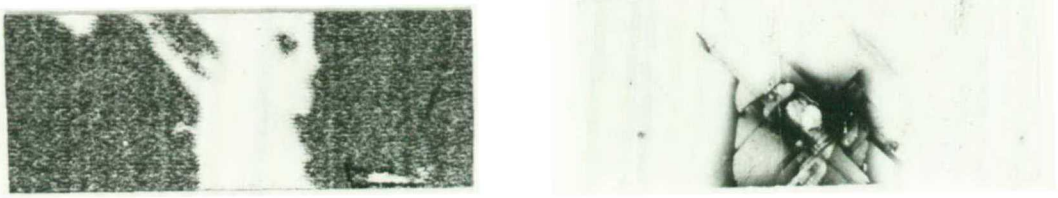
A 0.4 JOULES



B 1.33 JOULES



C 1.46 JOULES



D 4.0 JOULES

Figure 74

DEPLIED LAYERS OF AN EIGHT PLY (+/-45) COMPOSITE

HIGH VELOCITY IMPACT

3.0 JOULES

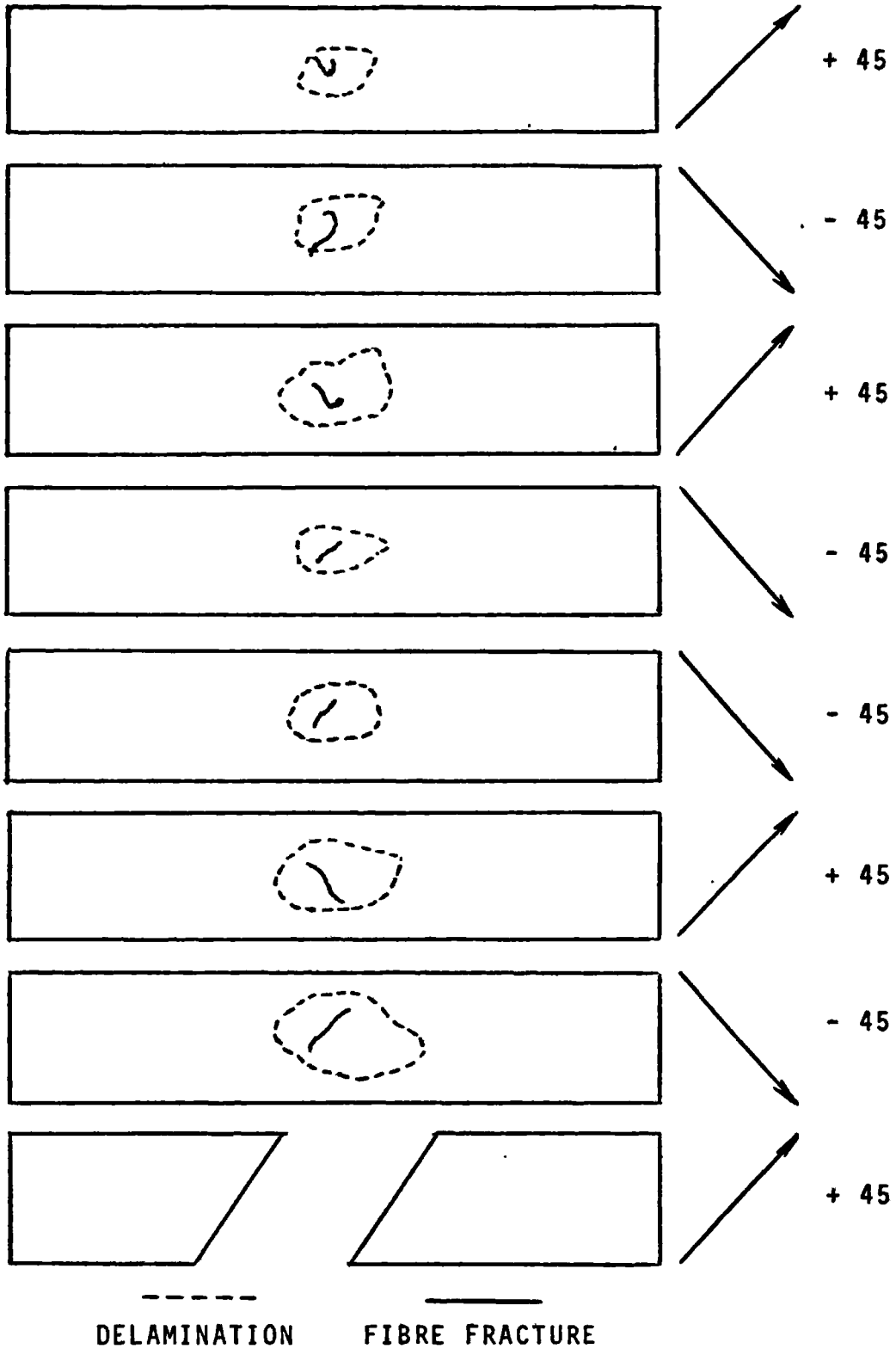
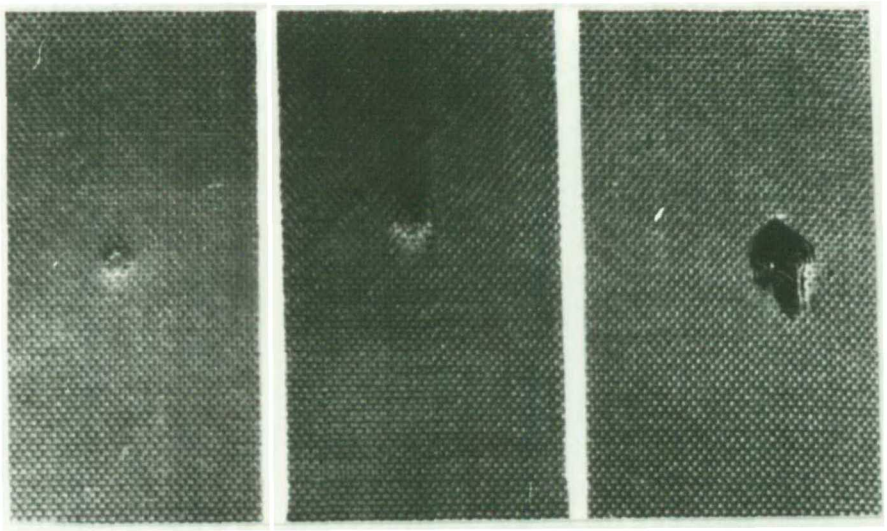


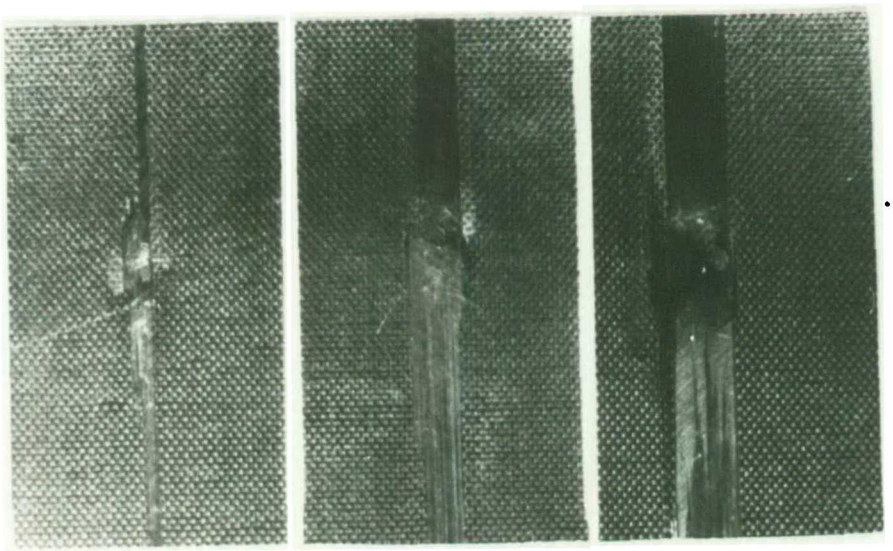
Figure 75

PHOTOGRAPHS DETAILING THE DAMAGE INCURRED IN THE EIGHT PLY (0,+/-45) COMPOSITE AFTER HIGH VELOCITY IMPACT.



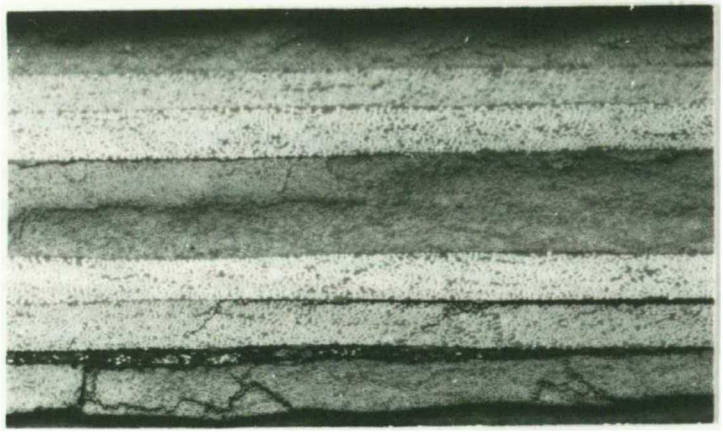
TOP SURFACE

0.9 J	2.7 J	3.2 J
A	B	C

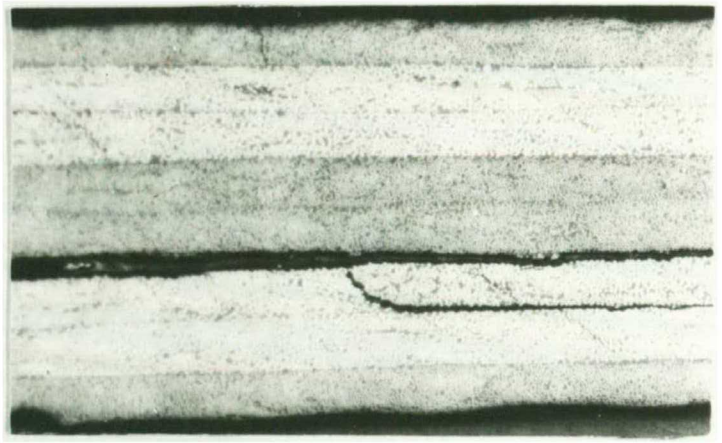


BACK SURFACE

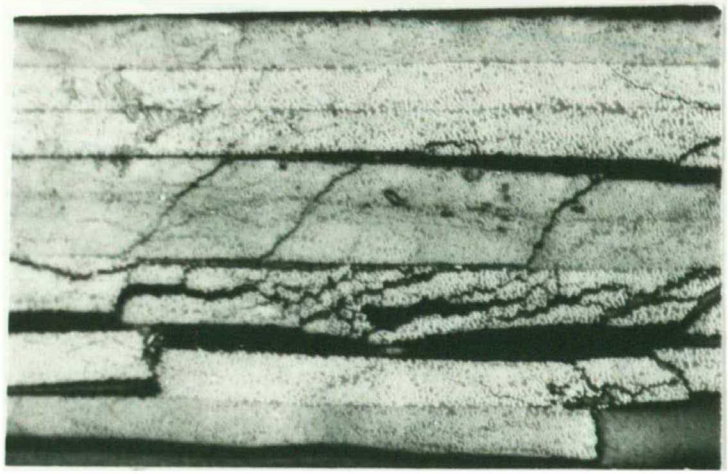
Figure 76



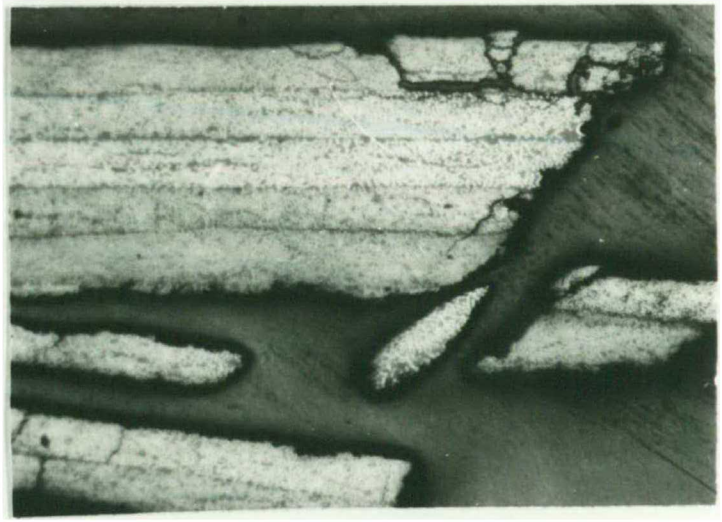
A 0.9 JOULES



B 1.7 JOULES



C 2.7 JOULES



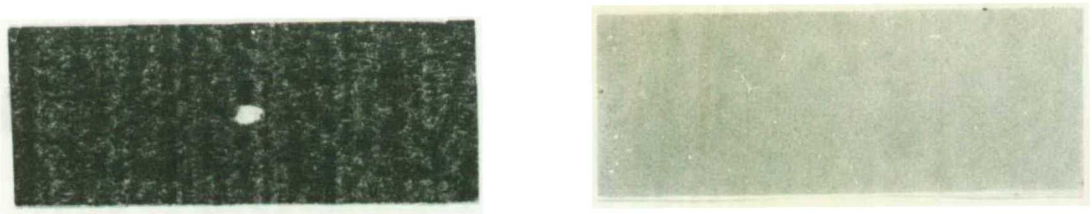
D 4.0 JOULES

Figure 77

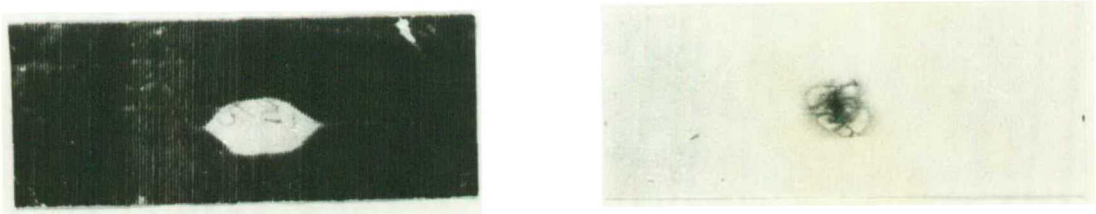
DAMAGE GROWTH IN EIGHT PLY (0_2/+/-45) COMPOSITE

HIGH VELOCITY IMPACT

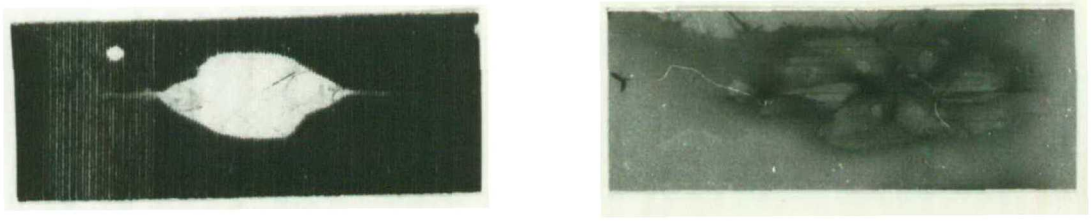
RADIOGRAPHS AND ULTRASONIC C-SCANS OF DAMAGED EIGHT PLY (0,+/-45) COMPOSITE TAKEN AFTER HIGH VELOCITY IMPACT.



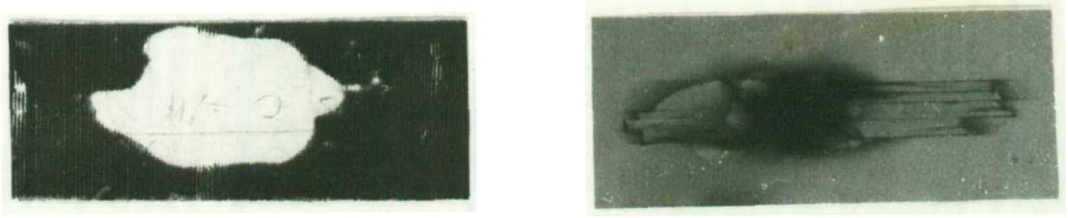
A 0.9 JOULES



B 1.7 JOULES



C 2.7 JOULES

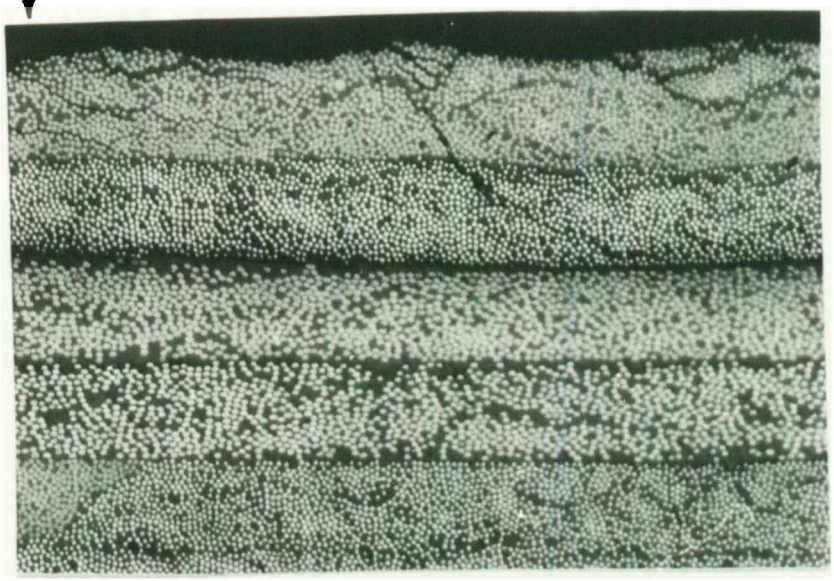


D 4.0 JOULES

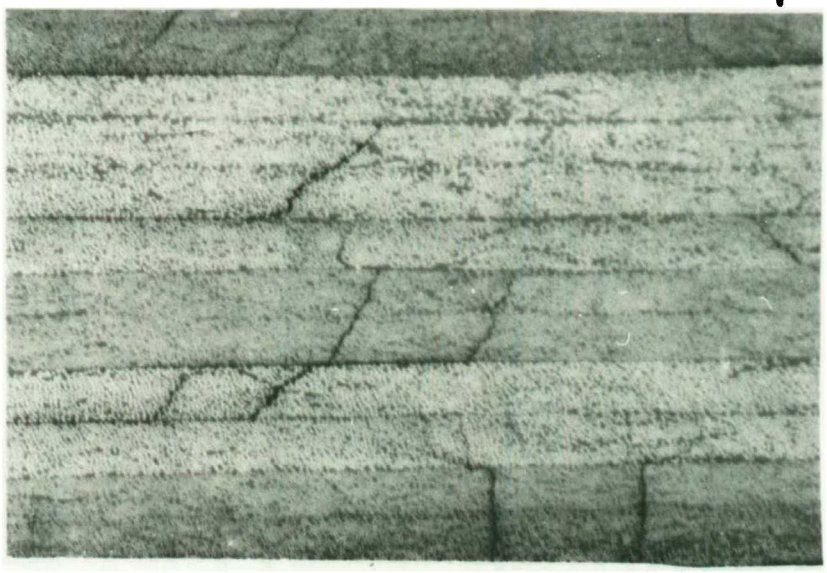
Figure 78

DAMAGE GROWTH IN SIXTEEN PLY (0,+/-45) COMPOSITE

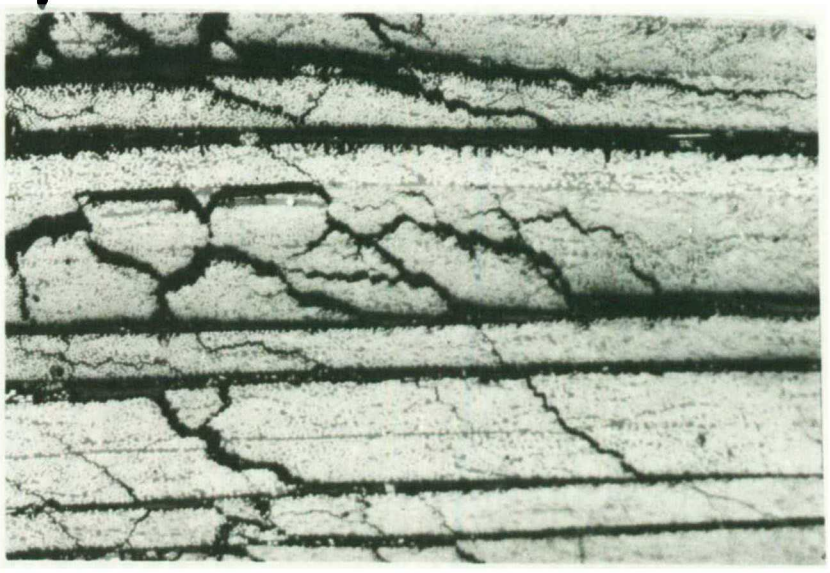
HIGH VELOCITY IMPACT



A 1.0 JOULES



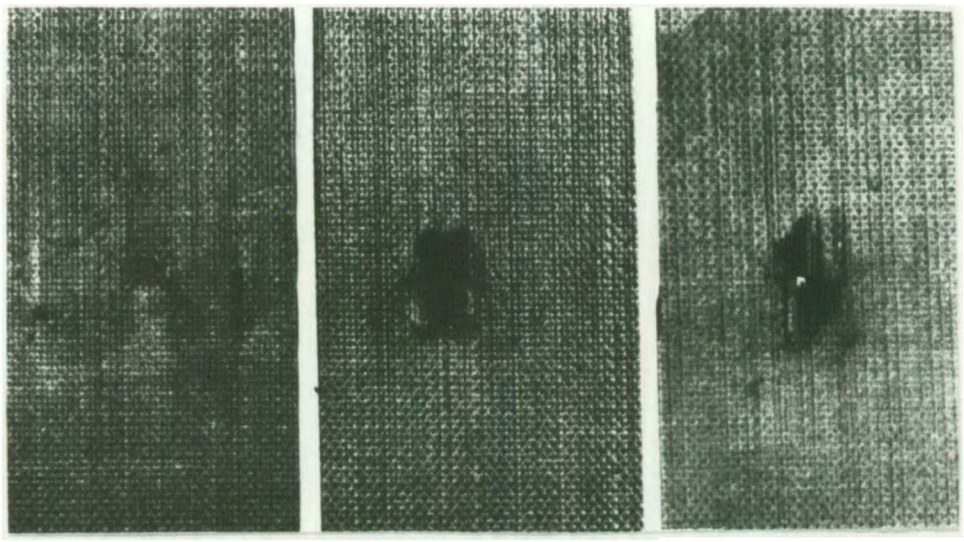
B 1.9 JOULES



C 5.7 JOULES

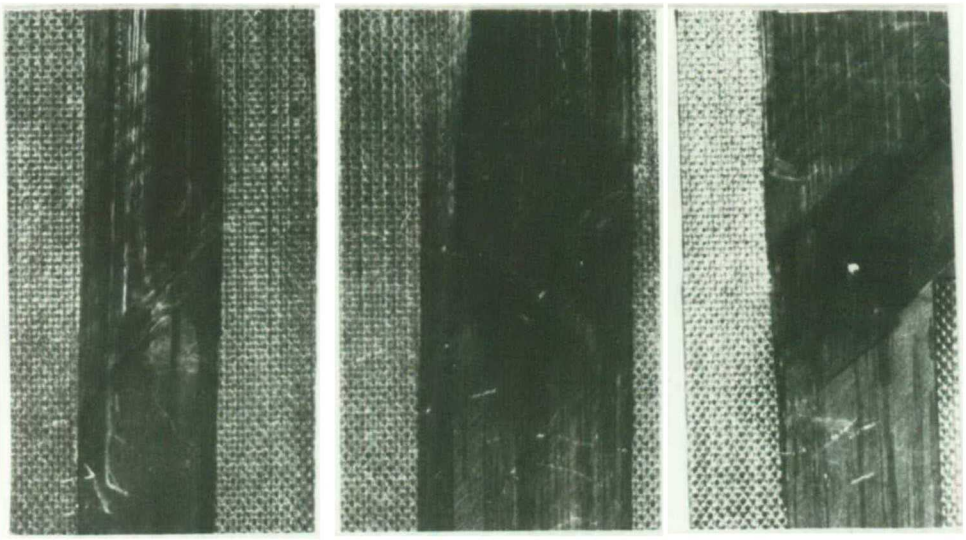
Figure 79

PHOTOGRAPHS DETAILING THE DAMAGE INCURRED IN THE SIXTEEN PLY $(0_2 +/-45)$ COMPOSITE AFTER HIGH VELOCITY IMPACT.



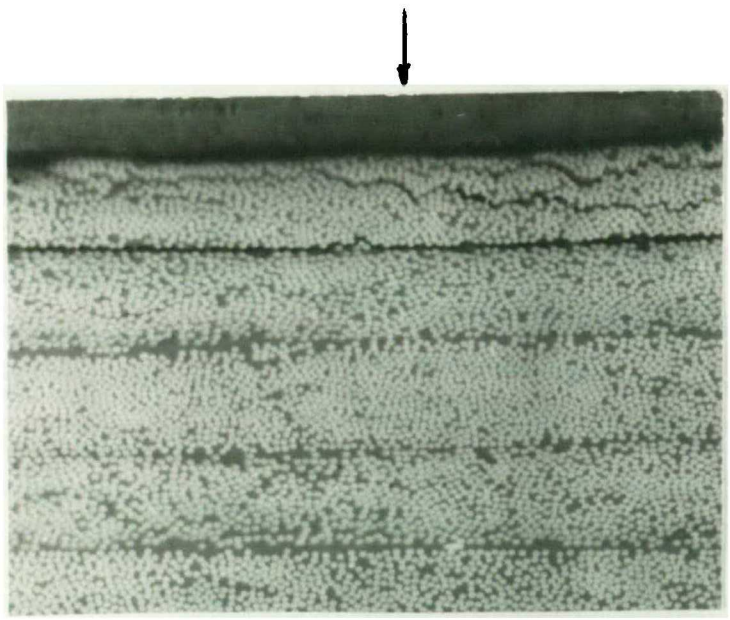
TOP SURFACE

2.1 J	5.7 J	6.9 J
A	B	C

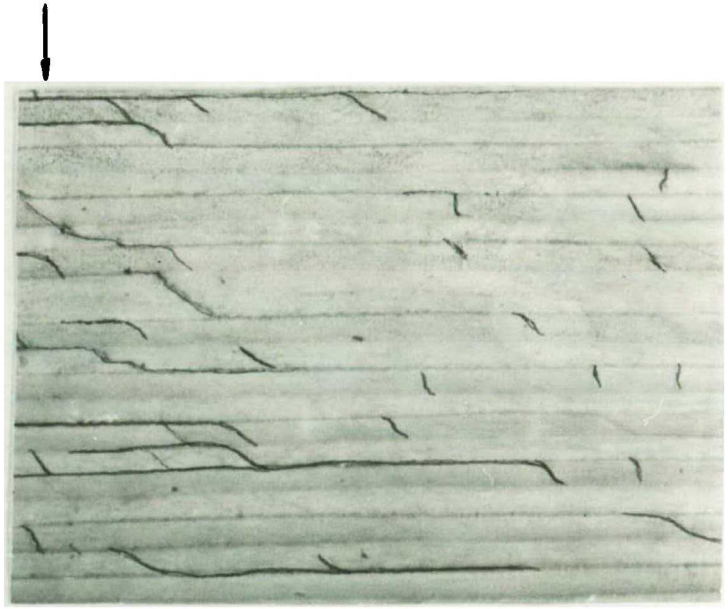


BACK SURFACE

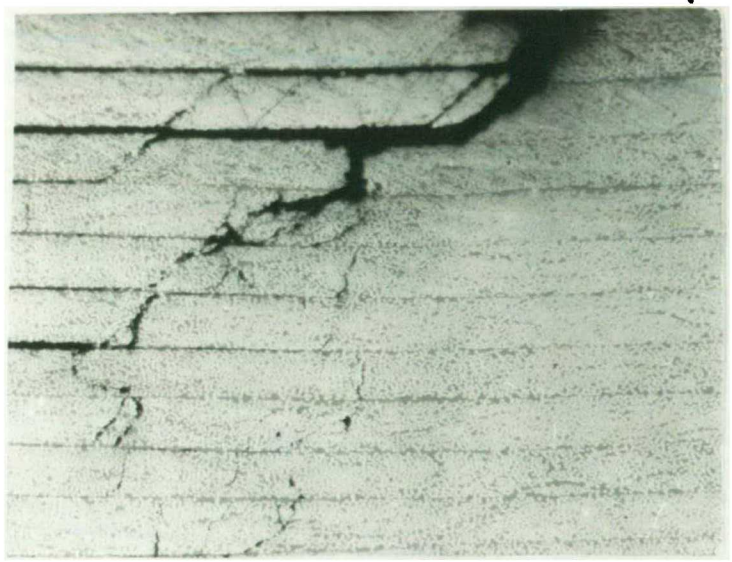
Figure 80



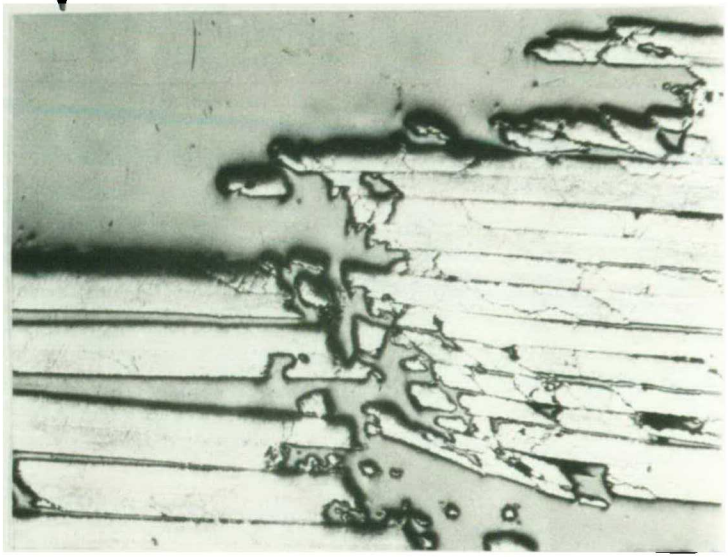
A 0.6 JOULES



B 3.9 JOULES



C 11.3 JOULES



D 20.5 JOULES

Figure 81

DAMAGE GROWTH IN THIRTY TWO PLY (+/-45)
COMPOSITE. HIGH VELOCITY IMPACT.

THE VARIATION OF PERFORATION ENERGY WITH TARGET THICKNESS FOR THE (+/-45°) COMPOSITE BEAMS

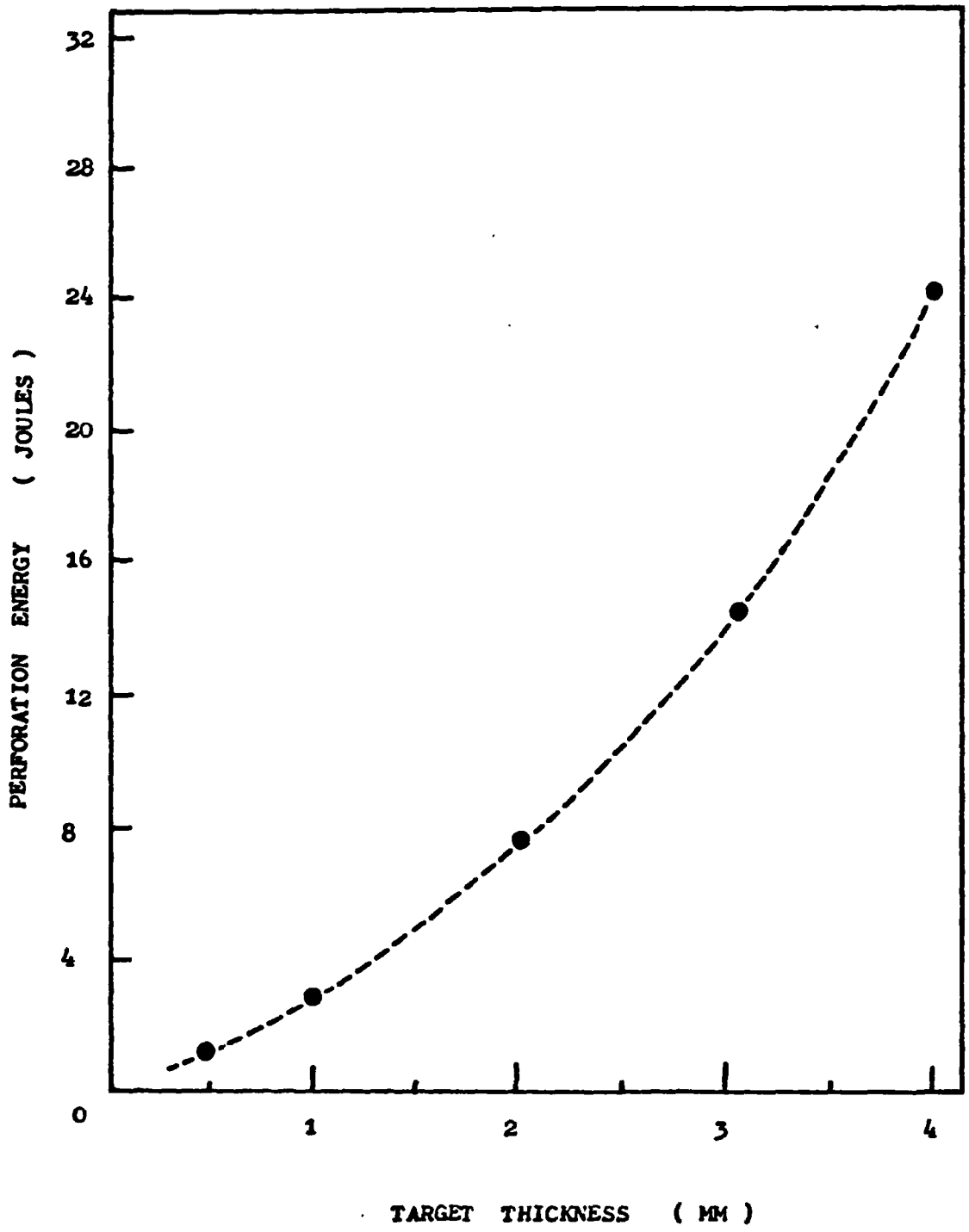
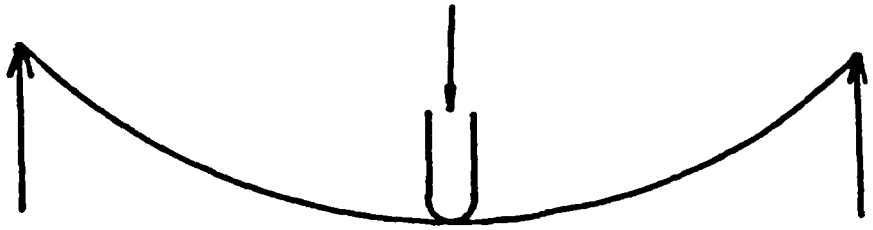


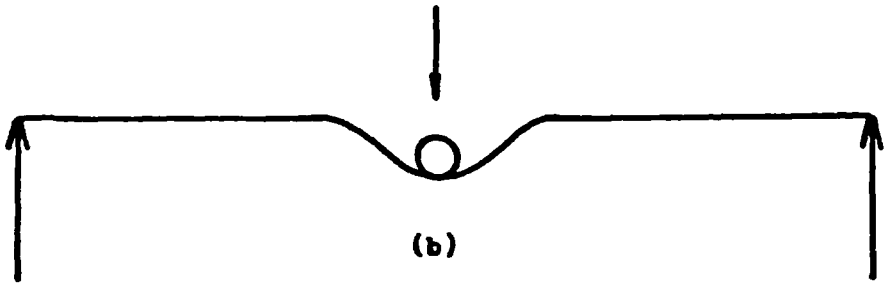
Figure 82

SCHEMATIC REPRESENTATIONS OF THE ASSUMED MODES OF RESPONSE AFTER LOW AND HIGH VELOCITY IMPACT.



(a)

THE PRIMARY MODE OF TARGET RESONSE GENERATED BY LARGE MASS, LOW VELOCITY IMPACT LOADING.



(b)

THE LOCALISED MODE OF TARGET RESPONSE GENERATED BY LOW MASS, HIGH VELOCITY IMPACT LOADING.

Figure 83

THE COMPARISON OF THE PREDICTED BALLISTIC PERFORATION THRESHOLD OBTAINED BY ASSUMING A PRIMARY MODE OF TARGET RESPONSE WITH THE (+/-45°) COMPOSITE EXPERIMENTAL DATA

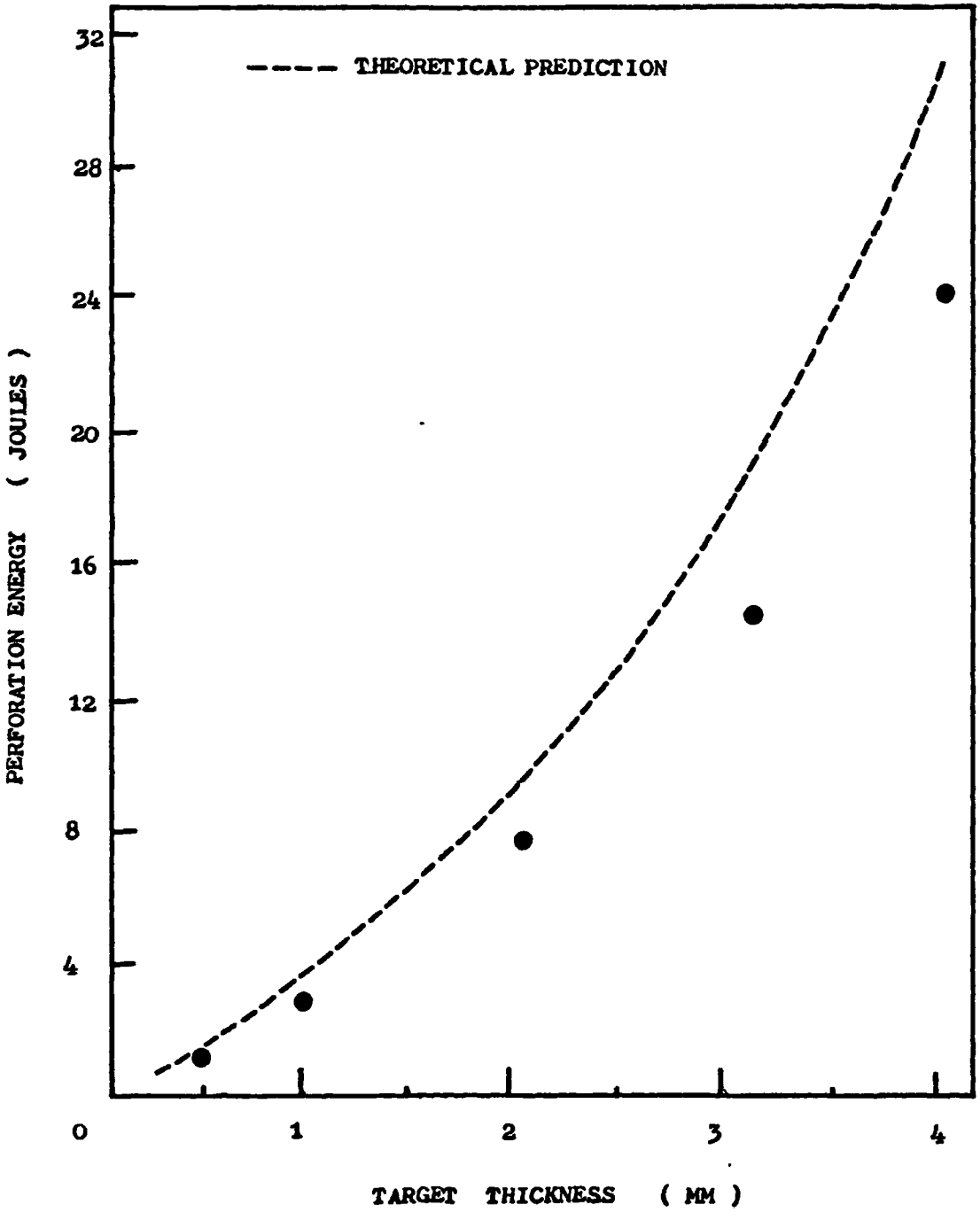


Figure 84

THE COMPARISON OF THE PREDICTED AND EXPERIMENTAL PERFORATION ENERGIES FOR THE BALLISTICALLY IMPACTED (+/- 45°) BEAMS.

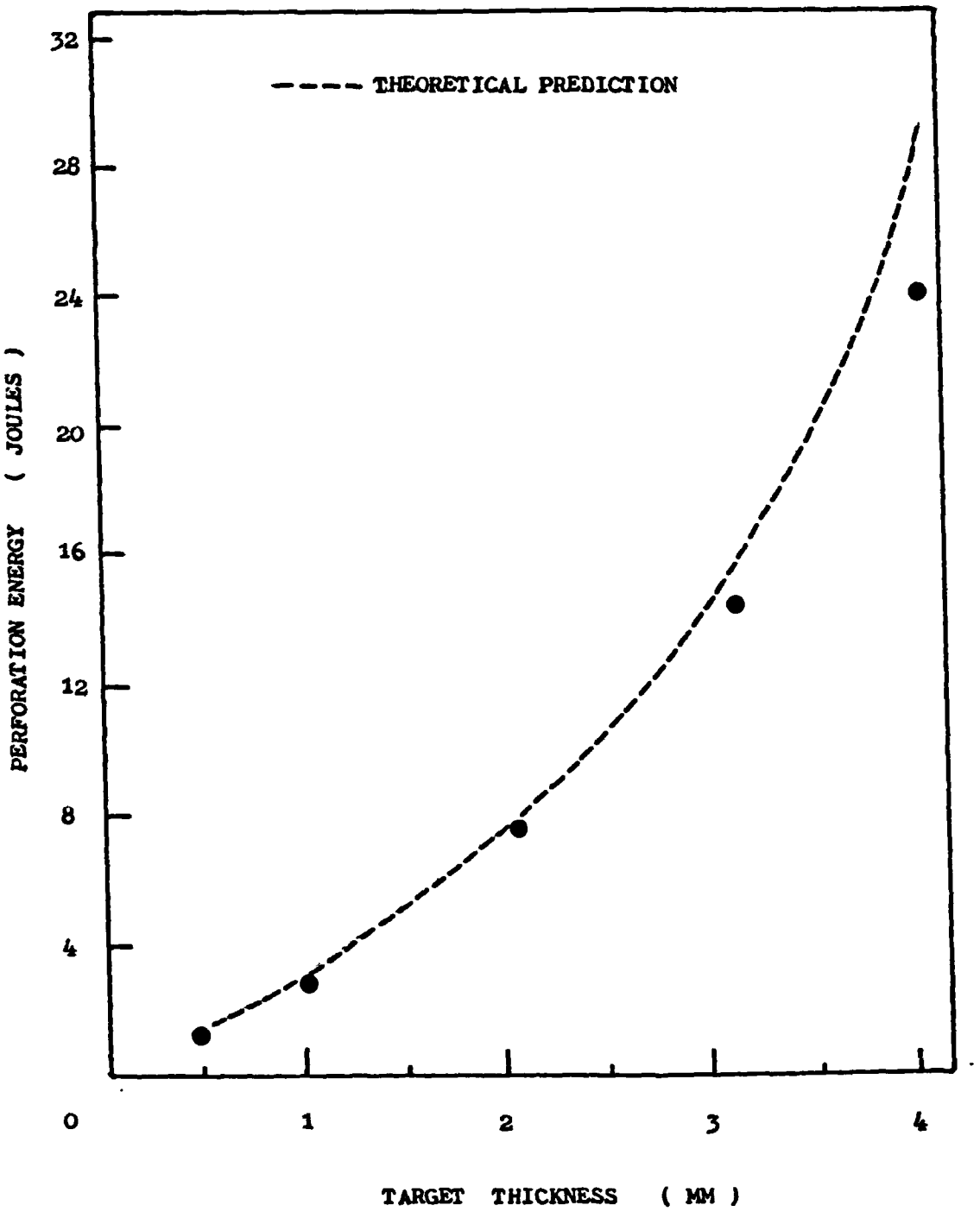


Figure 85

GRAPHICAL REPRESENTATION OF THE RELATIVE ENERGY ABSORPTION IN THE BALLISTICALLY IMPACTED (+/-45°) BEAM COUPONS.

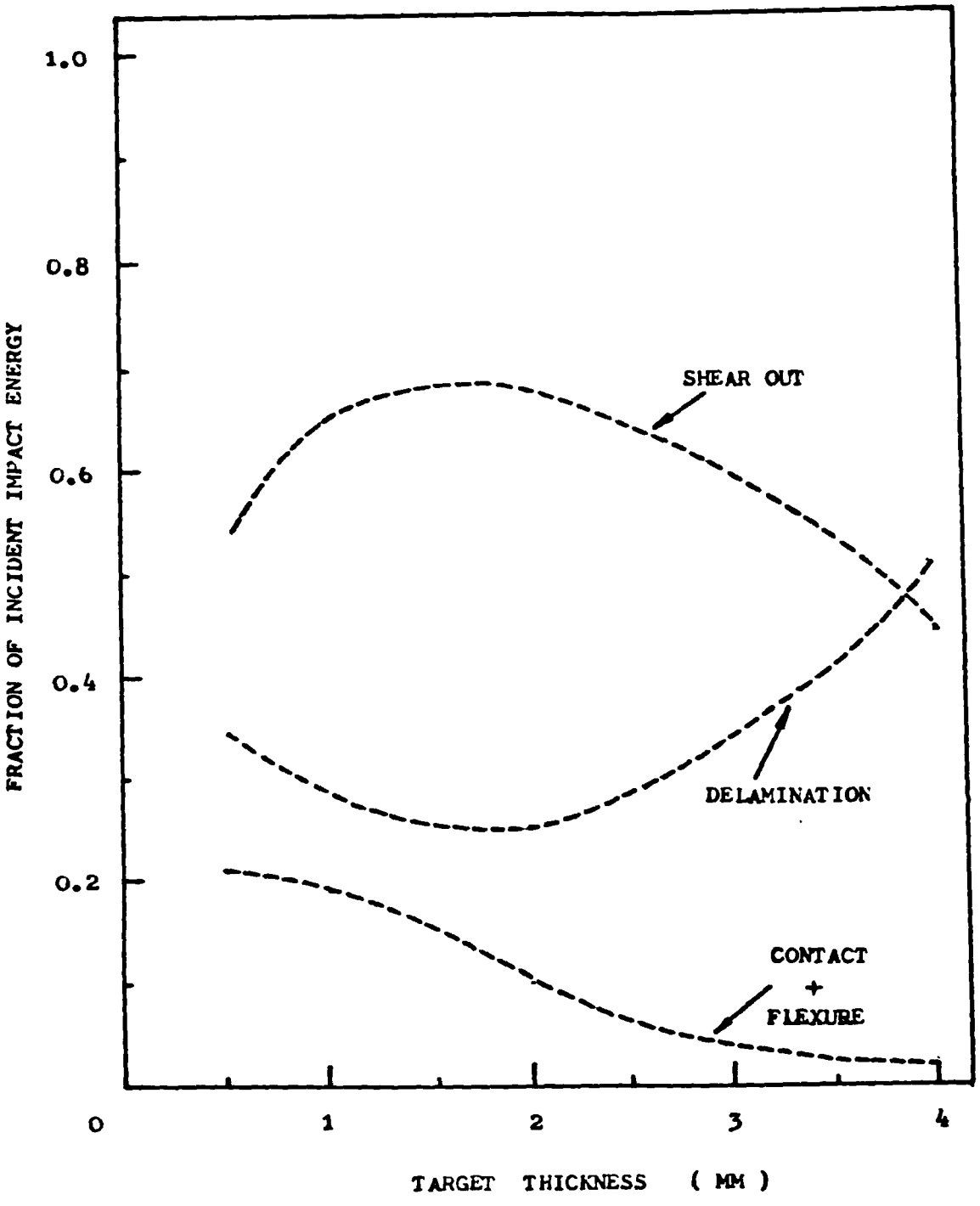


Figure 86

ENERGY DISSIPATED IN DELAMINATION vs TARGET THICKNESS .

HIGH VELOCITY PERFORATION OF (+/-45°) COMPOSITES

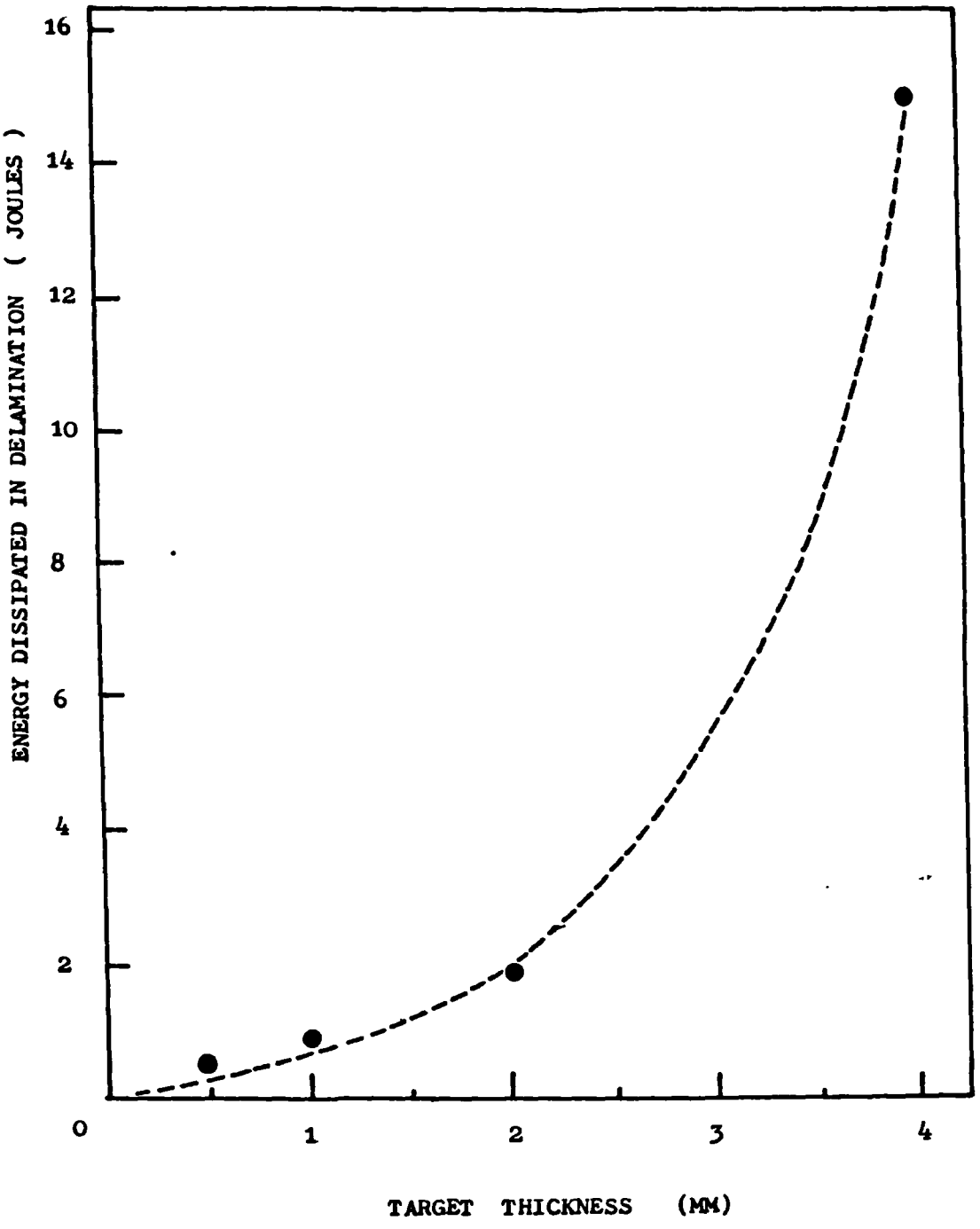


Figure 87

A COMPARISON OF THE PREDICTED AND EXPERIMENTAL PERFORATION ENERGIES FOR THE BALLISTICALLY IMPACTED (+/-45°) BEAMS.

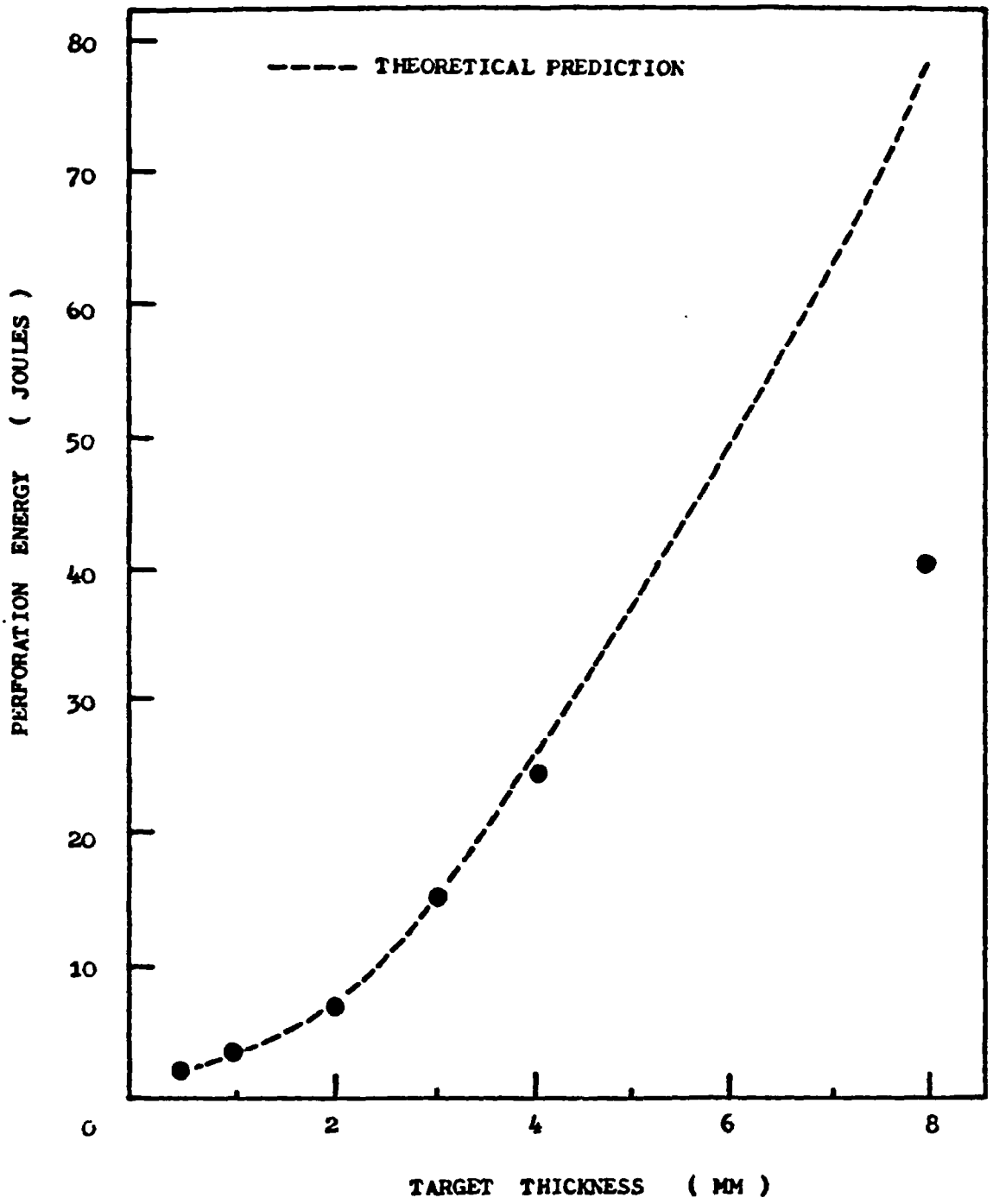
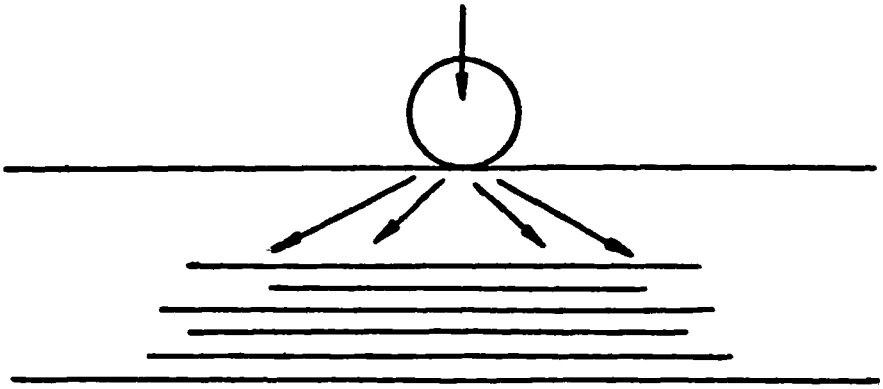


Figure 88

SCHEMATIC REPRESENTATION OF THE SHEAR ZONE IN THE BALLISTICALLY IMPACTED SIXTY-FOUR PLY (+/-45) COMPOSITE.

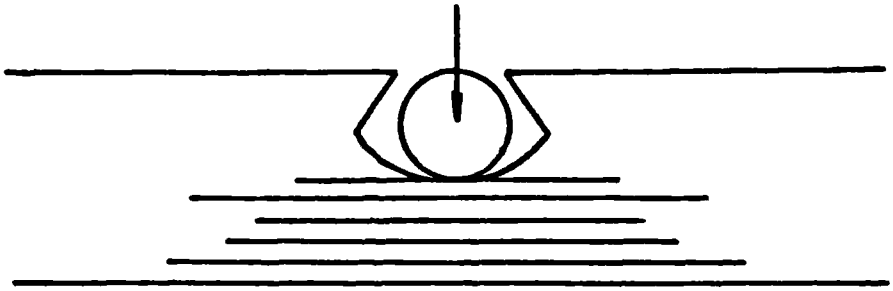
Figure 89

SCHEMATIC FIGURES SHOWING THE THREE STAGES OF DAMAGE DEVELOPMENT DURING PERFORATION OF THE SIXTY-FOUR PLY COMPOSITE.



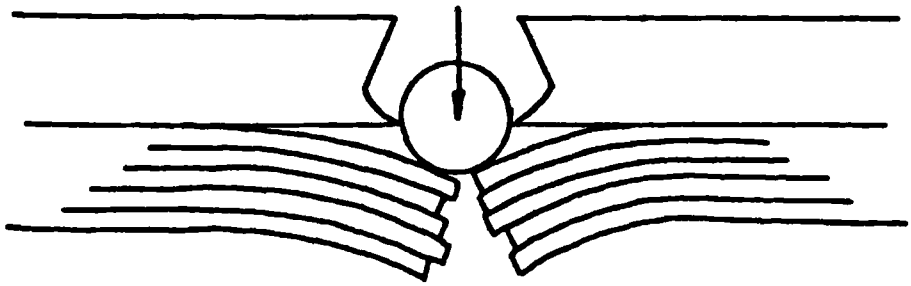
STAGE 1

STRESS WAVE PROPAGATION



STAGE 2

TOP SURFACE PENETRATION



LOWER SURFACE TENSILE FAILURE

Figure 90

THE VARIATION OF PERFORATION ENERGY WITH PROJECTILE MASS FOR THE (+/-45) COMPOSITE BEAMS SUBJECTED TO HIGH VELOCITY IMPACT LOADING.

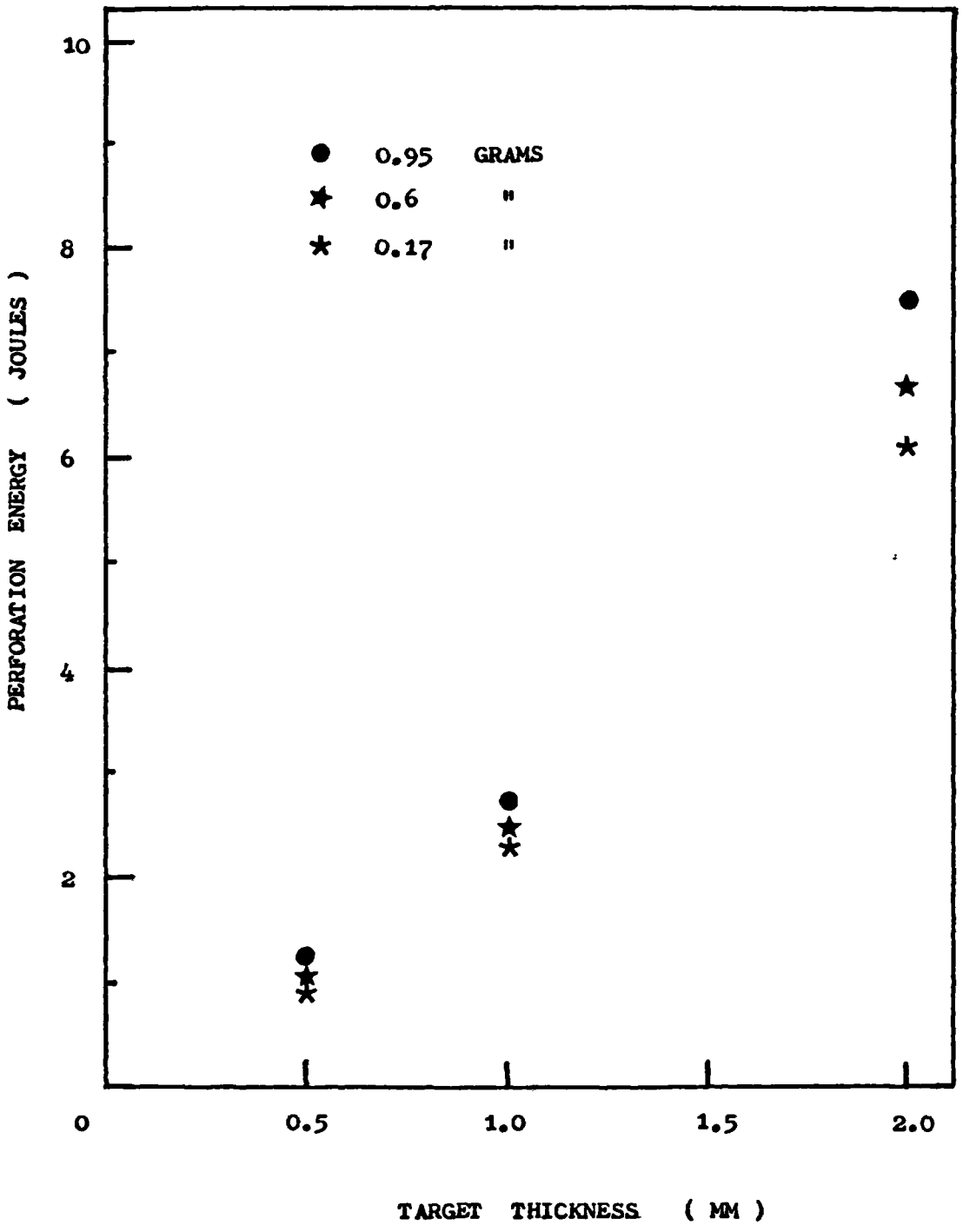


Figure 91

A COMPARISON OF THE VARIATION IN ENERGY DISSIPATION IN DELAMINATION AT PERFORATION WITH PROJECTILE MASS FOR THE EIGHT PLY (+/-45°) COMPOSITE.

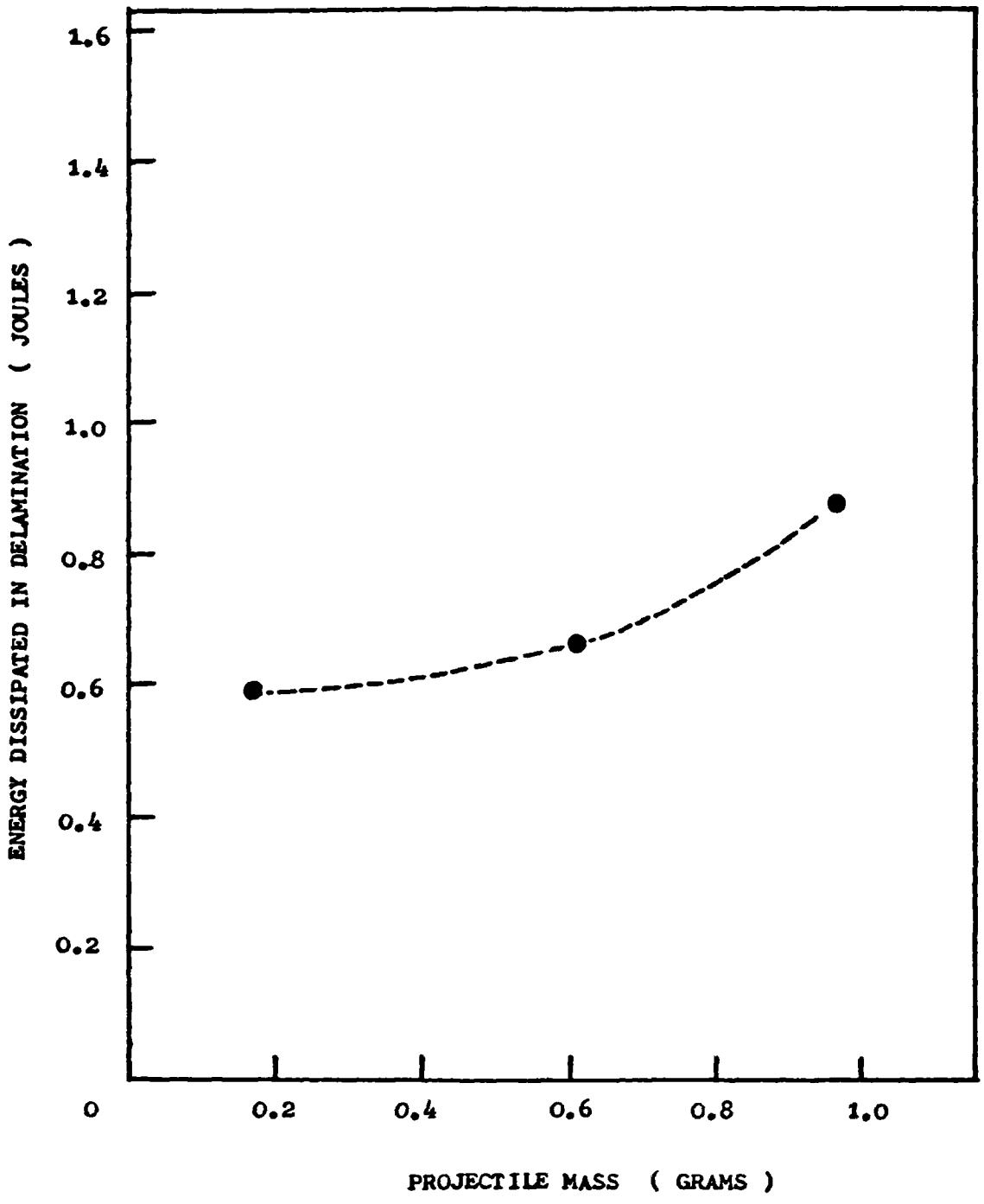


Figure 92

THE EFFECT OF PROJECTILE DIAMETER ON PERFORATION IN THE (+/-45) COMPOSITES.

TARGET DIMENSIONS 50MM x 50MM

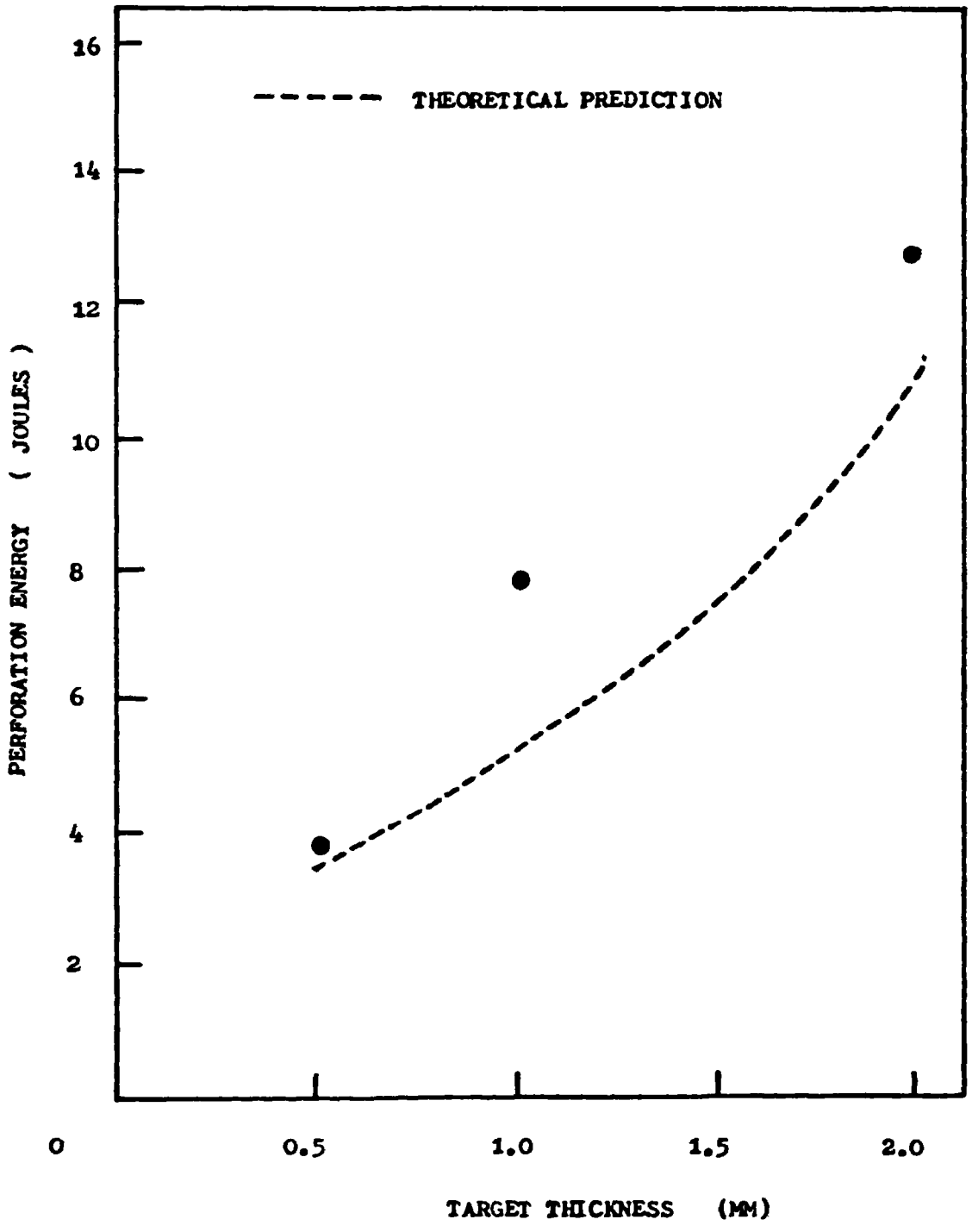
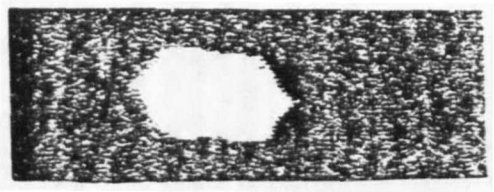


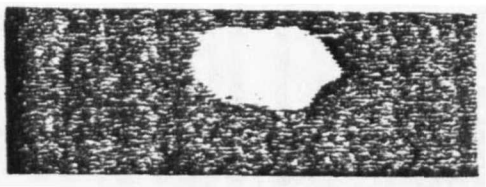
Figure 93

ULTRASONIC C-SCANS SHOWING THE EFFECT OF BEAM LENGTH ON HIGH VELOCITY IMPACT DAMAGE

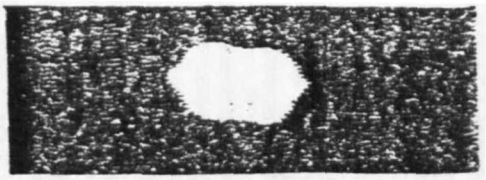
IMPACT ENERGY = 1.8 JOULES



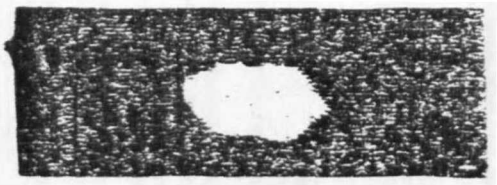
LENGTH = 50 MM



LENGTH = 75 MM

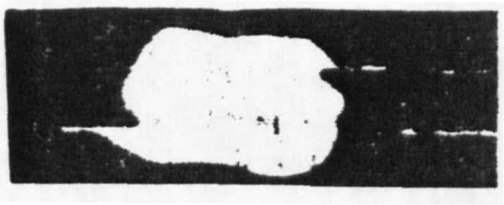


LENGTH = 100 MM



LENGTH = 150 MM

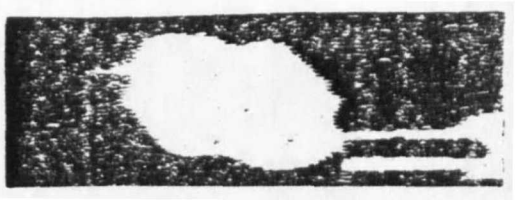
IMPACT ENERGY = 7.0 JOULES



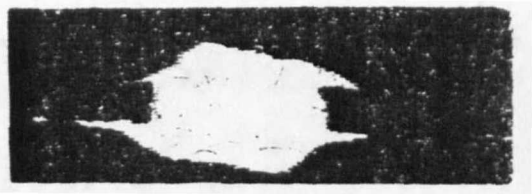
LENGTH = 50 MM



LENGTH = 75 MM



LENGTH = 100 MM



LENGTH = 150 MM

Figure 94

THE VARIATION OF DELAMINATED AREA WITH BEAM LENGTH FOR THE SIXTEEN PLY (0 ,+/-45) LAMINATE SUBJECTED TO HIGH VELOCITY IMPACT LOADING.

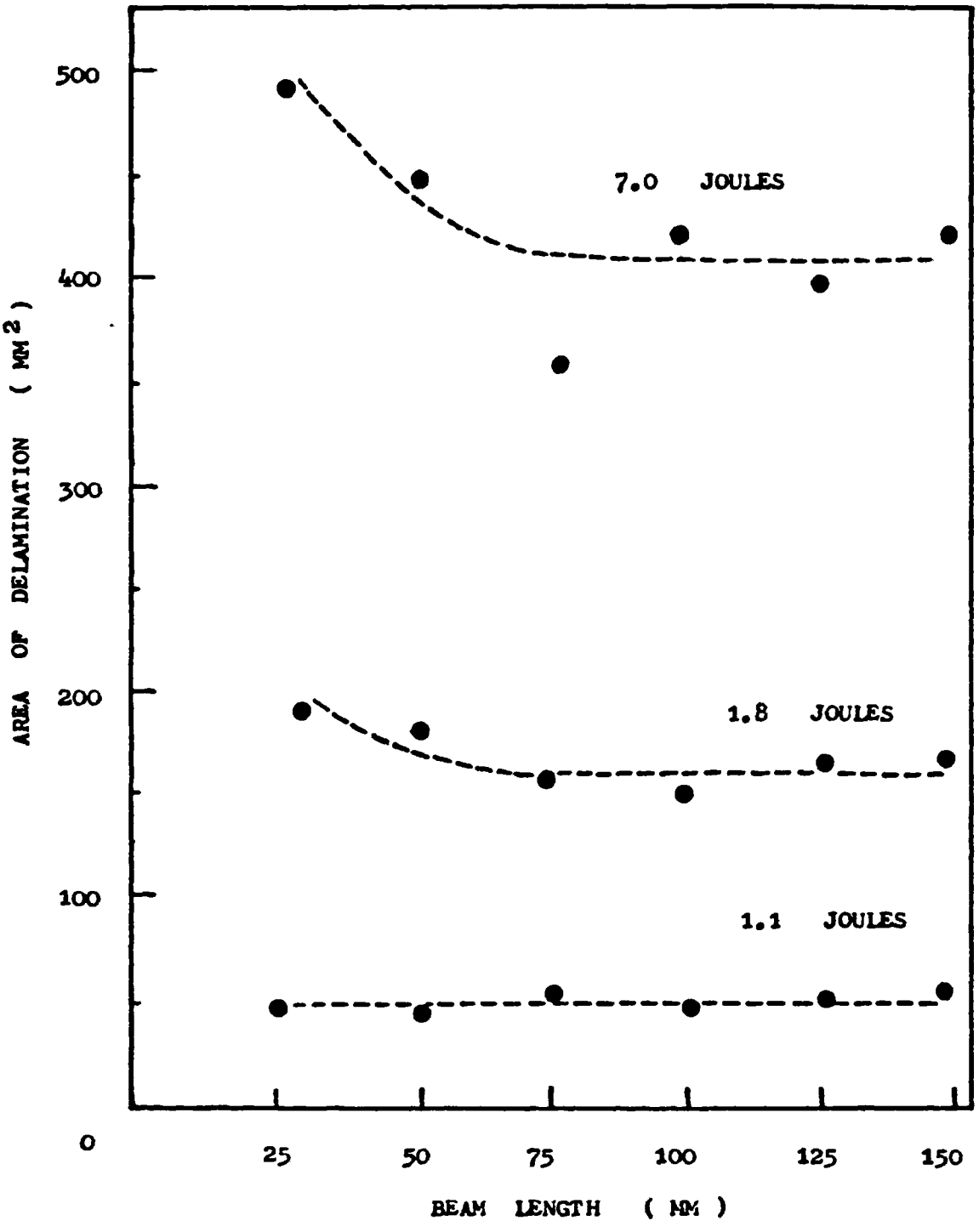


Figure 95

THE VARIATION OF IMPACT ENERGY TO INITIATE FIRST DAMAGE WITH BEAM LENGTH FOR THE SIXTEEN PLY (0,+/-45) COMPOSITE

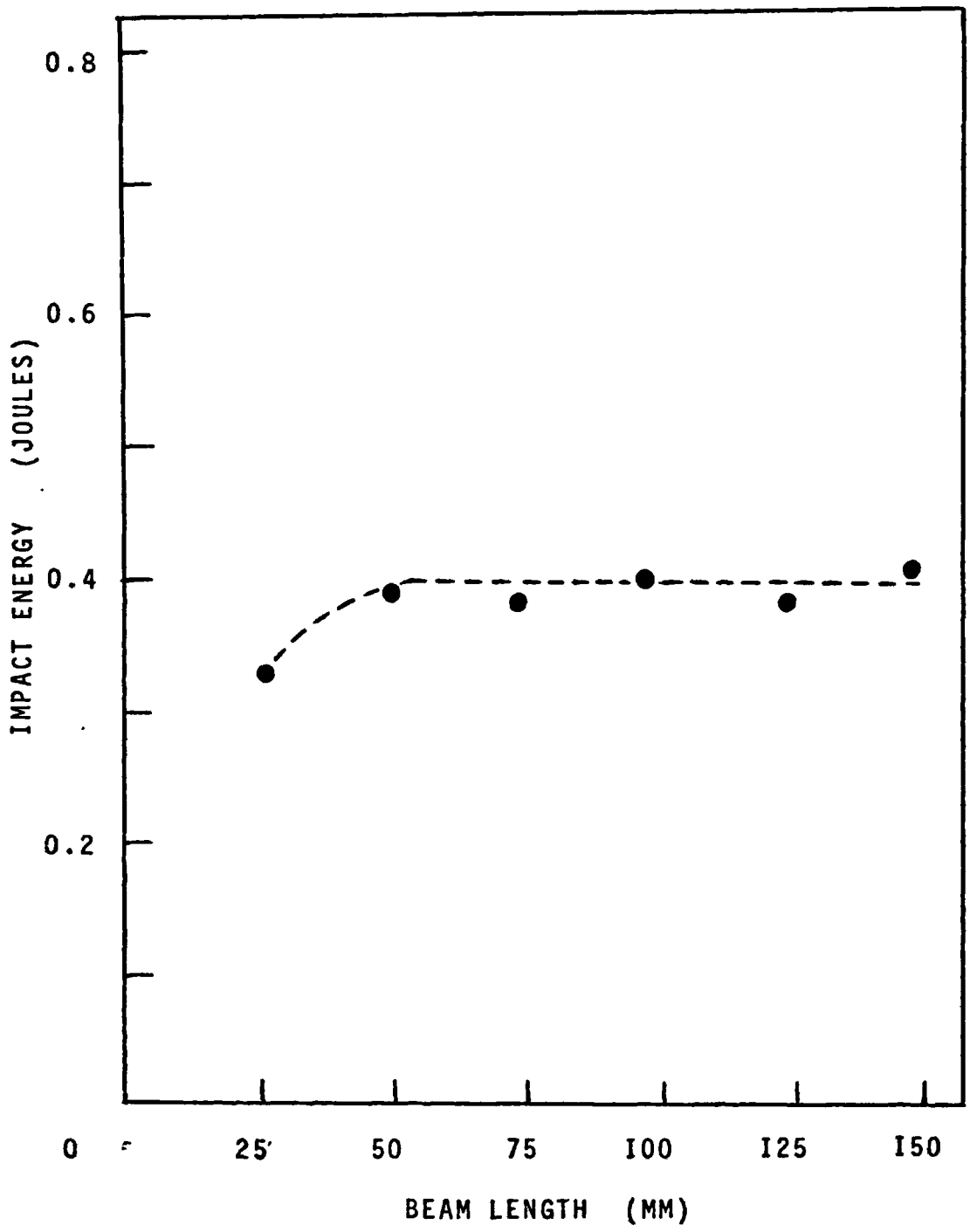


Figure 96

THE EFFECT OF BEAM LENGTH ON THE VARIATION OF BALLISTIC PERFORATION ENERGY WITH BEAM LENGTH.
SIXTEEN PLY (0,+/-45) COMPOSITE.

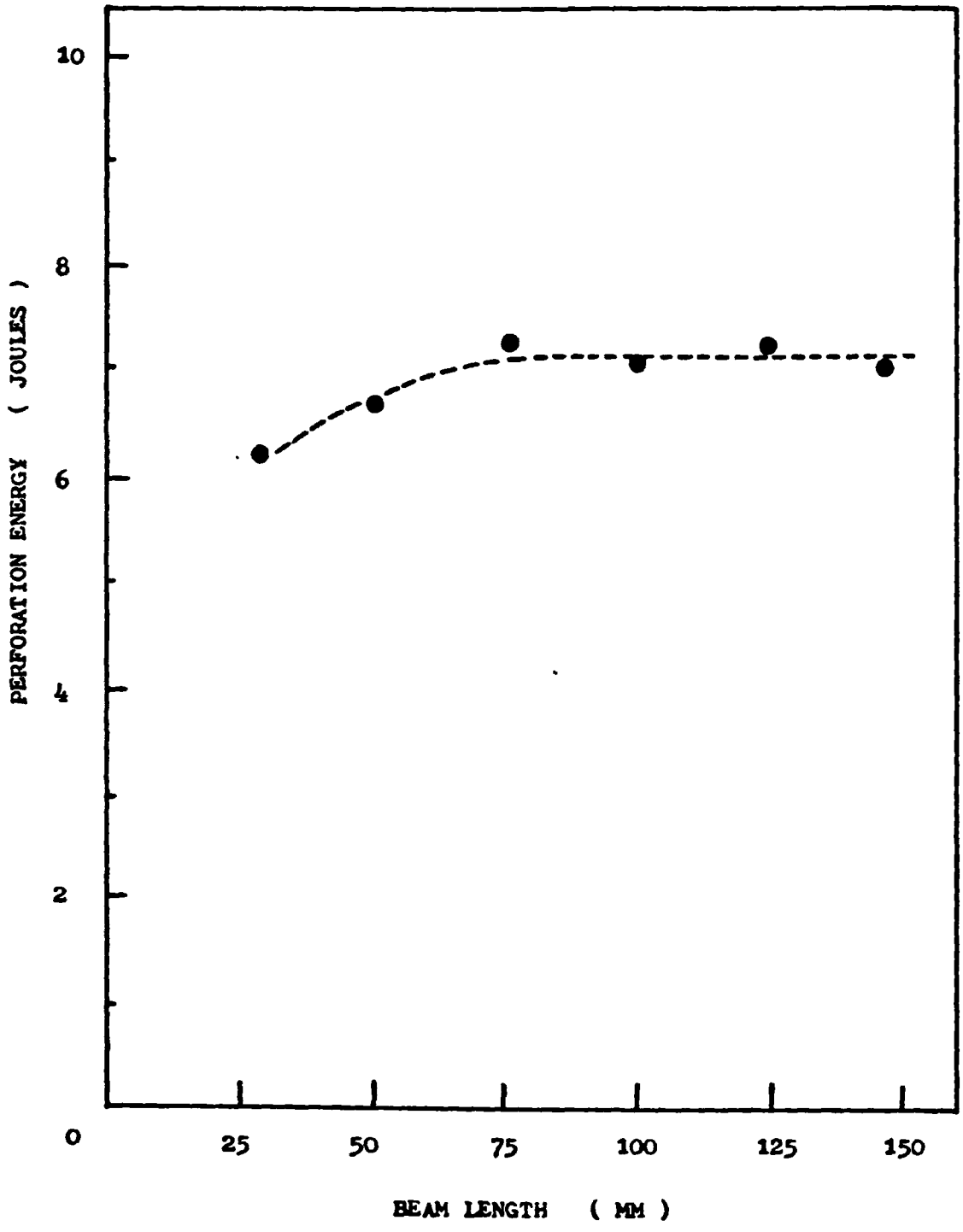
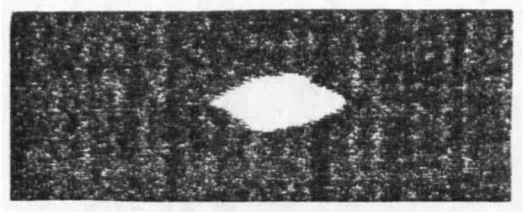


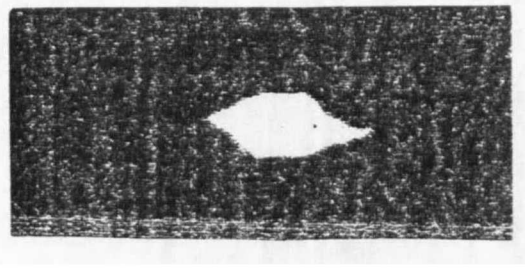
Figure 97

ULTRASONIC C-SCANS SHOWING THE EFFECT OF TARGET WIDTH ON HIGH VELOCITY IMPACT DAMAGE

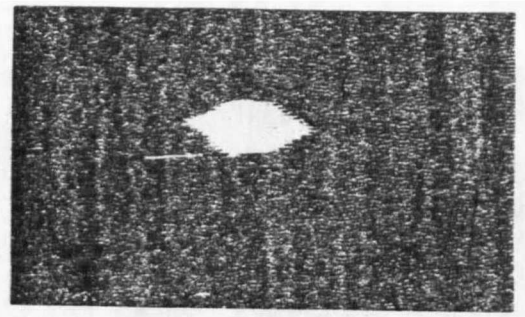
IMPACT ENERGY = 1.3 JOULES



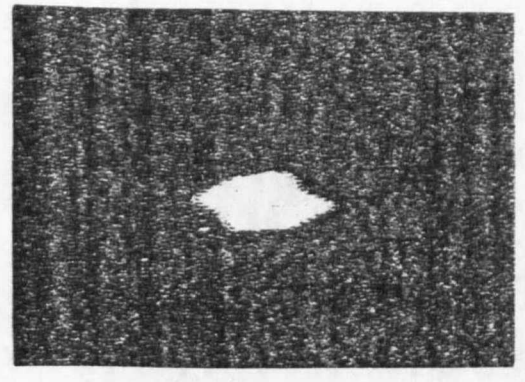
WIDTH = 25 MM



WIDTH = 30 MM



WIDTH = 40 MM



WIDTH = 50 MM

Figure 98

THE VARIATION OF PERFORATION ENERGY WITH TARGET WIDTH FOR THE SIXTEEN PLY (0,+/-45) COMPOSITE .

HIGH VELOCITY IMPACT.

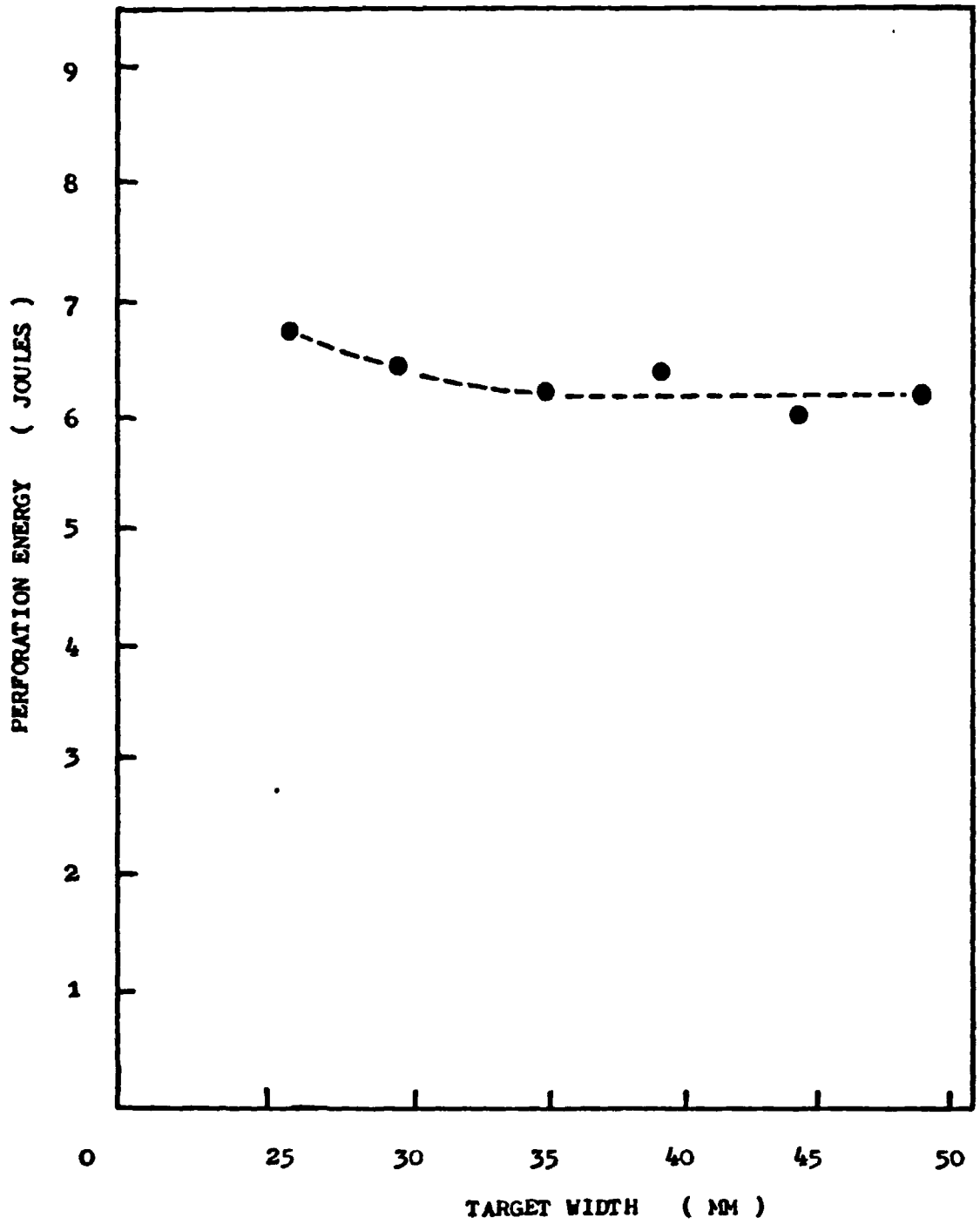


Figure 99

THE VARIATION OF PERFORATION ENERGY WITH TARGET WIDTH FOR THE SIXTEEN PLY (0,+/-45) COMPOSITE .

HIGH VELOCITY IMPACT.

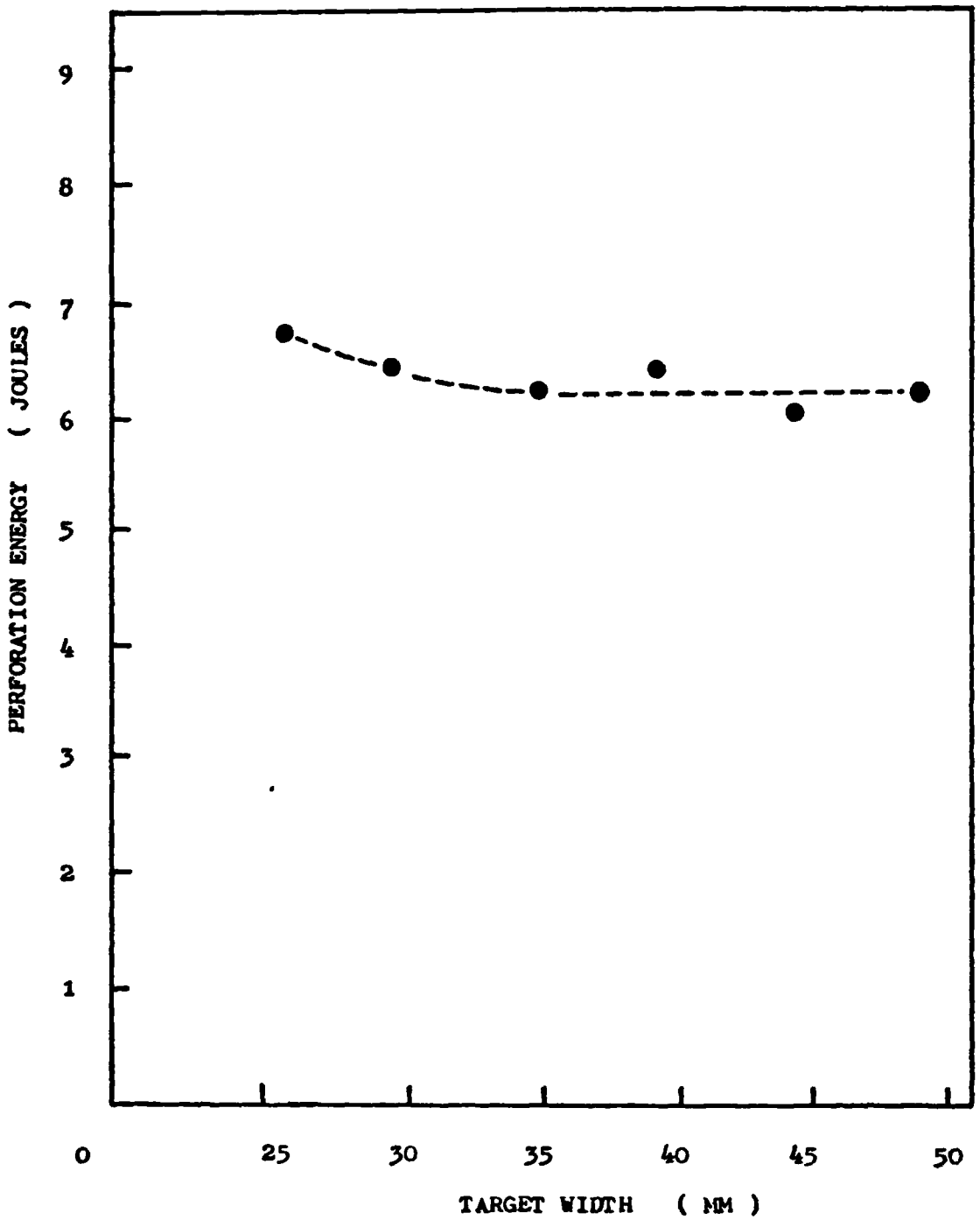


Figure 100

COMPARISON OF THE PREDICTED INCIDENT ENERGY TO INITIATE FIRST DAMAGE IN THE (+/-45) COMPOSITE PLATES CLAMPED BETWEEN TWO 130 MM CIRCULAR SUPPORTS.

HIGH VELOCITY IMPACT

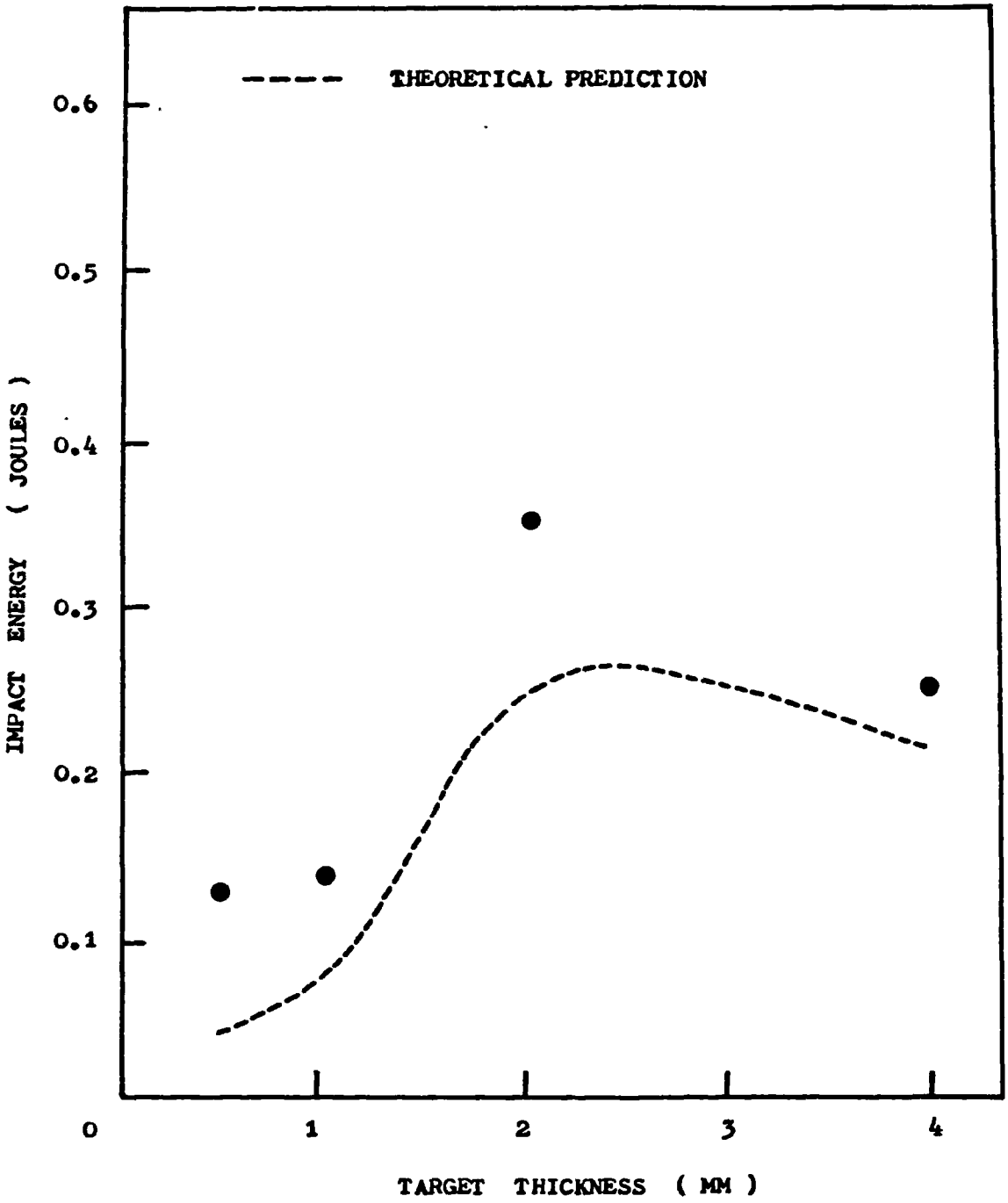
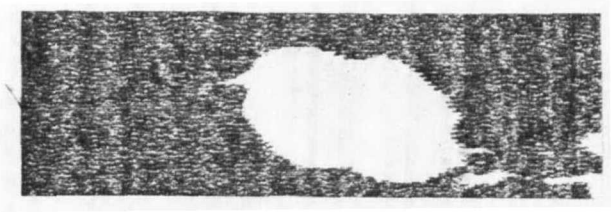


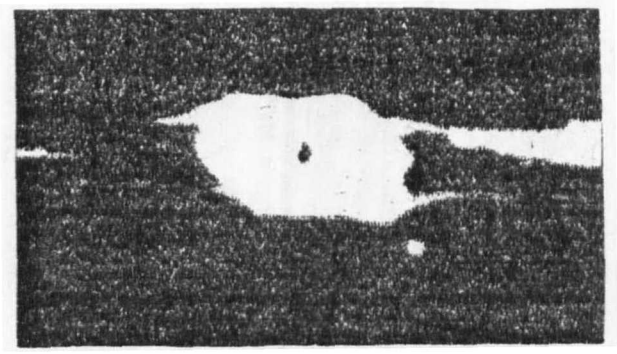
Figure 101

ULTRASONIC C-SCANS OF DAMAGED SIXTEEN PLY (0°, +/-45°) COMPOSITES DETAILING THE EFFECT OF GEOMETRY ON BALLISTIC IMPACT RESPONSE



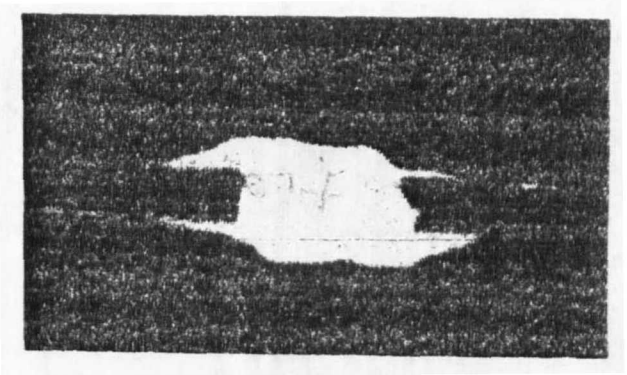
SIMPLY SUPPORTED BEAM. LENGTH = 50MM, WIDTH = 25MM

V = 110 M/S



SIMPLY SUPPORTED PLATE. LENGTH = 50MM, WIDTH = 50MM

V = 110 M/S



CIRCULAR CLAMPED PLATE. PLATE DIAMETER = 130MM.

V = 110 M/S

Figure 102

THE VARIATION OF PERFORATION ENERGY WITH TARGET THICKNESS FOR THE (+/-45) COMPOSITES CLAMPED BETWEEN CIRCULAR SUPPORTS DIAMETER 130 MM

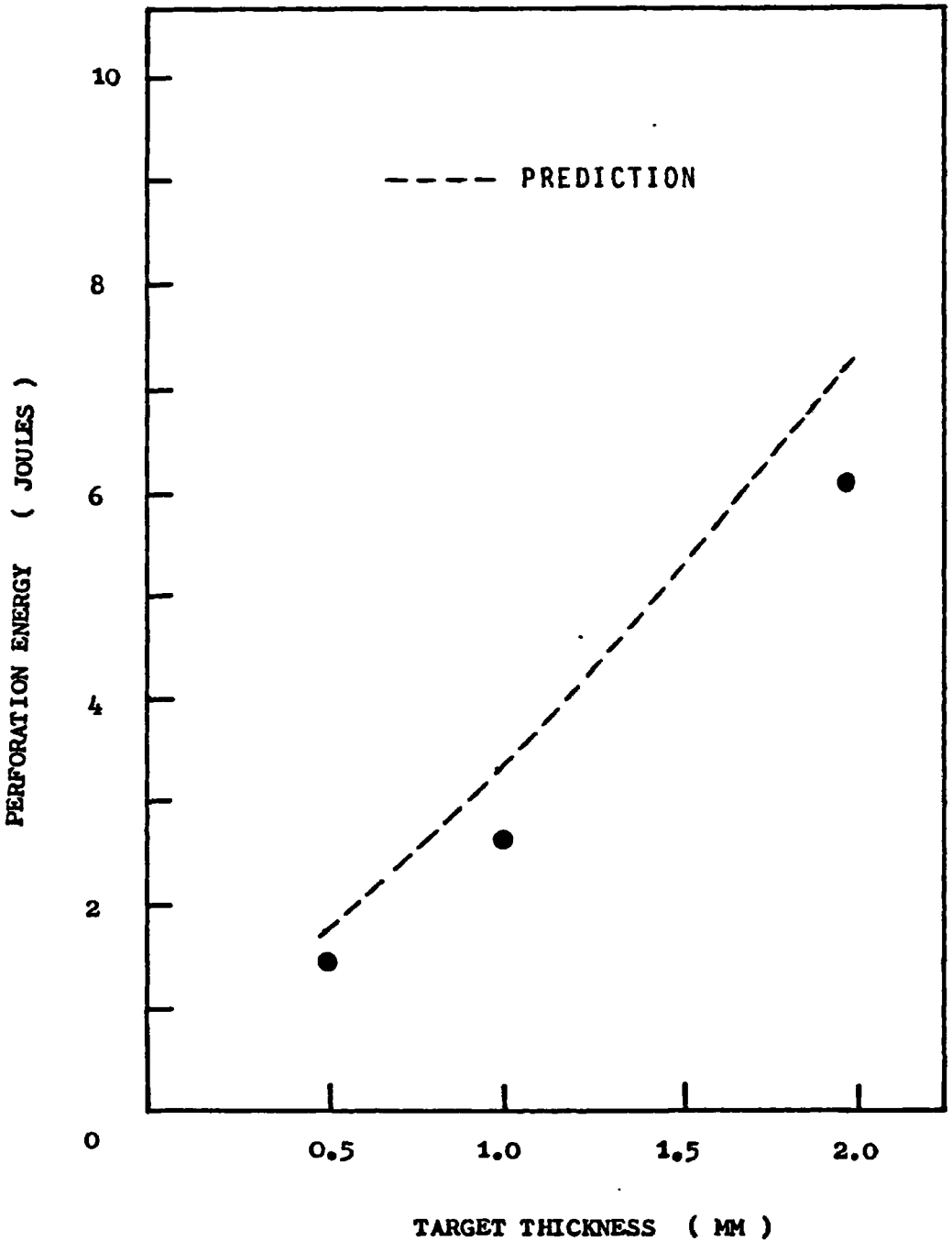


Figure 103

THE VARIATION OF NORMALISED TENSILE STRENGTH WITH IMPACT ENERGY

EIGHT PLY (+/-45) COMPOSITE

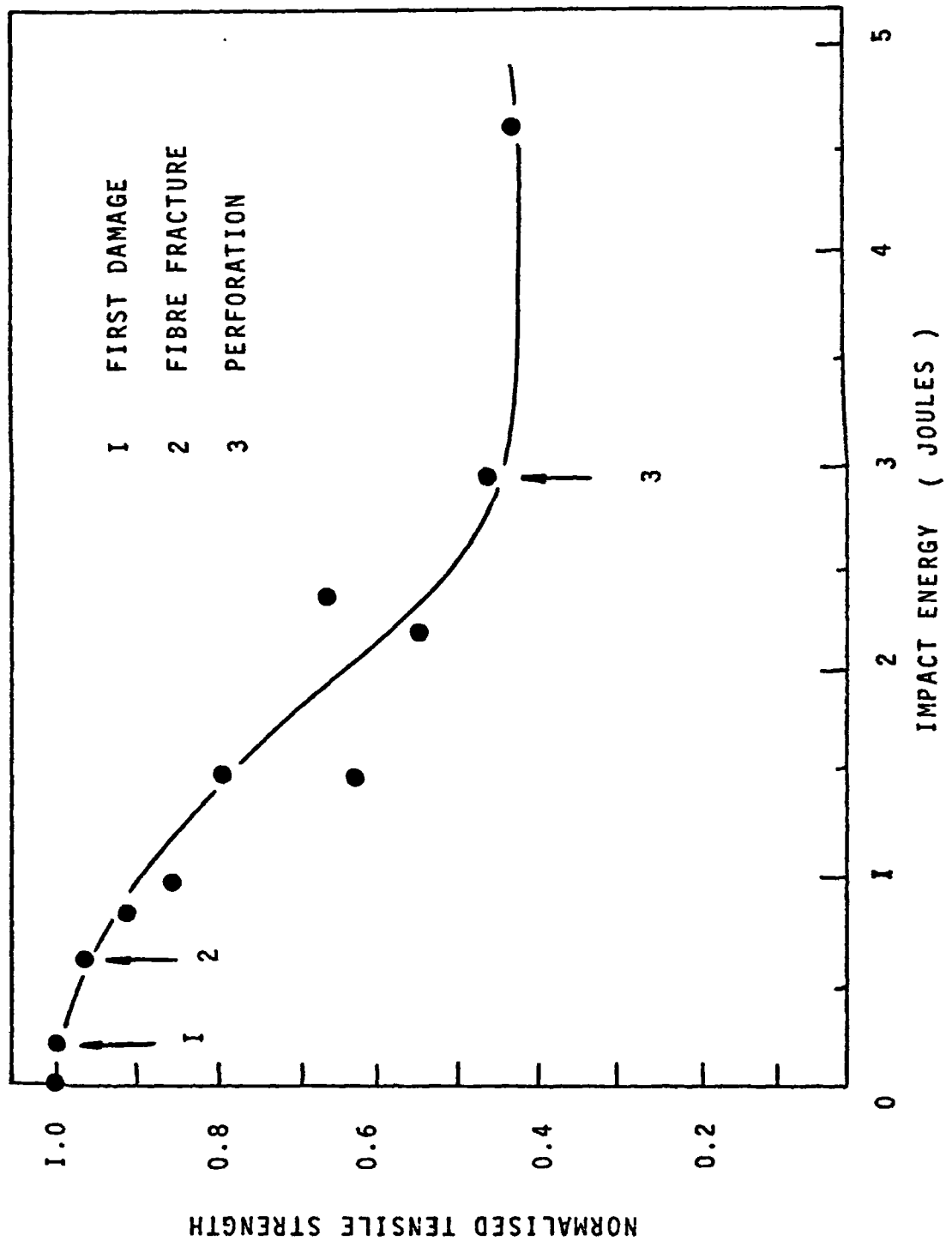


Figure 104

THE VARIATION OF NORMALISED TENSILE STRENGTH WITH IMPACT ENERGY

EIGHT PLY (0,+/-45) COMPOSITE

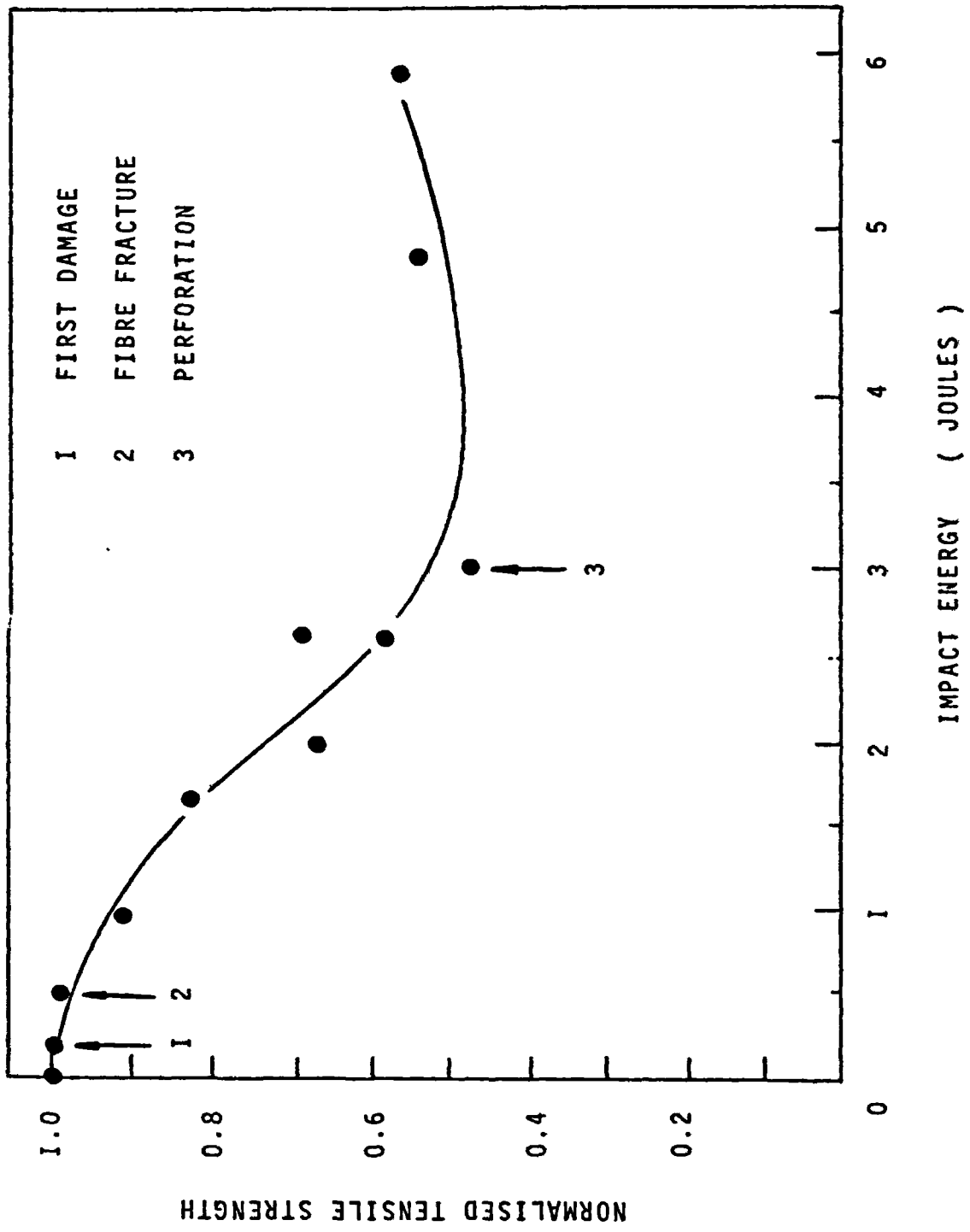


Figure 105

THE VARIATION OF NORMALISED TENSILE STRENGTH WITH IMPACT ENERGY

SIXTEEN PLY (0,+/-45) COMPOSITE

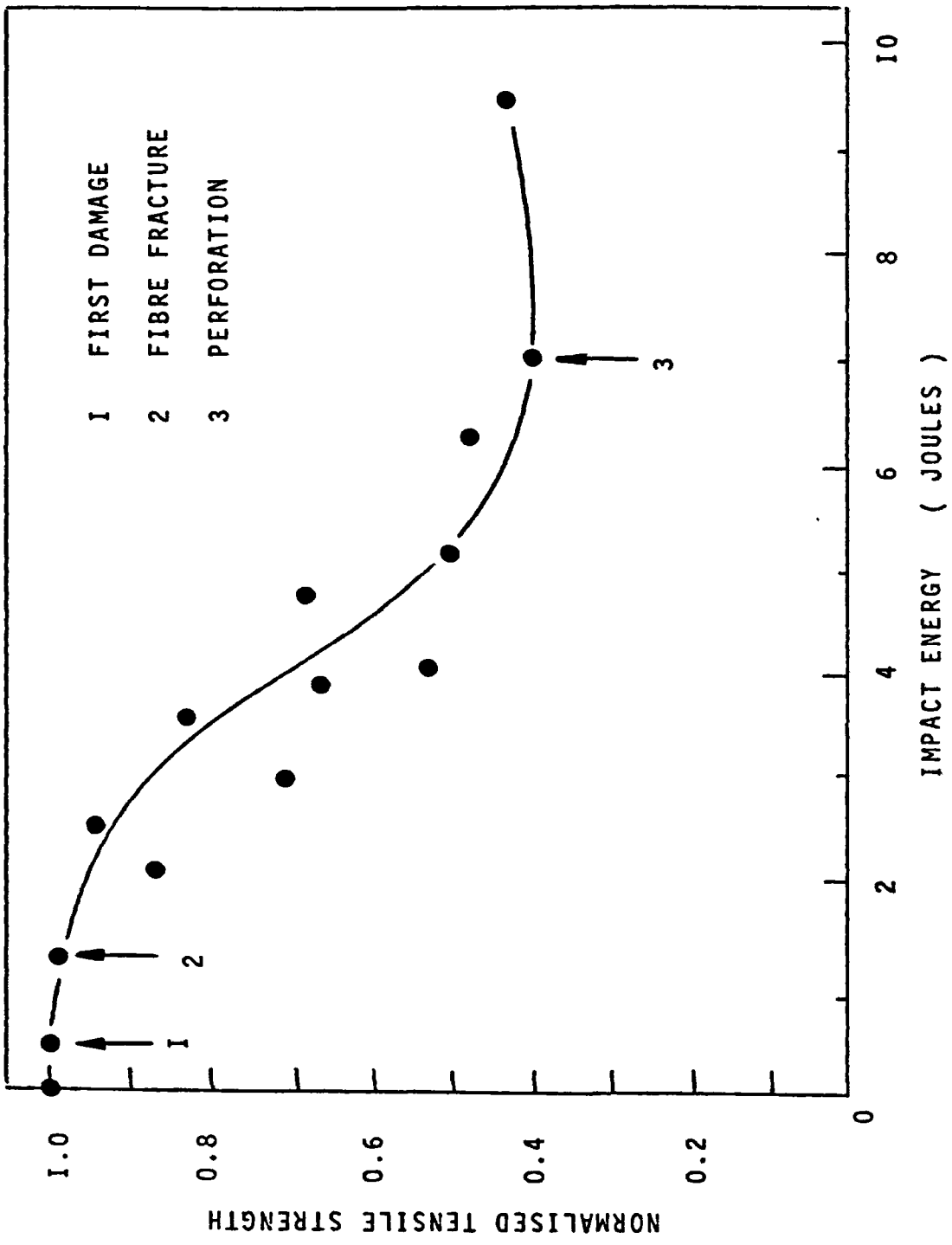


Figure 106

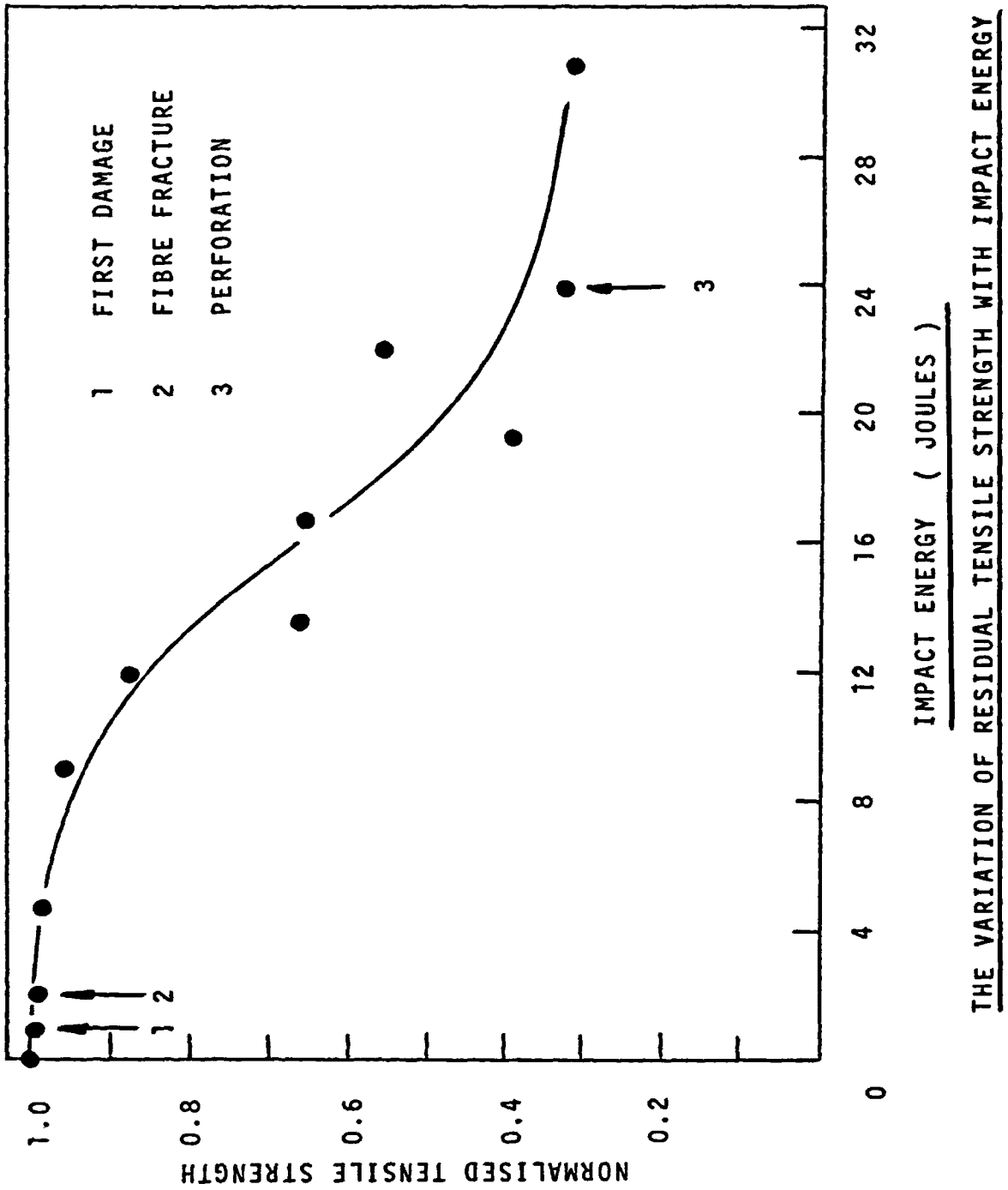

THE VARIATION OF RESIDUAL TENSILE STRENGTH WITH IMPACT ENERGY
NORMALISED TENSILE STRENGTH
1.0
0.8
0.6
0.4
0.2
0
4
8
12
16
20
24
28
32
IMPACT ENERGY (JOULES)
1 FIRST DAMAGE
2 FIBRE FRACTURE
3 PERFORATION
1
2
3

Figure 107

THE VARIATION OF TRANSVERSE LENGTH OF FIBRE FRACTURE WITH IMPACT ENERGY

EIGHT PLY (+/-45) COMPOSITE

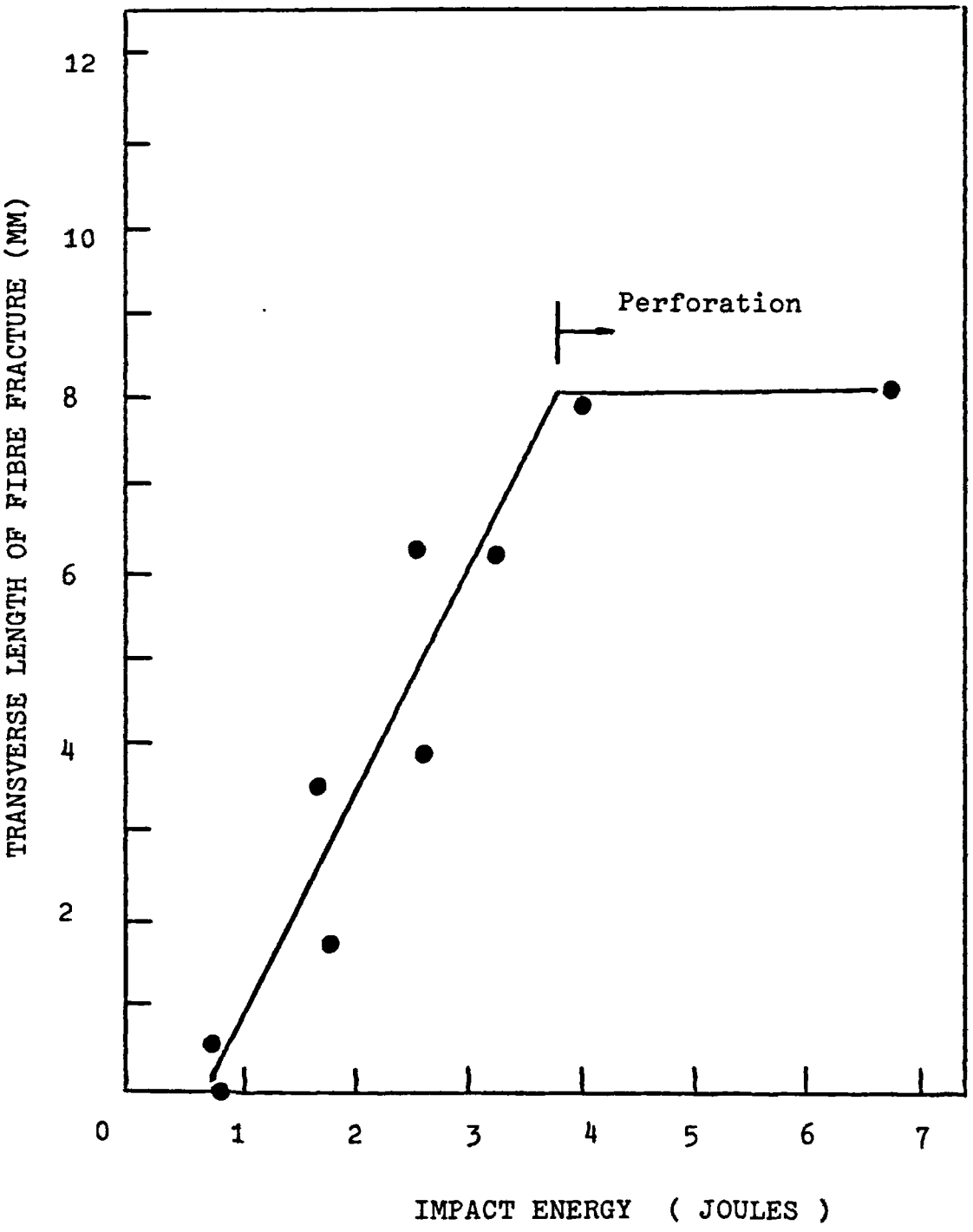


Figure 108

THE VARIATION OF TRANSVERSE LENGTH OF FIBRE FRACURE
WITH IMPACT ENERGY
EIGHT PLY (0,+/-45) COMPOSITE

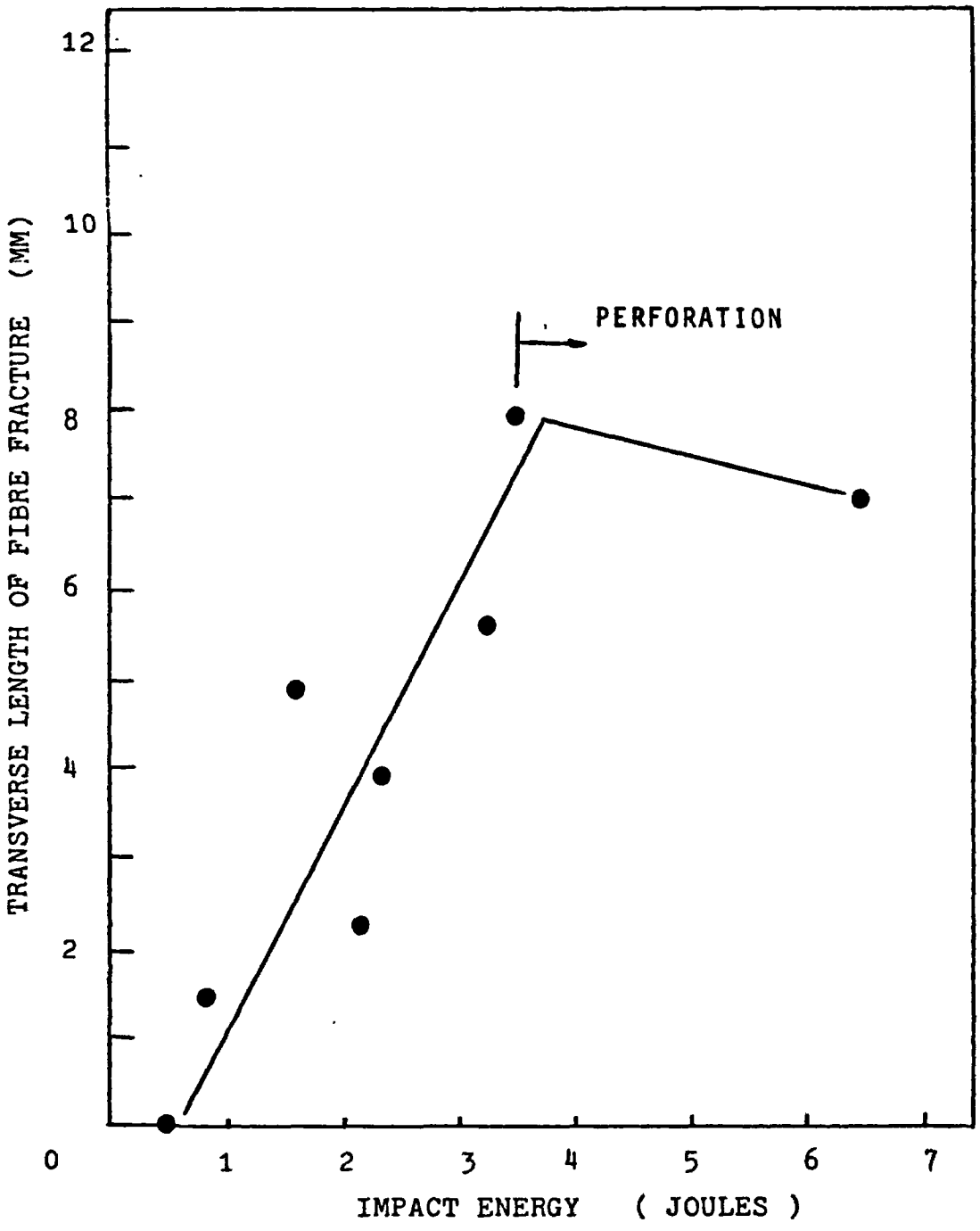


Figure 109

THE VARIATION OF TRANSVERSE LENGTH OF FIBRE FRACTURE WITH IMPACT ENERGY

SIXTEEN PLY (0,+/-45) COMPOSITE

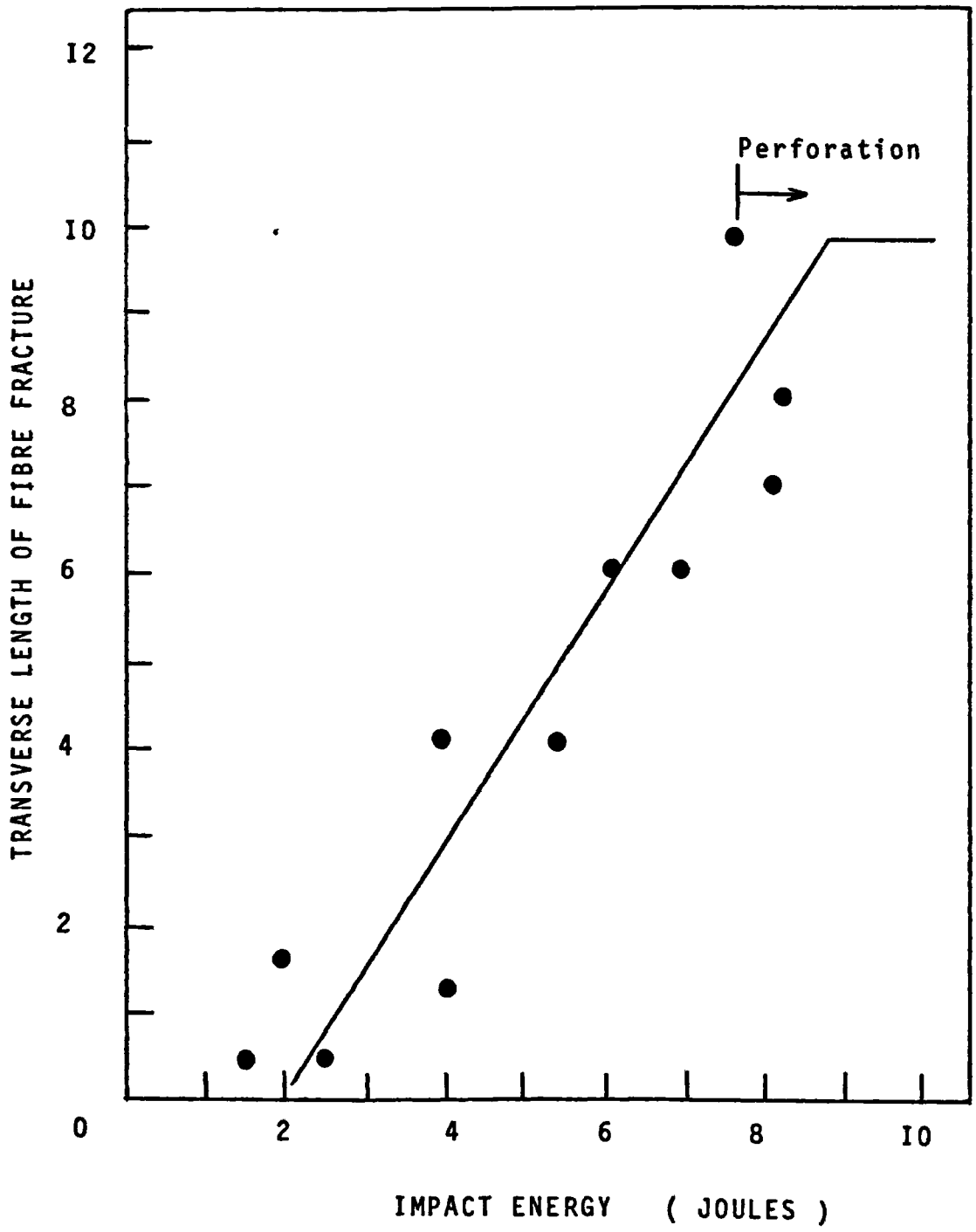


Figure 110

THE VARIATION OF NORMALISED TENSILE STRENGTH WITH IMPACT ENERGY

EIGHT PLY (+/-45) COMPOSITE

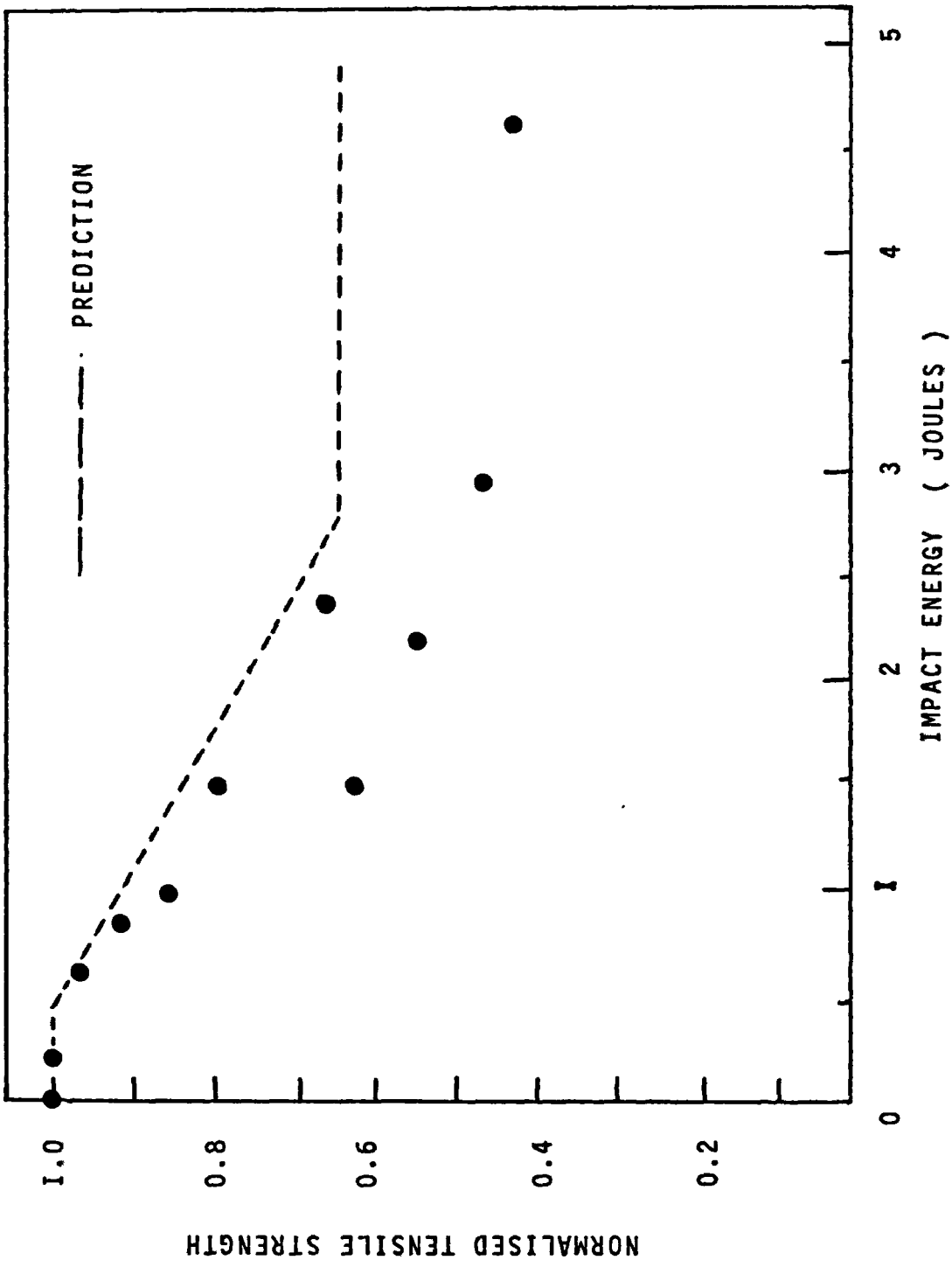


Figure 111

THE VARIATION OF NORMALISED TENSILE STRENGTH WITH IMPACT ENERGY

EIGHT PLY (0,+/-45) COMPOSITE

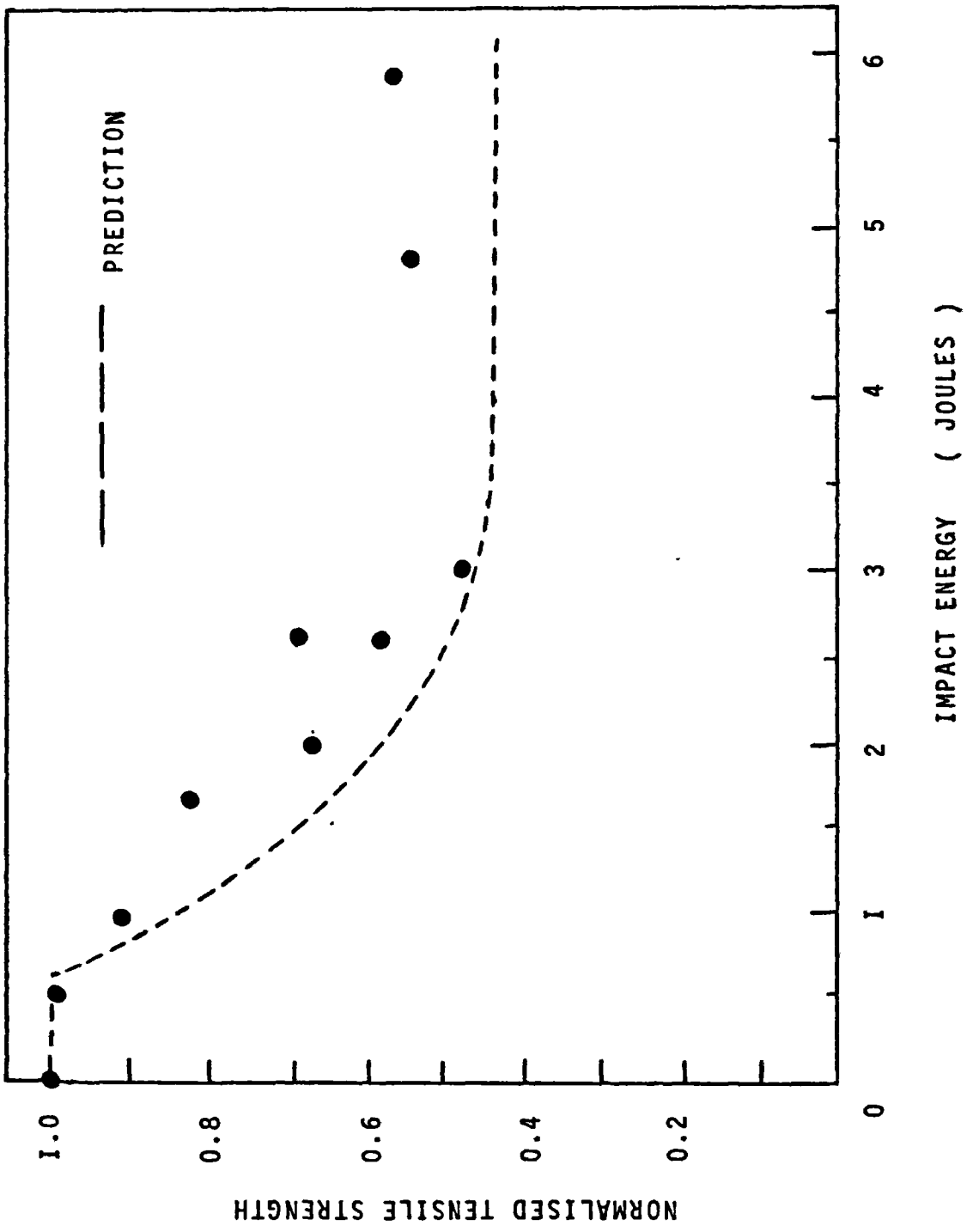


Figure 112

THE VARIATION OF NORMALISED TENSILE STRENGTH WITH IMPACT ENERGY

SIXTEEN PLY (0,+/-45) COMPOSITE

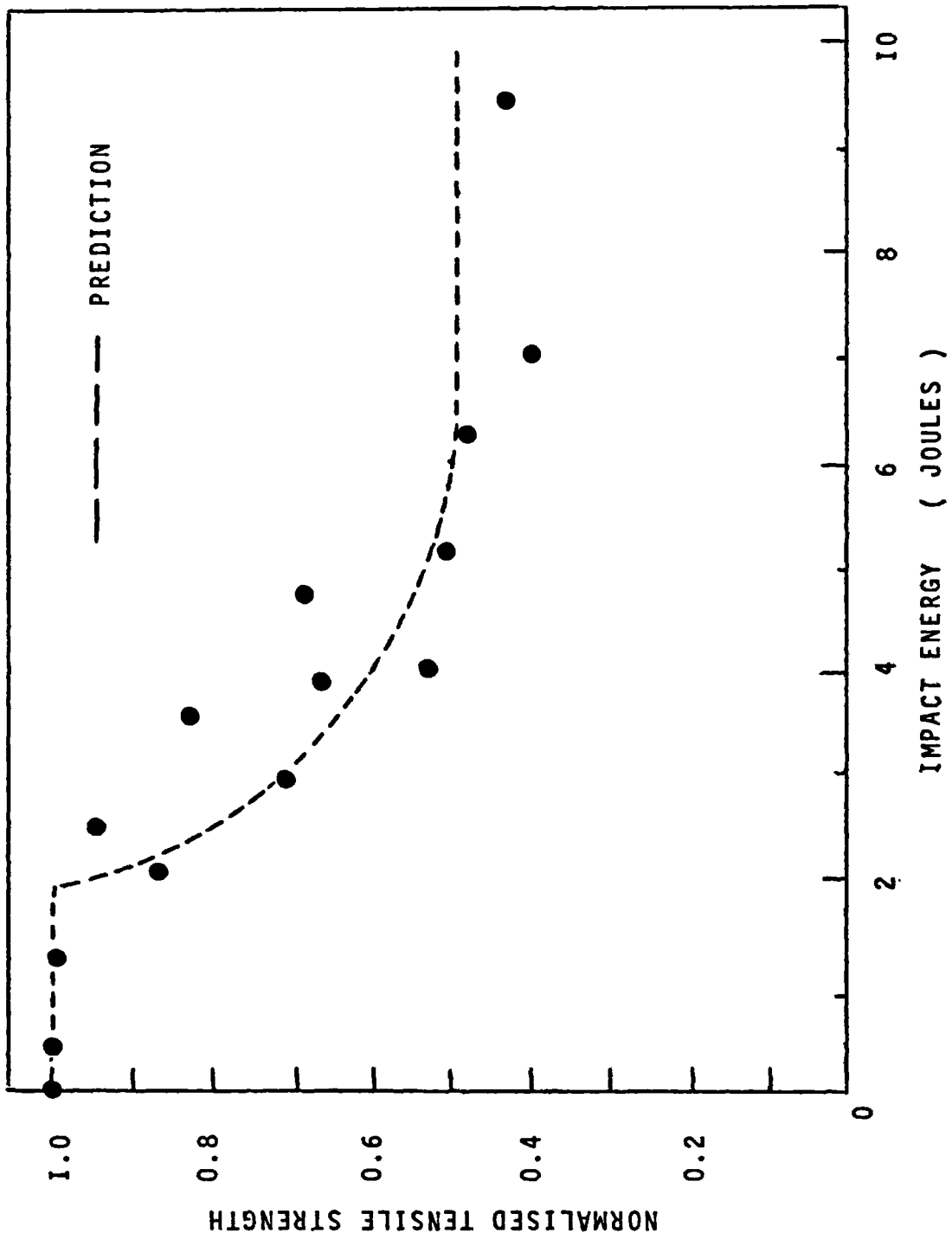


Figure 113

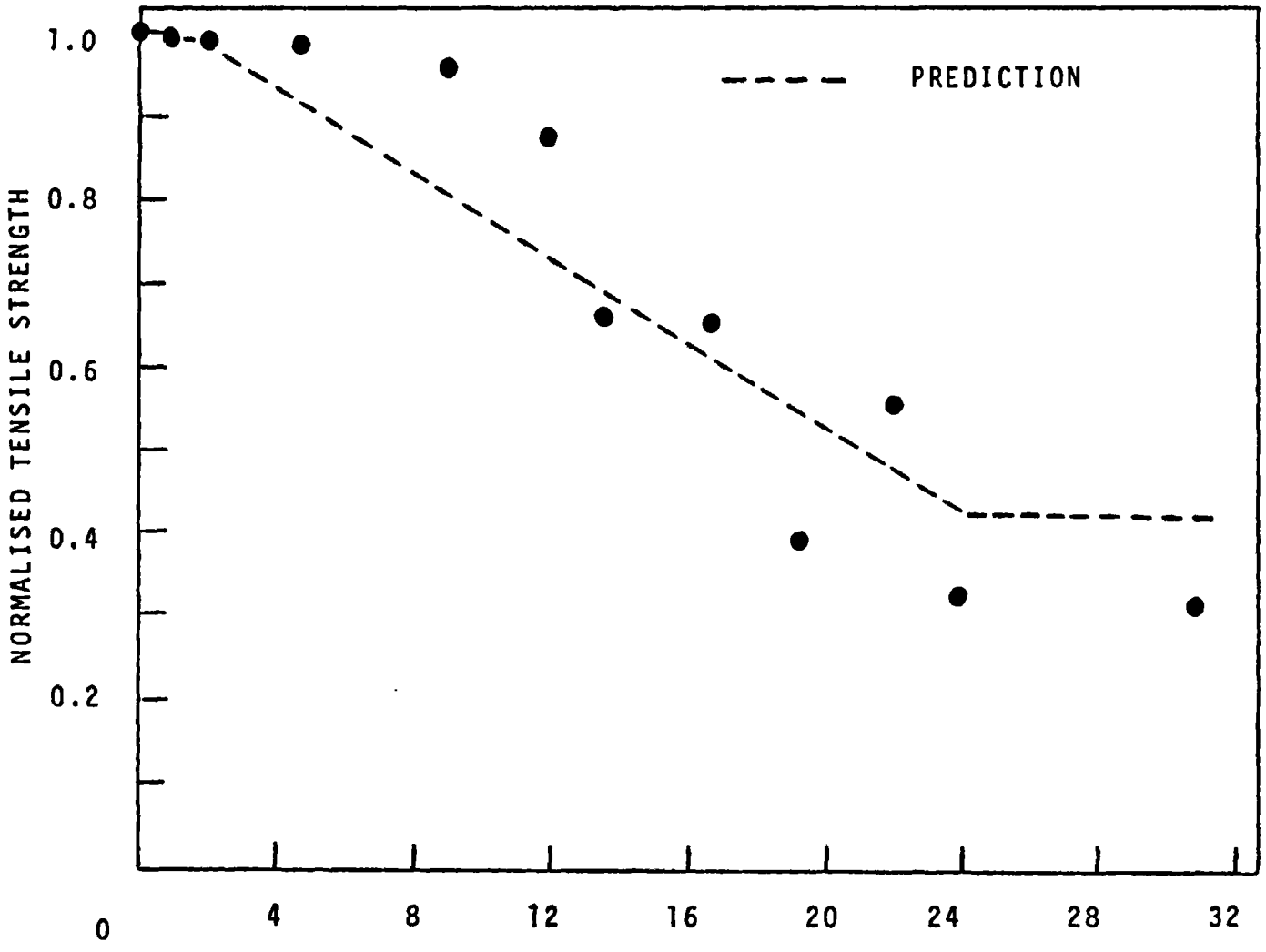


Figure 114

THE VARIATION OF RESIDUAL TENSILE STRENGTH WITH IMPACT ENERGY
FOR THE THIRTY-TWO PLY (+/-45) COMPOSITE

THE VARIATION OF DELAMINATION AREA WITH IMPACT ENERGY AFTER LOW AND HIGH VELOCITY IMPACT LOADING. SIXTEEN PLY (0,+/-45) COMPOSITE

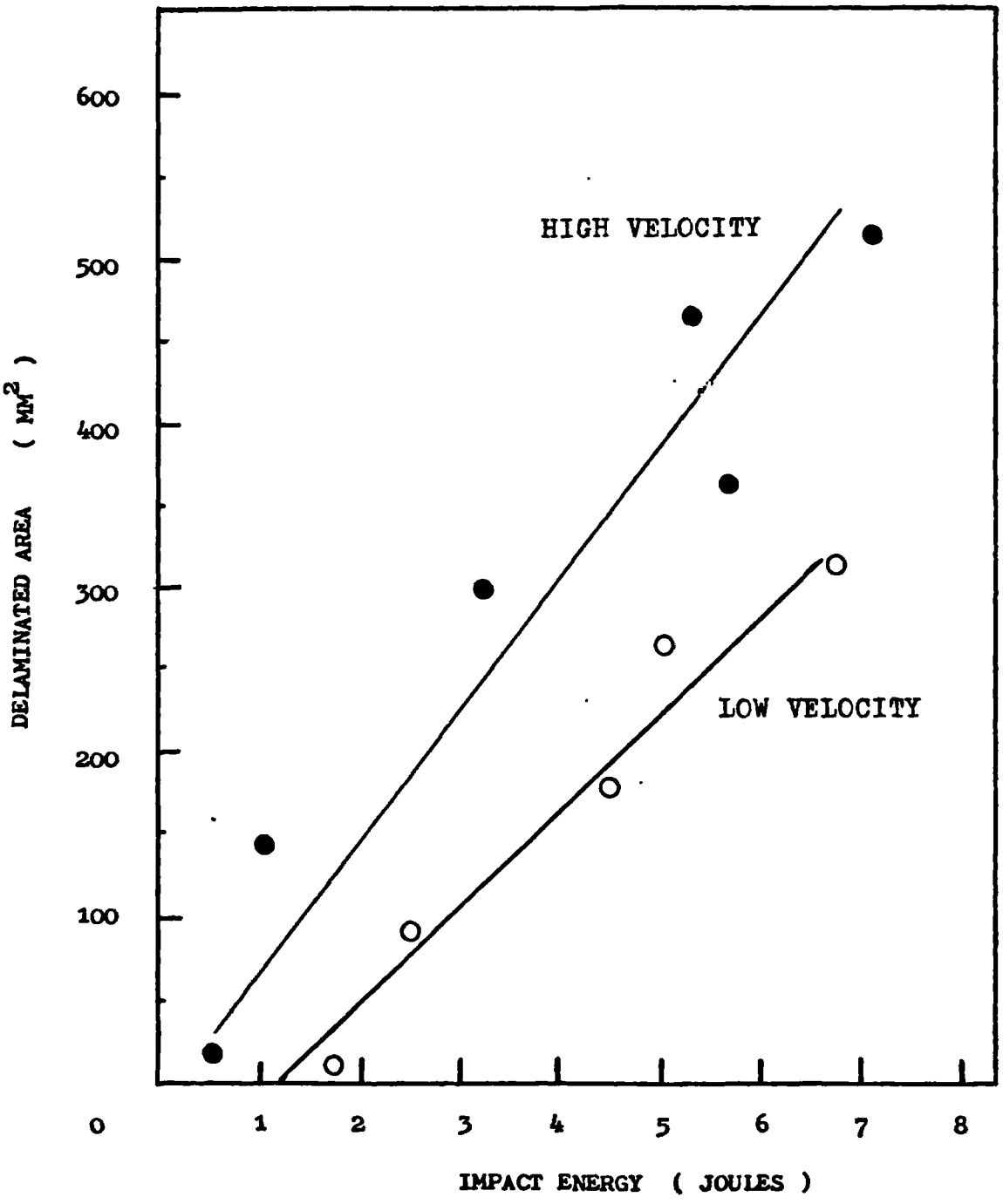


Figure 115

APPENDIX 1

Calibration of the Drop-weight Load Cell

Before conducting tests on the drop weight rig it was necessary to calibrate the response of the load cell. This can be accomplished in several ways, for example, removing it from the impact carriage and testing in a standard mechanical testing machine or by applying a series of weights on the in-situ load cell and measuring the resulting voltage. The latter technique was favoured here because Djahansouzi (90) has identified several difficulties involved with the former procedure. Figure 116 shows the resulting load-voltage characteristics for loads up to 200 Newtons. It was assumed that the load-voltage curve remained linear beyond the limits of this curve, indeed evidence suggests that it does (90).

CALIBRATION OF THE DROP WEIGHT LOAD CELL

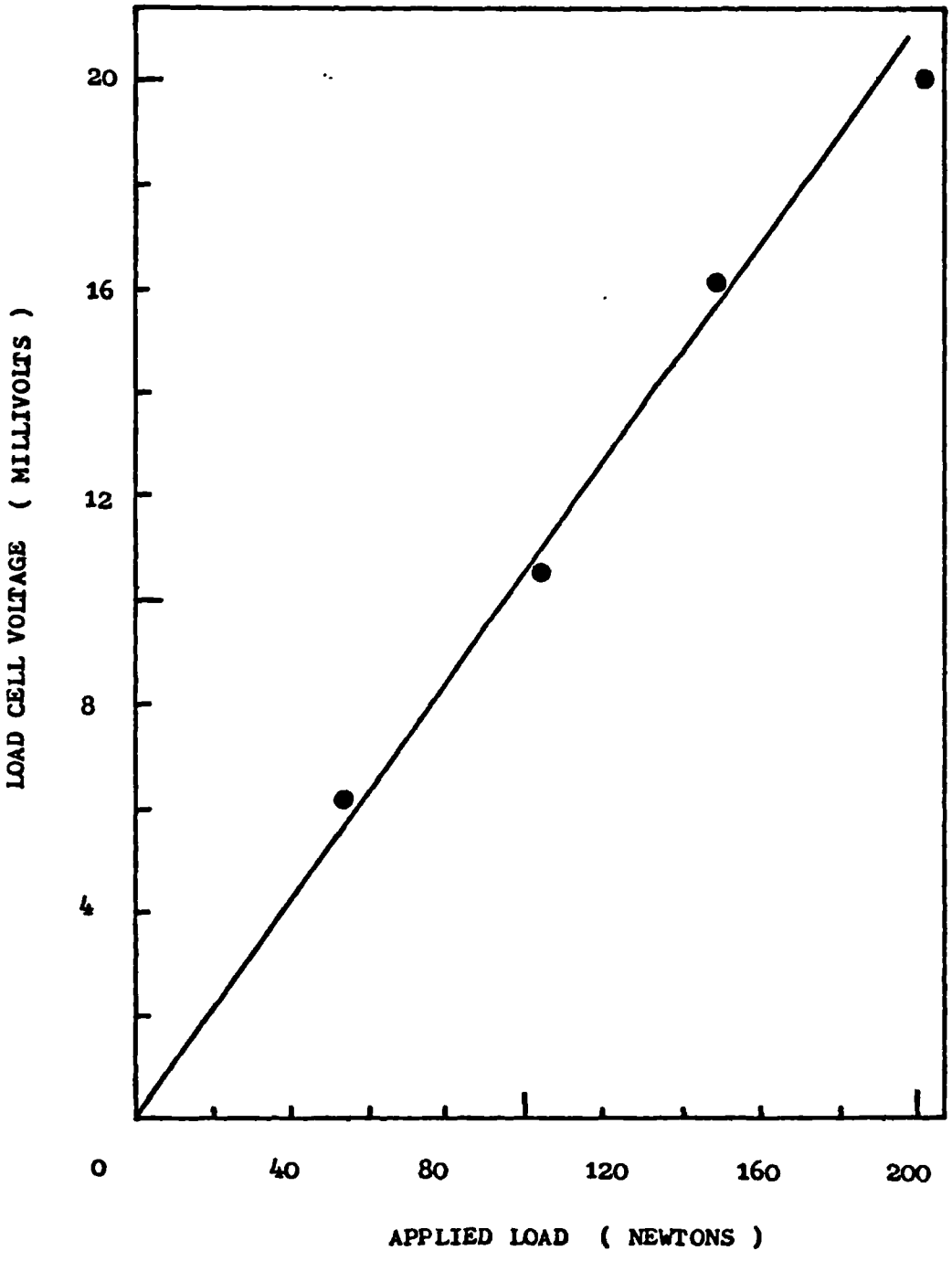


Figure 116

APPENDIX 2

Calibration of the high velocity gas gun

Before undertaking any experimental testing it was first necessary to calibrate the performance of the gas gun.

The design of the gun allowed the projectile velocity to be controlled in two ways, by varying either the chamber pressure or sabot mass, or indeed both. Both techniques were employed here enabling velocities in the range 20m/s to 400m/s to be achieved. The latter approach of varying sabot mass for a fixed chamber pressure was favoured for obtaining velocities in the range 20m/s to 400m/s.

The gun was fired by slowly increasing the chamber pressure until the plastic diaphragm ruptured, the resulting instantaneous release of pressure accelerating the projectile/ sabot combination along the barrel. This technique enabled the gun to be loaded and fired very quickly giving very consistant and reproducable results. Figures 118-120 contain the resulting calibration curve for sabot masses between 5 grams and 300 grams, these results emphasize the reproducability of the gas gun.

Projectile velocities in excess of 200m/s were achieved by varying the chamber pressure for a fixed sabot mass. Here an array of Melinex plastic diaphragms were used in order to

achieve bursting pressures in the range 300 psi to 1000 psi. With this procedure bursting of the diaphragms was achieved by raising the chamber pressure to seventy five per cent of its ultimate pressure and passing a current through a length of resistance wire located at the diaphragm centre. Figure 117 details the bursting characteristics of the Melinex diaphragms and includes the operating curve. Other bursting pressures outside this range were achieved by stacking several diaphragms together. The resulting calibration data for this technique is shown in figure 121. The figure indicates that velocities over 400m/s can be achieved for a chamber pressure of 1000 psi. The construction of the gun accommodates chambers pressures up to 2500 psi. However, the trends evident in figure 121 suggests the curve will approach a value of around 500m/s. To achieve velocities above this it may be likely that the gun barrel will have to be evacuated or perhaps the driver gas changed, helium is one possibility.

THE BURSTING CHARACTERISTICS OF THE MELINEX DIAPHRAGM

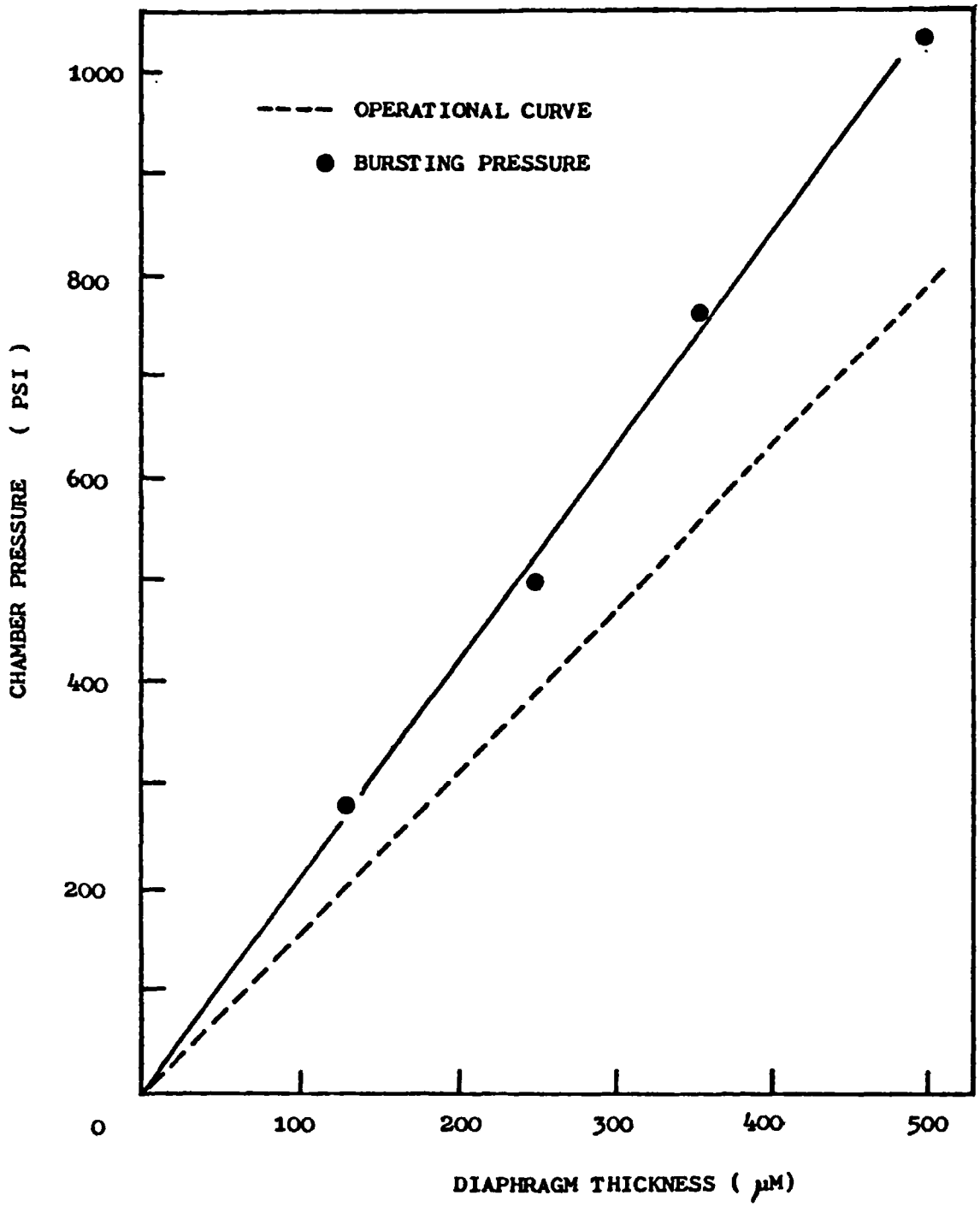


Figure 117

THE VARIATION OF PROJECTILE VELOCITY WITH SABOT MASS

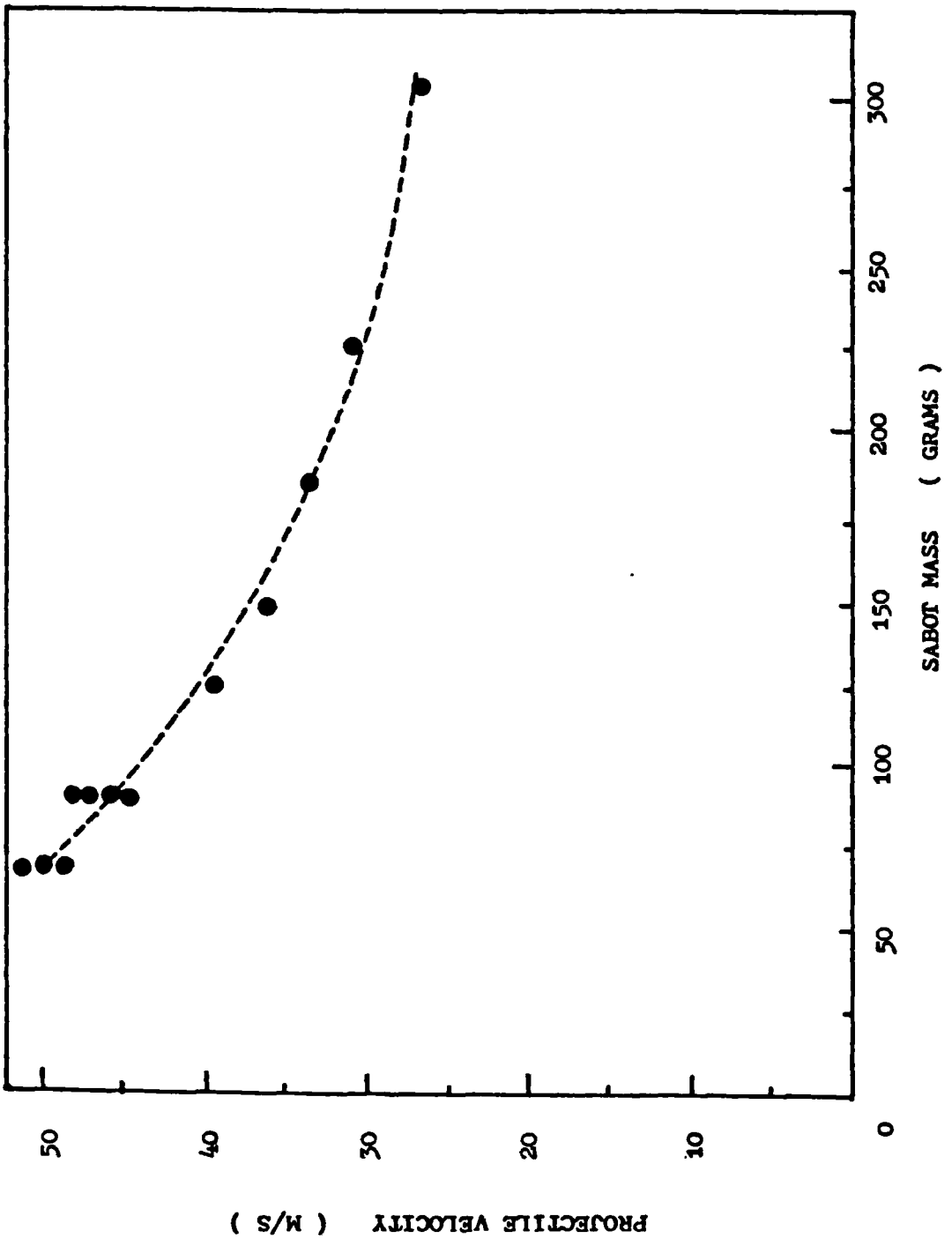


Figure 118

THE VARIATION OF PROJECTILE VELOCITY WITH SABOT MASS

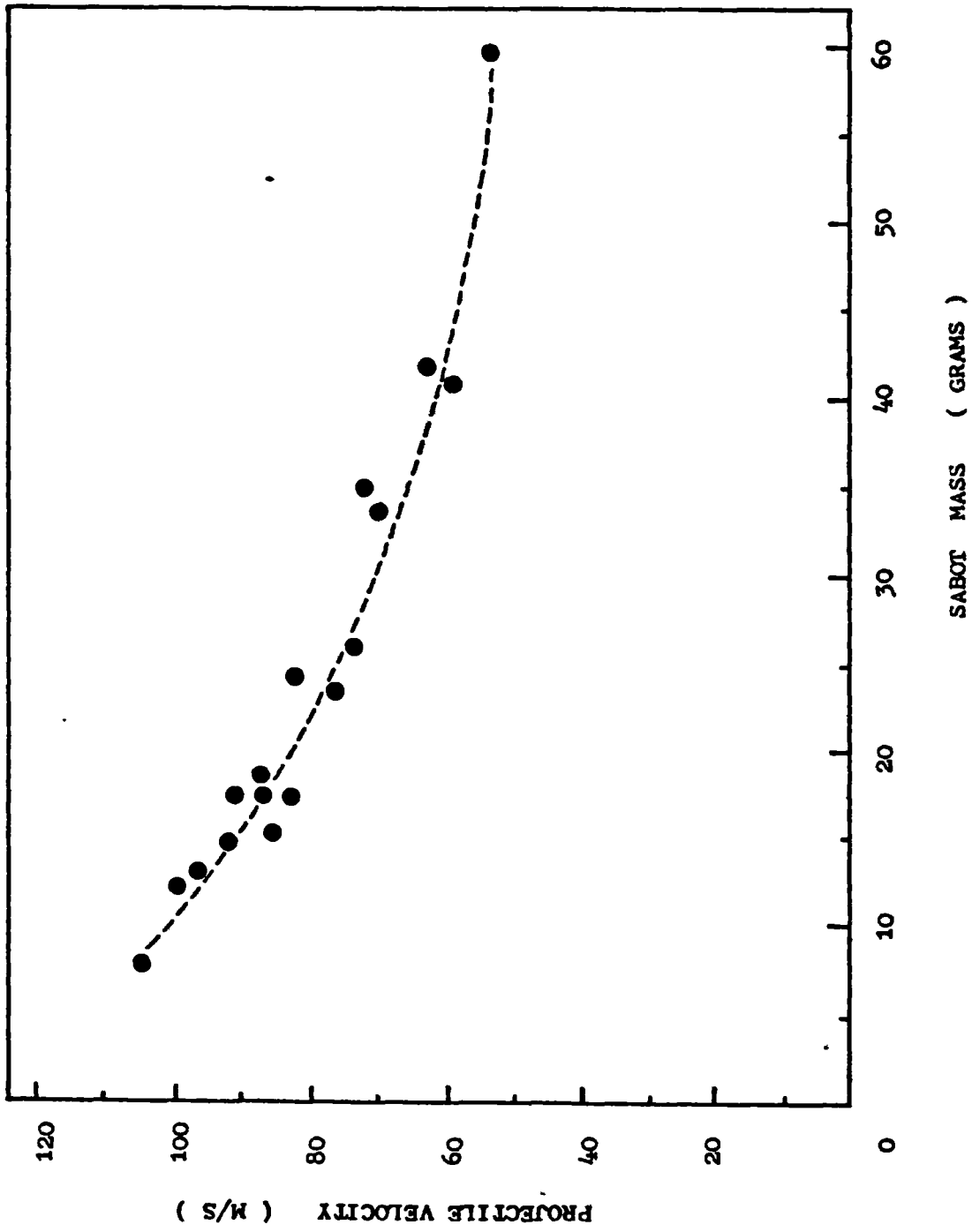


Figure 119

THE VARIATION OF PROJECTILE VELOCITY WITH SABOT MASS

HIGH PERFORMANCE PLASTIC

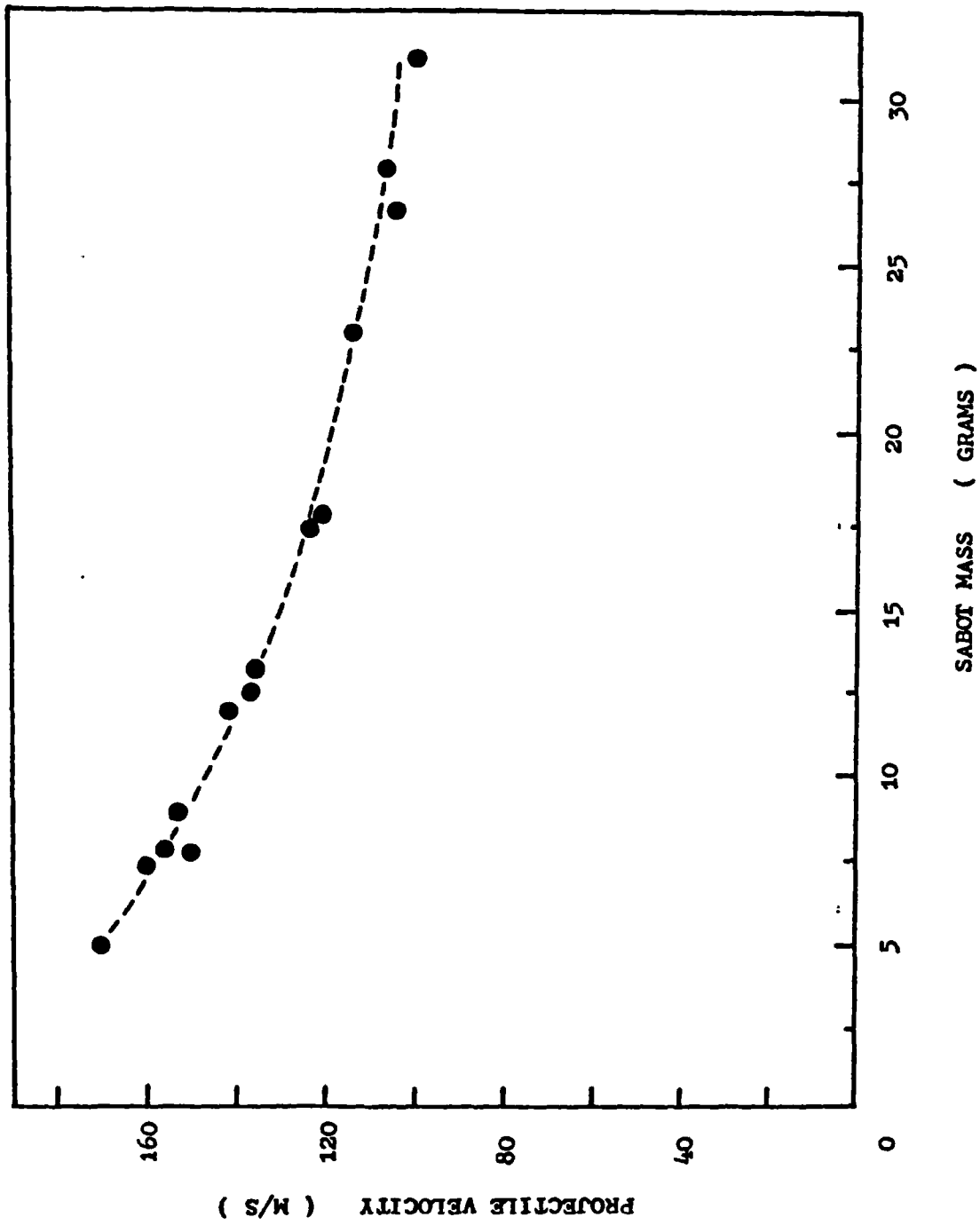


Figure 120

THE VARIATION OF PROJECTILE VELOCITY WITH CHAMBER PRESSURE

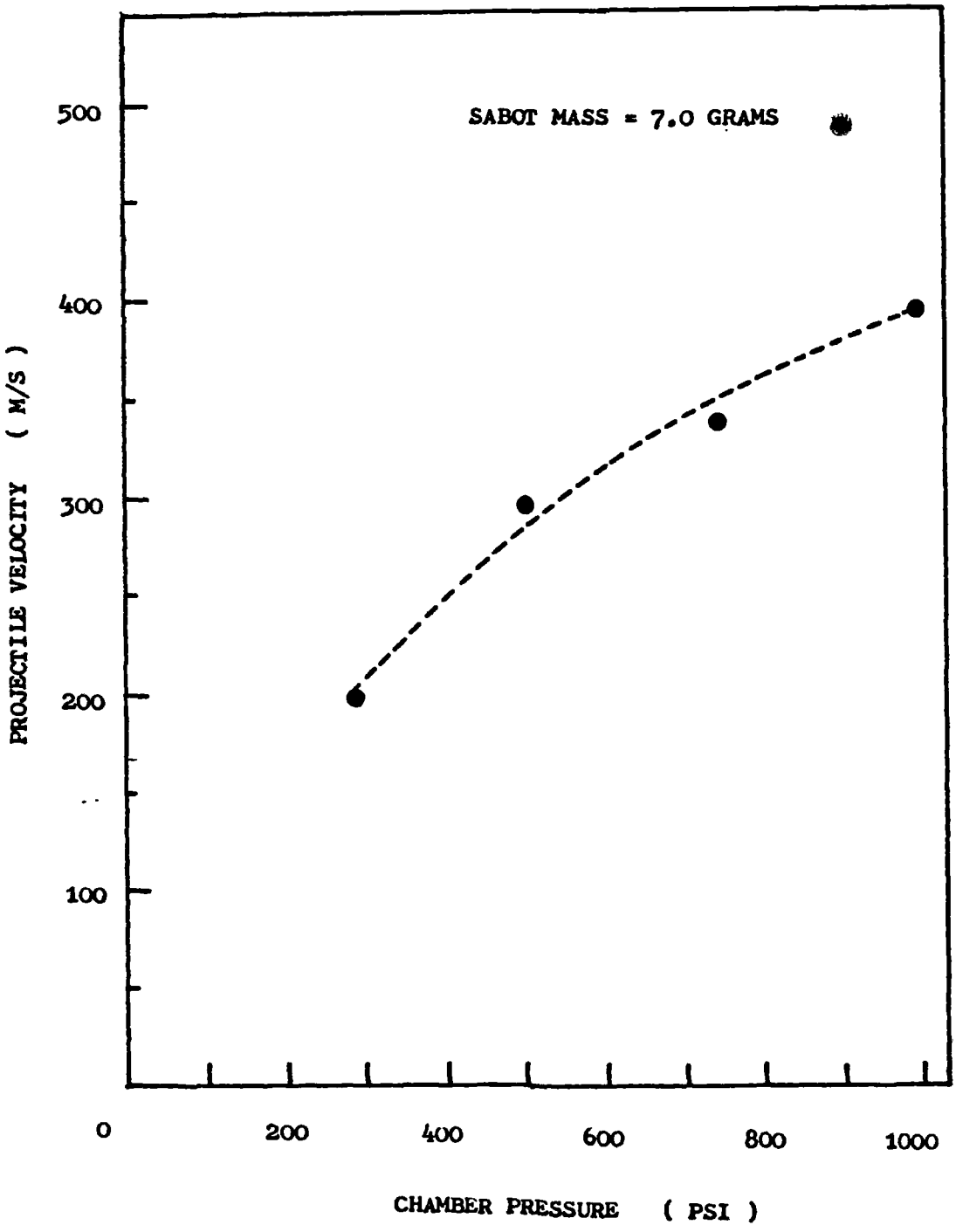


Figure 121

APPENDIX 3. LISTING OF COMPUTER PROGRAMME FOR CALCULATING THE A,B AND D MATRICES OF A LAMINATED COMPOSITE

```
   10 REM PROGRAM TO DETERMINE THE A B AND D MATRICIES OF A
COMPOSITE
   20 CLS
   30 PRINT
   40 PRINT"THIS PROGRAM DETERMINES THE EXTENSIONAL STIFFNESS"
   50 PRINT"BENDING STIFFNESSES AND COUPLING STIFFNESSES OF AN"
   60 PRINT"                                    ANGLE PLY COMPOSITE"

   70 PRINT
   80 DIM THETA(32)
   90 ICOUNT = -1
  110 E11=135E9
  111 E22=8E9
  130 V12=0.31
  150 G12=5.9E9
  170 T=.000125
  180 PRINT "INPUT THE NUMBER OF PLIES"
  190 INPUT N
  200 GOSUB 380
  210 PRINT " INPUT THE ORIENTATIONS OF THE PLIES":PRINT
  220 PRINT "STARTING ON THE UPPER SURFACE":PRINT
  230 PRINT "TYPE THEM IN ORDER USING A NEW LINE FOR EACH"
  240 FOR I = 1 TO N
  250 INPUT THETA(I)
  260 NEXT I
  270 FOR J = 1 TO N
  280 ICOUNT = ICOUNT + 2
  290 THICK = T*N
  300 ZK = (THICK/2*(1-ICOUNT/N))
  310 GOSUB 450
  320 GOSUB 680
  330 GOSUB 770
  340 GOSUB 860
  350 NEXT J
  360 GOSUB 950
  370 END
  380 REM     THIS ROUTINE CALCULATES Q
  390 V21 = V12*E22/E11
  400 Q11 = E11/(1-V12*V21)
  410 Q12 = V12*E22/(1-V12*V21)
  420 Q22 = E22/(1-V12*V21)
  430 Q66 = G12
  440 RETURN
  450 REM THIS ROUTINE CALCULATES QBAR
  460 REM                  DETERMINE THE SINES AND COSINES
  470 THETA = RAD(THETA(J))
  480 C1 = COS(THETA)
  490 S1 = SIN(THETA)
  500 C2 = C1*C1
  510 S2 = S1*S1
  520 C3 = C2*C1
  530 S3 = S2*S1
  540 C4 = C2*C2
  550 S4 = S2*S2
  560 REM
  570 QB11 = Q11*C4+2*(Q12+2*Q66)*S2*C2 +Q22*S4
  580 QB12 = (Q11+Q22-4*Q66)*S2*C2+Q12*(S4+C4)
```

```
590 QB22 = Q11*S4+2*(Q12+2*Q66)*S2*C2+Q22*C4
600 QB16 = (Q11-Q12-2*Q66)*S1*C3+(Q12-Q22+2*Q66)*S3*C1
610 QB26 = (Q11-Q12-2*Q66)*C1*S3+(Q12-Q22+2*Q66)*C3*S1
620 QB66 = (Q11+Q22-2*Q12-2*Q66)*S2*C2+Q66*(S4+C4)
670 RETURN
680 REM    THIS ROUTINE CALCULATES THE  " A " MATRIX
690 CLS
700 A11 = A11 + QB11*T
710 A12 = A12 + QB12*T
720  A16 = A16 + QB16*T
730 A22 = A22 + QB22*T
740 A26 = A26 + QB26*T
750 A66 = A66 + QB66*T
760 RETURN
770  REM      THIS ROUTINE CALCULATES THE " B " MATRIX
780 ZT = T*ZK
790 B11 = B11 + QB11*ZT
800 B12 = B12 + QB12*ZT
810 B16 = B16 + QB16*ZT
820 B22 = B22 + QB22*ZT
830 B26 = B26 + QB26*ZT
840 B66 = B66 + QB66*ZT
850RETURN
860 REM THIS ROUTINE CALCULATES THE " D " MATRIX
870 CON = ZK^2*T+T^3/12
880 D11 = D11 +QB11*CON
890 D12 = D12 + QB12*CON
900 D16 = D16 + QB16*CON
910 D22 = D22 + QB22*CON
920 D26 = D26 + QB26*CON
930 D66 = D66 + QB66*CON
940 RETURN
950 PRINT   "              THE STIFFNESS MATRICIES ARE AS
FOLLOWS"
960 PRINT
961 VDU2
970 PRINT "                          THE  A  MATRIX":PRINT
980 PRINT"                          A11  =  ";A11
990 PRINT"                          A12  =  ";A12
1000 PRINT"                         A16  =  ";A16
1010 PRINT"                         A22  =  ";A22
1020 PRINT"                         A26  =  ";A26
1030 PRINT"                         A66  =  ";A66:PRINT
1040 PRINT"                           THE  B  MATRIX":PRINT

1050 PRINT"                         B11  =  ";B11
1060 PRINT"                         B12  =  ";B12
1070 PRINT"                         B16  =  ";B16
1080 PRINT"                         B22  =  ";B22
1090 PRINT"                         B26  =  ";B26
1100 PRINT"                         B66  =  ";B66:PRINT
1110 PRINT"                           THE  D  MATRIX":PRINT

1120 PRINT"                         D11  =  ";D11
```

```
1130 PRINT"                    D12  =  ";D12
1140 PRINT"                    D16  =  ";D16
1150 PRINT"                    D22  =  ";D22
1160 PRINT"                    D26  =  ";D26
1170 PRINT"                    D66  =  ";D66
1171 VDU3
1180 RETURN
```

Appendix 4

Listing of a Computer Programme for Calculating the Distribution of Contact Stresses

```
 10 REM IMPACT CHARACTERISTICS
 20 PRINT "PROJECTILE DIAMETER"
 30 INPUT RP
 40PRINT"PROJECTILE VELOCITY"
 50INPUT V
 60PRINT"KTKP"
 70INPUT KTKP
 80PRINT"PROJECTILE MASS"
 90INPUT MP
100PRINT"BEAM MASS"
110INPUT MT
120N1=1/MP+1/MT
130N=SQR(RP)*4/(3*PI*KTKP)
140TEMP= 5*V^2/(4*N1*N)
150A=SQR(RP)*(TEMP)^0.2
160P=TEMP^0.6*4*SQR(RP)/(3*PI*KTKP)
170QO=3*P/(2*PI*A^2)
180REM DETERMINE STRESSES
200VDU3
205 FOR ZZ=1TO5
210 FOR RRO=1TO20
220 FOR RO=1TO5
230RO=RRO/1000
240Z=ZZ/1000
250REM DETERMINE LAMDA1
260BB=(A^2-Z^2-RO^2)
270AA=1
280CC=-(Z^2)*(A^2)
290BC=BB^2-4*AA*CC
300LAMDA=-BB+SQR(BC)
310LAMDA1=LAMDA/2
320IF LAMDA1>0 THEN GOTO 350
330LAMDA=-BB-SQR(BC)
340LAMDA1=LAMDA/2
350REM DETERMINE STRESSES
360SIGR1=0.12*A^2/(RO^2)*(1-(Z/SQR(LAMDA1))^3)
370TEMP=A/SQR(LAMDA1)
380SIGR2=1.32*Z/A*ATN(TEMP)
390SIGR3=0.68*Z*SQR(LAMDA1)/(A^2+LAMDA1)
400SIGR4=-2*Z/SQR(LAMDA1)
410SIGR5=A^2*Z^3/((LAMDA1^2+A^2*Z^2)*SQR(LAMDA1))
420SIGMAR = (SIGR1+SIGR2+SIGR3+SIGR4+SIGR5)*QO
430SIGMAT=(-SIGR1+SIGR2-SIGR3+0.32*SIGR4)*QO
440SIGMAZ=Z^3/((LAMDA1^2+A^2*Z^2)*SQR(LAMDA1))*3*P/(2*PI)
450VDU2
460PRINT"STRESSES AT Z = ";Z ;"RO =, ";RO
470PRINT"SIGMA RR = ";SIGMAR
480PRINT"SIGMA THETA = ";SIGMAT
490PRINT"SIGMA ZZ = ";SIGMAZ
```

```
491 NEXT RRO
492 NEXT ZZ
510END
520DATA 0.005,0.0011,0.01,0.0011,1.5,0.1,2,0.1,2.5,0.1
530DATA 0.5,1,1,1,1.5,1,2,1,2.5,1
540DATA 0.5,2,1,2,1.5,2,2,2,2.5,2
550DATA 0.5,3,1,3,1.5,3,2,3,2.5,3
560DATA 0.5,4,1,4,1.5,4,2,4,2.5,4
570DATA 0.5,5,1,5,1.5,5,2,5,2.5,5
580DATA 0.5,6,1,6,1.5,6,2,6,2.5,6
590DATA 0.5,7,1,7,1.5,7,2,7,2.5,7
600print"stresses at z = "; Z ;"RO =, ";RO
610PRINT"SIGMA RR = ";SIGMAR
620PRINT"SIGMA THETA = ";SIGMAT
630PRINT"SIGMA ZZ = ";SIGMAZ
```